



TECHNICAL REPORT 0-6813-1
TxDOT PROJECT NUMBER 0-6813

Investigation of High-Range Water Reducers on Inducing Micro-Cracking in Precast Concrete Elements

Raissa Ferron
Gwen Carris
Stephen Stacey
Michael Rung

February 2017; Published September 2018

<http://library.ctr.utexas.edu/ctr-publications/0-6813-1.pdf>



Technical Report Documentation Page

1. Report No. FHWA/TX-17/0-6813-1		2. Government Accession No.	3. Recipient's Catalog No.	
4. Title and Subtitle Investigation of High-Range Water Reducers on Inducing Micro-Cracking in Precast Concrete Elements			5. Report Date March 2017; Published September 2018	
			6. Performing Organization Code	
7. Author(s) Raissa Ferron, Gwen Carris, Stephen Stacey, Michael Rung			8. Performing Organization Report No. 0-6813-1	
9. Performing Organization Name and Address Center for Transportation Research The University of Texas at Austin 3925 W. Braker Lane, 4 th Floor Austin, TX 78759			10. Work Unit No. (TR AIS)	
			11. Contract or Grant No. 0-6813	
12. Sponsoring Agency Name and Address Texas Department of Transportation Research and Technology Implementation Office P.O. Box 5080 Austin, TX 78763-5080			13. Type of Report and Period Covered Technical Report July 2014–December 2016	
			14. Sponsoring Agency Code	
15. Supplementary Notes Project performed in cooperation with the Texas Department of Transportation and the Federal Highway Administration.				
16. Abstract An overarching objective of this project is to increase the understanding of the effect of polycarboxylate (PC) high-range water-reducers (HRWR) on the performance of concrete mixtures, with a special focus on concrete mixtures that will be used in precast concrete beam applications. The motivation for this research was based upon the results of Interagency Contract (IAC) No. 463MTIA034: Evaluation of Long-Term Durability of Concrete, which addresses potential mechanisms for unexplained cracking in girders cast at Texas precast plants, typically appearing 18–24 months after casting.				
17. Key Words Autogenous shrinkage, drying shrinkage, high range water reducer, micro-cracking			18. Distribution Statement No restrictions. This document is available to the public through the National Technical Information Service, Springfield, Virginia 22161; www.ntis.gov.	
19. Security Classif. (of report) Unclassified	20. Security Classif. (of this page) Unclassified	21. No. of pages 218	22. Price	

Form DOT F 1700.7 (8-72) Reproduction of completed page authorized



THE UNIVERSITY OF TEXAS AT AUSTIN
CENTER FOR TRANSPORTATION RESEARCH

Investigation of High-Range Water Reducers on Inducing Micro-Cracking in Precast Concrete Elements

Raissa Ferron
Gwen Carris
Stephen Stacey
Michael Rung

CTR Technical Report:	0-6813-1
Report Date:	March 2017; Published September 2018
Project:	0-6813
Project Title:	Evaluation of ASTM C 494 Procedures for Polycarboxylate Admixtures Used in Precast Concrete Elements
Sponsoring Agency:	Texas Department of Transportation
Performing Agency:	Center for Transportation Research at The University of Texas at Austin

Project performed in cooperation with the Texas Department of Transportation and the Federal Highway Administration.

Center for Transportation Research
The University of Texas at Austin
3925 W. Braker Lane, 4th Floor
Austin, TX 78759

<http://ctr.utexas.edu/>

Disclaimers

Author's Disclaimer: The contents of this report reflect the views of the authors, who are responsible for the facts and the accuracy of the data presented herein. The contents do not necessarily reflect the official view or policies of the Federal Highway Administration or the Texas Department of Transportation (TxDOT). This report does not constitute a standard, specification, or regulation.

Patent Disclaimer: There was no invention or discovery conceived or first actually reduced to practice in the course of or under this contract, including any art, method, process, machine manufacture, design or composition of matter, or any new useful improvement thereof, or any variety of plant, which is or may be patentable under the patent laws of the United States of America or any foreign country.

Engineering Disclaimer

NOT INTENDED FOR CONSTRUCTION, BIDDING, OR PERMIT PURPOSES.

Project Engineer: Raissa Ferron
Designation: Research Supervisor

Acknowledgments

The authors express appreciation to TxDOT Project Director, Ms. Sonya Badgley, and members of the Project Monitoring Committee: Andy Naranjo (CST), Hector Garcia (BRG), Jaime Gandara (CST), Rachel Cano (CST), Ruben Carrasco (CST), Patti Dathe (RTI), Darrin Jensen (RTI), and Jason Tucker (CST). The authors also express appreciation to the two employees at the two precast plants that allowed us access to their facilities, and UT Austin graduate student, Ms. Savitha Srinivasan, for her invaluable assistance and expertise during crack mapping at site visits to Dallas and Texarkana. Also appreciated are the intelligence, time, curiosity, assiduousness, and labor of the undergraduate researcher assistants that worked on this project: Esteban Gonzalez, Pamela Ruiz, Zige Zhang, and Jessica Milligan—may you all reach the heights of civil engineering in your future. Finally, the authors thank the CTR staff, especially Ms. Ashley Williams and Ms. Maureen Kelly, for their assistance with respect to the administrative aspects of this project.

Table of Contents

Chapter 1. Introduction.....	1
1.1 Background and Scope	1
1.2 Report Content and Organization	3
Chapter 2. Information Survey Review and a Summary of Forensic Investigations in the Field.....	4
2.1 Summary of Previous Project Investigations.....	4
2.2 Literature Survey Review Results	6
2.3 Forensic Investigations	6
2.3.1 Methodology	7
2.3.2 Crack Mapping.....	7
2.3.3 Results.....	10
2.3.4 Review of Relative Humidity Results.....	23
2.3.5 Qualitative Information from Surveys at Both Sites.....	24
2.4 Key Findings and Conclusions	26
2.4.1 Information Survey Review Results	26
2.4.2 Forensic Investigation Results	26
Chapter 3. Materials and Mixture Proportions	27
3.1 Introduction.....	27
3.2 Portland Cements	27
3.3 Fly Ash.....	27
3.4 Aggregates	27
3.4.1 Coarse Aggregate.....	27
3.4.2 Fine Aggregate.....	28
3.5 Chemical Admixtures	28
Chapter 4. Laboratory Testing: Evaluation of Suitability of ASTM C494 Procedures for Precast Concrete Mixtures.....	30
4.1 Introduction.....	30
4.2 Overview of ASTM C494 and Testing Matrix	31
4.2.1 Water Content	36
4.2.2 Time of Set.....	38
4.2.3 Compressive Strength	41
4.2.4 Drying Shrinkage	45
4.3 Suitability of ASTM C494: Results and Conclusions	60

Chapter 5. Parametric Study: Developing a Complementary Testing Matrix to ASTM C494	61
5.1 Introduction.....	61
5.2 Parametric Study: Concrete Testing	61
5.2.1 Restrained Shrinkage Rings	63
5.2.2 Parametric Study of Concrete:.....	82
5.2.3 Results and Conclusions for Concrete Testing	82
5.3 Parametric Study: Paste Testing	82
5.3.1 Time of Set.....	84
5.3.2 Autogenous Deformation.....	86
5.3.3 Corrugated Tube Results.....	92
5.3.4 Modifications to ASTM Corrugated Tube Standard Approach.....	93
5.3.5 Results from Enhanced Corrugated Tube Test	100
5.3.6 Conclusions for Parametric Testing	108
5.4 Isothermal Calorimetry Testing	108
5.4.1 Methodology	108
5.4.2 Results and Discussion	110
5.4.3 Key Findings and Results	118
5.4.4 Mini Ring Test	118
5.5 Key Findings.....	119
Chapter 6. Field Work	121
6.1 Introduction.....	121
6.2 TxDOT Exposure Site Visit.....	121
6.2.1 Block Examination.....	121
6.3 Precast Plant Site Visit.....	129
6.4 UT Austin Exposure Site	133
6.4.1 Methodology	133
6.4.2 Exposure Specimen Types	134
6.4.3 Block and Mini Girder Exposure Results	137
6.4.4 Exposure Block Expansion/Contraction Results	142
6.4.5 Carbonation Testing Results	147
6.4.6 Key Findings	153
Chapter 7. Conclusions	154
7.1 Summary of Task Findings.....	154
7.2 Recommendations and Future Work	157

Appendix I: Materials Identification	159
Appendix II: Mixture Identification According to Task.....	161
Appendix III: Compressive Strength Data.....	164
Appendix IV: Additional Cited Sources	167
Appendix V: Drying Shrinkage Curves.....	168
Appendix VI: Restrained Shrinkage Ring Program	183
Appendix VII: Cedar Park Blocks Included in Parametric Study	191
References.....	195

List of Figures

Figure 2-1: Micro-cracking focused on the top flange of a rejected precast girder.....	4
Figure 2-2: Precast plant exposure block replicate cast according to ASTM C1293 0.42 w/cm and 20% Class F fly ash.....	5
Figure 2-3: Precast plant straight cement exposure block replicate cast according to ASTM C1293 0.45 w/cm.....	6
Figure 2-4: Overall map of locations.....	7
Figure 2-5: Savitha Srinivasan (graduate student working on associated TxDOT project 0-6922) recording crack widths and lengths at the Dallas site visit	8
Figure 2-6: SHM40 Vaisala kit with plastic tubes, rubber plugs, and humidity sensor.	9
Figure 2-7: Holes sealed with cementitious grout	9
Figure 2-8: Overall view of bridge looking east; (exterior girder in this picture is labelled as G1).....	10
Figure 2-9: Overall photo of G7 with corresponding humidity measurement probes and crack map G7-2.....	14
Figure 2-10: Overall photo of G8, an adjacent cracked girder, with corresponding humidity measurement probes and crack map G8-1.....	14
Figure 2-11: Close-up photo of G7-2 corresponding sealed humidity probe drilled holes, showing minimal cracking.....	15
Figure 2-12: Close-up photo of G8-1 corresponding internal relative humidity probes, showing typical micro-cracking distress.....	15
Figure 2-13: Overall view of site facing north (visible exterior girder is referred to as G1).....	16
Figure 2-14: Overall photo of G1, an exterior uncracked girder, with corresponding humidity measurement probes and crack map G1-2.....	22
Figure 2-15: Overall photo of G2, a cracked girder, with corresponding humidity measurement probes and crack map G2-4.....	22
Figure 2-16: Close-up photo of G1-2 crack map, showing no cracks	23
Figure 2-17: Close-up photo of G2-4 crack map, showing typical micro-cracking distress	23
Figure 2-18: Plot of the four relative humidity gradients investigated.....	24
Figure 2-19: White powder on girders.....	25
Figure 2-20: Surface defects on cracked girder at Dallas site (1).....	25
Figure 2-21: Surface defects on cracked girder at Dallas site (2).....	25
Figure 2-22: Similar surface defects observed in cracked flange at Texarkana	26
Figure 4-1: Testing performed and qualification criteria used to evaluate the relevancy of ASTM C494 to predict the latent cracking observed in the precast concrete barriers	30
Figure 4-2: Tests performed for ASTM C494 and their respective limits and chapters.....	31

Figure 4-3: Time of set equipment used throughout this project.....	39
Figure 4-4: Drying shrinkage curve showing effect of w/cm ratio on base mixture, M1-NC (0.26 w/cm), for 1- and 28-Day curing.	48
Figure 4-5: Drying shrinkage curve showing effect of w/cm ratio for base mixture M3-NC (0.33 w/cm) for 1- and 28-Day curing.	48
Figure 4-6: Drying shrinkage curve showing effect of w/cm ratio for base mixture M4-SCC (0.31 w/cm) for 1- and 28-Day curing.	49
Figure 4-7: Drying shrinkage curve showing effect of cement source (PC-III-A and PC-III-B) for 0.26 and 0.31 w/cm ratios for base mixture M1-NC and M4-SCC respectively.	50
Figure 4-8: Drying shrinkage curve showing effect of cement type (PC-III-A and PC-I-A) and curing period for 0.28 w/cm ratios for mixtures T5-M5 and T5-M7.....	51
Figure 4-9: Drying shrinkage curve showing effect of HRWR dosage for base mixture for M1-NC for 1- and 28-Day curing.	52
Figure 4-10: Drying shrinkage curve showing effect of HRWR Dosage for base mixture M3-NC for 1- and 28-Day curing.	52
Figure 4-11: Drying Shrinkage Curve showing effect of HRWR type (HR-P1, HR-P2, and HR-P3) base mixture for M1-NC.....	53
Figure 4-12: Drying shrinkage curve showing effect of HRWR type (HR-P1, HR-P2, and HR-P3) for base mixture M4-SCC.	54
Figure 4-13: Drying shrinkage curve showing effect of cement content for base mixture M1-NC.	55
Figure 4-14: Drying shrinkage curve showing effect of cement content (658 lb/yd ³ and 517 lb/yd ³) for base mixture M3-NC.....	55
Figure 4-15: Drying shrinkage curve showing effect of fly ash addition (175 lb/yd ³ – 25% add. and 233 lb/yd ³ – 33% add.) for base mixture M1-NC.	56
Figure 4-16: Drying shrinkage curve showing effect of fly ash addition (219 lb/yd ³ – 33% add) for base mixture M3-NC.....	57
Figure 4-17: Drying shrinkage curve showing effect of fly ash addition (271 lb/yd ³ – 40% add and 165 lb/yd ³ – 25% add) for base mixture M4-SCC.	57
Figure 4-18: Drying shrinkage curve showing effect of fly ash addition (165 lb/yd ³ – 25% add) for base mixtures M6-CFA and M3-CWB.	58
Figure 4-19: Drying shrinkage curve showing effect of fine aggregate source (FA-A, FA-B and FA-LW) for mixtures M3-NC, M3-CSP and M3-CLWA (20% of the fine aggregate replacement with lightweight aggregate).	59
Figure 5 1: Parametric study testing breakdown between concrete and paste analysis.....	61
Figure 5 2: Stainless steel vise and CAD drawing used to align the 6-in. longitudinal slit in the outer HPVC 16-in. pipe	64
Figure 5 3: Locking locations for securing the inner and outer rings to the restrained shrinkage ring bases denoted in red	65

Figure 5 4: Strain gage locations on restrained shrinkage ring.....	66
Figure 5 5: Terminal diagram for restrained shrinkage ring strain gages.....	66
Figure 5 6: DAQ setup employed at UT Austin for collecting restrained shrinkage ring strain data.....	67
Figure 5 7: Diagram of the restrained shrinkage ring setup.....	68
Figure 5 8: Casting restrained shrinkage ring on vibrating table.....	69
Figure 5 9: Restrained shrinkage rings (four mixtures), monitored in the testing room	70
Figure 5 10: Net strain versus the square root of time (days) after demolding for Mixture 8.....	71
Figure 5 11: Tensile strength (psi) approximately determined through curve fit at time of cracking.....	73
Figure 5 12: Modulus of elasticity (ksi) approximately determined through curve fit at time of cracking.	74
Figure 5 13: Compressive strength (psi) approximately determined through curve fit at time of cracking	75
Figure 5 14: Cracking potential envelopes outlining the potential for each of the eight mixture designs cast.....	76
Figure 5 15: Net microStrain development over time (days) for all ring mixtures.	77
Figure 5 16: Restrained shrinkage ring data with respect to time.....	78
Figure 5 17: Compressive strength, splitting tensile, and modulus of elasticity for Mixture 1 and Mixture 3.....	78
Figure 5 18: Restrained Shrinkage ring data with respect to time modeling effect of w/cm for Mixture 1 – 0.28 w/cm and Mixture 2 – 0.33	79
Figure 5 19: Compressive strength, splitting tensile, and modulus of elasticity for Mixture 1 and Mixture 2.....	80
Figure 5 20: Restrained Shrinkage ring data with respect to time modeling effect of the HRWR type with Mixture 4 – HR-P1 and Mixture 5 – HR-P3 and *Mixture 7 – HR-P2	81
Figure 5 21: Compressive strength, splitting tensile and modulus of elasticity for Mixture 4, Mixture 5, and Mixture 7	81
Figure 5 22: Parametric study testing breakdown with chapter section designation for paste analysis	84
Figure 5 23: Vicat Needle Test, ASTM C191.	85
Figure 5 24: Averaged setting times plotted for each paste mixtures.....	86
Figure 5 25: Autogenous Shrinkage Test Setup via Volumetric/Buoyancy Method.....	87
Figure 5 26: Buoyancy shrinkage 0.31 PC-III-A for HR-P1 at 6.5, 8.25, and 12 fl oz/100 lb cement.....	89

Figure 5 27: Buoyancy shrinkage 0.31 PC-III-A for HR-P2 at 6.5, 8.25, and 12 fl oz/100 lb cement.....	89
Figure 5 28: Buoyancy shrinkage 0.31 PC-III-A for HR-P3 at 6.5, 8.25, and 12 fl oz/100 lb cement.....	90
Figure 5 29: Buoyancy shrinkage 0.31 PC-III-A for HR-P1, HR-P2, and HR-P3 at fixed 6.5 fl oz/100 lb cement.....	91
Figure 5 30: Buoyancy shrinkage 0.31 PC-III-A for HR-P1, HR-P2, and HR-P3 at fixed 8.25 fl oz/100 lb cement.....	91
Figure 5 31: Buoyancy shrinkage 0.31 PC-III-A for HR-P1, HR-P2, and HR-P3 at fixed 12 fl oz/100 lb cement.....	92
Figure 5 32: Corrugated polyethylene autogenous test setup (Germann Instruments).....	93
Figure 5 33: CAD drawing of corrugated tube test rig	94
Figure 5 34: Test setup for the corrugated tube test developed at UT Austin.	95
Figure 5 35: Corrugated tube being filled and vibrated.....	96
Figure 5 36: Diagram of the non-contact LVDT setup.....	96
Figure 5 37: Excerpt of Version 2 corrugated tube set-up showing the non-contact LVDT eddy current sensor and adjacent steel plate in situ	97
Figure 5 38: Typical LVDT calibration curve	98
Figure 5 39: LABview program screen of three samples voltage readings with respect to time	99
Figure 5 40: Signal conditioning input modules set in the signal conditioning input board	100
Figure 5 41: Effect of w/cm on autogenous shrinkage of paste containing low dosage of HR-P1 HRWR	101
Figure 5 42: Effect of w/cm on autogenous shrinkage of paste containing moderate dosage of HR-P1 HRWR	101
Figure 5 43: Effect of w/cm on autogenous shrinkage of paste containing high dosage of HR-P1 HRWR	102
Figure 5 44: Effect of w/cm on autogenous shrinkage of paste containing low dosage of HR-P2 HRWR	103
Figure 5 45: Effect of w/cm on autogenous shrinkage of paste containing moderate dosage of HR-P2 HRWR	104
Figure 5 46: Effect of w/cm on autogenous shrinkage of paste containing high dosage of HR-P3 HRWR	105
Figure 5 47: 6.5 and 8.25 oz/cwt dosages show no significant bleed bump and overlap at a higher dosage than the 12 oz/cwt dosage.....	105
Figure 5 48: 6.5 and 8.25 oz/cwt dosages show a similar, though not as significant bleed bump and both overlap at a higher dosage than the 12 oz/cwt dosage	106

Figure 5 49: 6.5 and 8.25 oz/cwt dosages show a similar, though not as significant bleed bump and both overlap at a higher dosage than the 12 oz/cwt dosage	107
Figure 5 50: Comparison of pastes in concrete mixtures with known performance history, excepting the 0.31 w/cm which did not have a comparable paste mixture.....	108
Figure 5 51: Isothermal calorimetry apparatus	109
Figure 5 52: A screenshot of the Grace AdiaCal software monitor showing voltage over time from thermocouples underneath cement paste.....	109
Figure 5 53: Calorimetry results for three mixes.	110
Figure 5 54: Typical heat flow curve with demarcated periods shown (Zhang et al. 2015)	111
Figure 5 55: Heat flow curve of all 0.26 w/cm mixes using HR-P2 admixture	111
Figure 5 56: Cumulative heat evolved of all 0.26 w/cm mixes using HR-P2 admixture	111
Figure 5 57: Heat flow curve of all 0.28 w/cm mixes using HR-P1 admixture	112
Figure 5 58: Cumulative heat evolved of all 0.28 w/cm mixes using HR-P1 admixture	112
Figure 5 59: Heat flow curve of all 0.28 w/cm mixes using HR-P2 admixture	112
Figure 5 60: Cumulative heat evolved of all 0.28 w/cm mixes using HR-P2 admixture.	113
Figure 5 61: Heat flow curve of all 0.28 w/cm mixtures to compare the effect of HRWR dosage and addition of fly ash	113
Figure 5 62: Cumulative heat evolved for all 0.28 w/cm mixtures	113
Figure 5 63: Effect of dosage of HR-P1 and fly ash on heat flow over time for 0.31 w/cm	114
Figure 5 64: Effect of dosage of HR-P1 and fly ash on total heat evolved for 0.31 w/cm.....	114
Figure 5 65: Effect of HR-P2 dosage on heat flow curve.....	114
Figure 5 66: Heat flow curve of 0.31 w/cm mixtures evaluated.....	115
Figure 5 67: Heat flow curve of all 0.31 w/cm mixes using HR-P3 admixture	115
Figure 5 68: Total energy curve of all 0.31 w/cm mixes using HR-P3 admixture	115
Figure 5 69: Heat flow curve of all 0.33 w/cm mixes evaluated using HR-P1	116
Figure 5 70: Total heat evolved for 0.33 w/cm mixes incorporating HR-P1	116
Figure 5 71: Heat flow curve of 0.33 w/cm mixtures incorporating HR-P2	116
Figure 5 72: Total heat evolved curved of 0.33 w/cm curves incorporating HR-P2	117
Figure 5 73: Heat flow curve of 0.33 w/cm curves incorporating HR-P3	117
Figure 5 74: Heat flow curves of 0.33 w/cm mixtures incorporating HR-P3.....	117
Figure 5 75: Mini restrained ring test	118
Figure 5 76: Crack development in mini-ring restrained test:	119
Figure 6 1: Example of Crack Rating = 0	122
Figure 6 2: Example of Crack Rating = 1	123
Figure 6 3: Example of Crack Rating = 2	123

Figure 6 4: Example of Crack Rating = 3	124
Figure 6 5: Example of Crack Rating = 4.5	124
Figure 6 6: Exposure block crack ratings with respect to month of casting.	125
Figure 6 7: Exposure block crack ratings according to variation in HR-P1 dosage with all other properties held constant; data represents nine distinct blocks.	125
Figure 6 8: Exposure block crack ratings according to variation in HR-P1 and HR-P1+NR-1 with all other properties held constant; data represents 16 distinct blocks.	126
Figure 6 9: Exposure block crack ratings according to a given water-to-cement ratio for a fixed cement content of 658 lb/yd ³ ; data represents 38 distinct blocks.	126
Figure 6 10: Exposure block crack ratings according to a given cementitious content lb/yd ³ ; data represents 12 distinct blocks.	127
Figure 6 11: Concentration of map cracking pattern.	130
Figure 6 12: Girder located at Precast Plant PP-A (micro-cracking concentrated on upper and lower flange)	131
Figure 6 13: Girder located at Precast Plant PP-B (micro-cracking concentrated on web).....	131
Figure 6 14: (A) Photo of girder located at Precast Plant PP-B with fingers pointing to diagonal release strand cracks. (B) Photo of a separate girder located at Precast Plant PP-B showing that the micro-cracks stem away from the release strand cracks and form in new space between release strand cracks.....	132
Figure 6 15: Close up image of Figure 6-14(b).	133
Figure 6 20: Carbonation exposure site at UT Austin with shelter (Stevenson Screen).....	137
Figure III-1: Compressive Strength Results Task 3.....	164
Figure III 2: Compressive Strength Results Task 4.....	165
Figure III 3: Compressive Strength Results Task 5	166
Figure IV 1: Time vs Temperature curve for precast concrete elements containing Alamo III and Capitol III cement taken from Implementation of Concrete Works Software in Texas Highway Construction (Meeks 2012).....	167
Figure VI 1: Drying Shrinkage 0.26 PC-III-A 517lb + FA-1 129lb HR-P1 5.25 oz + NR-1 3 oz.....	168
Figure VI 2: Drying Shrinkage 0.56 PC-III-A 658lb FA-1 219lb HR-P1 6.5 oz + NR-1 3 oz TRIAL A	168
Figure VI 3: Drying Shrinkage 0.56 PC-III-A 658lb FA-1 219lb HR-P1 6.5 oz + NR-1 3 oz TRIAL B	169
Figure VI 4: Drying Shrinkage 0.26 PC-III-A 663lb FA-1 271lb HR-P1 7 oz + NR-1 2.5 oz.....	169
Figure VI 5: Drying Shrinkage 0.26 PC-III-A 705lb FA-1 175lb HR-P1 5.25 oz + NR-1 3 oz.....	170

Figure VI 6: Drying Shrinkage 0.26 PC-III-A 705lb FA-1 175lb HR-P1 6.5 oz + NR-1 1.5 oz.....	170
Figure VI 7: Drying Shrinkage 0.26 PC-III-A 705lb FA-1 175lb HR-P1 8.25 oz + NR-1 1.5 oz.....	171
Figure VI 8: Drying Shrinkage 0.26 PC-III-A 663lb FA-1 271lb HR-P1 7 oz + NR-1 2.5 oz.....	171
Figure VI 9: Drying Shrinkage 0.33 PC-III-A 663lb FA-1 271lb HR-P1 5 oz + NR-1 2.5 oz.....	172
Figure VI 10: Drying Shrinkage 0.31 PC-III-A 663lb FA-1 165lb HR-P1 5.5 oz + NR-1 2.5 oz.....	172
Figure VI 11: Drying Shrinkage 0.26 PC-III-A 705lb FA-1 233lb HR-P1 6.5 oz + NR-1 3 oz.....	173
Figure VI 12: Drying Shrinkage 0.28 PC-III-A 705lb FA-1 175lb HR-P1 12 oz + NR-1 3 oz.....	173
Figure VI 13: Drying Shrinkage 0.31 PC-III-A 663lb FA-1 271lb HR-P1 5.5 oz + NR-1 2.5 oz.....	174
Figure VI 14: Drying Shrinkage 0.31 PC-III-A 640lb FA-1 213lb HR-P1 6 oz + NR-1 2 oz.....	174
Figure VI 15: Drying Shrinkage 0.31 PC-III-A 663lb FA-1 271lb HR-P2 5.5 oz + NR-1 2.5 oz.....	175
Figure VI 16: Drying Shrinkage 0.31 PC-III-A 663lb FA-1 271lb HR-P3 7.25 oz + NR-2 2.5 oz.....	175
Figure VI 17: Drying Shrinkage 0.31 PC-III-B 663lb FA-1 271lb HR-P1 6 oz + NR-1 2.5 oz.....	176
Figure VI 18: Drying Shrinkage 0.33 PC-III-A 517lb HR-P1 30.5 oz + NR-1 3 oz.....	176
Figure VI 19: Drying Shrinkage 0.33 PC-III-A 658lb HR-P1 11.88 oz + NR-1 3 oz.....	177
Figure VI 20: Drying Shrinkage 0.33 PC-III-A 658lb HR-P1 6.5 oz + NR-1 3 oz.....	177
Figure VI 21: Drying Shrinkage 0.33 PC-III-A 658lb HR-P1 5.5 + NR-1 2 oz.....	178
Figure VI 22: Drying Shrinkage 0.33 PC-III-A 658lb HR-P1 5 + NR-1 2.5 oz w/ FA-LW	178
Figure VI 23: Drying Shrinkage 0.33 PC-III-A 663lb FA-1 271lb HR-P1 5 oz + NR-1 2.5 oz.....	179
Figure VI 24: Drying Shrinkage 0.38 PC-III-A 705lb FA-1 175lb	179
Figure VI 25: Drying Shrinkage 0.4 PC-III-A 658lb FA-1 165lb HR-P1 2 oz + NR-1 2 oz	180
Figure VI 26: Drying Shrinkage 0.4 PC-III-A 658lb HR-P1 2 oz + NR-1 2 oz.....	180
Figure VI 27: Drying Shrinkage 0.45 PC-III-A 705lb FA-1 175lb	181
Figure VI 28: Drying Shrinkage 0.52 PC-III-A 658lb.....	181
Figure VI 29: Drying Shrinkage 0.56 PC-III-A 658lb.....	182

List of Tables

Table 2-1: Crack mapping data recorded in Dallas	11
Table 2-2: Relative humidity results.....	15
Table 2-3: Crack mapping data.....	17
Table 2-4: Relative humidity probe measurements	23
Table 3-1: Oxide analysis for different cement sources and types	27
Table 3-2: Oxide analysis for Class F fly ash.....	27
Table 3-3: Physical properties of the coarse aggregates.....	28
Table 3-4: Physical properties of the fine aggregates.....	28
Table 3-5: Classification of admixtures used throughout this study.....	29
Table 4-1: Initial testing matrix for ASTM C494: three “bad performers” (yellow) and two “good performers” (blue).....	32
Table 4-2: Mixture proportions for the different control types used for ASTM C494 qualification	33
Table 4-3: Mixtures organized with respect to their control mixture.	34
Table 4-4: Reasoning behind the control mixtures selected	35
Table 4-5: Water content pass/fail for ASTM C494 in reference to control mixtures.	37
Table 4-6: Time of set pass/fail for ASTM C494 in reference to control mixtures.....	40
Table 4-7: Compressive strength pass/fail for ASTM C494 in reference to control mixtures (1-7 Day).....	42
Table 4-8: Compressive strength pass/fail for ASTM C494 in reference to control mixtures (7-Day through 28-Day).	43
Table 4-9: Compressive strength pass/fail for ASTM C494 in reference to control mixtures (90-Day through 6-Month).	44
Table 4-10: Drying shrinkage pass/fail for ASTM C494 in reference to control mixtures (1-Day Cure).	46
Table 5 1: Concrete mixtures subjected to the restrained ring test parametric study 62	
Table 5 2: Net time-to-cracking and stress rate for all ring mixture.....	72
Table 5 3: Pastes mixtures subjected to parametric study	83
Table 5 4: Mixture proportions and averaged time of set through ASTM C191.....	85
Table 5 5: Autogenous shrinkage according to mixture designs at 72 hours after introduction of cement to water	88
Table 5 6: Time of cracking for restrained paste mixes that did crack.....	119
Table 6 1: Material Selection Criterion for Crack Investigation of Cedar Park TxDOT Site	121
Table 6 2: Blocks cast at UT Austin exposure site for TxDOT 0-6813.	138

Table 6 3: Mini girder matrix at UT Austin Exposure Site.	140
Table 6 4: Pinned exposure block matrix at UT Austin exposure site.....	142
Table 6 5: Carbonation testing matrix at UT Austin Exposure Site and results comparing sheltered (IN) specimens versus unsheltered (OUT) specimens	149
Table I-1: Cement nomenclature, distributor and oxide analysis	159
Table I-2: Fly ash nomenclature, distributor and oxide analysis	159
Table I-3: Coarse aggregate nomenclature, source and properties	159
Table I-4: Fine aggregate nomenclature, source and properties	159
Table I-5: Admixture nomenclature, source, classification and properties	160
Table II-1: Task 3 Mixture ID's and mixture designs	161
Table II-2: Task 4 Mixture ID's and mixture designs	162
Table II-3: Task 5 Mixture ID's and mixture designs	163

Chapter 1. Introduction

Over the past few decades surface cracking has become more and more apparent on girders produced at precast plants all throughout the state of Texas. Originally, the concern was that the cracking was a result of alkali-silica reaction (ASR) and delayed ettringite formation (DEF), yet that theory was dismissed due to the results of field and lab investigations. The type of cracking seen has been perceived as a map and or micro-cracking pattern, and analogous to all cracks in concrete, it is due to volumetric change. However, the exact mechanism causing the volumetric changes is not fully understood. The cracks have been labeled as “micro-cracks” as they do not appear to increase in crack width, but rather seem to densify and scatter across the concrete structure. The cracking appears to intensify as the concrete is exposed to the environment (typically apparent in 18 to 24 months after casting). The cracking became a cause for concern when TxDOT’s quality control noticed that the map cracking would develop even prior to the girders being put in service, occurring simply by sitting in the precast yard. Additionally, there was some concern that the cracks may extend down to the reinforcement.

As a result of this widespread cracking, girders have been rejected and terminated from future service. Therefore, these micro-cracks have resulted in sizable expenses to the precast producers as well as the state DOT, who has been responsible for inspecting and researching with regards to the cracking issue on the existing girders currently in service. Despite the considerable amount of effort that was put into improving the precast high performance concrete (HPC) mixture designs, the micro-cracking issue still persist. Concrete cast at precast plants less than a year ago shows the development of micro-cracking all along the concrete’s exposed surfaces.

After ASR and DEF were eliminated through petrographic examination, the investigation began to look at the concrete pathology, in order to see if something had been altered to cause the material related cracking issue (IAC). The typical 0.28 to 0.33 w/cm ratio ranges implemented at precast plants paired with the need to increase the use of high range water reducers (HRWRs) has guided Texas Department of Transportation (TxDOT) to consider whether the HRWRs, specifically the polycarboxylate admixtures, could be contributing to the cracking issue. Currently, three-fourths of the major precast plants in the state of Texas have begun to experiment and utilize self-consolidating concrete (SCC) mixture designs. The incorporation of viscosity-modifying admixtures (VMAs) which are used to minimize segregation has prompted new developments in HRWRs and therefore created an additional cause for concern with respect to the micro-cracking seen in the field. In this project, we examined the performance of actual precast plant mixtures as well as examine the effect of HRWR admixture dosage on volumetric changes with respect to shrinkage

The goal of this research was to increase our understanding of the role that HRWRs, particularly polycarboxylate-based HRWRs, have on the micro-cracking in precast concrete. A key aspect of this project was to determine the suitability of ASTM C494, Standard Specification for Chemical Admixtures for Concrete, to be used as a tool to screen mixtures containing HRWRs in order to determine the micro-cracking susceptibility of the mixture.

1.1 Background and Scope

From the second that water is introduced to concrete, the mixture undergoes volumetric changes that will continue to develop over the concrete’s lifetime. In the very initial stages of the

concrete the volume change is mainly attributed to autogenous and thermal changes. Delayed shrinkage of the concrete is induced by the concrete's exposure to the environment, through drying shrinkage and to a lesser extent, carbonation shrinkage.

The rising concern is that these volumetric changes are occurring far beyond the fresh and fluid state of the mixture and are causing tensile stresses to develop in the concrete much later into the final set state of the mixture. Unfortunately, predicting and modeling the cracking phenomenon in considering all of the concrete system's mechanical properties, creep, size and restraint conditions has yet to be fully understood. In addition, the present knowledge on free deformation effects have yet to be fully understood, as mixture designs and admixtures are continually changing to meet the growing needs of the precast industry.

Since the 1970s, the development of high-performance concrete (HPC) has been a focal point of the concrete industry, allowing designers and contractors to enter an entirely new regime of structural performance. The increasing high cement content mixture designs in conjunction with low w/cm (0.28 to 0.33) and high range water reducing admixtures made high early strength and long-term durability attainable. Precast production plants continue to develop increasing higher early strengths permitting a shorter timeline for form stripping and strand release. Concerns for material based onset concrete deterioration was originally thought to have been subsided due to the highly stringent guidelines placed on mixture designs such as with approved aggregate suppliers that have been documented in the Concrete Related Source Quality Catalog (TxDOT 2016).

Despite meeting TxDOT's qualification standards for the prevention of concrete deterioration or cracking related issues, the micro-cracking problem persisted at precast plants in Texas. A brief investigation proved that the cracks were not causing any volumetric expansion, and therefore could not be ASR or DEF related. Despite the amount of effort that was put into improving the HPC mixture designs, the drastically decreasing w/cm content and implementation of new portland cements (PC) and high range water reducers has proven to be the ultimate pitfall as it drastically increased the concrete's susceptibility to early age cracking. The micro-cracking issue is still prevalent in the most up to date HPC mixtures. Concrete cast at precast plants less than a year ago shows the develop the micro-cracking all along the concrete's exposed surfaces.

Results have confirmed that the typical 0.28 to 0.33 w/cm ratio ranges implemented at precast plants paired with the need to increase the use of high range water reducers has had a direct influence the high early age shrinkage of concrete. The investigation led by the The Texas Department of Transportation (TxDOT) in conjunction with work performed by The Construction Materials Research Group (CMRG) at the University of Texas at Austin has guided research to target the superplasticizers and specifically the polycarboxylate admixtures as the subject of focus for eliminating the cracking issue. In this project we examine the performance of actual precast plant mixtures as well as examine the effect of superplasticizer admixture dosage on volumetric changes with respect to shrinkage. The work program was performed in two phases:

- Phase 1 consisted of casting concrete and paste mixtures and testing them against current testing protocol for qualifying admixtures.
- Phase 2 consisted of implementing a series of additional tests with the hopes of better quantifying an admixture's potential for provoking shrinkage cracking.

1.2 Report Content and Organization

The study composed in this report has sought out to quantify the precast field observations along with the observed cracking seen at both UT and TxDOT concrete exposure sites in order to distinguish the potential shrinkage causing mechanisms. The research outlined in the following sections has been performed in order to better guide a build of a testing matrix that is capable of testing high range water reducing admixtures and discerning if they are appropriate for future field use according to their shrinkage effects.

This report has been segmented into seven unique chapters. Chapter 2 consists of Task 1, which focused upon gathering information about (1) the use and qualification of polycarboxylates in precast elements, especially precast girders, and (2) cracking observed in precast girders. Chapter 3 describes the materials that were used throughout this project. Chapter 3 outlines the selections based on Task 2, which focused on the selection of materials and mixture proportions that will be used for ASTM C494 testing and other tests related to the project, and assess key physical, chemical, and mineralogical properties of the constituent materials. Materials were selected based upon their past and continued use at two major pre-cast plants in Texas.

Chapter 4 outlines Tasks 3-4, which involved testing procedures performed in the laboratory to identify and single out the driving proponent of the cracking phenomenon with respect to the different admixture dosages and actual precast plant mixture designs. The work performed made use of the existing protocol for testing admixtures qualification, ASTM C494, in concrete mixtures through drying shrinkage, compression, time of set, and water content measurements.

Chapter 5 describes the testing program and equipment employed for testing pastes and concrete mixtures through an amended testing procedure series that quantifies a mixture's shrinkage and cracking response. Paste testing included autogenous shrinkage through volumetric, linear and visual inspection, and concrete testing included restrained autogenous shrinkage testing.

Chapter 6 presents the research related to field exposure specimens including precast plant visits, exposure site visits, large cast exposure blocks and carbonation front ingress for long term monitoring. Mixtures were either cast in the lab conditions or in the field and selected to mimic actual precast mixtures as well as mixtures with varying admixture dosages to identify superplasticizer's potential cracking effect in the field. Similar mixtures were also selected and monitored at the TxDOT exposure site and a visual examination and scale of cracking deterioration was developed.

Chapter 7 summarizes key findings and makes recommendations.

Chapter 2. Information Survey Review and a Summary of Forensic Investigations in the Field

2.1 Summary of Previous Project Investigations

Since the 1990s, TxDOT has been working intensely to create a prescriptive based means of preventing ASR and DEF in concrete structures. Since the early 2000s, TxDOT, along with research based out of the University of Texas at Austin helped to develop a matrix to identify aggregates prone to ASR as well as setup a system for mitigating ASR in concrete. Yet even after the introduction of the ASR mitigation techniques, a map cracking pattern type of distress still developed on several girders in TxDOT's producer pre-cast plant yards.

The cracking was originally discovered by TxDOT's quality control department that had been directed to monitor pouring and handling of precast girders at a New Braunfels plant. It was noticed that several girders that were left in the "bone yard" waiting to be put into service had developed significant map cracking on the surface on both the flange and web sections of the girders. Figure 2-1 from a precast plant in Waco shows a severe case of this micro-cracking.



Figure 2-1: Micro-cracking focused on the top flange of a rejected precast girder

The girders were subsequently rejected and a funded investigation was setup by the Federal Highway Administration (FHWA) ASR Development and Deployment Program. This investigation was led by Dr. Kevin Folliard with the University of Texas at Austin, Dr. Michael D.A Thomas with the University of New Brunswick, and Dr. Benoit Fournier with Laval University in order to determine the root cause behind the observed cracking. The original 4 that led to this study were composed of straight cement mixtures ranging from 0.33 to 0.35 w/cm apart from one that contained 20% replacement of the cement with Class F fly ash. While the cracking pattern seemed indicative of ASR, ASR lab analysis paired with field exposure blocks and petrographic analysis of cores pulled from several girders suggested that the observed cracking was not the result of ASR. Recently, replicate exposure blocks were cast at UT using concrete mixtures ranging from 0.28 to 0.42 w/cm through graduate researcher Nicolas Tiburzi's work outlined in his master's report, "Evaluation of volume changes and cracking potential of low water-to-cementitious material ratio concrete mixtures" (Tiburzi 2015).

Recently more rejected girders for other TxDOT projects have emerged in various precast plants across Texas. Although the testing ruled out ASR as the deleterious mechanism, the same distinct micro-cracking developed on the ASR exposure blocks as pictured in Figure 2-2 and Figure 2-3 were seen on the girders.

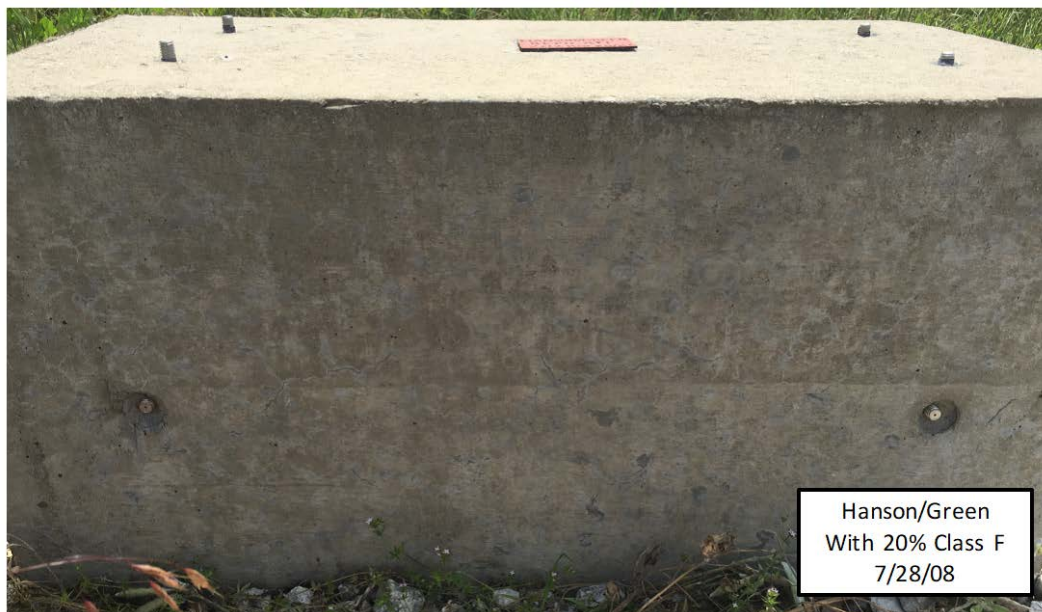


Figure 2-2: Precast plant exposure block replicate cast according to ASTM C1293 0.42 w/cm and 20% Class F fly ash



Figure 2-3: Precast plant straight cement exposure block replicate cast according to ASTM C1293 0.45 w/cm

2.2 Literature Survey Review Results

A thorough review of the Transportation Research Database, ACI journals, and Cement and Concrete Research journals was conducted looking for similar cracking in precast concrete made using polycarboxylate high range water reducing admixtures that was not due to ASR. No similar micro-cracking was found. A recent paper by Aïcha F. Ghezal, Ph.D. and Gabriel J. Assaf demonstrates that naphthalene-based super plasticizers in SCC concrete mixtures result in higher creep and drying shrinkage than the same mixtures made with the same dosage of polycarboxylate-based admixtures (Ghezal et al.).

2.3 Forensic Investigations

The objective of the in-service visits was to perform a detailed site evaluation and forensic investigation. Both sites were located in the northern and eastern portion of the state as shown in Figure 2-4. While the mixture designs are currently unknown, the concretes were cast at a similar age (precast labels state 2005 at the Dallas site and 2007 at the Texarkana site). The trips were performed in coordination with TxDOT Project 0-6922, which will continue to monitor the growth of cracks in future years.

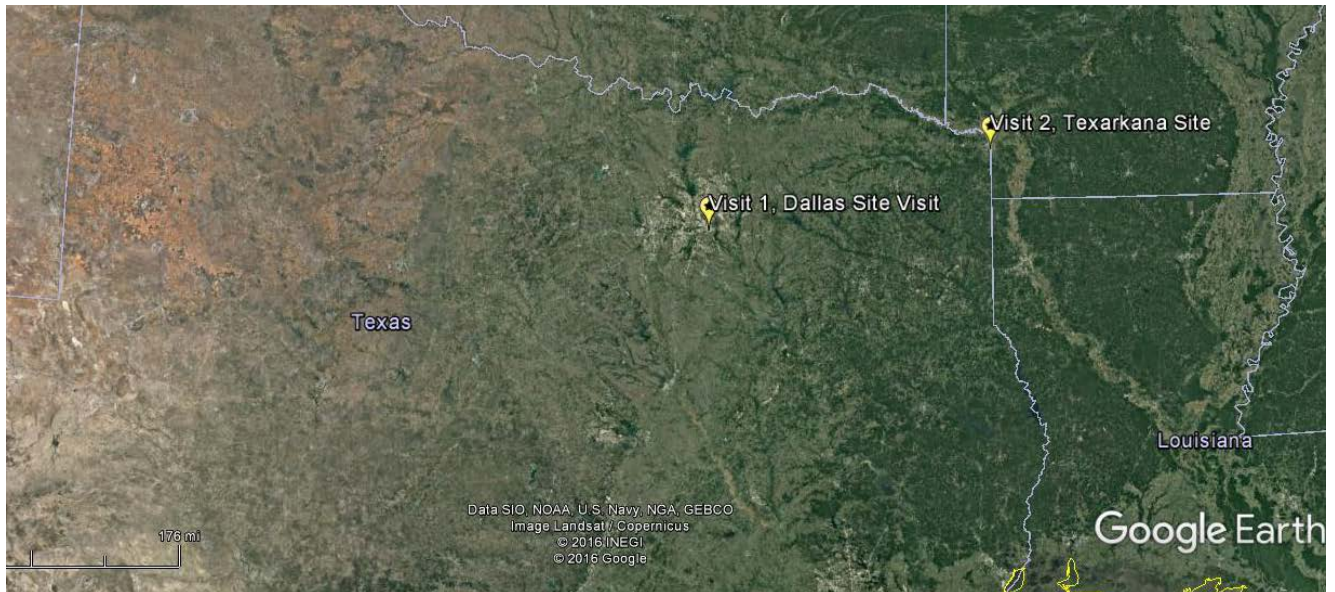


Figure 2-4: Overall map of locations

2.3.1 Methodology

Besides photo and visual surveys of the two bridges, quantitative crack mapping and internal relative humidity measurements were performed as described in the sections below.

2.3.2 Crack Mapping

The 8”x8” measurement squares were placed at areas of interest (where accessible areas of cracking were observed and near necessary relative humidity probe measurements). An optical microscope was used to examine the 8” perimeter length of each side of the square. The number of cracks, length of cracks, and crack widths were recorded. The final value recorded is the average crack width/the length of the square examined. The data was gathered in coordination with TxDOT Project 0-6922, which will continue monitoring these crack maps in future years. Figure 2-5 shows the crack mapping being conducted.



Figure 2-5: Savitha Srinivasan (graduate student working on associated TxDOT project 0-6922) recording crack widths and lengths at the Dallas site visit

2.3.2.1 Internal Relative Humidity Measurement

The Vaisala SHM40 structural humidity kit (Figure 2-6) was used to measure the relative humidity at 1", 2", and 3" depths into a girder to determine if a distinct drying gradient could be a driving mechanism of the cracking. The accuracy of the SHM40 relative humidity measurements and temperature measurements is $\pm 1.5\%$ and $\pm 0.2\text{ }^{\circ}\text{C}$, respectively. The stress created by a drying gradient is directly proportional to the internal relative humidity measured and areas of cracking due to drying shrinkage are generally found where the drying shrinkage stress differentials are greatest (Grasley et al.). For this purpose, the measurements were taken at two adjacent girders, one that had cracked and one that had not or did not seem to be cracked. The holes were drilled at approximately 3" apart and near a corresponding crack map. The holes were drilled and then cleaned of dust using compressed air. All equipment used is shown in Figure 2-6 to take the relative humidity measurement. The exterior of a plastic tube was coated in epoxy and inserted into the hole. A rubber plug was inserted into the top of the plastic tube to keep the system sealed. After a period of at least 24 hours, the relative humidity probe was inserted, left to equalize for 30 minutes, and then relative humidity and temperature measurements were recorded. Finally, the exposed portion of the plastic tube was removed using a razor blade and the holes were sealed using a cementitious grout (Figure 2-7).



Figure 2-6: SHM40 Vaisala kit with plastic tubes, rubber plugs, and humidity sensor.
The orange caps are for visibility and water protection.



Figure 2-7: Holes sealed with cementitious grout

2.3.3 Results

2.3.3.1 Visit 1: Dallas

Location: Hampton/Inwood at Trinity River (Figure 2-8)

Bridge width: 16 girders

Date Visited: 11/19-11/20/2016

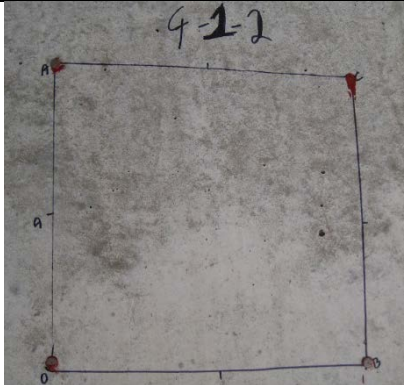
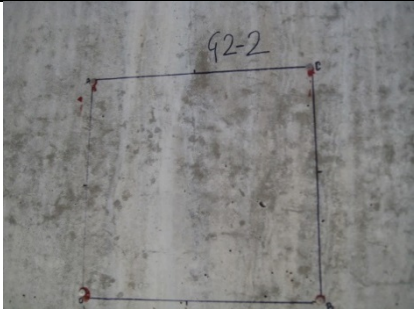


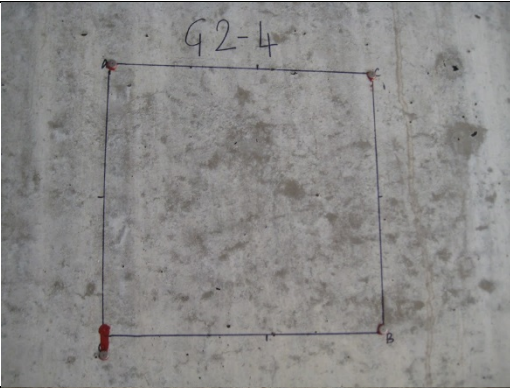

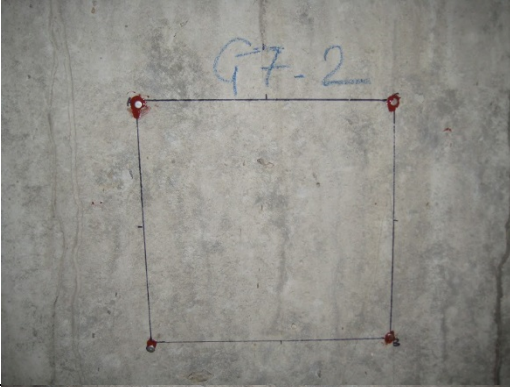
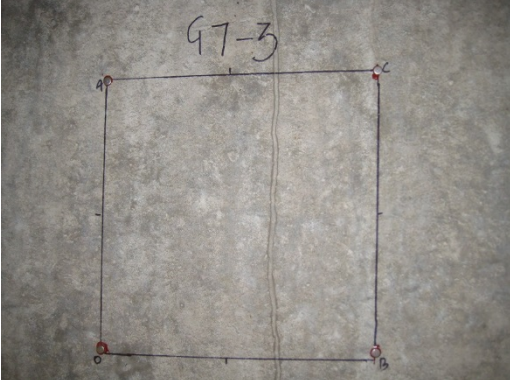
Figure 2-8: Overall view of bridge looking east; (exterior girder in this picture is labelled as G1)

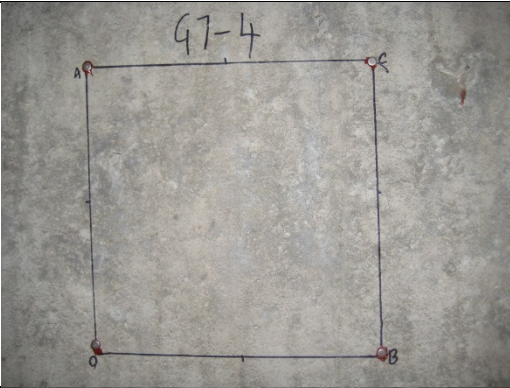
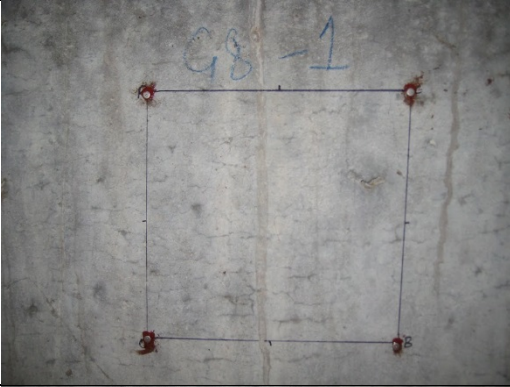
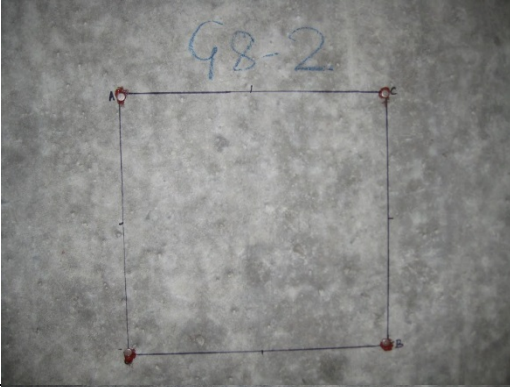

Crack ratings were conducted on the exterior girder shown in Figure 2-8 (labelled as G1) as well as the adjacent girders going into the page (labelled G2, G3, etc.). At least one crack grid, but sometimes as many as three were placed on a girder and the second number denotes which side of the girder the crack grid was on, where odd numbers correspond to the girder surface located closest to the initial exterior of the G1 girder and even numbers correspond to the interior surface. The number of even and odd numbers denotes how many crack grids were applied to that surface. Thus G2-1 and G2-3 represents crack grids that are located on the second girder and that both grids are located on the side of second girder that is closest to the exterior face of the G1 girder (i.e., the exterior face of the second girder). Since there are two odd numbers this means that more than one crack map was made on that side of the girder (in this case two crack grids). At

least one photo was taken on each girder, however not all crack grids were photographed. Based upon visual and photographic inspection, the cracking severity varied from girder to girder and along the length and depth of the girder. Girders 1, 2, 7, and 9 appeared to have lower levels of cracking than other girders. This is shown quantitatively in Table 2-1, where Girder 8 has the greatest average cracking index and crack width in G8-3. This assessment matched with the previous inspection results by a TxDOT team.

Table 2-1: Crack mapping data recorded in Dallas

Section	Average Crack Width (in)	Average Cracking Index (in/yd)	Picture
G1-1	0.000635	0.014453	
G1-2	0.000359	0.005469	
G2-1	0.000414	0.053789	
G2-2	0.00025	0.054688	
G2-3	0.000465	0.030859	

Section	Average Crack Width (in.)	Average Cracking Index (in/yd)	Picture
G2-4	0.000446	0.016797	
G7-1	0.000188	0.003906	
G7-2	0.000146	0.004297	
G7-3	0.000188	0.001172	

Section	Average Crack Width (in.)	Average Cracking Index (in/yd)	Picture
G7-4	0.000388	0.004297	
G8-1	0.000485	0.120703	
G8-2	0.000188	0.007422	
G8-3	0.000722	0.110547	

Section	Average Crack Width (in.)	Average Cracking Index (in/yd)	Picture
G8-4	0.000407	0.012238	

Relative humidity measurements were conducted with humidity probes (see Figures 2-9 through 2-12). The relative humidity results and corresponding girder section crack ratings from the Dallas site are shown in Table 2-2.



Figure 2-9: Overall photo of G7 with corresponding humidity measurement probes and crack map G7-2

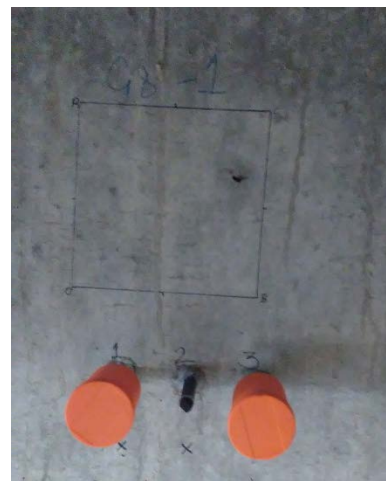


Figure 2-10: Overall photo of G8, an adjacent cracked girder, with corresponding humidity measurement probes and crack map G8-1

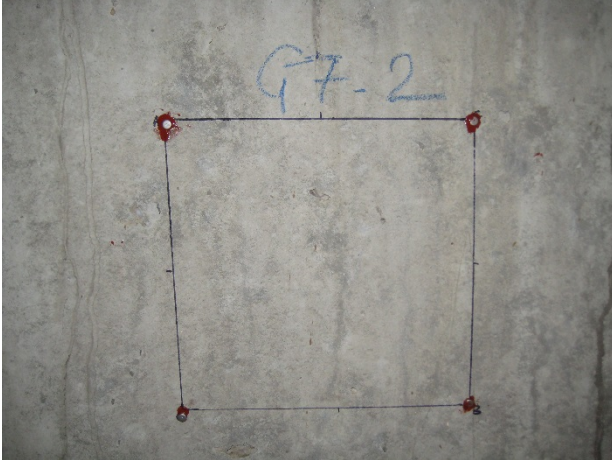


Figure 2-11: Close-up photo of G7-2 corresponding sealed humidity probe drilled holes, showing minimal cracking

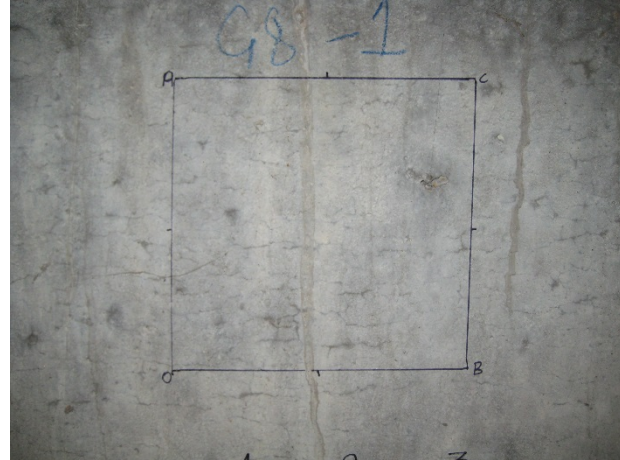


Figure 2-12: Close-up photo of G8-1 corresponding internal relative humidity probes, showing typical micro-cracking distress

Table 2-2: Relative humidity results

	Girder G7-2 (Visibly Uncracked by Naked Eye)	Girder G8-1 (Visibly Cracked by Naked Eye)
Crack Rating (avg. cracking width/length reviewed)	0.004297 in./yd.	0.033203125 in./yd.
1" Relative Humidity	67.3%, 21.6°C	65.9%, 23.1°C
2" Relative Humidity	72.2%, 21.4°C	73.9%, 22.2°C
3" Relative Humidity	76.0%, 21.0°C	75.5%, 22.0°C

2.3.3.2 Visit 2: *Texarkana*

Location: IH-30 WB Ramp to US-59 SB (Figure 2-13)

Bridge width: 11 girders

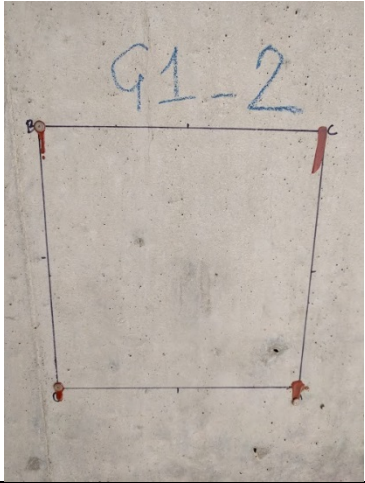
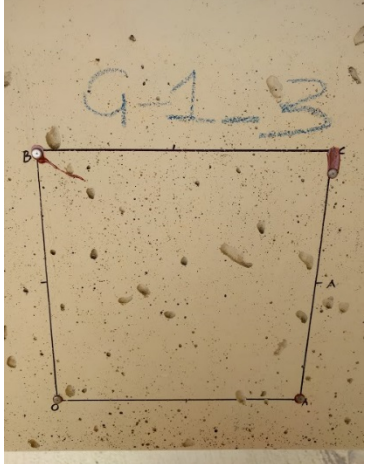
Date Visited: 12/7-12/8/2016


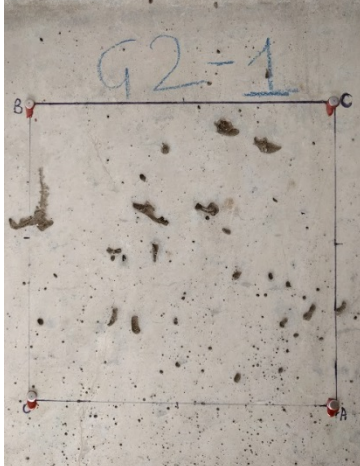
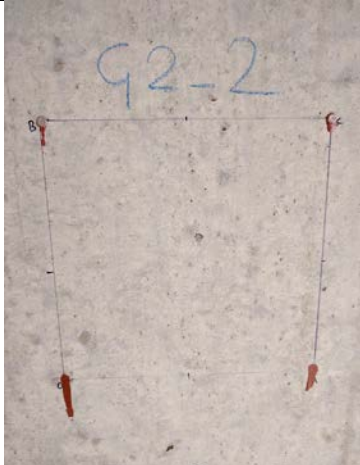


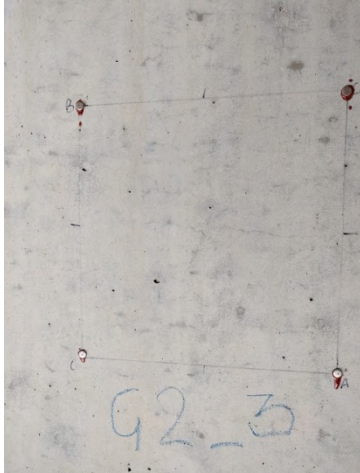
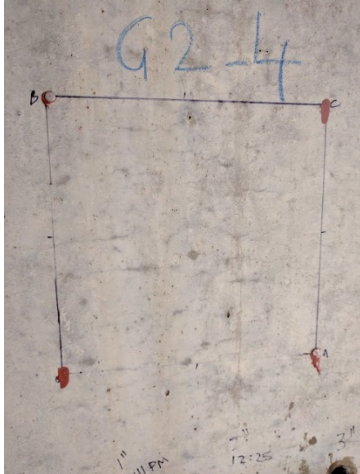
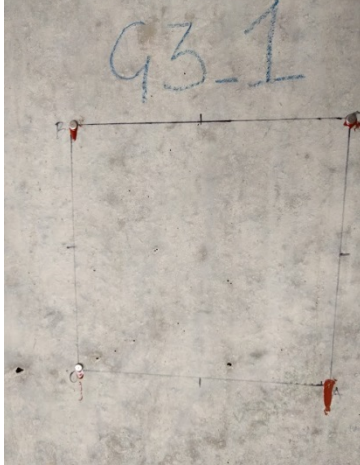
Figure 2-13: Overall view of site facing north (visible exterior girder is referred to as G1)

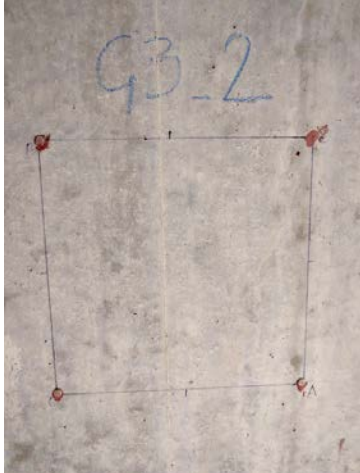
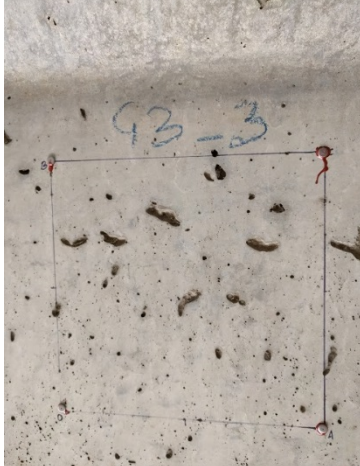
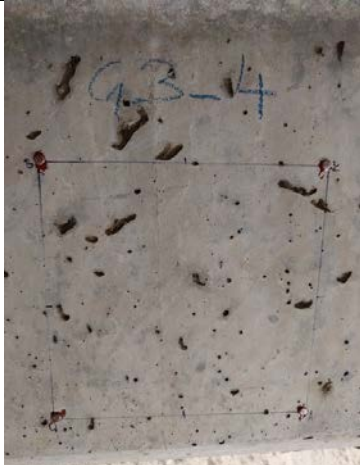
The crack mapping data for the Texarkana bridge is summarized in Table 2-3. Similar to before, G1 represents the exterior girder and measurements were conducted on girders going into the page.

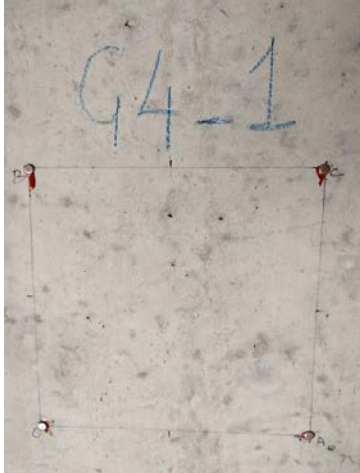
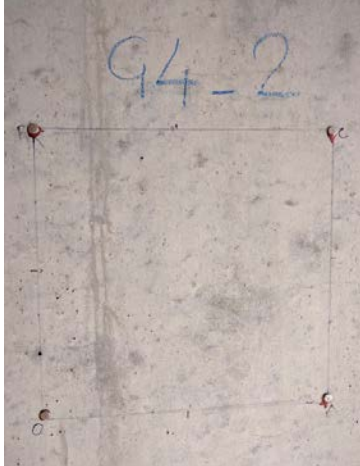
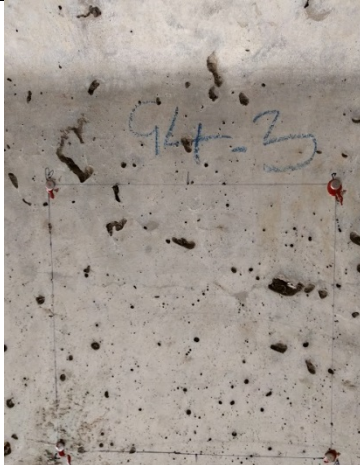
Table 2-3: Crack mapping data

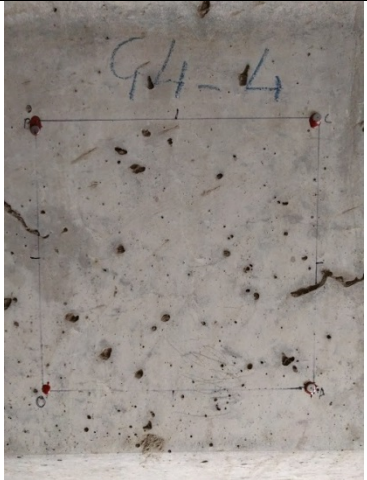
Section	Average Crack width (in.)	Average Cracking Index (in/yd)	Picture
G1-2	0	0	 <p>A photograph of a concrete surface with a square mapping grid drawn in blue ink. The vertices of the square are marked with red pushpins. The label 'G1-2' is handwritten in blue ink at the top of the grid.</p>
G1-3	0	0.003125	 <p>A photograph of a concrete surface with a square mapping grid drawn in blue ink. The vertices are marked with red pushpins. A crack is visible on the right side of the grid, labeled 'A'. The label 'G1-3' is handwritten in blue ink at the top of the grid.</p>

Section	Average Crack width (in.)	Average Cracking Index (in/yd)	Picture
1-4	4.69E-05	0.008789	
G2-1	0.000565	0.030078	
G2-2	0.000479	0.025781	

Section	Average Crack width (in.)	Average Cracking Index (in/yd)	Picture
G2-3	0.000313	0.032031	
G2-4	0.000188	0.033203	
G3-1	0	0.003516	

Section	Average Crack width (in.)	Average Cracking Index (in/yd)	Picture
G3-2	0.000167	0.001563	
G3-3	0.000156	0.022656	
G3-4	0.000175	0.021484	

Section	Average Crack width (in.)	Average Cracking Index (in/yd)	Picture
G4-1	0.000804	0.005859	 <p>A photograph showing a concrete surface with a grid of four red pins. The handwritten label 'G4-1' is visible at the top of the grid. The surface appears relatively smooth with some minor discoloration.</p>
G4-2	0.000504	0.030469	 <p>A photograph showing a concrete surface with a grid of four red pins. The handwritten label 'G4-2' is visible at the top of the grid. The surface shows some vertical streaking and minor discoloration.</p>
G4-3	0.000297	0.014844	 <p>A photograph showing a concrete surface with a grid of four red pins. The handwritten label 'G4-3' is visible at the top of the grid. The surface is heavily stained with dark spots and appears more textured than the other two sections.</p>

Section	Average Crack width (in.)	Average Cracking Index (in/yd)	Picture
G4-4	0.000503	0.027344	

Relative humidity measurements were conducted with humidity probes (see Figures 2-14 through 2-17). The relative humidity results and corresponding girder section crack ratings from the Dallas site are shown in Table 2-4.



Figure 2-14: Overall photo of G1, an exterior uncracked girder, with corresponding humidity measurement probes and crack map G1-2

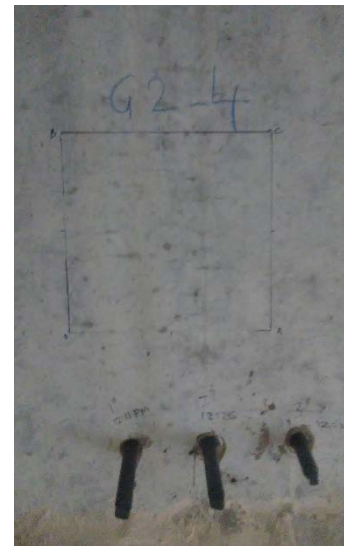


Figure 2-15: Overall photo of G2, a cracked girder, with corresponding humidity measurement probes and crack map G2-4

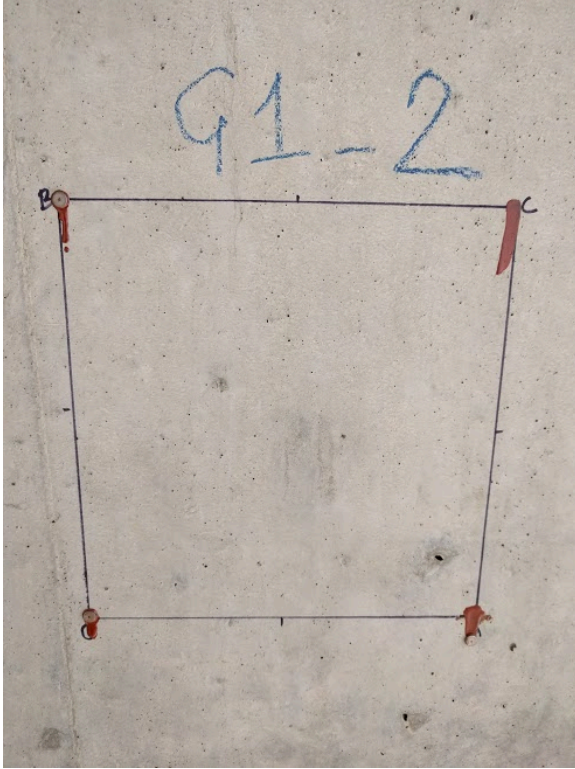


Figure 2-16: Close-up photo of G1-2 crack map, showing no cracks

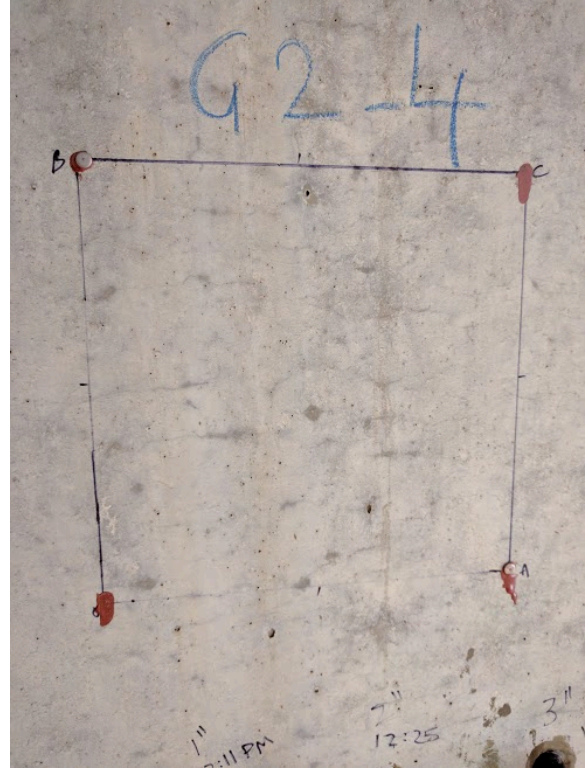


Figure 2-17: Close-up photo of G2-4 crack map, showing typical micro-cracking distress

Table 2-4: Relative humidity probe measurements

	Girder G1-2 (Visibly Uncracked by Naked Eye)	Girder G2-4 (Visibly Cracked by Naked Eye)
Crack Rating (in./yd.)	0 in./yard	0.033203125 in./yard
1" Relative Humidity, Temperature	73%, 8.9°C	70.6%, 9.1°C
2" Relative Humidity, Temperature	77%, 9.1°C	78.4%, 9.2°C
3" Relative Humidity, Temperature	83.9%, 9.3°C	79.1%, 9.3°C

2.3.4 Review of Relative Humidity Results

Figure 2-18 shows the variation of internal relative humidity from both sites. The median annual ambient relative humidity for both sites is recorded at 0". The plot shows a more distinct variation in the drying gradient for the cracked girder. As stress from drying shrinkage and internal relative humidity are directly related, this shows that there is a greater stress variation in the cracked girder. However, the cracks are likely limited to the surface and the gradient from 0" to 1" is higher for both of the uncracked girders. Our equipment could only measure internal relative humidity at depths of 1" and greater. A previous study of micro-cracking using nuclear magnetic resonance found the moisture gradient driving drying shrinkage-based micro-cracking extended to a maximum depth of 0.6" in the studied cement-based material (Bisschop).

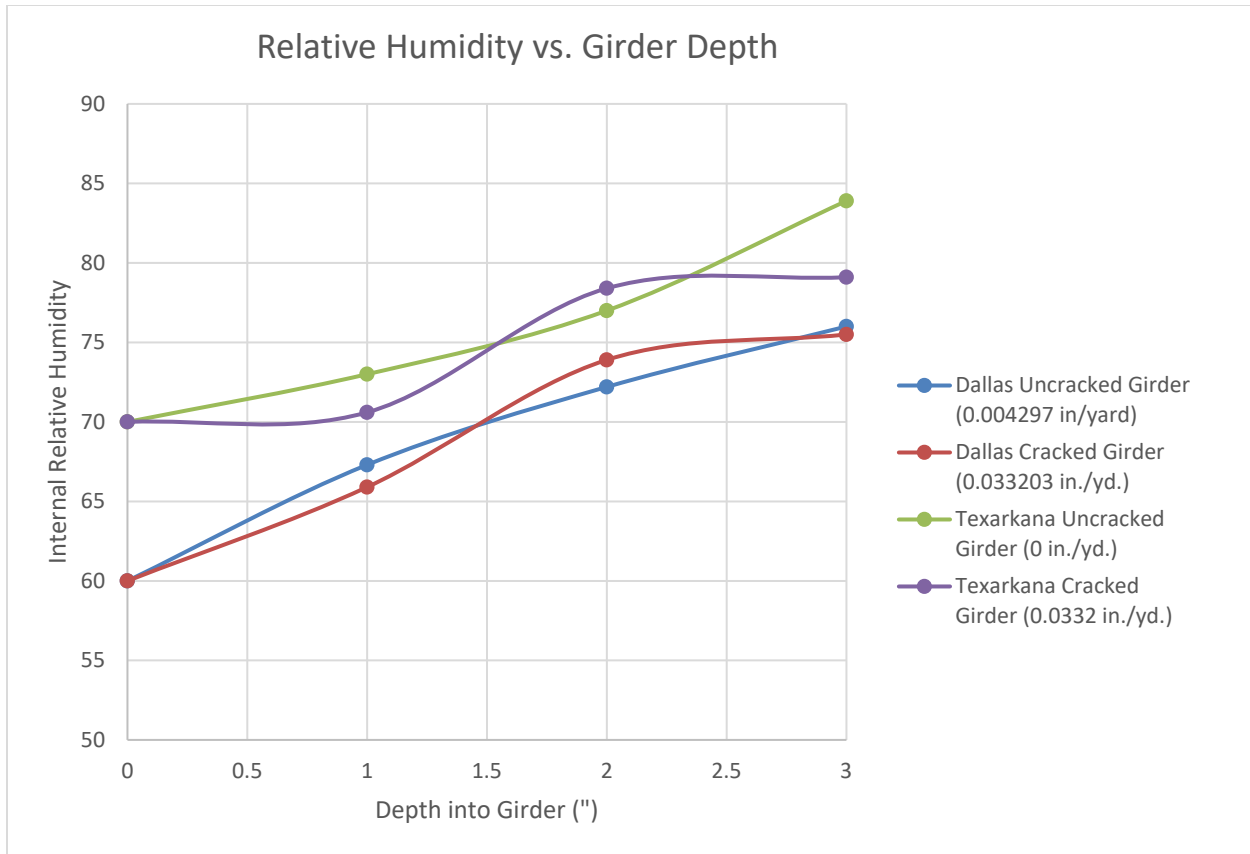


Figure 2-18: Plot of the four relative humidity gradients investigated.
The relative humidity at 0" was specified as the median annual relative humidity for both locations.

2.3.5 Qualitative Information from Surveys at Both Sites

The review of both sites revealed that there is no directional pattern (e.g., more cracking on northern/eastern girders) in the cracking or consistency along the length of the girder. One similarity between both sites is that the girders had white powder on them (see Figure 2-19). Future monitoring by TXDOT project 0-6922 will monitor the growth of these cracks. Another is that multiple surface defects (e.g., bug holes or pop outs) exposing aggregates were found at both sites along cracked girders (see Figures 2-20 through 2-22).



Figure 2-19: White powder on girders.

This powder was present on fingers after rubbing them on girders at both sites and has been viewed at exposure blocks at lab.

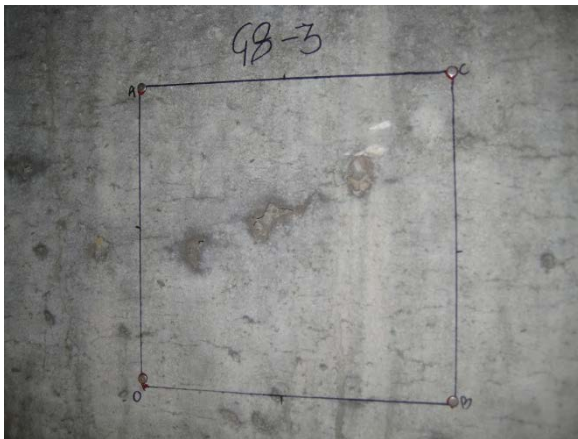


Figure 2-20: Surface defects on cracked girder at Dallas site (1)



Surface defect

Figure 2-21: Surface defects on cracked girder at Dallas site (2)



Figure 2-22: Similar surface defects observed in cracked flange at Texarkana

2.4 Key Findings and Conclusions

2.4.1 Information Survey Review Results

- A recent study shows that naphthalene HRWRs induce more long-term creep and drying shrinkage than polycarboxylate HRWR's (G. Assaf et al.).
- Jan Bisschop's work (2012) with nuclear magnetic resonance showed a correlation between high moisture gradient or relative humidity gradient and propensity of cracking.
- Crack patterns seen on girders seems consistent with crazing types of cracks.

2.4.2 Forensic Investigation Results

- Girders were evaluated for crack ratings and relative humidity at a site in Texarkana and Dallas. The results indicate a trend between higher variation in relative humidity up to 2" of depth and higher crack rating.

Chapter 3. Materials and Mixture Proportions

3.1 Introduction

This chapter outlines the materials utilized to evaluate the micro-cracking issue throughout this project. Appendix I includes information about the source of the materials.

3.2 Portland Cements

Two Type III portland cements (coined “PC-III-A” and “PC-III-B”) and one Type I/II portland cement (coined “PC-I-A”) in accordance with ASTM C150 were used for this project (2015). The bulk of the study made use of Type III cements due to its common if not exclusive use in precast plants across the state of Texas. The Type III cements were taken from two different commercially used Texas cement plants. Table 3-1 provides the oxide analysis obtained for the different cement sources and types as per determined by TxDOT’s cement laboratory.

Table 3-1: Oxide analysis for different cement sources and types

Cement	SiO ₂	Al ₂ O ₃	Fe ₂ O ₃	CaO	MgO	SO ₃	Na ₂ O	K ₂ O
	mass %	mass %	mass %	mass %	mass %	mass %	mass %	mass %
PC-III-A	19.8	4.3	3.1	64.2	0.6	4.1	0.1	0.7
PC-III-B	19.8	5.1	1.9	63.5	1.1	5	0.1	0.6
PC-I-A	18.6	5.4	2.6	64.9	1.1	3.3	0.1	1

3.3 Fly Ash

One Class F fly ash in accordance with ASTM C618 was used for this project (2015). The fly ash was taken from a local Texas source. Table 3-2 provides the chemical composition analysis as per determined by TxDOT for the fly as used.

Table 3-2: Oxide analysis for Class F fly ash

Fly Ash	SiO ₂	Al ₂ O ₃	Fe ₂ O ₃	CaO	MgO	SO ₃	Na ₂ O	K ₂ O
	mass %	mass %	mass %	mass %	mass %	mass %	mass %	mass %
Class F	52.07	23.07	3.95	11.65	2.06	0.48	0.403	0.74

3.4 Aggregates

3.4.1 Coarse Aggregate

Three different coarse aggregate sources were used for this project. All sources were composed of siliceous river gravel and/or limestone and were graded according to ASTM C33

grading size 57 (2016). Table 3-3 shows the specific gravity and absorption capacity of the coarse aggregates.

Table 3-3: Physical properties of the coarse aggregates

Coarse Aggregate	Mineralogy Type	Specific Gravity	Absorption Capacity (%)
CA-R	Siliceous	2.54	1.31
CA-L	Limestone	2.47	3.25
CA-RII	Siliceous	2.26	1.52

3.4.2 Fine Aggregate

Three different fine aggregates sources were used for this project. The majority of the mixture designs were composed of siliceous river gravel (FA-R). Several mixtures were composed of a limestone source (FA-RII), and a light weight fine aggregate (FA-LW). Table 3-4 shows the specific gravity and absorption capacity of the fine aggregates.

Table 3-4: Physical properties of the fine aggregates

Fine Aggregate	Mineralogy Type	Specific Gravity	Absorption Capacity (%)
FA-R	Siliceous	2.47	1.14
FA-RII	Siliceous	2.57	1.96
FA-LW	Manufactured	1.86	22.50

3.5 Chemical Admixtures

Since the focus of this study was to identify the potential harmful effects of the use of high range water reducing admixtures (HRWRA) on HPC at precast plants, only the most current and future proposed HRWRAs used in TxDOT precast concrete applications were utilized. Exclusively polycarboxylate-based high range water reducers (HR-P1, HR-P2, HR-P3, HR-P4, and HR-P5) along with stabilizing agents or viscosity modifying admixtures (VMA) (NR-1, NR-2) were selected for use from two chief distributors used at the precast plants in Texas. Table 3-5 contains details about the recommended dosages and specific gravity of the chemical admixtures used in this work.

Table 3-5: Classification of admixtures used throughout this study

Admixture Name	C-Polymer Type	ASTM C494 Classification	Specific gravity
HR-P1	Polycarboxylate	F	1.1
HR-P2	Polycarboxylate	F	1.1
HR-P3	Polycarboxylate	F	1.1
HR-P4	Polycarboxylate	F	1.1
HR-P5	Polycarboxylate	F	1.1
NR-1	Normal Range Water Reducer and Retarder	B & D	1.2
NR-2	Normal Range Water Reducer and Retarder	B & D	1.2
VMA-1	Viscosity Modifier	S	1.1

Chapter 4. Laboratory Testing: Evaluation of Suitability of ASTM C494 Procedures for Precast Concrete Mixtures

4.1 Introduction

In this chapter our goal was to test the following hypothesis: that if ASTM C494, Standard Specification for Admixtures in Concrete, performance requirements are valid for predicting the micro-crack development observed in precast girders, then mixtures that have observed cracking (herein called “poor performance mixtures”) in the field should also fail in ASTM C494 testing (2010). Thus, in the event that the poor performance mixtures pass all or some of the tests outlined in ASTM C494, then the standard is considered inadequate or not fully adequate. Figure 4-1 provides a graphical representation of the devised ASTM C494 qualification process.

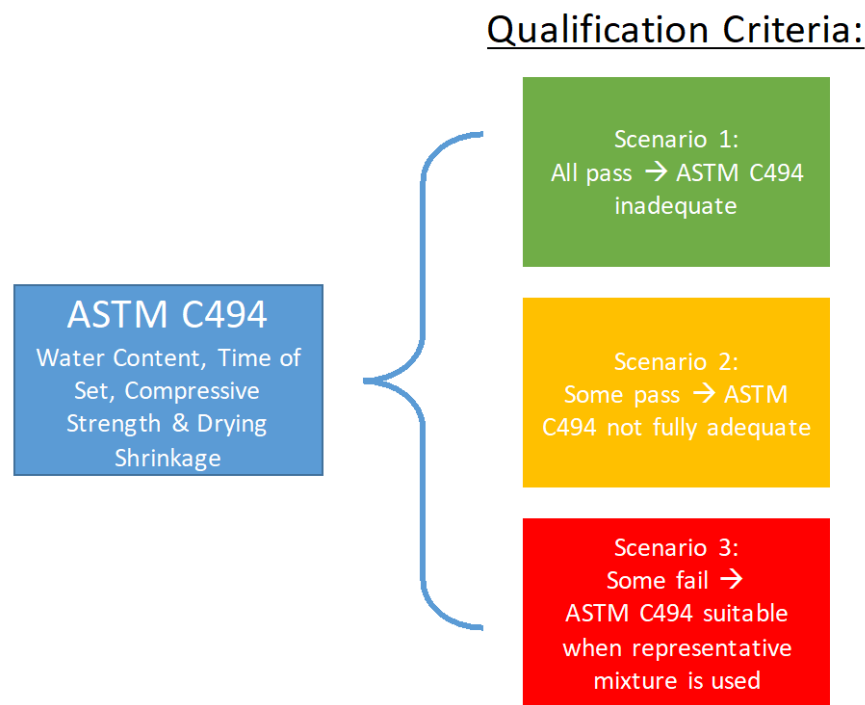


Figure 4-1: Testing performed and qualification criteria used to evaluate the relevancy of ASTM C494 to predict the latent cracking observed in the precast concrete barriers

ASTM C494 was initially carried out through the “specific approach” and the goal was to use the the results from the ASTM C 494 tests (water content, ASTM C403 time of set, ASTM C39 compressive strength, and ASTM C157 free shrinkage, ASTM C78 flexural strength, and ASTM C666 freeze-thaw testing) to quantify a mixture design’s cracking potential. In this project, the flexural strength and freeze-thaw testing were omitted since both TxDOT and the research team at University of Texas at Austin was in agreement that testing concrete in flexural and freeze thaw for HPC would not aid the investigation efforts. Additional mixtures were carried out via the “non-specific approach,” as specified in ASTM C494, which suggests specific changes in mixture proportions based on specific mixture property alterations. Figure 4-2 outlines the tests employed as a part of the ASTM C494 testing, the passing limits and their respective chapter locations.

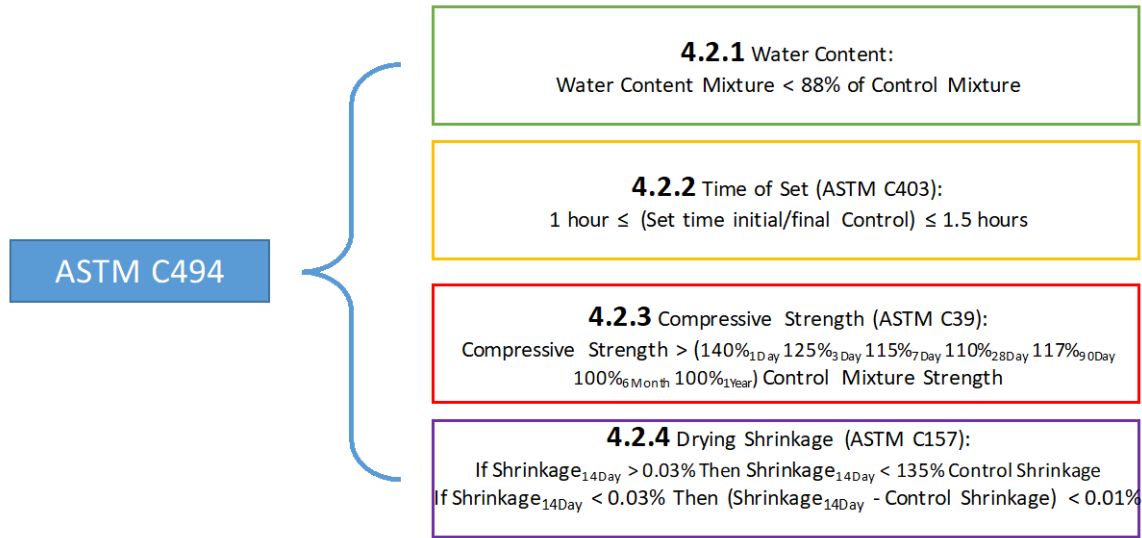


Figure 4-2: Tests performed for ASTM C494 and their respective limits and chapters

4.2 Overview of ASTM C494 and Testing Matrix

Each of the sections within this chapter will begin by outlining the particular laboratory testing procedure and its potential relevance with ASTM C494. All concrete mixtures for ASTM C494 testing were mixed in a rotary drum mixer in accordance with ASTM C192 mixing procedure. For assurance of quality control, each mixture was tested for air content and unit weight (ASTM C231, Standard test method for air content of freshly mixed concrete by the pressure method) and slump test (ASTM C143, standard test method for slump of hydraulic-cement concrete) (2014) (2015). In the event that the standard deviation of air content (%) or slump (in.) deviated from the goal set by precast plants or prescribed in our matrix the was repeated. Details about the material properties and characteristics of the cement, aggregates and chemical admixtures used in these concrete mixtures were detailed in Chapter 3. Unless otherwise stated, the primary aggregates used throughout this study were CA-R and FA-R.

Initially, three mixtures that failed in the field in terms of micro-cracking (herein called “bad” performers) and two mixtures that have no observed cracking, herein called “good” performers, were cast and subjected to the testing prescribed by ASTM C494. Table 4-1 outlines the five mixtures selected for testing. As shown in the key included in Table 4-1, there were three “bad” and two “good” performance mixtures.

Table 4-1: Initial testing matrix for ASTM C494: three “bad performers” (yellow) and two “good performers” (blue)

w/cm	Cement Type	Cement Content (lb/yd ³)	SCM Content (lb/yd ³)	Admixtures			
				Type	(floz/100 lb cement)	Type	(floz/ 100 lb cement)
0.26		705	175		6.5		1.5
0.28		705	175		12		3
0.31	PC-III-A	663	271	HR-P1	5.5	NR-1	2.5
0.31		640	213		6		2
0.33		658	0		6.5		3

KEY:		-"Bad" Performer
		-"Good" Performer

The “bad” (highlighted in yellow in Table 4-1) and “good” (highlighted in blue in Table 4-1) nomenclature was used throughout this chapter as a means of illuminating the original testing series used for evaluating the effectiveness of ASTM C494 testing through the specific approach. An additional matrix of 22 mixtures were cast, which focused on determining the sensitivity of ASTM C494 testing limits for “tests not for a specific approach.” The testing “not for a specific approach” implemented variations in mixture proportioning, specifically mixture proportions related to precast mixtures commonly used in Texas. The study compared mixtures through the evaluation with variations in HRWR dosage and type, cement content and source, water to binder ratio and fly ash content as a means of using ASTM C494 in discerning differences in future micro-cracking potential. Thus 14 “comparison” mixtures were also evaluated in addition to good and bad performers mixtures (See Table 4-3). The data from these mixes were investigated to understand the effect of mixture proportioning on time of set, compressive strength, and free shrinkage.

However, because a true control mixture in reference to a mixture design requiring the usage of HRWR is not possible, four pseudo-control mixtures were created by imposing either increasing the water content (as in the CWB control), adding a small dosage of HRWR (as in the CSP-1 and CSP-2 controls), or replacement of fine aggregate with lightweight aggregate (as in the CLWA control). The CWB control was developed in an attempt to reduce the superplasticizer used in the mixture by increasing the water-to-binder ratio of one the concretes. Table 4-2 displays the mixture designs of the controls. In addition to showing the comparison mixtures, Table 4-3 also presents the corresponding control mixtures that the comparison mixtures, good performing mixtures and bad performing mixtures were compared with for the ASTM C494 qualification. Table 4-4 explains the basis for selecting which pseudo-control would be used to evaluate the comparison, good, and bad performing mixtures. All mixtures with known performers were analyzed with respect to the CWB control, which does not match any parameter of their mixture proportion. However, it was considered useful to evaluate these mixtures with respect to a known good performer that was the same for all mixtures. Thus, we will be able to determine whether there are any similarities among the behavior of the comparison mixtures with the bad and good performing mixtures. For example, if a comparison mixture and bad performing mixture both fail the same ASTM C494 tests, then this may suggest that the comparison mixture would also perform badly in the field. The methodology used also provides insight about the effect of the method used

to design the control mixture in the determining the potential for the mixture to would perform badly.

Table 4-2: Mixture proportions for the different control types used for ASTM C494 qualification

Control ID	w/cm	Cement Type	Cement Content (lb/yd ³)	SCM Content (lb/yd ³)	Admixtures			
					Type	(floz/100 lb cement)	Type	(floz/ 100 lb cement)
CSP-1	0.26	PC-III-A	705	175	HR-P1	8.25	NR-1	1.5
CWB	0.4		658	0		2		2
CSP-2	0.33		658	0		5.5		2
CLWA			658	0		5		2.5

<p>CSP1 & 2: Control Mixtures based on HRWR dosage CWB: Control Mixtures based on water to binder ratio CLWA: Control Mixtures based on lightweight fine aggregate replacement</p>
--

Table 4-3: Mixtures organized with respect to their control mixture.

Mixtures highlighted in yellow are known “bad performers” and mixes highlighted in blue are known “good performers.”

Mix ID	w/b	Cement Type	Cement Content (lb/yd. ³)	SCM Content (lb/yd. ³)	HRWR Type	HRWR Dosage (fl.oz./100 cwt)	NR Type	NR Dosage (fl.oz./100 cwt)	Evaluated against Control			
									CSP-1	CWB	CSP-2	CLWA
1	0.26	PC-III-A	705	175	HR-P1	5.25	NR-1	1.5	Yes	No	No	No
2	0.26	PC-III-A	517	129	HR-P1	25.75	NR-1	3	Yes	No	No	No
3	0.26	PC-III-A	705	175	HR-P2	8.25	NR-1	3	Yes	No	No	No
4	0.26	PC-III-A	705	175	HR-P3	10	NR-2	3	Yes	No	No	No
5	0.26	PC-IIIB	705	175	HR-P1	8.25	NR-1	3	Yes	No	No	No
6	0.26	PC-III-A	705	233	HR-P1	6.5	NR-1	3	Yes	No	No	No
7	0.38	PC-III-A	700	175	-	-	-	-	No	Yes	No	No
8	0.45	PC-III-A	705	175	-	-	-	-	Yes	No	No	No
B1	0.26	PC-III-A	705	175	HR-P1	6.5	NR-1	3	Yes	Yes	No	No
B2	0.28	PC-III-A	705	175	HR-P1	12	NR-1	3	Yes	Yes	No	No
G1	0.31	PC-III-A	663	271	HR-P1	5.5	NR-1	3	No	Yes	No	No
B3	0.31	PC-III-A	640	213	HR-P1	6	NR-1	3	No	Yes	No	No
G2	0.33	PC-III-A	658	0	HR-P1	6.5	NR-1	3	No	Yes	Yes	Yes
9	0.26	PC-III-A	658	219	HR-P1	6.5	NR-1	3	No	Yes	Yes	Yes
10	0.33	PC-III-A	517	0	HR-P1	30.5	NR-1	3	No	Yes	Yes	Yes
11	0.33	PC-III-A	658	0	HR-P1	11.88	NR-1	3	No	Yes	Yes	Yes
13	0.52	PC-III-A	658	0		-	-	-	No	Yes	Yes	Yes
14	0.56	PC-III-A	658	0	-	-	-	-	No	Yes	Yes	Yes

Table 4-4: Reasoning behind the control mixtures selected

Mix ID	Control Mixture Selected for Comparison; Reason for Selection	Evaluated against Control			
		CSP-1	CWB	CSP-2	CLWA
1	<ul style="list-style-type: none"> CSP-1; HRWR dosage of CSP-1 is greater than Mix 1 but all else is the same. Represents an opposite to how ASTM C494 tests against a control. 	Yes	No	No	No
2	<ul style="list-style-type: none"> CSP-1; Mixtures have same w/b but binder composition and HRWR dosage changed in Mix 2. 	Yes	No	No	No
3	<ul style="list-style-type: none"> CSP-1; Similar composition to CWB but HRWR type differs in Mix 3 and other admixtures were adjusted to get stable mixture at targeted slump. 	Yes	No	No	No
4	<ul style="list-style-type: none"> CSP-1; Similar composition to CWB but HRWR type differ in Mix 3 and other admixtures type and content adjusted to get stable mixture at targeted slump 	Yes	No	No	No
5	<ul style="list-style-type: none"> CSP-1; Similar composition to CSP-1 but cement type differs in Mix 5 	Yes	No	No	No
6	<ul style="list-style-type: none"> CSP-1; Similar composition but fly ash content increases; other admixtures adjusted to get stable mixture at targeted slump 	Yes	No	No	No
7	<ul style="list-style-type: none"> CWB; same composition as CWB but no admixture in Mix 7. Therefore, the effect of admixture inclusion from this mix was evaluated. 	No	Yes	No	No
8	<ul style="list-style-type: none"> CSP-1; similar mixture as CSP-1 but no admixture in Mix 8. 	Yes	No	No	No
B1	<ul style="list-style-type: none"> CSP-1; same w/b, so that the effect of reducing the HRWR dosage is evaluated. 	Yes	Yes	No	No
B2	<ul style="list-style-type: none"> CSP-1; most similar match as w/b of B2, although greater than CSP-1 so we see the effect of increasing w/b ratio and the effect of an increase in admixture dosage. 	Yes	Yes	No	No
G1	<ul style="list-style-type: none"> CWB; No good control for this mixture, so CWB selected as a standard known non-cracking mix to compare with. 	No	Yes	No	No
B3	<ul style="list-style-type: none"> CWB; No good control for this mixture, so CWB selected as a standard known non-cracking mix to compare with for the same purpose as those explained in G1. 	No	Yes	No	No
G2	<ul style="list-style-type: none"> CWB; Lower w/b ratio and admixture added as needed to get flow. CLWA; Similar mixture proportion but G2 also has fly ash. CSP-2; Similar but G2 also has fly ash. 	No	Yes	Yes	Yes
9	<ul style="list-style-type: none"> CSP-2; Same cement content, except Mix 9 has Fly ash. Same justifications as G2 for the comparison against CLWA and CWB 	No	Yes	Yes	Yes
10	<ul style="list-style-type: none"> Compared against all CWB, CSP-2, and CLWA to understand the impact of cement content and the sensitivity of the controls 	No	Yes	Yes	Yes
11	<ul style="list-style-type: none"> CSP-2; Similar w/b but now looking at the effect of removing fly ash (HRWR adjusted accordingly to get target flow) CLWA; Similar w/b but now looking at the effect of removing fly ash (HRWR adjusted accordingly to get targeted flow) 	No	Yes	Yes	Yes
13	<ul style="list-style-type: none"> CWB; similar composition but Mix 13 has a higher w/b and admixture removed 	No	Yes	Yes	Yes
14	<ul style="list-style-type: none"> CWB; same mixture but higher w/b and admixture removed Same justifications as G2 for the comparison against CLWA and CSP-1 	No	Yes	Yes	Yes

4.2.1 Water Content

4.2.1.1 Procedure and Experimental Setup

The qualification for ASTM C494 with respect to HRWR Type F requires that the water content of the admixture test mixture in question not exceed 88% of the control total water content. Considering that the intent of HRWR addition in concrete mixtures is to reduce the need for water to obtain a workable mixture, exceeding the control mixtures water content is not a concern. Yet because the controls are not a “true” control mixture designs with respect to the admixtures or mixture designs results have been tabulated purely as a means of complete fulfillment of ASTM C494 testing procedures.

4.2.1.2 Results

Mixture design comparison stated the water content as “pass” for water addition less than or equal to 88% of the respective control or “fails” for water greater than 88% of the control. Table 4-5 provides the Pass/Fail results of the mixtures with respect to their controls.

Table 4-5: Water content pass/fail for ASTM C494 in reference to control mixtures.

Additionally, “bad performers” (yellow) and “good performers” (blue) have been highlighted.

Mix ID	w/b	Cement Type	Cement Content (lb/yd. ³)	SCM Content (lb/yd. ³)	HRWR Type	HRWR Dosage (fl.oz./100 cwt)	NR Type	NR Dosage (fl.oz./100 cwt)	Evaluation with Respect to Control			
									CSP-1	CWB	CSP-2	CLWA
1	0.26	PC-III-A	705	175	HR-P1	5.25	NR-1	1.5	Pass			
2	0.26	PC-III-A	517	129	HR-P1	25.75	NR-1	3	Pass			
3	0.26	PC-III-A	705	175	HR-P2	8.25	NR-1	3	Pass			
4	0.26	PC-III-A	705	175	HR-P3	10	NR-2	3	Pass			
5	0.26	PC-III-B	705	175	HR-P1	8.25	NR-1	3	Pass			
6	0.26	PC-III-A	705	233	HR-P1	6.5	NR-1	3	Pass			
7	0.38	PC-III-A	700	175	-	-	-	-	Fail	Fail		
8	0.45	PC-III-A	705	175	-	-	-	-	Fail			
B1	0.26	PC-III-A	705	175	HR-P1	6.5	NR-1	3	Fail	Pass		
B2	0.28	PC-III-A	705	175	HR-P1	12	NR-1	3	Fail	Pass		
G1	0.31	PC-III-A	663	271	HR-P1	5.5	NR-1	3		Pass		
B3	0.31	PC-III-A	640	213	HR-P1	6	NR-1	3		Pass		
G2	0.33	PC-III-A	658	0	HR-P1	6.5	NR-1	3		Pass	Fail	Fail
9	0.26	PC-III-A	658	219	HR-P1	6.5	NR-1	3		Pass	Fail	Fail
10	0.33	PC-III-A	517	0	HR-P1	30.5	NR-1	3		Pass	Fail	Fail
11	0.33	PC-III-A	658	0	HR-P1	11.88	NR-1	3		Pass	Pass	Pass
12	0.52	PC-III-A	658	0						Pass	Pass	Pass
13	0.56	PC-III-A	658	0						Pass	Fail	Fail

Because “good” and “bad” performers both primarily passed with respect to their controls, water content cannot be used as a proper means of evaluating a mixture’s potential towards micro-cracking. Therefore, ASTM C494-water content is inadequate for micro-cracking prediction.

4.2.2 Time of Set

4.2.2.1 Procedure and Experimental Setup

The qualification for ASTM C494 with respect to HRWR Type F requires that both initial and final time of set of the admixture test mixture is within a certain range of the control mixture’s initial and final set time. Each mixture employed the time of set analysis through ASTM C403, Standard test method for time of setting of concrete mixtures by penetration resistance (2008). For this test, approximately 0.25-ft³ of concrete was sieved through a No. 4 sieve with the aid of a vibrating table in order to ascertain a mortar mixture. The mortar was then set into a 6x6-in steel cylindrical tin, capped and held in a 73°C testing environment. The time of set testing equipment is shown in Figure 4-3.



Figure 4-3: Time of set equipment used throughout this project

Time of set measurements were initiated 3 hours after the introduction of cement to water. Thereafter, 15-minute increments were employed to determine the length of time until the mortar achieved 500 psi for an indication of initial set or 4000 psi as an indication of final set of the concrete.

4.2.2.2 Results

According to ASTM C494, the HRWR test mixture set time cannot be less than 1 hour and not more than 1.5 hours in reference to the control time of initial and final set measurement. Table 4-6 presents the Pass/Fail results of the mixtures with respect to their control for the ASTM C494 set time requirements.

Table 4-6: Time of set pass/fail for ASTM C494 in reference to control mixtures.

Additionally, “bad performers” (yellow) and “good performers” (blue) have been highlighted.

Mix ID	w/b	Cement Type	Cement Content (lb/yd. ³)	SCM Content (lb/yd. ³)	HRWR Type	HRWR Dosage (fl.oz./100 cwt)	NR Type	NR Dosage (fl.oz./ 100 cwt)	Initial Time of Set				Final Time of Set			
									CSP-1	CWB	CSP-2	CLWA	CSP-1	CWB	CSP-2	CLWA
1	0.26	PC-III-A	705	175	HR-P1	5.25	NR-1	1.5	Fail				Pass			
2	0.26	PC-III-A	517	129	HR-P1	25.75	NR-1	3	Fail				Fail			
3	0.26	PC-III-A	705	175	HR-P2	8.25	NR-1	3	Pass				Pass			
4	0.26	PC-III-A	705	175	HR-P3	10	NR-2	3	Pass				Pass			
5	0.26	PC-III-B	705	175	HR-P1	8.25	NR-1	3								
6	0.26	PC-III-A	705	233	HR-P1	6.5	NR-1	3	Fail				Fail			
7	0.38	PC-III-A	700	175						-						
8	0.45	PC-III-A	705	175					Fail				Fail			
B1	0.26	PC-III-A	705	175	HR-P1	6.5	NR-1	3	-	Pass				Pass		
B2	0.28	PC-III-A	705	175	HR-P1	12	NR-1	3	-	Fail				Pass		
G1	0.31	PC-III-A	663	271	HR-P1	5.5	NR-1	3		Pass				Pass		
B3	0.31	PC-III-A	640	213	HR-P1	6	NR-1	3		Fail				Fail		
G2	0.33	PC-III-A	658	0	HR-P1	6.5	NR-1	3		Fail	Fail	Fail		Fail	Fail	Fail
9	0.26	PC-III-A	658	219	HR-P1	6.5	NR-1	3		Fail	Fail	Fail		Fail	Fail	Fail
10	0.33	PC-III-A	517	0	HR-P1	30.5	NR-1	3		Fail	Fail	Fail		Fail	Fail	Fail
11	0.33	PC-III-A	658	0	HR-P1	11.88	NR-1	3		Fail	Fail	Fail		Fail	Fail	Fail
12	0.52	PC-III-A	658	0						Pass	Pass	Pass		Pass	Pass	Pass
13	0.56	PC-III-A	658	0						Pass	Pass	Pass		Pass	Pass	Pass

Table 4-6 indicates that overall there were fewer “passes” with respect to initial set as compared to final set. Also, lower w/cm ratio mixtures (<0.31) had more variability in passing and failing as compared to higher w/cm mixtures. With regards to the “good” and “bad” performing mixtures half of the “good” (two out of four) performers passed and half of the “bad” (three out of six) performers failed. Based on the inconclusiveness of the time of set testing results, ASTM C494, Time of Set, is deemed inadequate for micro-cracking prediction. Based on the inconclusiveness of the time of set testing results, ASTM C494, Time of Set, is deemed inadequate for micro-cracking prediction.

4.2.3 Compressive Strength

4.2.3.1 Procedure and Experimental Setup

The qualification for ASTM C494 with respect to HRWR Type F requires that compressive strength of the admixture test mixture in question exceeds a certain percentage of the compressive strength of the control for 1, 3, 7, 28, and 90 days, and 6 and 12 months. To evaluate the compressive strength of the concrete, 3x6-in specimens were cast and subsequently subjected to the ASTM C39, Compressive Strength of Cylindrical Concrete Cylinders (2016). 24 3x6-in concrete cylinders were cast in plastic compressive cylinder molds for each mixture. The 24 specimens were cured for a 24-hour period and stored in a temperature controlled room at 23 ± 3 °C and covered with wet burlap and plastic sheeting to prevent evaporation. In order to provide a representation of concrete cast and demolded in the precast yard 3 cylinders were stripped and measured at 18 hours after cement was added to water. After which, the specimens were demolded and set in a moist curing environment at 23 ± 3 °C up until they were to be tested in compression. Three cylinders were tested in compression for each compression date. The average compressive stresses along with standard deviations for each concrete mixture are included in the Appendix III of this report.

4.2.3.2 Result

The pass/fail limits for each of the dates according to ASTM C494 for Type F HRWR are listed in Tables 4-7 through 4-9. A cell highlighted in red denotes mixture that failed the compressive strength qualification criteria for that specific date; whereas a green highlighted denotes a mixture that passed the compressive strength qualification criteria for that specific date. Percentages in header row lists the ASTM C494 minimum strength ratio for that specific day. Percentage number in cells indicate the percentage that the base mixture varies from the control mixture. Values over 100% means that the strength of the base mixture exceeded the control mixture. Additionally, “bad performers” (Yellow) and “good performers” (Blue) are highlighted.

Table 4-7: Compressive strength pass/fail for ASTM C494 in reference to control mixtures (1-7 Day).

Minimum percentages needed to pass listed in header row. Red indicates fail; green indicates pass. “Bad performers” (yellow) and “good performers” (blue) are highlighted.

Mix ID	w/b	Cement Type	Cement Content (lb/yd. ³)	SCM Content (lb/yd. ³)	HRWR Type	HRWR Dosage (fl.oz./100 cwt)	NR Type	NR Dosage (fl.oz./100 cwt)	1 Day - 140%				3 Day-125%			
									CSP-1	CWB	CSP-2	CLWA	CSP-1	CWB	CSP-2	CLWA
1	0.26	PC-III-A	705	175	HR-P1	5.25	NR-1	1.5	92%				58%			
2	0.26	PC-III-A	517	129	HR-P1	25.75	NR-1	3	62%				42%			
3	0.26	PC-III-A	705	175	HR-P2	8.25	NR-1	3	77%				65%			
4	0.26	PC-III-A	705	175	HR-P3	10	NR-2	3	3800%				36%			
5	0.26	PC-III-B	705	175	HR-P1	8.25	NR-1	3	94%				63%			
6	0.26	PC-III-A	705	233	HR-P1	6.5	NR-1	3	18%				41%			
7	0.38	PC-III-A	700	175	-	-	-	-		38%				42%		
8	0.45	PC-III-A	705	175	-	-	-	-	88%				63%			
B1	0.26	PC-III-A	705	175	HR-P1	6.5	NR-1	3	82%	140%	-	-	122%	130%	-	-
B2	0.28	PC-III-A	705	175	HR-P1	12	NR-1	3	18%	126%	-	-	110%	118%	-	-
G1	0.31	PC-III-A	663	271	HR-P1	5.5	NR-1	3		113%	-	-		87%	-	-
B3	0.31	PC-III-A	640	213	HR-P1	6	NR-1	3		113%	-	-		93%	-	-
G2	0.33	PC-III-A	658	0	HR-P1	6.5	NR-1	3		111%	117%	96%		117%	140%	89%
9	0.26	PC-III-A	658	219	HR-P1	6.5	NR-1	3		90%	95%	78%		23%	27%	17%
10	0.33	PC-III-A	517	0	HR-P1	30.5	NR-1	3		133%	140%	115%		74%	88%	57%
11	0.33	PC-III-A	658	0	HR-P1	11.88	NR-1	3		132%	140%	114%		76%	90%	58%
12	0.52	PC-III-A	658	0		-	-	-		131%	139%	114%		78%	92%	60%
13	0.56	PC-III-A	658	0	-	-	-	-		119%	125%	103%		78%	92%	60%

Table 4-8: Compressive strength pass/fail for ASTM C494 in reference to control mixtures (7-Day through 28-Day).

Minimum percentages needed to pass listed in header row. Red indicates fail; green indicates pass. “Bad performers” (yellow) and “good performers” (blue) are highlighted.

Mix ID	w/b	Cement Type	Cement Content (lb/yd. ³)	SCM Content (lb/yd. ³)	HRWR Type	HRWR Dosage (fl.oz./100 cwt)	NR Type	NR Dosage (fl.oz./100 cwt)	7 Day-115%				28 Day-110%			
									CSP-1	CWB	CSP-2	CLWA	CSP-1	CWB	CSP-2	CLWA
1	0.26	PC-III-A	705	175	HR-P1	5.25	NR-1	1.5	52%				45%			
2	0.26	PC-III-A	517	129	HR-P1	25.75	NR-1	3	42%				36%			
3	0.26	PC-III-A	705	175	HR-P2	8.25	NR-1	3	55%				47%			
4	0.26	PC-III-A	705	175	HR-P3	10	NR-2	3	35%				30%			
5	0.26	PC-III-B	705	175	HR-P1	8.25	NR-1	3	51%				44%			
6	0.26	PC-III-A	705	233	HR-P1	6.5	NR-1	3	53%				46%			
7	0.38	PC-III-A	700	175	-	-	-	-		47%				85%		
8	0.45	PC-III-A	705	175	-	-	-	-	62%				53%			
B1	0.26	PC-III-A	705	175	HR-P1	6.5	NR-1	3	127%	129%	-	-	158%	148%	-	-
B2	0.28	PC-III-A	705	175	HR-P1	12	NR-1	3	140%	124%	-	-	150%	129%	-	-
G1	0.31	PC-III-A	663	271	HR-P1	5.5	NR-1	3		94%	-	-		108%	-	-
B3	0.31	PC-III-A	640	213	HR-P1	6	NR-1	3		100%	-	-		107%	-	-
G2	0.33	PC-III-A	658	0	HR-P1	6.5	NR-1	3		118%	136%	94%		115%	126%	99%
9	0.26	PC-III-A	658	219	HR-P1	6.5	NR-1	3		68%	57%	39%		51%	56%	44%
10	0.33	PC-III-A	517	0	HR-P1	30.5	NR-1	3		84%	79%	55%		64%	70%	55%
11	0.33	PC-III-A	658	0	HR-P1	11.88	NR-1	3		84%	82%	57%		64%	70%	55%
12	0.52	PC-III-A	658	0		-	-	-		84%	79%	55%		64%	70%	55%
13	0.56	PC-III-A	658	0	-	-	-	-		84%	80%	55%		64%	70%	55%

Table 4-9: Compressive strength pass/fail for ASTM C494 in reference to control mixtures (90-Day through 6-Month).

Minimum percentages needed to pass listed in header row. Red indicates fail; green indicates pass. “Bad performers” (yellow) and “good performers” (blue) are highlighted.

Mix ID	w/b	Cement Type	Cement Content (lb/yd. ³)	SCM Content (lb/yd. ³)	HRWR Type	HRWR Dosage (fl.oz./100 cwt)	NR Type	NR Dosage (fl.oz./100 cwt)	90 Day - 117%				6 Month - 100%			
									CSP-1	CWB	CSP-2	CLWA	CSP-1	CWB	CSP-2	CLWA
1	0.26	PC-III-A	705	175	HR-P1	5.25	NR-1	1.5	73%				76%			
2	0.26	PC-III-A	517	129	HR-P1	25.75	NR-1	3	68%				68%			
3	0.26	PC-III-A	705	175	HR-P2	8.25	NR-1	3	96%				100%			
4	0.26	PC-III-A	705	175	HR-P3	10	NR-2	3	70%				73%			
5	0.26	PC-III-B	705	175	HR-P1	8.25	NR-1	3	91%				91%			
6	0.26	PC-III-A	705	233	HR-P1	6.5	NR-1	3	86%				82%			
7	0.38	PC-III-A	700	175	-	-	-	-								
8	0.45	PC-III-A	705	175	-	-	-	-	90%				50%			
B1	0.26	PC-III-A	705	175	HR-P1	6.5	NR-1	3	148%	140%	-	-	146%	149%	-	-
B2	0.28	PC-III-A	705	175	HR-P1	12	NR-1	3	129%	126%	-	-	133%	149%	-	-
G1	0.31	PC-III-A	663	271	HR-P1	5.5	NR-1	3		113%	-	-		133%	-	-
B3	0.31	PC-III-A	640	213	HR-P1	6	NR-1	3		113%	-	-		116%	-	-
G2	0.33	PC-III-A	658	0	HR-P1	6.5	NR-1	3		111%	117%	96%		118%	117%	94%
9	0.26	PC-III-A	658	219	HR-P1	6.5	NR-1	3		90%	95%	78%		99%	99%	79%
10	0.33	PC-III-A	517	0	HR-P1	30.5	NR-1	3		133%	140%	115%		145%	145%	116%
11	0.33	PC-III-A	658	0	HR-P1	11.88	NR-1	3		132%	140%	114%		137%	137%	110%
12	0.52	PC-III-A	658	0		-	-	-		131%	139%	114%		137%	137%	110%
13	0.56	PC-III-A	658	0	-	-	-	-		119%	125%	103%		122%	122%	98%

Table 4-6 indicates that strengths of HRWR tested mixtures primarily failed with respect to their controls especially in early ages (≤ 28 Days). The bad performing mixtures exceeded the strength of the controls for just over half of the testing dates. The good performing mixtures exceeded the strength of their controls for just less than half of the testing dates. The remainder of the matrix with the HRWR controls (CSP-1 and CSP-2) and the lightweight aggregate control (CLWA) produces a high number of failures especially in the early ages. Due to the variability in compressive strengths with respect to good and bad performers, ASTM C494-compressive strength is inadequate for micro-cracking prediction.

The compressive strength pass/fail and percentage have only been presented to provide proof of fulfillment if ASTM C494 testing as a part of Task 3 of this research project. The collection of compressive strength data for each mixture performed in this project is located in the Appendix III of this report.

4.2.4 Drying Shrinkage

4.2.4.1 Procedure and Experimental Setup

In accordance with ASTM C494, testing procedures for free shrinkage due to drying shrinkage was assessed. To evaluate the drying shrinkage effects on concrete the length change of concrete prisms was subjected to the ASTM C157 testing method (2008). Six concrete prisms were cast in rigid molds for each mixture. The six specimens were cured for a 24-hour period and stored in a temperature controlled room at $23 \pm 3^\circ\text{C}$ and covered with wet burlap and plastic sheeting to prevent evaporation. After which, the specimens were demolded and set in a moist curing environment at $23 \pm 3^\circ\text{C}$ for a 15- to 30-minute period. Initial readings were immediately taken with a comparator along with mass measurements. Of the six prisms, three specimens were stored in a climate-controlled room at 50% RH and 23°C ; the remaining three specimens were cured in a saturated lime solution for a 28-day period from the date of casting. Both sets of prisms had successive measurement readings taken at ages of 4, 7, 14, 28, 56, 112 and 224 days. If applicable additional measurements were taken beyond the dates required in the ASTM standard. The length change for each specimen, $\Delta L_x(\%)$ was calculated using the following equation:

$$\Delta L_x = \frac{CRD_t - CRD_{initial}}{G} * 100\% \quad \text{Equation 4-1}$$

where CRD_t is the difference between the comparator reading of specimen and the reference bar at time “t”. $CRD_{initial}$ is the difference between the comparator reading of specimen and the reference bar at t=0 (i.e., the initial reading), and G is the length separation between inner gage faces embedded in the concrete specimen (250 mm).

4.2.4.2 Results

The following sections first provide the complete drying shrinkage matrix alongside the qualification for ASTM C 494 with respect to HRWR Type F. ASTM C 494 requires that if the shrinkage at 14 days (in accordance to ASTM C 157) exceeds 0.03% than the shrinkage relative to the control mixture should not exceed 135% (2008). However, if the shrinkage at 14 days is less than 0.03% than the difference between the control and tested mixture should not be less than 0.01%. Table 4-10 provides the Pass/Fail along with the shrinkage percentage or difference of mixture designs with respect to their controls. Green denotes mixtures that passed the qualification criteria, whereas red highlighted cells denote mixtures that failed. The remainder of the drying shrinkage results section provides comparisons of drying shrinkage in accordance with Task 4: effect of w/cm ratio, cement source, cement type, HRWR type, HRWR dosage, cement content, fly ash addition and shrinkage reducing parameters such a lightweight aggregate. All drying shrinkage curves can be found in Appendix V.

Table 4-10: Drying shrinkage pass/fail for ASTM C494 in reference to control mixtures (1-Day Cure).

Additionally, “bad performers” (yellow) and “good performers” (blue) have been highlighted.

Mix ID	w/b	Cement Type	Cement Content (lb/yd. ³)	SCM Content (lb/yd. ³)	HRWR Type	HRWR Dosage (fl.oz./100 cwt)	NR Type	NR Dosage (fl.oz./100 cwt)	1 Day Cure				28 Day Cure			
									CSP-1	CWB	CSP-2	CLWA	CSP-1	CWB	CSP-2	CLWA
1	0.26	PC-III-A	705	175	HR-P1	5.25	NR-1	1.5	78%				60%			
2	0.26	PC-III-A	517	129	HR-P1	25.75	NR-1	3	74%				57%			
3	0.26	PC-III-A	705	175	HR-P2	8.25	NR-1	3	76%				193%			
4	0.26	PC-III-A	705	175	HR-P3	10	NR-2	3	84%				71%			
5	0.26	PC-III-B	705	175	HR-P1	8.25	NR-1	3	77%				60%			
6	0.26	PC-III-A	705	233	HR-P1	6.5	NR-1	3	100%				61%			
7	0.38	PC-III-A	700	175	-	-	-	-		131%				30%		
8	0.45	PC-III-A	705	175	-	-	-	-	78%				51%			
B1	0.26	PC-III-A	705	175	HR-P1	6.5	NR-1	3	94%	103%			69%	148%		
B2	0.28	PC-III-A	705	175	HR-P1	12	NR-1	3	-0.01%	104%				90%		
G1	0.31	PC-III-A	663	271	HR-P1	5.5	NR-1	3		133%				111%		
B3	0.31	PC-III-A	640	213	HR-P1	6	NR-1	3		141%				145%		
G2	0.33	PC-III-A	658	0	HR-P1	6.5	NR-1	3		124%	0.015%	140%		111%	-0.001%	54%
9	0.26	PC-III-A	658	219	HR-P1	6.5	NR-1	3		106%	0.01%	100%		142%	0.00%	69%
10	0.33	PC-III-A	517	0	HR-P1	30.5	NR-1	3		129%	0.016%	122%		99%	-0.004%	48%
11	0.33	PC-III-A	658	0	HR-P1	11.88	NR-1	3		112%	0.012%	106%		174%	0.006%	85%
12	0.52	PC-III-A	658	0		-	-	-		104%	0.01%	99%		119%	0.000%	58%
13	0.56	PC-III-A	658	0	-	-	-	-		102%	0.01%	97%		79%	-0.009%	38%

Although not mandated by ASTM C 494 drying shrinkage at an extended time frame (referred to here as the “ultimate” shrinkage) of each mixture was also determined. It must be noted that the same pass and fail criterion with respect to the control used at 14-day was used at the “ultimate” shrinkage date. This was done as to not stray too far away from the ASTM standard for the “ultimate” shrinkage data comparison. For bad performing mixtures, half of the mixtures (one out of three) subjected to a 1-day curing period failed within the 14-day period. Additionally, the bad performing mixtures with 28-day curing (2 out of 3) failed within the 14-day period. The measurements compared at ultimate for 1-day curing failed all good and bad performing mixtures. Whereas the ultimate measurements compared with the 28-day curing procedure passed all the good and bad performers. The variability in pass/fail results for drying shrinkage confirms that ASTM C494-compressive strength is inadequate for micro-cracking prediction. The drying shrinkage pass/fail and percentages have only been presented to provide proof of fulfillment of ASTM C494 testing as a part of Task 3 of this research project.

Since drying shrinkage holds a great deal of relevance to the potential shrinkage induced micro-cracking seen in the field, a more detailed investigation of mixture design effects on drying shrinkage was performed in the following sections. Although the prescribed “good” and “bad” performers are no longer being directly compared to their respective controls in the following sections, their comparisons have been illuminated and discussed where applicable. In addition, shorthand mixture identifications are used throughout this chapter, where only the variable in the mixture designs being compared is presented throughout each figure.

4.2.4.2.1 Effect of w/cm Ratio

Figure 4-4, Figure 4-5, and Figure 4-6 show the drying shrinkage curve for three base concrete mixtures (M1-NC, M3-NC, and M4-SCC), each of which have three additional variations in w/cm ratios. NC and SCC are normally consolidated and self-consolidating concrete mixture design notations. Air and lime water storage curing procedures at 1 and 28-day accordingly for drying shrinkage measurements have been overlaid on the same graph in order to provide fulfillment of ASTM C157 specimen measurement procedures as previously described in Section 4.2.4.1.

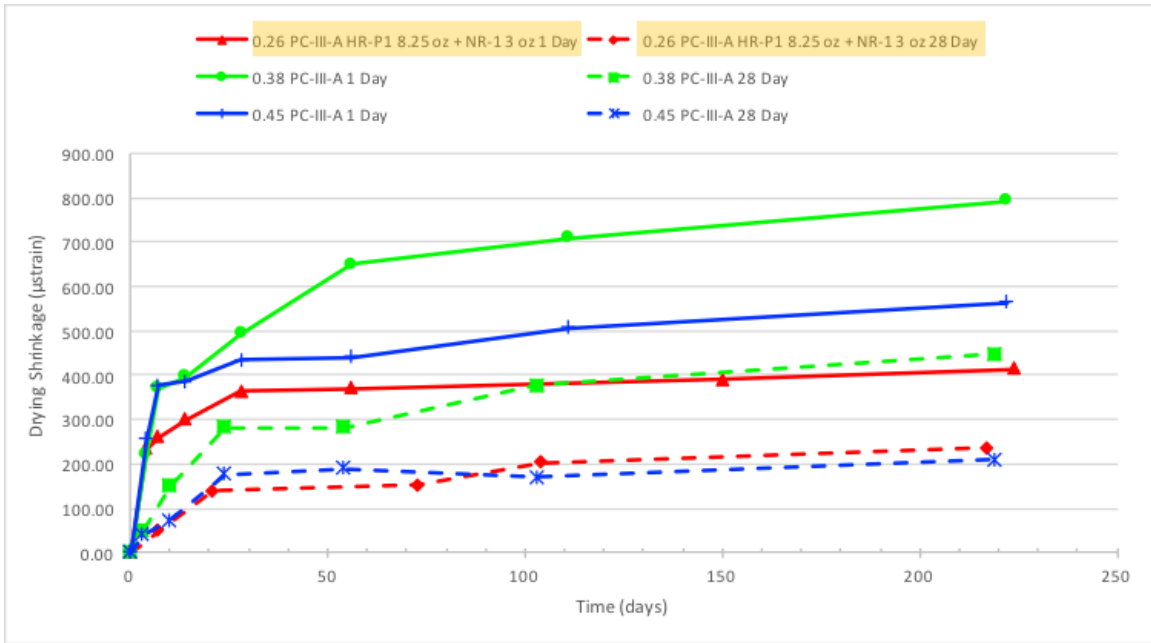


Figure 4-4: Drying shrinkage curve showing effect of w/cm ratio on base mixture, M1-NC (0.26 w/cm), for 1- and 28-Day curing.

For a given w/cm ratio, solid lines correspond to 1-day cure; dashed line corresponds to 28-day cure. Yellow shading denotes “bad performer” mixture.

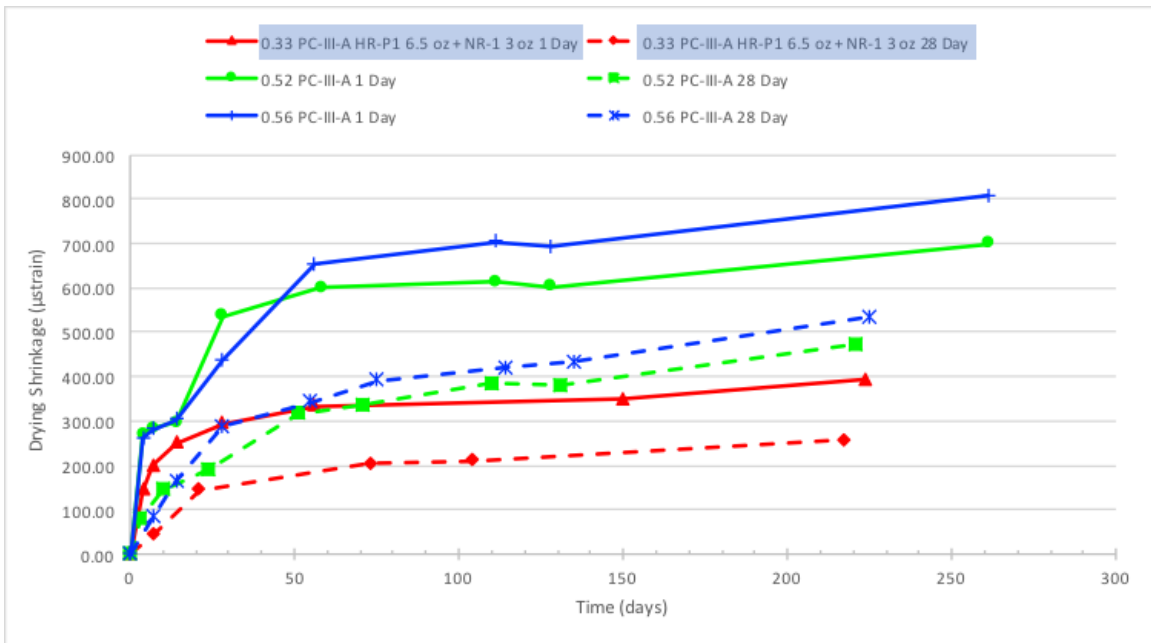


Figure 4-5: Drying shrinkage curve showing effect of w/cm ratio for base mixture M3-NC (0.33 w/cm) for 1- and 28-Day curing.

For a given w/cm ratio, solid lines correspond to 1-day cure; dashed line corresponds to 28-day cure. Blue shading denotes “good performer” mixture.

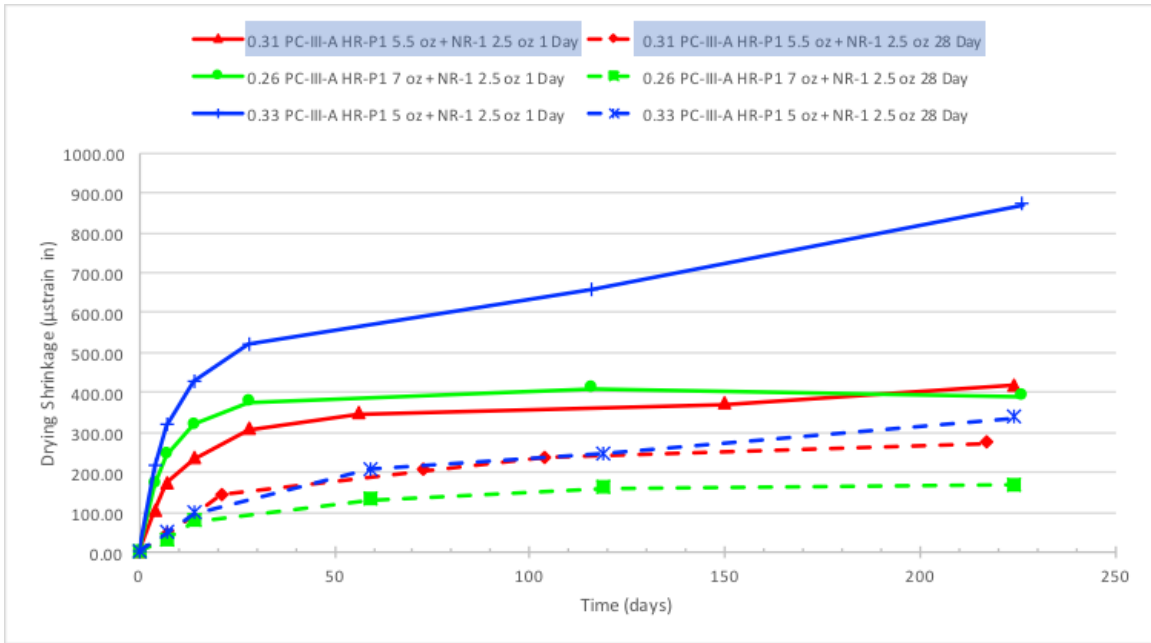


Figure 4-6: Drying shrinkage curve showing effect of w/cm ratio for base mixture M4-SCC (0.31 w/cm) for 1- and 28-Day curing.

For a given w/cm ratio, solid lines correspond to 1-day cure; dashed line corresponds to 28-day cure. Blue shading denotes “good performer” mixture.

In order to provide comparative results for these mixtures purely on the basis of w/cm ratio, the cement and coarse aggregate values per cubic yard were held constant. Thus, the true differences in the mixture designs is the water and fine aggregate content, thereby changing the paste content between each mix. Each of these mixtures and their adjacent comparative w/cm ratio mixtures do not initially confirm the established concept that with an increased w/cm ratio (cement and coarse aggregate held constant) the drying shrinkage, micro-strain, of the specimen should also be increased. However, the long-term shrinkage data collected proved to be more in agreement that as the w/cm increases the drying shrinkage also increases. Concrete mixtures with lower w/cm not only develop lower shrinkage strain but also discontinue advancement shrinkage sooner by establishing a RH equilibrium with the environment at a faster rate. With respect to good and bad performers, both showed similar degrees of shrinkage, (e.g., 400 microstrains when cured for 1 day and approximately 300 microstrain when cured for 28 days).

4.2.4.2.2 Effect of Cement Source

Figure 4-7 shows the drying shrinkage curve for two base concrete mixtures (M1-NC and M4-SCC), each of which have a direct duplicate with different Type III cement sources (PC-III-A and PC-III-B) for 0.26 and 0.31 w/cm.

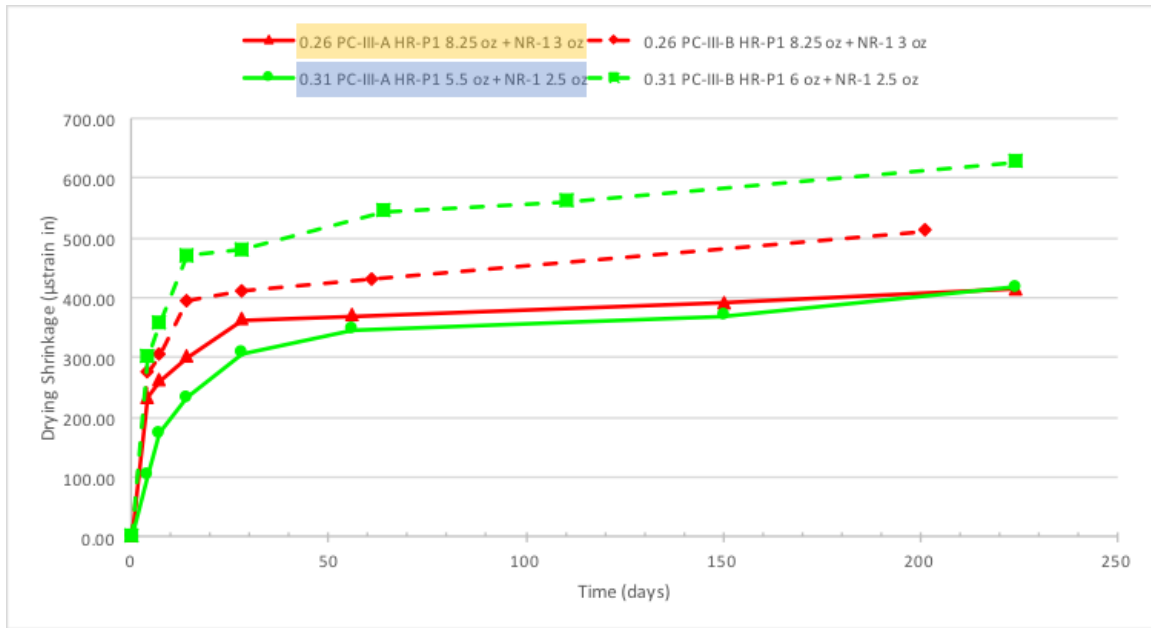


Figure 4-7: Drying shrinkage curve showing effect of cement source (PC-III-A and PC-III-B) for 0.26 and 0.31 w/cm ratios for base mixture M1-NC and M4-SCC respectively.

Dashed line corresponds to PC-III-B cement source; solid lines correspond to PC-III-A cement source. Yellow and blue shading denotes “bad performer” and “good performer,” respectively.

The graph shows that for both w/cm ratios the PC-III-B cement source develops more shrinkage initially as well as in the long-term shrinkage compared to PC-III-A cement source. In order to provide reasoning for the shrinkage difference based on cement source the Blaine fineness of the cement was determined. As previously discussed in Chapter 3 of this report, the Blaine fineness of PC-III-A and PC-III-B were reported as 486.3 and 519.8m²/kg, respectively. Smaller cement grain size increases autogenous shrinkage effects at an earlier age (Ei-ichi et al. 1994); therefore, the increased rate of shrinkage with PC-III-B as compared with PC-III-A as seen Figure 4-7 may be attributed to an increase in autogenous shrinkage occurring in conjunction with drying shrinkage. A precast temperature history profile performed and displayed in Figure 121 in the Appendix IV of this report proved that PC-III-A mixtures showed a greater delay in the initiation of the acceleration period as compared with PC-III-B.

4.2.4.2.3 Effect of Cement Type

Figure 4-8 shows the drying shrinkage curve for two concrete mixtures (T5-M5 and T5-M7), where both have all the same mixture design apart from cement types (PC-III-A and PC-I-A) accordingly for 0.28 w/cm.

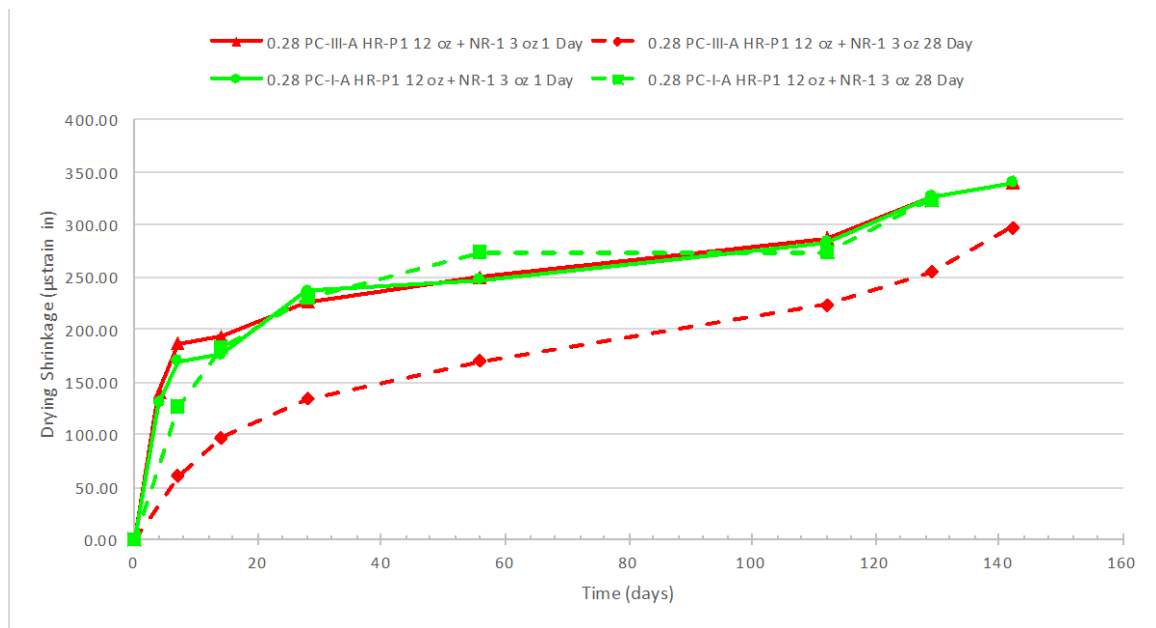


Figure 4-8: Drying shrinkage curve showing effect of cement type (PC-III-A and PC-I-A) and curing period for 0.28 w/cm ratios for mixtures T5-M5 and T5-M7.

Green lines correspond to an ASTM C150 Type I cement; red line corresponds to an ASTM C150 Type III cement. Dashed lines correspond to 28-day cure; solid lines correspond to 1-day cure.

Figure 4-8 clearly indicates that there is no difference between the use of a type III vs a type I cement taken from the same source from 1-day cure. The minimal strain difference between 1-day cure and 28-day cure for type I cement lacks reasoning and has been attributed to potential measurement error.

4.2.4.2.4 Effect of HRWR Dosage

Figure 4-9 and Figure 4-10 show the drying shrinkage curve for two base concrete mixtures (M1-NC and M3-NC), each of which have a direct duplicate with varying HRWR dosages for 0.26 and 0.33 w/cm.

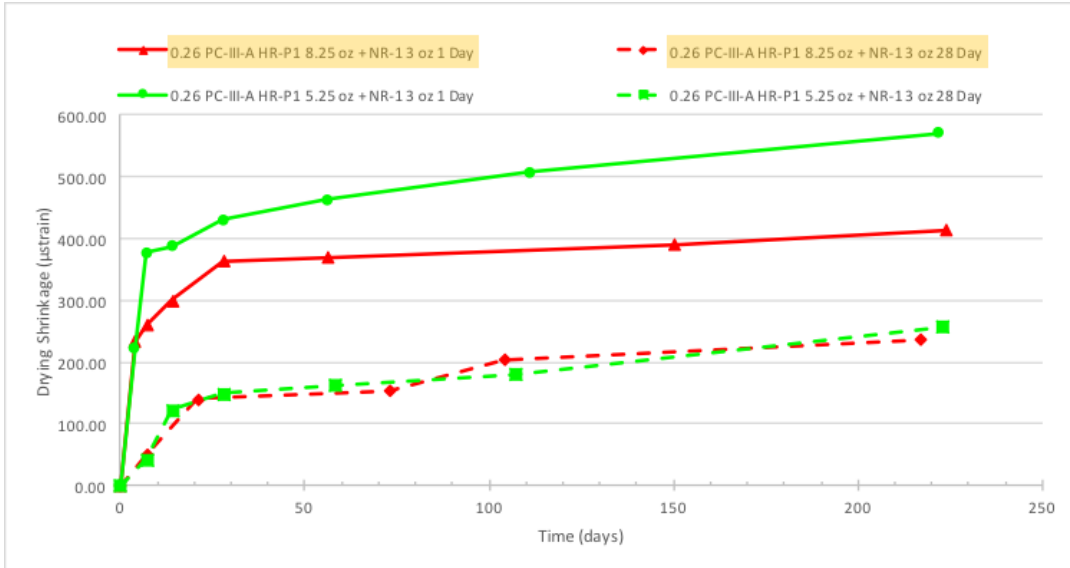


Figure 4-9: Drying shrinkage curve showing effect of HRWR dosage for base mixture for M1-NC for 1- and 28-Day curing.

Dashed lines correspond to 28-day cure; solid lines correspond to 1-day cure. Yellow shading denotes “bad performer” mixture from Table 4-1.

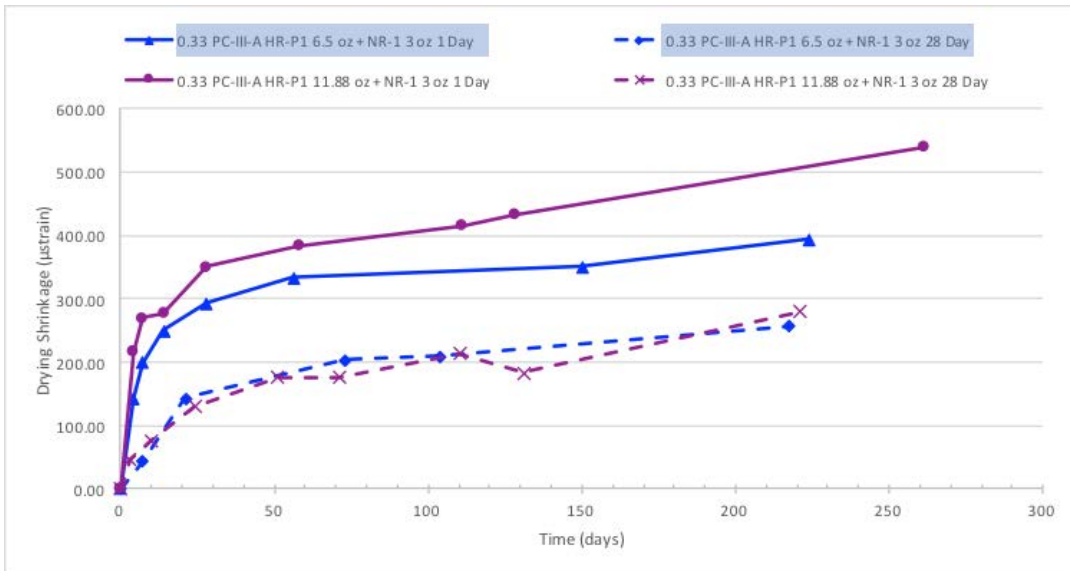


Figure 4-10: Drying shrinkage curve showing effect of HRWR Dosage for base mixture M3-NC for 1- and 28-Day curing.

Dashed lines correspond to 28-day cure; solid lines correspond to 1-day cure. Blue shading denotes “good performer” mixture from Table 4-1.

Figure 4-9 models base mixture M1-NC (0.26 w/cm with a HR-P1 8.25 fl oz/100 lb cement dosage and NR-1 3 fl oz/100 lb cement) compared to 0.26 w/cm mixture with a HR-P1 5.25 fl oz/100 lb cement with NR-1 3 fl oz/100 lb cement mixture. The mixture with lower HRWR dosage proves to continue to develop extensive shrinkage beyond the base M1-NC mixture. However,

Figure 4-10 tells a different story, as the increase in HRWR from 6.5 fl oz/100 lb cement to 11.88 fl oz/100 lb cement proves to develop shrinkage at a greater rate.

4.2.4.2.5 Effect of HRWR Type

Figure 4-11 and Figure 4-12 show the drying shrinkage curve for two base concrete mixtures (M1-NC and M4-SCC), each of which have a direct duplicate with three different HRWR types (HR-P1, HR-P2, and HR-P3) for 0.26 and 0.31 w/cm.

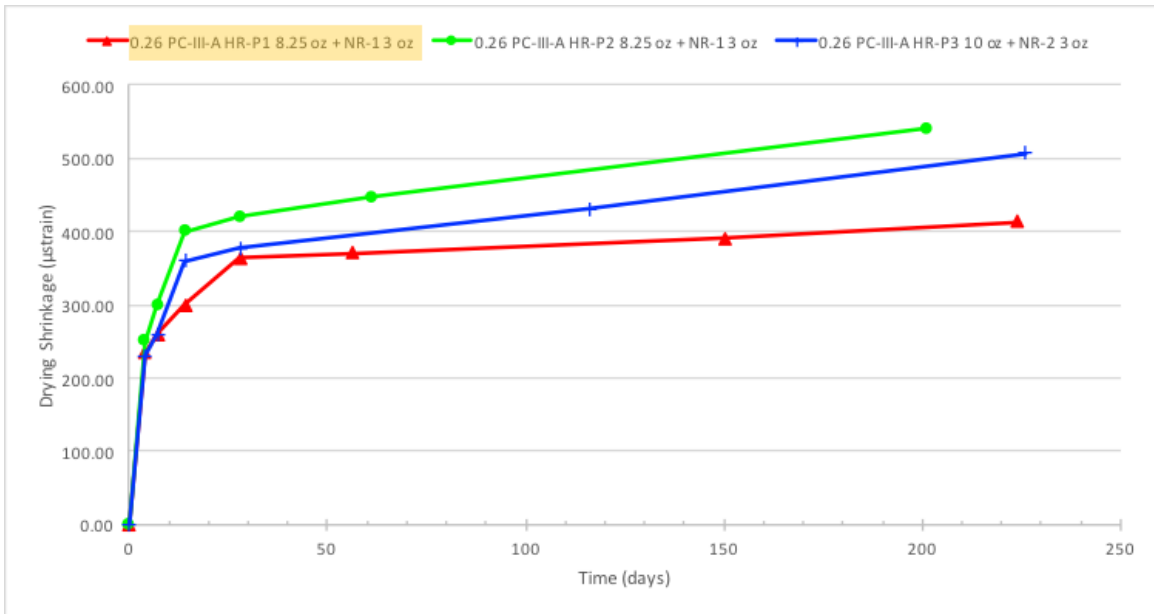


Figure 4-11: Drying Shrinkage Curve showing effect of HRWR type (HR-P1, HR-P2, and HR-P3) base mixture for M1-NC.

Yellow shading denotes “bad performer” mixture from Table 4-1.



Figure 4-12: Drying shrinkage curve showing effect of HRWR type (HR-P1, HR-P2, and HR-P3) for base mixture M4-SCC.

Blue shading denotes “good performer” mixture from Table 4-1.

Three different polycarboxylate-based HRWRs (HR-P1, HR-P2, and HR-P3) in conjunction with two different normal range water reducing and retarding (Type D) admixture (NR-1 and NR-2) were used for the comparison. The selection of the HRWR types along with their corresponding dosages were based on common admixture practices observed at precast plants, as well as targeted slumps obtained in the lab for proper consistency between different mixture designs.

For w/cm 0.26 mixtures, the comparison of drying shrinkage proved fairly similar between the three polycarboxylate (HR-P1, HR-P2 and HR-P3) mixtures, especially early ages, as shown in Figure 4-11. Continued development of shrinkage shows that HR-P1 shows the least amount of shrinkage followed by HR-P3 and HR-P2 with the largest amount of shrinkage. Whereas, Figure 4-12 with w/cm 0.31 mixtures, shows that the HR-P1 developed a significantly lower rate of shrinkage as compared with the other 0.31 w/cm mixtures with HR-P2 and HR-P3. Note, that in order to establish a similar slump to the other mixtures, the mixture containing the HR-P3 HRWR agent required an additional 2.25 fl oz/100 lb (i.e., dosage was 7.25 fl oz/100 lb cement in total) as compared to the mixtures. However, similar shrinkage between HR-P2 and HR-P3 was seen (see Figure 4-12).

4.2.4.2.6 Effect of Cement Content

Figure 4-13 and Figure 4-14 show the drying shrinkage curve for two base concrete mixtures (M1-NC and M3-NC), each of which have a direct duplicate with different Portland cement contents (705 lb/yd³, 517 lb/yd³, 658 lb/yd³ and 517 lb/yd³) for 0.26 and 0.33 w/cm. In order to have proper comparisons between each mixture with the w/cm ratio was held as a constant alongside the changing cement content.



Figure 4-13: Drying shrinkage curve showing effect of cement content for base mixture M1-NC.

Red line corresponds to mixtures with 705 lb/yd³ cement; green corresponds to 517 lb/yd³. Dashed lines correspond to 28-day cure; solid lines correspond to 1-day cure. Yellow shading denotes “bad performer” mixture from Table 4-1.

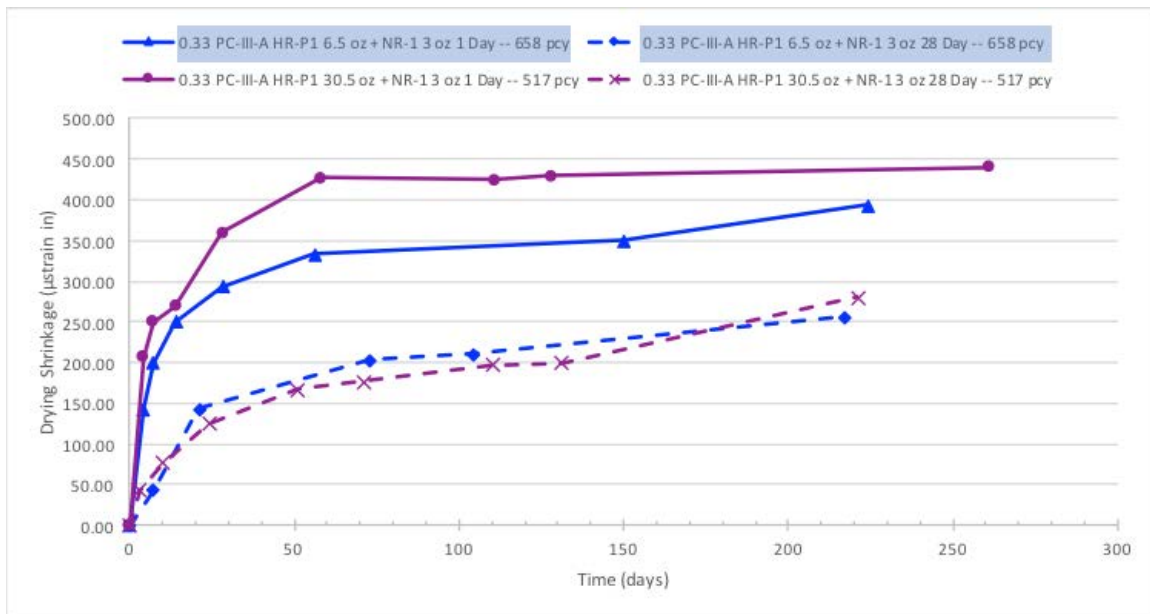


Figure 4-14: Drying shrinkage curve showing effect of cement content (658 lb/yd³ and 517 lb/yd³) for base mixture M3-NC.

Dashed lines correspond to 28-day cure; solid lines correspond to 1-day cure. Blue shading denotes “good performer” mixture from Table 4-1.

In order to establish similar slumps between the two cementitious contents shown in Figure 4-14, 30.5 oz was required with the 517 pcy mixture as compared with 6.5 oz for the 658 pcy mixture. Even still, the ultimate shrinkage did not appear to be affected by this substantial increase

in dosage. Since drying shrinkage is majorly experienced by the paste, it is reasonable that the mixtures with greater cement content develops greater volume change. Until equilibrium is met between the concrete specimen and the testing chamber continued shrinkage measurements should reveal that the mixtures with higher paste contents develop the largest amount of shrinkage.

4.2.4.2.7 Effect of Fly Ash Addition

Figure 4-15, Figure 4-16, and Figure 4-17 show the drying shrinkage curve for five base concrete mixtures (M1-NC, M3-NC, M4-SCC, M6-CFA, and M3-CWB), each of which have a comparative duplicate with different fly ash additions (25%, 33%, and 40% addition) for 0.26, 0.31, 0.33, and 0.40 w/cm.

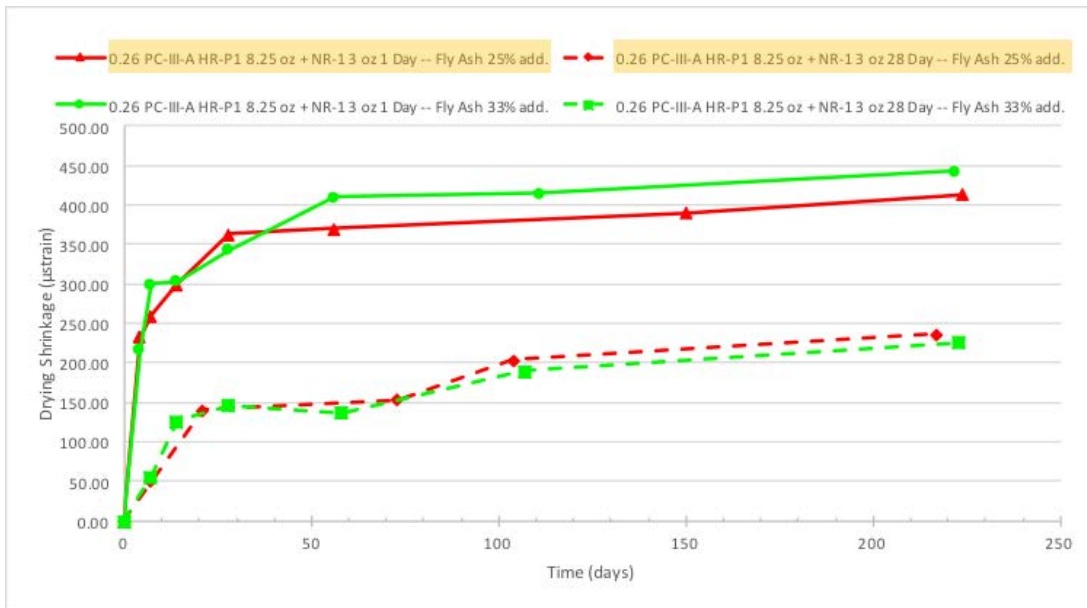


Figure 4-15: Drying shrinkage curve showing effect of fly ash addition (175 lb/yd³ – 25% add. and 233 lb/yd³ – 33% add.) for base mixture M1-NC.

Dashed lines correspond to 28-day cure; solid lines correspond to 1-day cure. Yellow shading denotes “bad performer” mixture from Table 4-1.

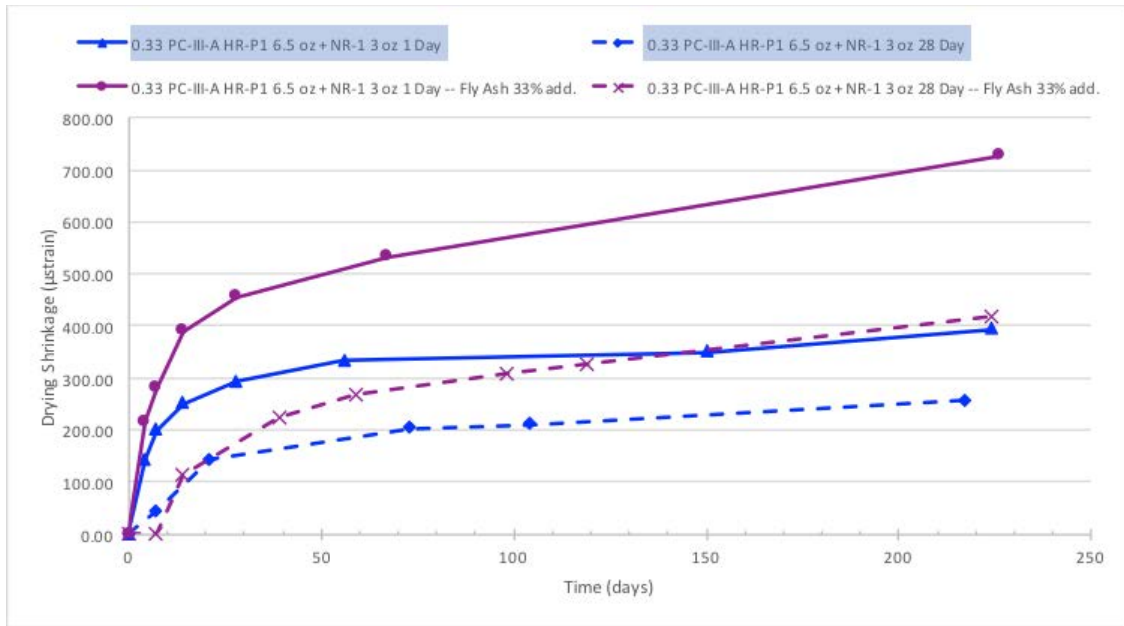


Figure 4-16: Drying shrinkage curve showing effect of fly ash addition (219 lb/yd^3 – 33% add) for base mixture M3-NC.

Dashed lines correspond to 28-day cure; solid lines correspond to 1-day cure. Blue shading denotes “good performer” mixture from Table 4-1.

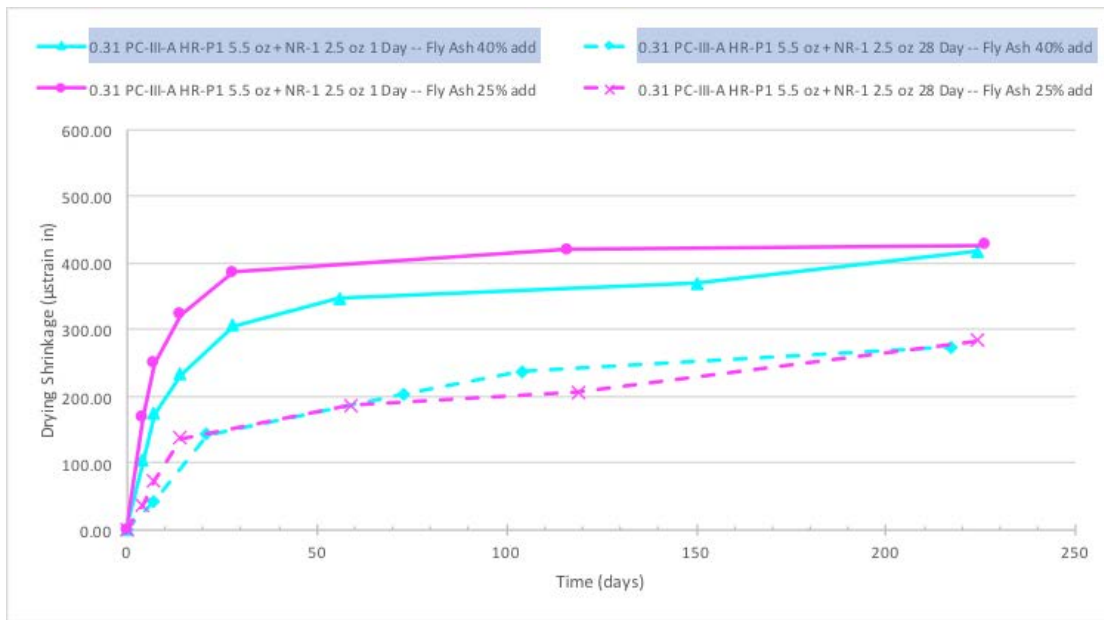


Figure 4-17: Drying shrinkage curve showing effect of fly ash addition (271 lb/yd^3 – 40% add and 165 lb/yd^3 – 25% add) for base mixture M4-SCC.

Dashed lines correspond to 28-day cure; solid lines correspond to 1-day cure. Blue shading denotes “good performer” mixture from Table 4-1.

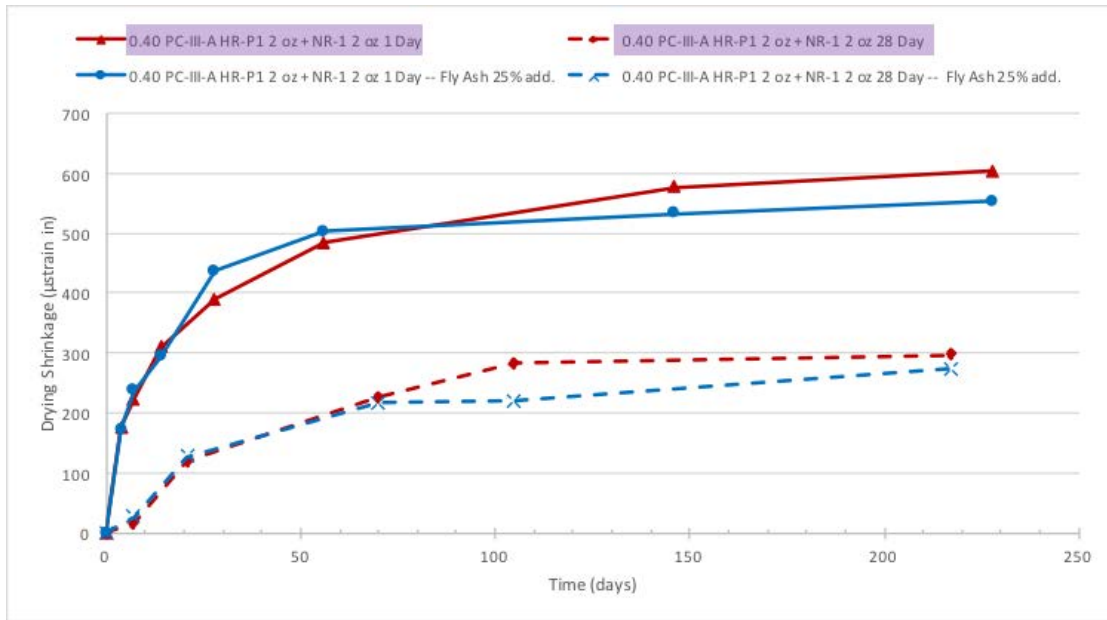


Figure 4-18: Drying shrinkage curve showing effect of fly ash addition (165 lb/yd³ – 25% add) for base mixtures M6-CFA and M3-CWB.

Dashed lines correspond to 28-day cure; solid lines correspond to 1-day cure. Purple shading denotes “CWB” control mixture from Table 4-2.

As depicted in all Figures 4-15 through 4-18, the greater the addition of fly ash by mass of cement (25%, 33% and 40%) the more shrinkage experienced by the specimen as compared with lower cementitious contents. This phenomenon is explained by the fact that the water-to-cementitious materials ratio was held constant and therefore with the increased addition of fly ash the mixing water was also increased. The increase in drying shrinkage can be attributed to the increase in both the mixing water content and paste content. If the mixing water was to be held constant or reduced despite the fly ash addition the shrinkage of the fly ash incorporated mixtures would be substantially lower than the straight cement mixtures (Thomas 2007) (Brooks and Jiang 1999).

4.2.4.2.8 Effect of Lightweight Aggregate

Figure 4-19 shows the drying shrinkage curve for three concrete mixtures (M3-NC, M3-CSP and M3-CLWA) all with 0.33 w/cm ratio, but varying fine aggregate sources FA-A, FA-B and FA-LW.

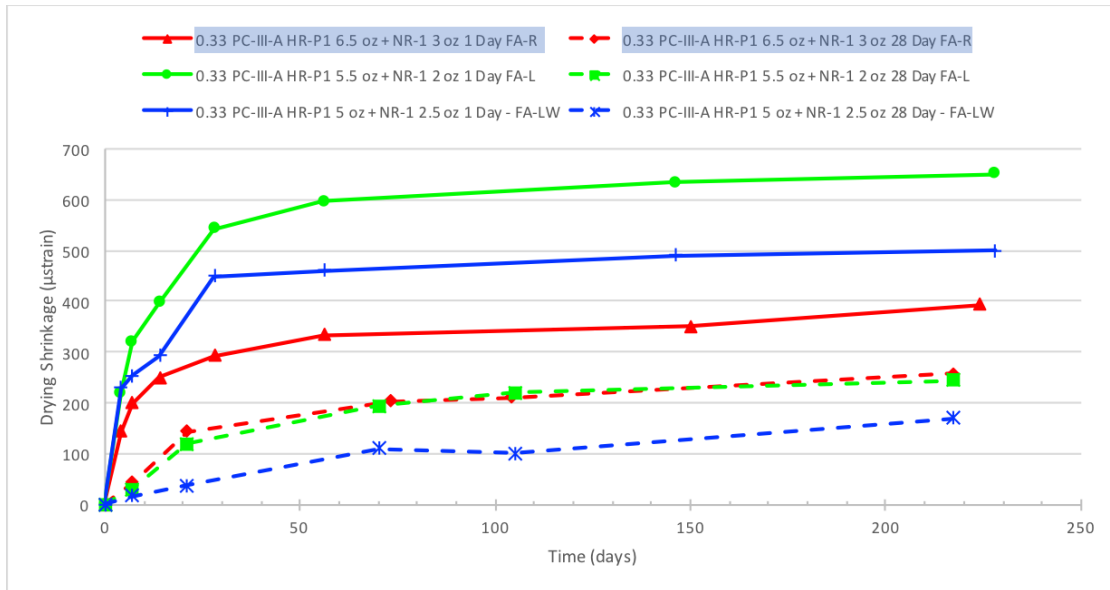


Figure 4-19: Drying shrinkage curve showing effect of fine aggregate source (FA-A, FA-B and FA-LW) for mixtures M3-NC, M3-CSP and M3-CLWA (20% of the fine aggregate replacement with lightweight aggregate).

Dashed lines correspond to 28-day cure; solid lines correspond to 1-day cure.

Literature has shown that the use of saturated lightweight fine aggregate can aid in internal curing of the concrete and mediate or even eliminate autogenous shrinkage effects, while maintaining the critical tensile stress well under the tensile capacity of the concrete (Cusson 2008). Yet in order to have true comparison of w/cm ratio proper care must be taken as to not provide excess water to the mixture with respect to the saturated light aggregate. Prior to mixing the manufactured light weight aggregate the sand was oven dried. Then 24 hours prior to mixing, the water required to get the sand in a saturated surface dried state (SSD) in addition to several pounds of mixing water was used to fully submerge and soak the sand. Despite the special attention that was provided to mixing with FA-LW the benefits of using the lightweight aggregate remain to be unseen with respect to drying shrinkage measurements.

4.2.4.3 Summary and Conclusions

Based on the results of this section the following conclusions may be drawn:

- “Good” and “Bad” Performers: ASTM C494 cannot properly discern between mixtures prone to cracking and not prone to cracking through the non-specific approach. For example, for each individual comparison both the “good” and “bad” performance mixtures showed less shrinkage than the mixtures that the individual parameter was compared to.
- The increase in w/cm ratio when the paste volume is held as a constant was directly related to an increase in ultimate drying shrinkage of the concrete. The w/cm ratio proved to be the greatest governing factor with respect to effecting ultimate drying shrinkage measurements.
- The two cement sources (PC-III-A and PC-III-B) for the same mixture designs developed different drying shrinkage curves. PC-III-B in all cases developed significantly greater

linear strain from drying shrinkage as compared with PC-III-A. This could be related to the coarser cement grain size of PC-III-A, which creates a less porous microstructural network structure than the PC-III-B cement. This has the effect of reducing chemical and thereby autogenous shrinkage in the initial weeks after casting (Ei-ichi et al. 1994).

- Differences in cement type PC-I-A and PC-III-A proved to have minimal effects with respect to drying shrinkage.
- It has been well established in literature that higher paste content results in greater drying shrinkage. It is believed that the ultimate drying shrinkage for the mixtures compared in this report will inevitably confirm that higher paste content results in higher linear drying shrinkage stain.
- The incorporation of fly ash addition as compared to straight cement mixtures resulted in increased drying shrinkage. This can be attributed to the increase in paste content that was a result of holding the water-to-cementitious ratios constant.
- No conclusion can be drawn from the incorporation of FA-LW with respect to drying shrinkage. Continued measurements may reveal more latent effect of the ultimate reduction in drying shrinkage as compared with the other two aggregate sources. At 224 days the mixture with the siliceous aggregate FA-A has experienced the least amount of shrinkage for 1-day cure.

4.3 Suitability of ASTM C494: Results and Conclusions

Currently, the Standard Specification for Chemical Admixtures in Concrete, ASTM C494, attempts to evaluate admixtures based on limited testing procedures, none of which are able to properly quantify the extent of the latent cracking effect as seen in the field as a result of excessive shrinkage. Therefore, the tests revealed that the hypothesis of implementing a specific and nonspecific approach with ASTM C494 is not capable of discerning “good” and “bad” performers. Below is a bulleted summary of the results of each individual test performed:

- *Water Content:* Both the “good” and “bad” performers passed with respect to the CWB control mixture. Therefore, water content evaluation cannot be used to predetermine a mixture designs cracking potential.
- *Time of Set:* Both the “good” and “bad” performers passed and failed for half of their respective mixtures. Therefore, time of set should not be used as a discernable means of evaluating a mixture designs cracking potential.
- *Compressive Strength:* Both of the “good” and “bad” performers passed or failed approximately half of the set compression limits and according dates for ASTM C494. Therefore, compressive strength should not be used as a discernable means of evaluating a mixture designs cracking potential.
- *Drying Shrinkage:* Both of the “good” and “bad” performers passed or failed half of limits set in ASTM C494 and at the last available measurement date (6-months). Therefore, drying shrinkage should not be used as a discernable means of evaluating a mixture designs cracking potential.

Chapter 5. Parametric Study: Developing a Complementary Testing Matrix to ASTM C494

5.1 Introduction

Based on the preconceived notion that ASTM C494 testing procedures would likely be inadequate towards testing HRWR’s potential towards inciting micro-cracking in concrete mixtures, a complementary testing matrix to ASTM C494 was developed. This matrix consisted of a parametric study based on concrete mixtures and paste mixtures to the restrained shrinkage and autogenous shrinkage behavior of the mixtures (see Figure 5-1). Due to the disconnect between concrete and paste results with respect to autogenous testing the results of each were discussed separately. Thus, this chapter is divided into two major sections: Concrete Testing (5.2) and Paste Testing (5.3). Both concrete and paste analysis testing required completely new integration and development of instrumentation. Detailed information is provided regarding the newly developed testing setups to ensure that the testing setups can be replicated and/or improved upon in the future.

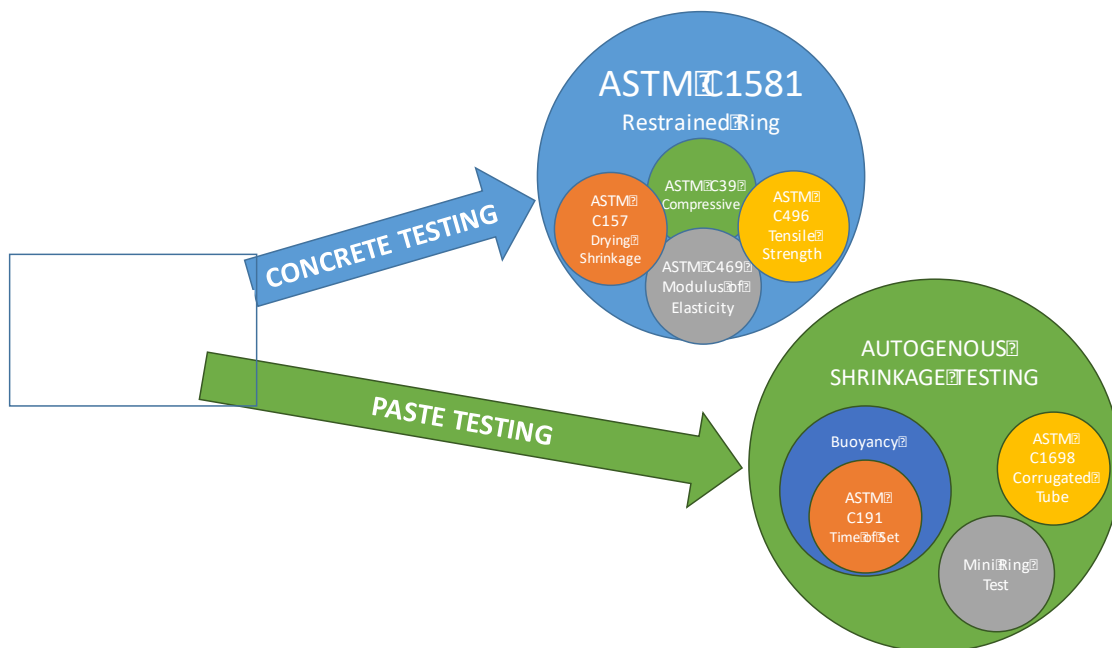


Figure 5-1: Parametric study testing breakdown between concrete and paste analysis

5.2 Parametric Study: Concrete Testing

This section presents the laboratory parametric study that was developed to investigate HRWR ASTM C494 Type F prevalence towards increased latent micro-cracking in concrete. The testing involved evaluating select concrete mixtures with HRWR in order to study their effect on causing cracking in the restrained shrinkage ring test, ASTM C1581. The mixtures employed were selected based on actual precast plant mixtures that had proven to develop latent micro cracking in the field. Table 5-1 presents the mixtures selected for concrete evaluation in the restrained ring test.

Table 5-1: Concrete mixtures subjected to the restrained ring test parametric study

Mix ID	w/cm	Cement Type	Cement Content (lb/yd ³)	SCM Content (lb/yd ³)	Aggregate Source		Admixtures			
					FA	CA	Type	(floz/100 lb cement)	Type	(floz/ 100 lb cement)
Mix 7	0.26	PC-III-A	705	175	FA-R	CA-R	HR-P2	8.25	NR-1	3
Mix 6			705	175	FA-R	CA-R	HR-P3	10	NR-2	2
Mix 4		PC-III-B	705	175	FA-R	CA-R	HR-P1	8.25	NR-1	3
Mix 3	0.28	PC-I-A	705	-	FA-R	CA-R	HR-P1	12	NR-1	3
Mix 1		PC-III-A	705	-	FA-R	CA-R	HR-P1	12		3
Mix 5	0.3	PC-III-A	564	188	FA-RII	CA-RII	HR-P3	8.25	NR-2	2
Mix 8	0.31	PC-III-A	663	271	FA-R	CA-R	HR-P4	7.25	NR-2	2.5
Mix 2	0.33	PC-III-A	658	-	FA-R	CA-R	HR-P2	12	NR-1	3

**Note: mix nomenclature here (“Mix 7”) is entirely separate from previous nomenclature presented in Chapter 4.*

It is important to note that the Mix 7 presented in Table 5-1 is not the same as the Mix 7 presented in Chapter 4. However, there is some overlap between mixture proportioning. Unfortunately, because of the necessary targeting of a workable slump, the dosage of HRWR varies so that no mixture tested in restrained shrinkage perfectly matches the mixture proportioning of mixtures in Chapter 4. When comparing mixture proportions between good performers and poor performers, the difference in mixture proportioning is often extremely sensitive, as evidenced by exposure blocks at the UT exposure site made with supposedly the same mixture proportions, but resulting in poor performance when made by 1 institution and good performance when made by another. Nevertheless, the details about the mixtures in Table 5-1 are provided with context with the other mixtures evaluated in this project.

- Mix 5 is very similar (slightly higher admixture dosage and different admixture type) to “G1” in Chapter 4, which is a known good performer.
- Mix 1 is similar to an exposure block at the UT site (Block B1) which has not cracked.
- Mix 3 is similar to an exposure block at the UT site (Block BP-1) which has not cracked and also similar to (varying types of admixture used and dosage of NR) B1, a known poor performer.
- Mix 8 is similar to 2 exposure blocks at UT, one of which has cracked (Block PP-A, different dosage of NR), and one of which has not cracked (Block PP-A Lab SCC, has a different admixture type).
- Mix 7 has the same proportions as BP-5, an exposure block at the UT site has cracked.
- Mix 6 is also similar to BP-5, an exposure block at the UT site which has cracked, but was made with a different HRWR and the HRWR dosage was lower than that used in BP-5.
- Mix 2 has a similar exposure block at the UT site (BP-2) which has not yet cracked at 18 months of age. However BP-2 was made with a different HRWR

5.2.1 Restrained Shrinkage Rings

5.2.1.1 Procedure and Experimental Setup

As described in Chapter 2, the testing program employed for measuring stress development in concrete due to restrained shrinkage is the restrained shrinkage ring test as per ASTM C 1581. The restrained shrinkage ring test was implemented along with drying shrinkage prisms with like surface area to volume ratio as well with 3x6-in. cylinders that were subjected to the same drying and temperature conditions. These complementary samples were cast with the rings to procure compressive, tensile and modulus of elasticity properties at 1, 3, 7, and 28 days after casting. This section will discuss how the measured mechanical properties coincide as well as how these properties may be used to predict the results derived from the restrained ring setup.

The setup that was implemented at the University of Texas at Austin was created to fulfill the requirements outlined in ASTM C1581, as well to as implement cost-effective modifications as per current literature and developments in the test. The core of the setup is built around a mild, 0.5 ± 0.05 -in thick, steel ring. The outer diameter of the ring was 13.0 ± 0.12 -in. The inner and outer circumferences of the rings were machined to a specification of at least 63 micro-inches. An

outer ring constructed of HPVC pipe was placed around the steel ring. The diameter of the HPVC ring was 16.0 ± 0.12 -in. and the height of the HPVC ring was 6.0 ± 0.25 -in. The HPVC ring was cut or “slit” longitudinally in order to allow the user to de-mold the concrete ring at final set. The slit was re-aligned through a stainless steel vise, Figure 5-2 shows (pictured alongside the CAD drawing).

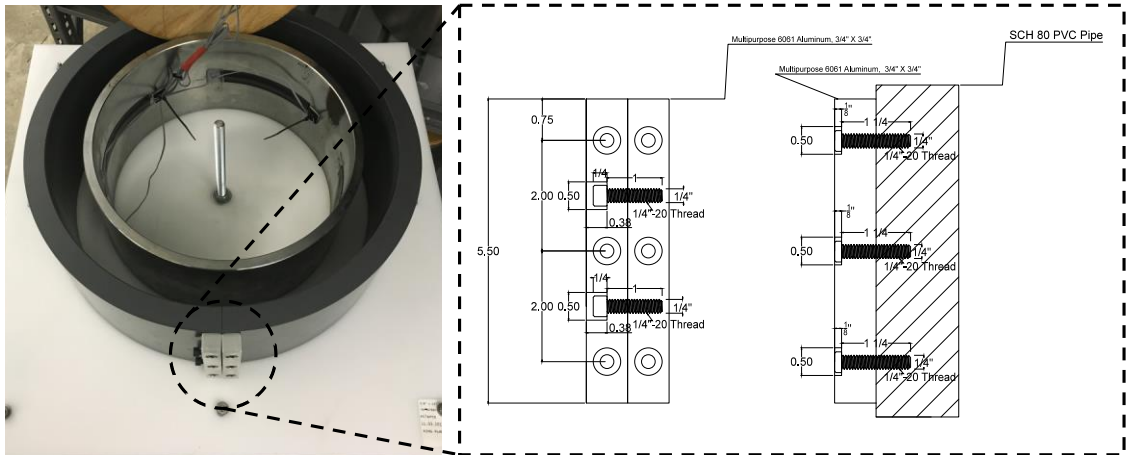


Figure 5-2: Stainless steel vise and CAD drawing used to align the 6-in. longitudinal slit in the outer HPVC 16-in. pipe

Both the steel ring and the outer HPVC rings were set on a 3/8-in. thick, 24x24-in. dimensions, rigid HDPE polyethylene plastic sheet. The plastic was selected for its low friction, non-absorptive and economical cost properties. The plastic bases were routed or grooved in order to accept both the inner steel ring and the outer HPVC 16-in. inner diameter pipe. The grooved edges created a tight seal between the rings and the plastic substrate as well as assured that the rings were set perfectly centered within one another. The bases have three locations to secure and lock down the outer HPVC ring into place as and the inner ring is locked into place through the use of a centralized piece of 1/2” stainless steel all-thread. Both mechanisms for securing the inner and outer rings during casting are pictured in Figure 5-3.



Figure 5-3: Locking locations for securing the inner and outer rings to the restrained shrinkage ring bases denoted in red

The strain monitoring aspect of the restrained shrinkage rings is composed of four two-wire strain gauges (FLA-6-11-1L). The gages are set at the midpoint of the ring and at a quarter circumferential distance from one another. The gages are set using Loctite (496 Instant Adhesive) epoxy and have been carefully oriented to measure solely lateral deformation. The gages are each covered by viscoelastic membrane (Dow 700) to assure that they are not disturbed during the casting process and/or encounter future corrosion issues. The gage wire is carefully tapered around the ring and the bound up and set into a terminal that is seated on a wood casing. The wire terminal accepts the +/- from each of the strain gauges and strategically organizes the wire within the box denoting the gage location on each of the rings. Figure 5-4 and Figure 5-5 provide a photo of the gages that are set in each of the restrained rings as well as a diagram of the input terminal with each of the gages H (+) and L (-). These figures also show the location of the strain gage relative to one another. Note that Figure 5-4 denotes the location of where the collection of strain gage wires have been set through. At this location the strain gage wire leads are accepted on the other side into the input terminal as shown in Figure 5-6.

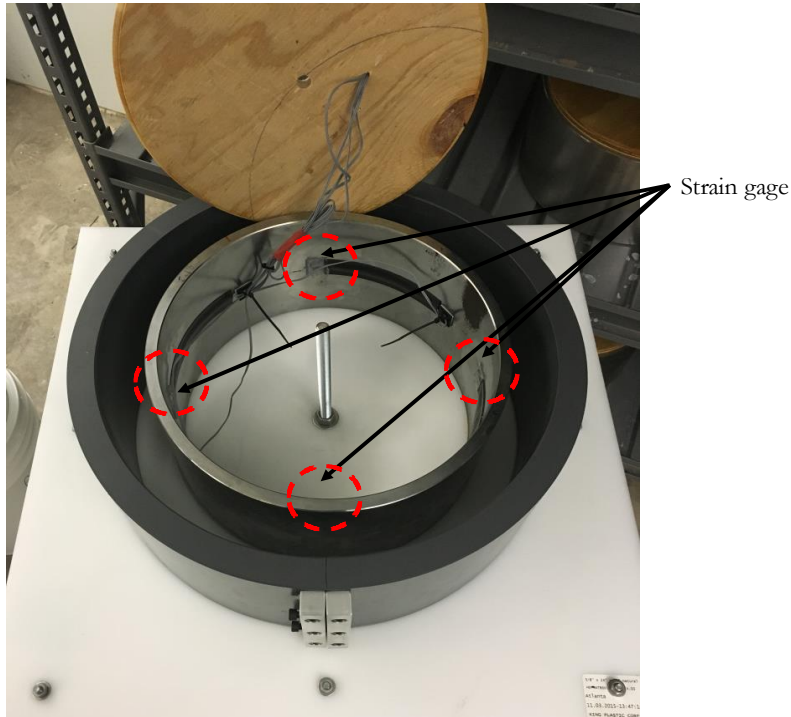


Figure 5-4: Strain gage locations on restrained shrinkage ring

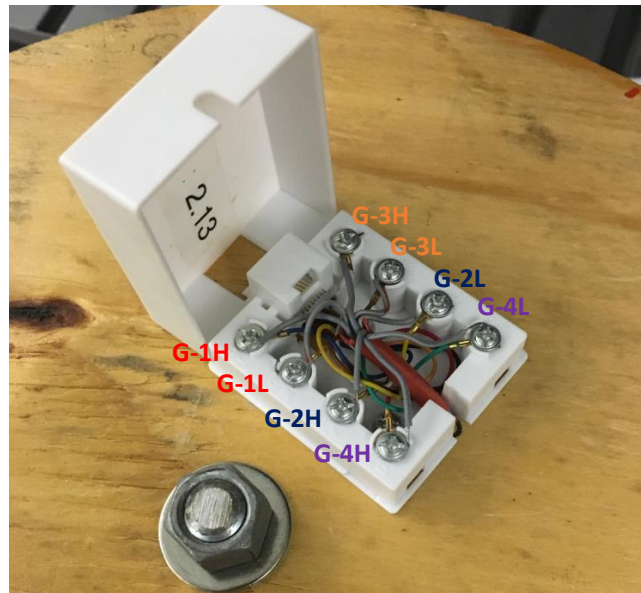


Figure 5-5: Terminal diagram for restrained shrinkage ring strain gages

From the terminal input an Ethernet cable with wires that are individually insulated to reduce interference is used. The Ethernet cable was selected based on the gage wire similarity to the strain gages as well as its economic properties and individually insulated cabling. The Ethernet cables are set just above each of the rings dropping down just over the top of the terminal inputs as pictured in Figure 5-4. From the rings the Ethernet cables are run to the data acquisition system

(DAQ). Figure 5-6 denotes the setup implemented at the University of Texas at Austin for collecting strain data on the restrained shrinkage rings.

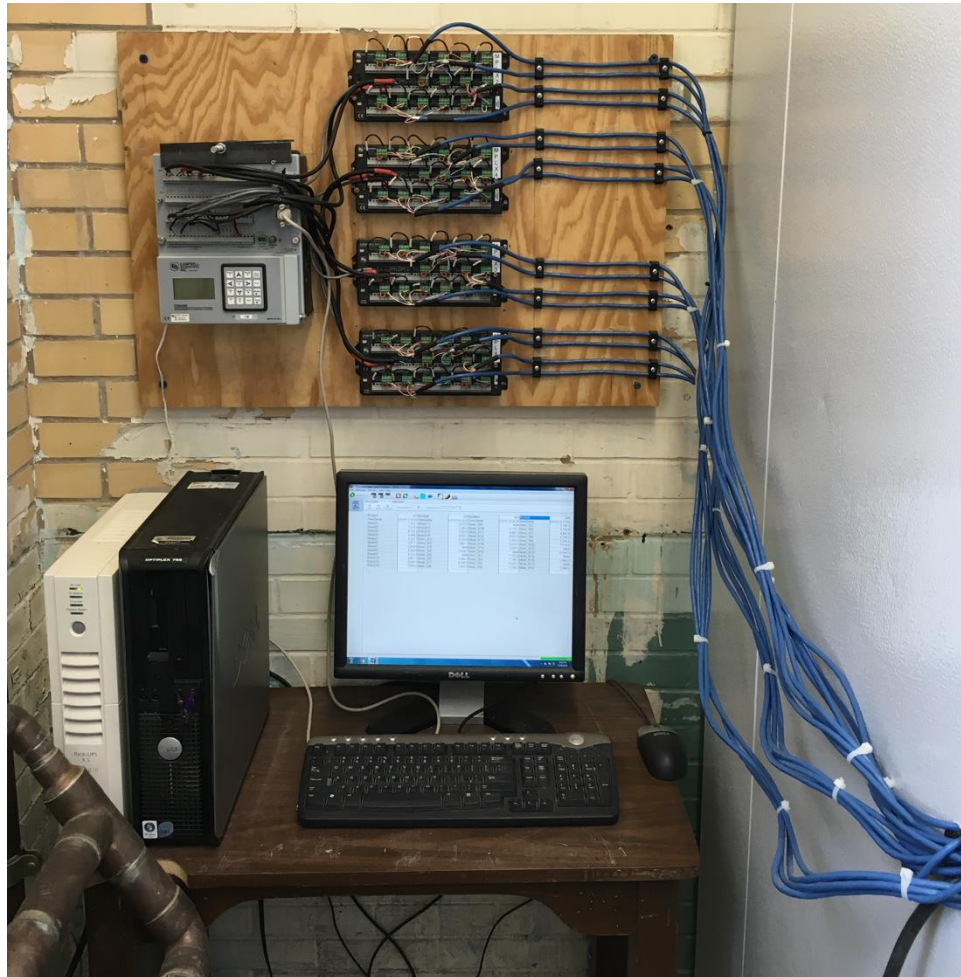


Figure 5-6: DAQ setup employed at UT Austin for collecting restrained shrinkage ring strain data

The central component of the restrained shrinkage ring DAQ is a Campbell Scientific CR 5000. Extending from the CR 5000 is a set of four multiplexers (AM 16/32). Each of the multiplexers have the capacity to collect data from 16 strain gages and therefore the capacity to measure four restrained rings setups. From the multiplexers, calibrated terminal input modules (TIM) (4SWB120's) have been used in order to collect the data from each of the strain gages. The TIM each act as the three other quadrants of a Wheatstone bridge. Each of the strain gages are directly connected to a TIM. A diagram of the DAQ and how it is interconnected with the restrained shrinkage ring is shown in Figure 5-7.

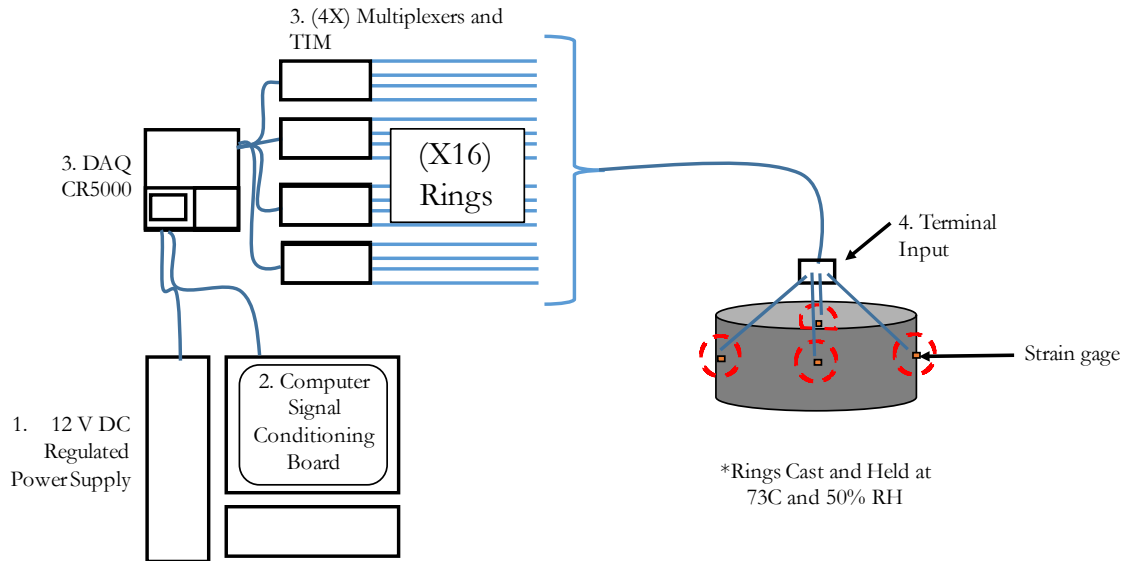


Figure 5-7: Diagram of the restrained shrinkage ring setup

The DAQ was programed in Campbell Scientific CR Basic program via PC400. The program calls to excite the strain gages every minute and collect data on each of the gages at 5 min intervals. The excitations were supplied with a second of interim delay between each subsequent reading to not provide interference between adjacent gages. The shortcut programing code implemented for this projects has been outlined in Appendix V.

The casting procedure of the restrained shrinkage rings followed the process outlined in ASTM C1581. The concrete was cast and set in thermally controlled rooms at $23 \pm 3^{\circ}\text{C}$. Prior to casting the ring molds were sufficiently oiled and individually set on a vibrating table. Each ring was cast in two lifts, where each lift was subjecting to rodding for a 75 count as well as 30 sec of vibrating on a vibrating table to eliminate entrapped air and reduce “bugholes” on the concrete’s surface. Assuring that the surface has limited imperfections is key to determine the true time of cracking. In the event that large entrapped air voids propagate along the surface, the concrete ring will have a smaller cross sectional area to combat the tensile stresses and can cause the ring to crack and fail prematurely. Three rings were cast for each mixture. Figure 5-8 provides a photo of the ring on the vibration table.



Figure 5-8: Casting restrained shrinkage ring on vibrating table

Since the rings were cast in the testing environment, the rings went directly from the vibrating table and into position on the drying racks. Once the rings were set into position, the Ethernet cables were connected to the terminal input and wet burlap was applied as well as plastic sheets to insulate the wet burlap over the exposed concrete surface. The outer HPVC ring was released and removed at the time of final set. Final set was determined by ASTM C403, measuring penetration resistance of mortar specimens obtained from the concrete by sieving through a number-4 sieve. The strain was taken as zero from the point at which the rings were demolded and re-positioned onto the drying racks. The rings were sealed with HVAC tape on the tops and bottoms of the rings to facilitate solely circumferential drying shrinkage effects. Figure 5-9 shows four mixtures (three rings for each) being monitored in the testing environment (23°C and 50% relative humidity).



Figure 5-9: Restrained shrinkage rings (four mixtures), monitored in the testing room

As discussed in Chapter 2 of this report, the stress rate in the steel rings was calculated using Equation 2-10. The average of all four strain gages was plotted with respect to the square root of time. An example for Mixture 8 is shown in Figure 5-10. The alpha, α , in Equation 2-10 is obtained using a best fit linear line for the strain development measured from the strain gages on the steel from the shrinking concrete. The strain is plotted over the square root of time after demolding the specimens.

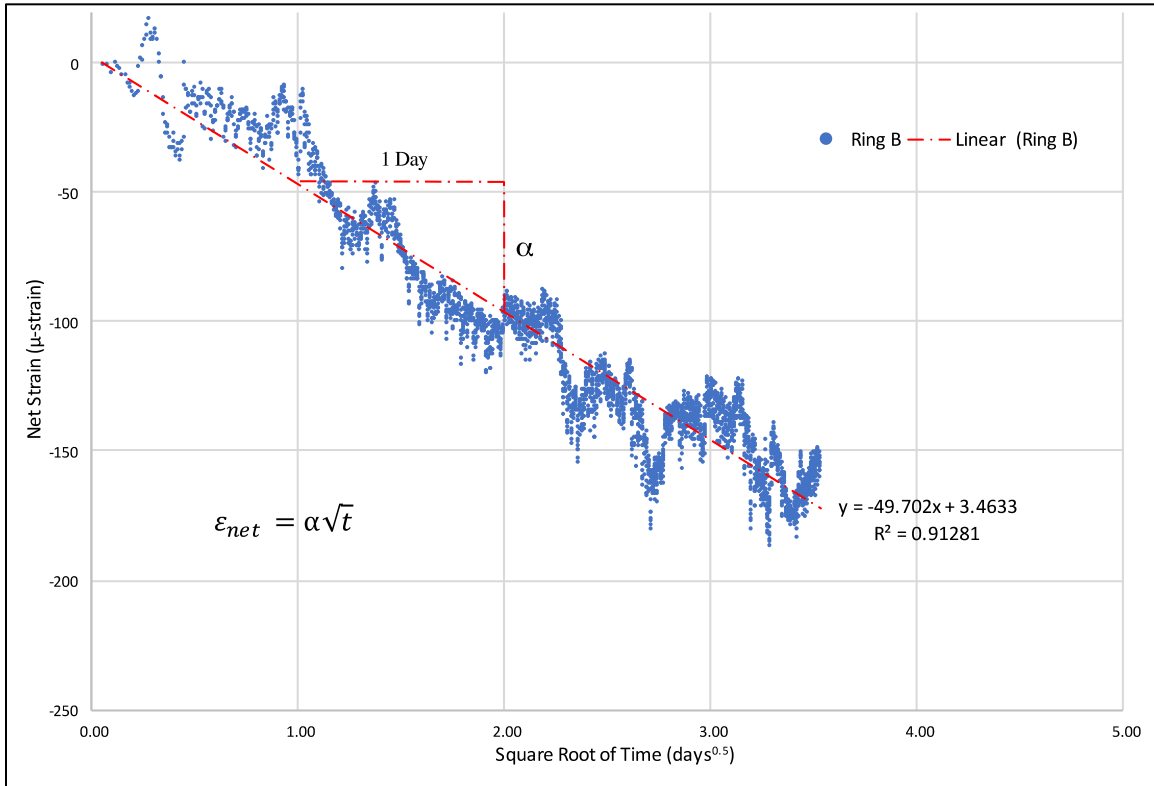


Figure 5-10: Net strain versus the square root of time (days) after demolding for Mixture 8

Furthermore, based on work performed by See et al. (2004), complementary cylinders held in the same curing conditions as the restrained shrinkage rings were cast for evaluation of mechanical properties with respect to strength and modulus as well as prisms for drying shrinkage. These complementary specimens were evaluated at 1, 3, 7, 14, and 28 days after casting. Assuming that the steel ring provides the degree of restraint, R_m , as a function of concrete's modulus, E_c , can be determined using Equation 5-1 (See et al. 2004):

$$R_m \cong 1.0-7.4 \cdot 10^{-3} E_c \quad \text{Equation 5-1}$$

5.2.1.2 Result and Discussion

To gain insight about the temporal development of the concrete's mechanical properties, cylinders for mechanical properties measurements and prisms for free drying shrinkage measurements were cast in conjunction with the restrained shrinkage rings. Table 5-2 shows the mechanical properties development at 1, 3, 7, and 28 days relative to the stress rate and net time to cracking observed in the restrained ring test.

Table 5-2: Net time-to-cracking and stress rate for all ring mixture

RSF Mixture ID	Age (days)	Compressive Strength (psi)	Splitting Tensile Strength (psi)	Modulus of Elasticity (ksi)	Net Time to Cracking (days)	Stress Rate Cracking Psi/Day
Mix 1	1	5591	790	2478	25	20.5
	3	8127	790	3108		
	7	8698	1059	3498		
	28	9594	979	2720		
Mix 2	1	3606	501	1885	26	11.7
	3	5953	655	2655		
	7	6728	584	2934		
	28	8017	1009	2650		
Mix 3	1	1292	275	873	5	99.5
	3	5037	706	2513		
	7	5980	840	2467		
	28	6790	774	2576		
Mix 4	1	6096	578	2059	5	105.4
	3	9583	928	2628		
	7	10529	947	2877		
	28	11614	1101	2865		
Mix 5	1	3566	576	2200	TBD	TBD
	3	5016	838	2543		
	7	5395	809	2905		
	28	-	-	-		
Mix 6	1	7597	860	1901	22	37.9
	3	9921	1125	3041		
	7	11028	1090	2907		
	28	-	-	-		
Mix 7	1	1915	857	1421	14	47.6
	3	9375	986	2946		
	7	11066	929	2977		
	28	-	-	-		
Mix 8	1	7110	839	2675	TBD	TBD
	3	5016	838	2867		
	7	10801	1012	2869		
	28	-	-	-		

Table 5-2 shows that the greater the stress rate (psi/day) the sooner the cracking of the concrete ring occurs. Time of cracking and mechanical properties with respect to tensile strength modulus and compression strength for all completed (cracked) mixtures was further analyzed in Figures 5-11 through 5-13. The plots were constructed to approximate the mechanical properties at the mixture's cracking point through linear interpretation.

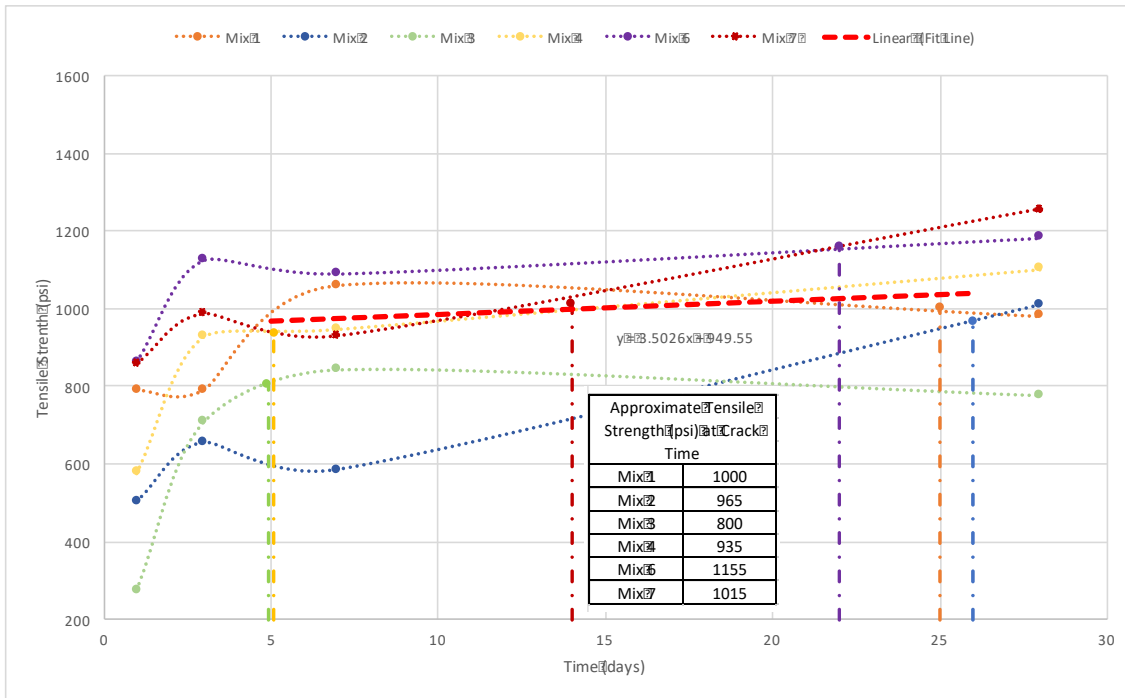


Figure 5-11: Tensile strength (psi) approximately determined through curve fit at time of cracking

Although tensile strength does not show significant development or rate of change between 1 and 28 day measurements, the standard deviation between the date of cracking and the best fit linear interpretation of the approximated tensile strength (psi) data points at cracking is approximately 100 psi (105 psi). Eliminating mixture 3, which is a Type I cement mixture (used for comparison purposes), the standard deviation is reduced to 75 psi. Based on the data tabulated in Figure 5-12, there is a strong correlation between the concrete’s tensile strength development and cracking date.

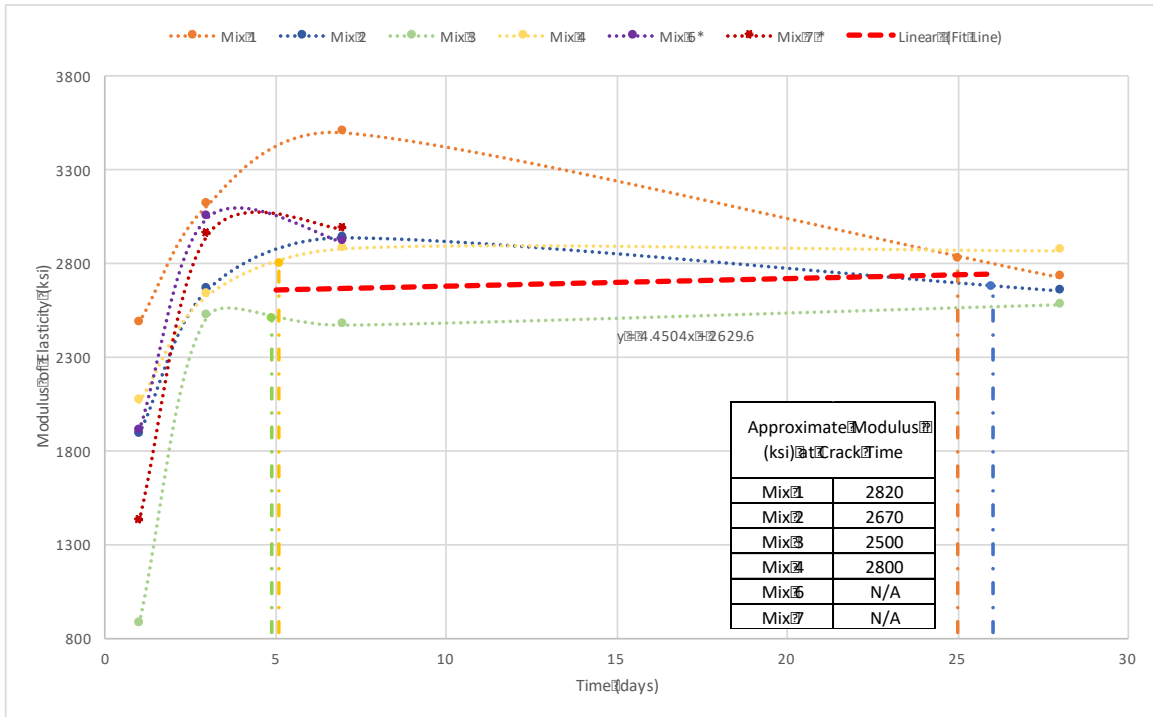


Figure 5-12: Modulus of elasticity (ksi) approximately determined through curve fit at time of cracking.

Best fit line (linear) outlined in red.

The average plotted modulus of elasticity development is shown by the best fit interpretation of modulus (ksi) at cracking, which has a very small slope and centers around 2600 ksi (2629.6 ksi). Unfortunately, results were based upon four mixtures as Mixes 6 and 7 cracked at an unusual age and Mix 8 segregated so that it did not exhibit a standard single crack, but rather steadily cracked through the segregated paste. The standard deviation between approximate modulus at cracking is less than 130 ksi (128 ksi). Again, after eliminating Mixture 3 (which is a Type I cement mixture), the standard deviation is reduced to 65 ksi. Based on the data tabulated in Figure 5-13 there is a very strong correlation between the concrete's modulus of elasticity and cracking date.

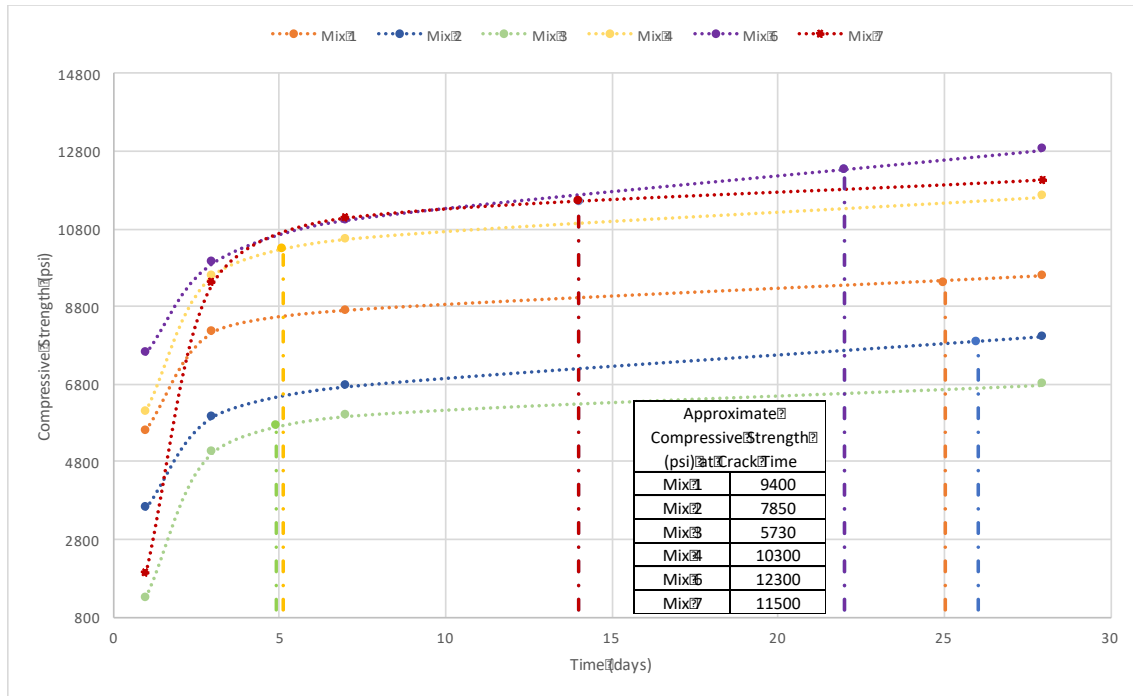


Figure 5-13: Compressive strength (psi) approximately determined through curve fit at time of cracking

The standard deviation for compressive strength data for the six mixtures that had a distinct cracking strain at under 30 days was over 2000 psi (2214 psi). Even omitting Mixture 3 data the standard deviation of compressive strength at approximate time of cracking was over 1500 psi. Due to this disconnect a more detailed investigation was performed to determine cracking performance with respect to previous literature.

A data set was mapped correlating 7-day drying shrinkage and 7-day modulus of concrete, and this data set was compared against the cracking potential envelopes (high, moderate-high, moderate-low and low) developed by See et al. (2004) (see Figure 5-14). Figure 5-14 shows that in reference to See’s work (2004) the cracking potential of the mixture designs performed in this project have extremely low cracking potential. All mixtures employed in this study displayed cracking potentials that were lower or on par with the HPC mixtures evaluated in See’s investigation (2004).

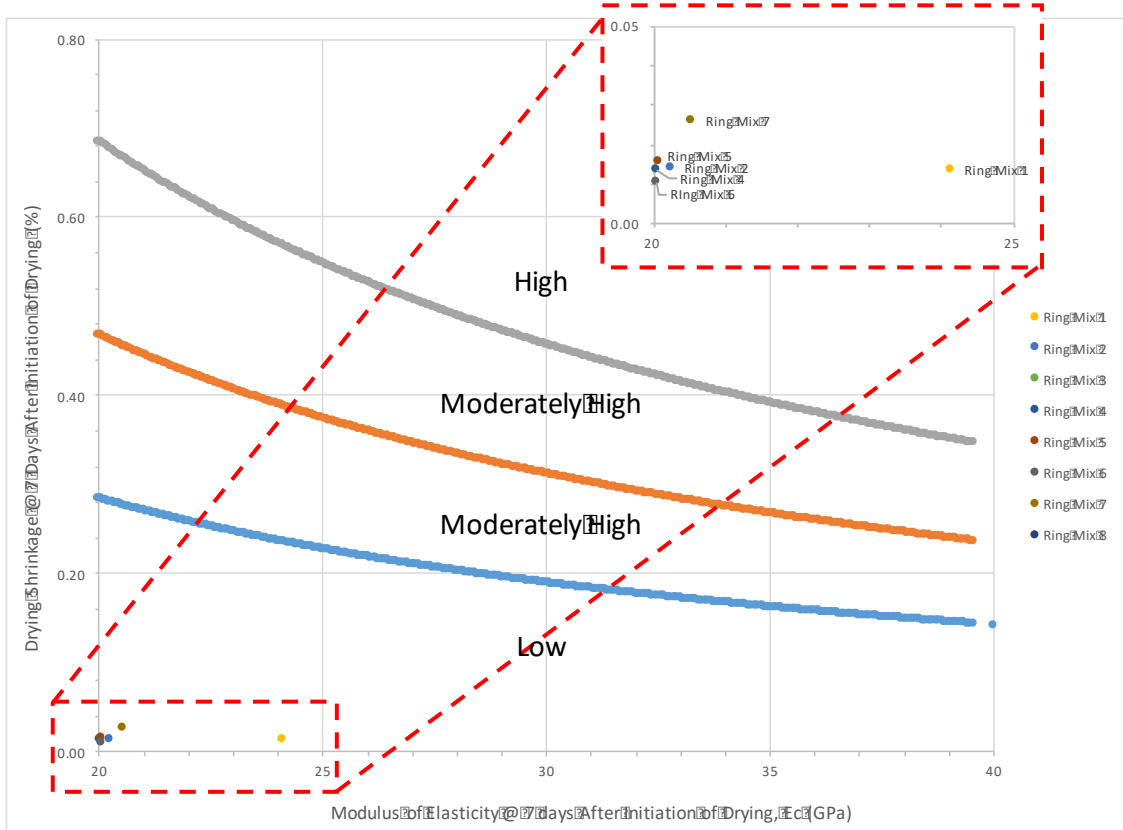


Figure 5-14: Cracking potential envelopes outlining the potential for each of the eight mixture designs cast

Figure 5-15 displays the average temporal evolution of strain data for each mixture (note that it is based on the average of three rings). Individual mixture design ring strain shrinkage results may be found in Appendix VII.

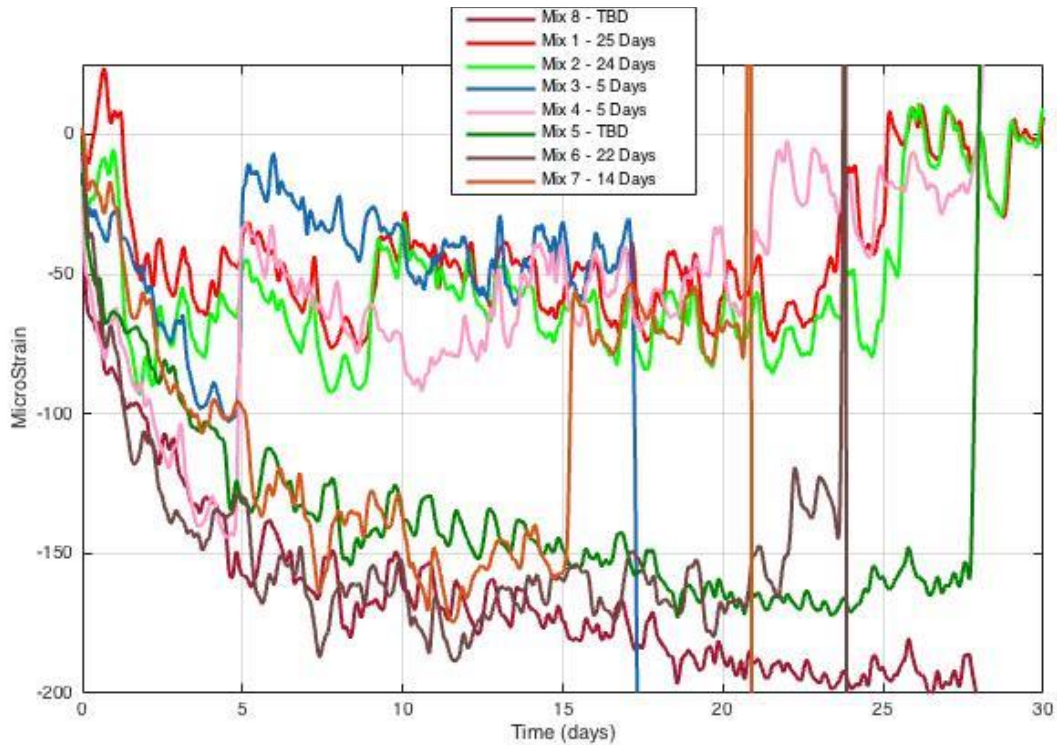


Figure 5-15: Net microStrain development over time (days) for all ring mixtures.
 Number after mix id in legend denotes the age of specimen when cracking occurred.

5.2.1.2.1 Effect of Cement Type

Figure 5-16 shows the effect switching from cement type III (displayed as Mix 1 and made using cement PC-III-A) to a Type I cement (denoted as Mix 3 and is comprised of cement PC-I-A). Figure 5-17 provides the mechanical property development of the two mixtures in terms of compressive strength, tensile strength and elastic modulus at 1, 3, 7, and 28 days. All mechanical properties apart from net strain observed from the strain gages were procured through cylinder testing.

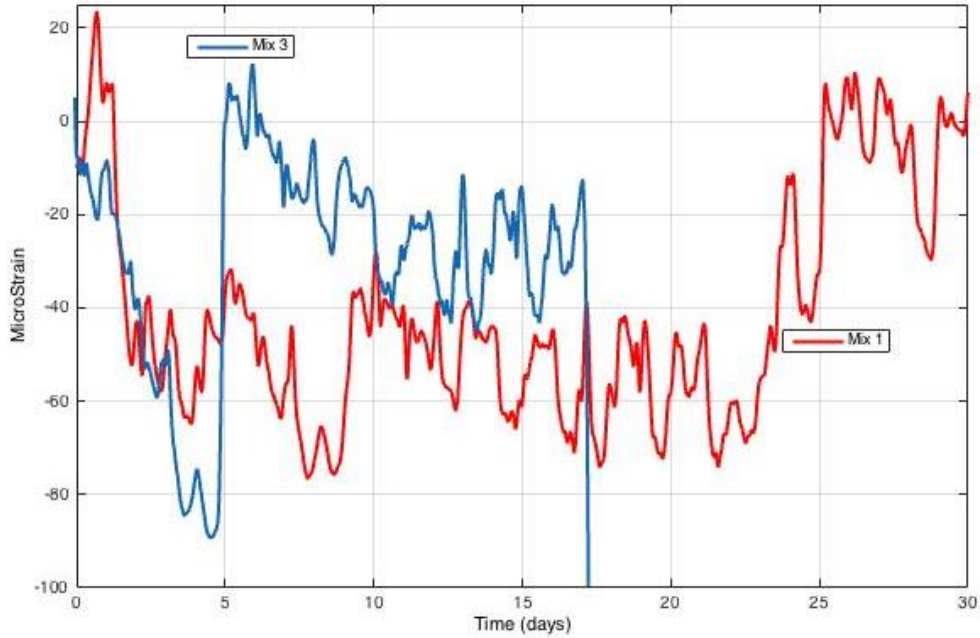


Figure 5-16: Restrained shrinkage ring data with respect to time
Effect of cement type: Mixture 1 – PC-III-A and Mixture 3 – PC-I-A

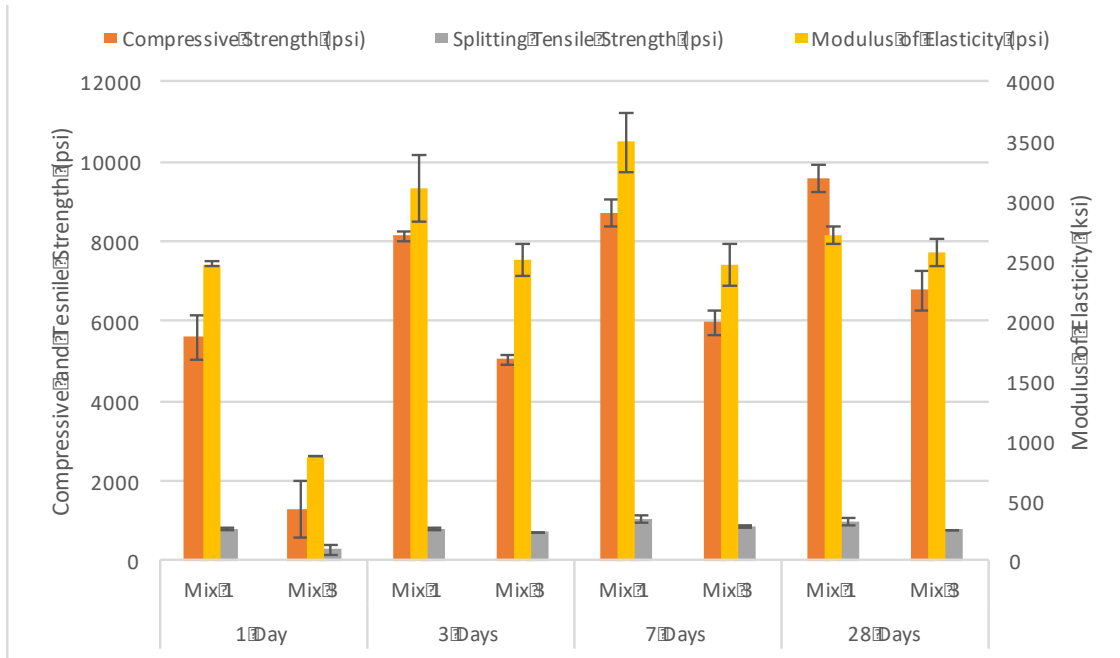


Figure 5-17: Compressive strength, splitting tensile, and modulus of elasticity for Mixture 1 and Mixture 3

Based on the data plotted in Figures 5-14 and 5-15, the cement type (Mixture 1 – Type III and Mixture 3 – Type I) plays a considerable role in the strain rate and cracking date of the rings. The concrete containing the Type III developing strain five times faster than the concrete containing the Type I cement. The early cracking date of the Type I cement in comparison to Type

III may be attributed to the significantly higher rate of strength and modulus development shown in Figure 5-15.

5.2.1.2.2 Effect of w/cm ratio

Figure 5-18 shows the stress development that occurred in the restrained shrinkage test based on analyzing mixtures according to their w/cm ratio. Mixture 1 has a w/cm of 0.28, whereas Mixture 2 has a w/cm of 0.33. Figure 5-19 presents the mechanical property development of the two mixtures with respect to compressive strength, tensile strength and elastic modulus at 1, 3, 7, and 28 days.

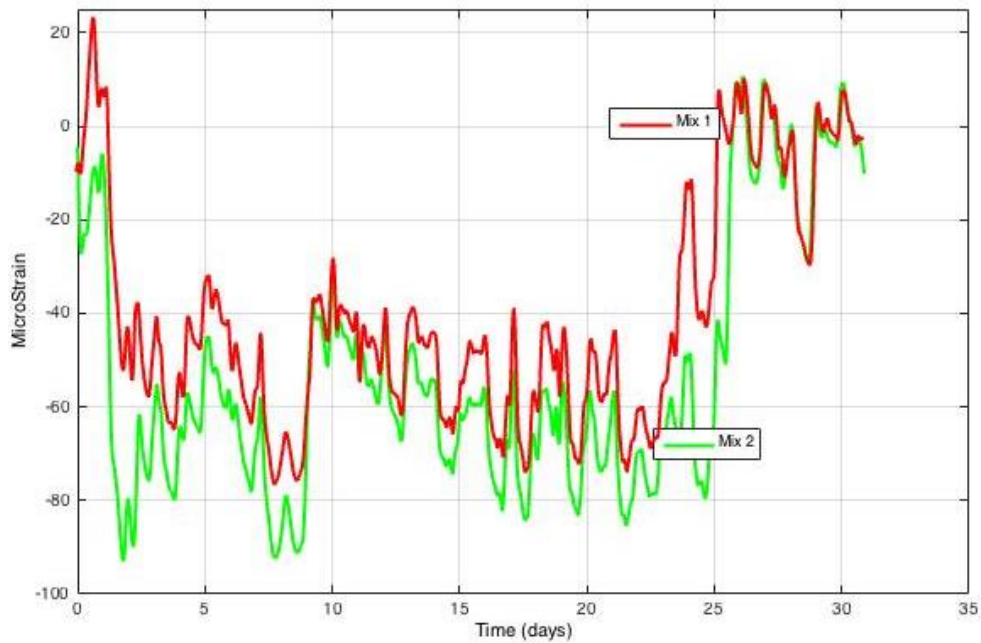


Figure 5-18: Restrained Shrinkage ring data with respect to time modeling effect of w/cm for Mixture 1 – 0.28 w/cm and Mixture 2 – 0.33

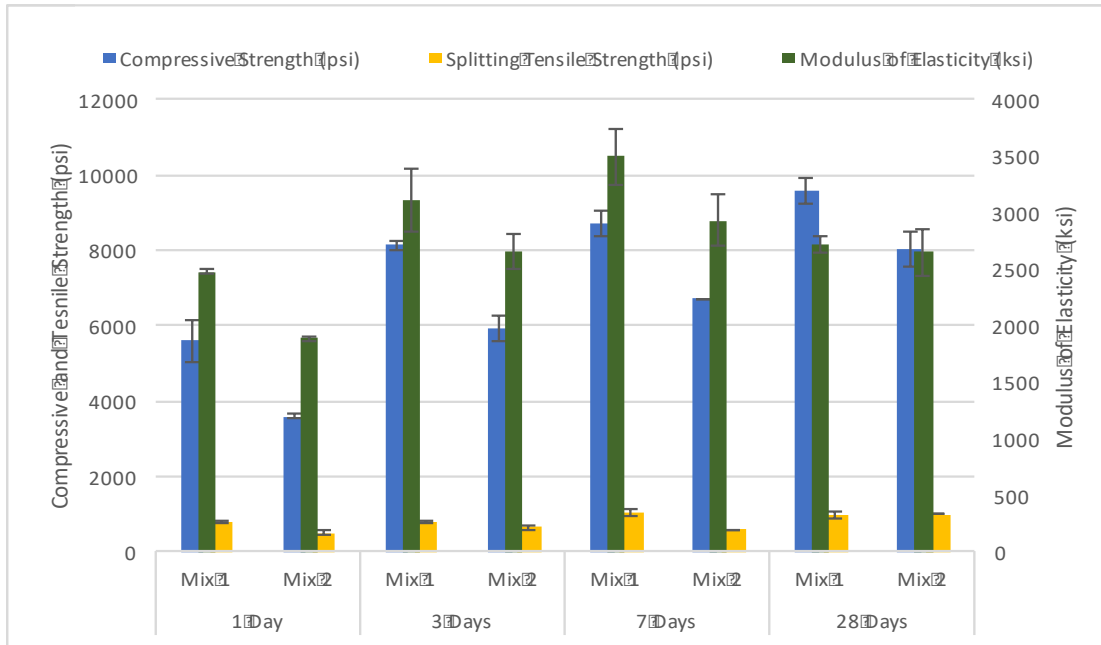


Figure 5-19: Compressive strength, splitting tensile, and modulus of elasticity for Mixture 1 and Mixture 2

Based on the data plotted in Figure 5-17, the w/cm content (Mixture 1 – 0.28 and Mixture 2 – 0.33) did not play a decisive role in the strain seen by the steel ring and the crack date. Although Mixture 1 had greater compressive strength ($\cong 2000$ psi more) than Mixture 2, the splitting tensile and modulus of the two mixtures were no more than 25% of one another.

5.2.1.2.3 Effect of HRWR Type

Figure 5-20 outlines the stress development seen by the restrained shrinkage test analyzing the effect of changing the HRWR type; three HRWRs were considered: HR-P1 (Mix 4), HR-P3 (Mix 5), and HR-P2 (Mix 7). Mix 7 utilizes a different cement source PC-III-B than the other two mixtures, but was inserted here to provide an additional mixture comparison. Figure 5-21 provides mechanical property development of the three mixtures in terms of compressive strength, tensile strength, and elastic modulus at 1, 3, 7, and 28 days.

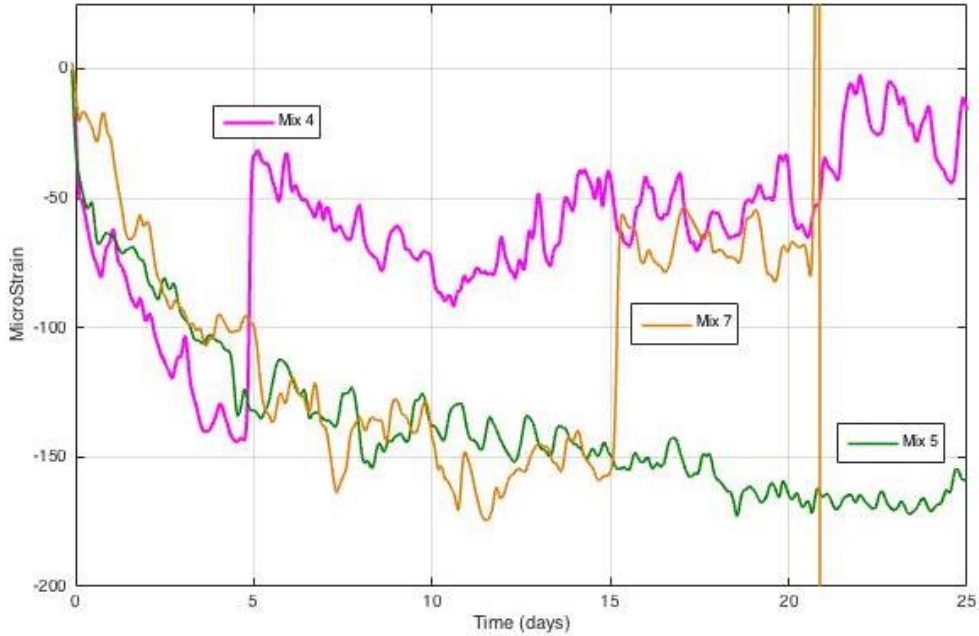


Figure 5-20: Restrained Shrinkage ring data with respect to time modeling effect of the HRWR type with Mixture 4 – HR-P1 and Mixture 5 – HR-P3 and *Mixture 7 – HR-P2

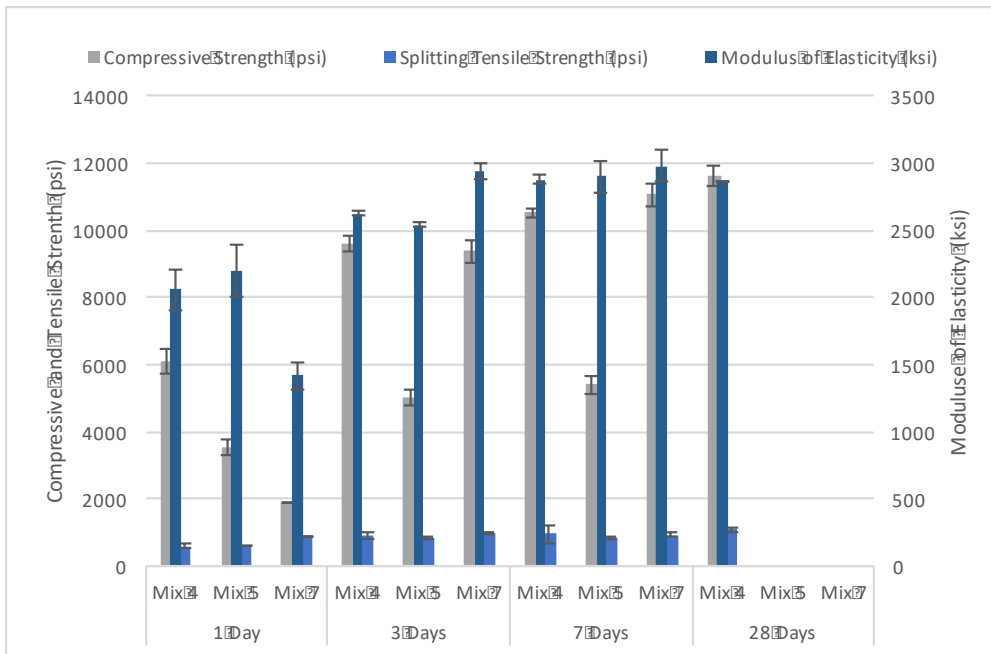


Figure 5-21: Compressive strength, splitting tensile and modulus of elasticity for Mixture 4, Mixture 5, and Mixture 7

Based on the data plotted in Figures 5-18 and 5-19, the w/cm content (Mixture 4 – HR-P1 and Mixture 5 – HR-P3 and *Mixture 7 – HR-P2) did play a considerably decisive role in the crack date of the concrete rings. Dates of cracking for the HR-P1 (Mix 5) was 5 days, followed by HR-P2 (Mix 7) at 15 days, followed by HR-P3 (Mix 4), which cracked beyond the month-long period

within which the rings were monitored. Figure 5-19 shows that the low compressive strength of Mixture 5 and the slower development of compressive strength for Mixture 7 may indicate that slower development of compressive strength with each of the different HRWR's effects the cracking date.

5.2.2 Parametric Study of Concrete:

5.2.3 Results and Conclusions for Concrete Testing

The mixtures selected for the restrained ring test all were selected based upon their usage in precast plants in Texas. The mixtures are all classified as HPC mixture designs and therefore had a very low likelihood of cracking due to high early strength development. However, comparing between the different HPC mixtures the following may be concluded:

- Type III cement, as compared to Type I cement, is more effective in developing strength and increasing the length of time at which cracking occurs in the restrained ring test.
- Differences in w/cm ratio did not affect the rate or time of cracking in the restrained ring test.
- Type of HRWR plays a pivotal role with respect to the rate at which strength is developed as well as the time to cracking. However, referring to data from Chapter 4, HRWR type HR-P1 showed the least amount of drying shrinkage with respect to HR-P2 and HR-P3, yet Mix 4 containing HR-P1 showed the earliest date to cracking (5 days). This shows that although drying shrinkage and restrained ring testing expose the concrete to similar conditions the shrinkage performance is not analogous to one another. Therefore, drying shrinkage for precast mixtures may not be a good indicator of cracking performance with respect to autogenous shrinkage ring testing. More work is required to verify this conclusion.

A more complete matrix should be composed to continue creating comparisons between precast plant HPC mixture designs showing both good and bad performance. It should also be noted that Mixes 1 and 2 should be performed again due to learning curve that is associated with the DAQ and strain gage equipment that was sorted out with the mixtures that followed (Mixes 3–8).

5.3 Parametric Study: Paste Testing

The parametric study also looked into testing paste mixtures with varying HRWR dosage and w/cm ratio in several autogenous testing apparatuses: buoyancy test, corrugated tube test and mini ring rest. Table 5-3 presents the paste mixtures that were evaluated by all tests undertaken throughout the paste study. All 0.31 w/cm mixtures in this project incorporated fly ash, so this paste matrix was designed specifically to understand the influence of admixture type and admixture dosage.

Table 5-3: Pastes mixtures subjected to parametric study

w/cm	Cement Type	Admixtures	
		Type	(floz/100 lb cement)
0.31	PC-III-A	HR-P1	6.5
			8.25
			12
		HR-P2	6.5
			8.25
			12
		HR-P3	6.5
			8.25
			12

A single w/cm ratio of 0.31 was selected because it represents the average of the w/cm ratios employed at Texas precast plants. Likewise, one source of cement (PC-III-A) was selected as a means of reducing the matrix to provide comparison purely based on HRWR type, dosage and their effects on paste autogenous shrinkage testing. Figure 5-22 outlines how the following sections in this chapter have been segmented and cross-referenced with one another.

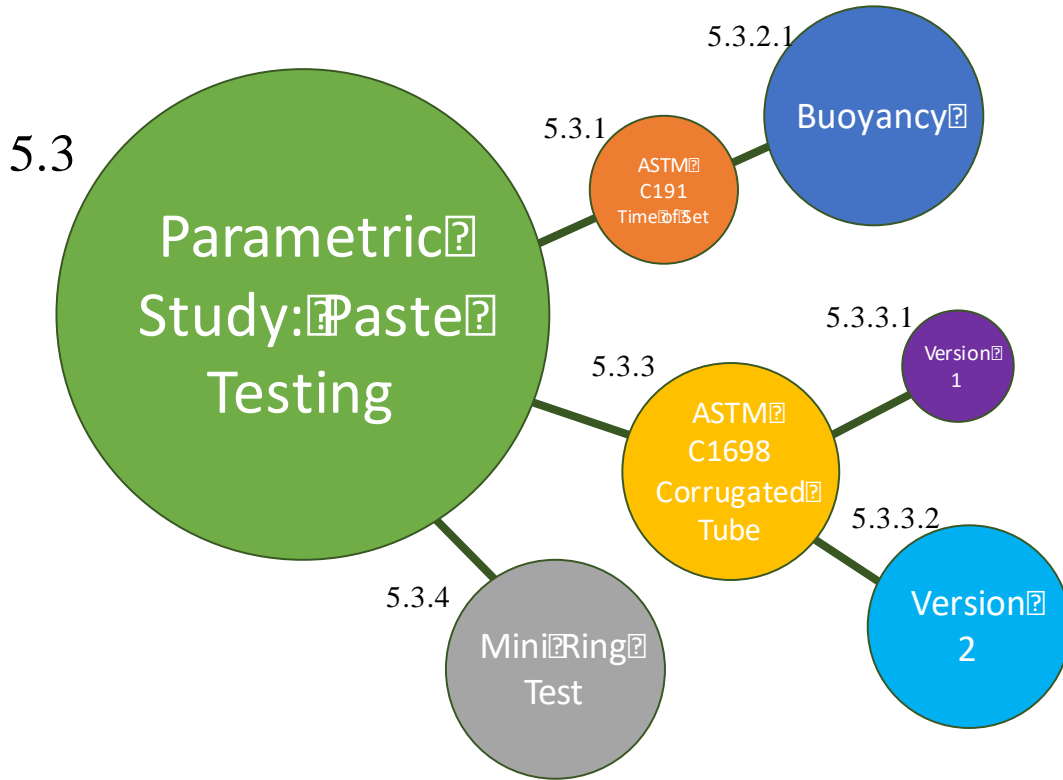


Figure 5-22: Parametric study testing breakdown with chapter section designation for paste analysis

5.3.1 Time of Set

5.3.1.1 Procedure and Experimental Setup

In order to collect the initial and final set times for the paste samples listed in Table 5-3, the Vicat needle test, ASTM C191, Time of Setting of Hydraulic Cement by Vicat Needle, was utilized. The paste was mixed in a Hobart mixer in accordance with ASTM C305. Depending on the slump of the paste produced, two unique procedures were followed. A slump of approximately zero permitted the user to fill the Vicat conical mold by following the procedure listed in ASTM C191. The user would collect the paste into a spherical ball with gloves tossing from one hand to the other for six times. The paste sample is then set into the larger radius of the Vicat mold and the paste and mold is then moved to be seated on the larger radii mold end. For a paste mixture with a slump greater than zero (typical for most samples), the mixture was poured into the conical Vicat mold while the larger end was set securely onto a weigh boat.

In order to mimic the isothermal conditions associated with all of the autogenous shrinkage testing performed throughout this research, the time of set sample was set on a cold plate. The cold plate circulated 23 °C from the base of the Vicat paste sample. The Vicat needle setup was also housed in an insulated box to further stabilize temperature as well as limit drying shrinkage from ambient air flow. At least two samples from separate mixing dates were used to verify consistent initial and final set time results. The Vicat needle apparatus works by the release of a rod with a needle that uses gravity to impress the needle into the paste sample. The depth of the needle was collected and recorded based on a metric reading attached to the Vicat apparatus. Each sample

required an initial reading 30 minutes after the addition of cement and water, followed by readings at 10-minute intervals until a penetration reading of 25 mm or less was achieved. The Vicat setup employed for all paste samples is shown and annotated in Figure 5-23.

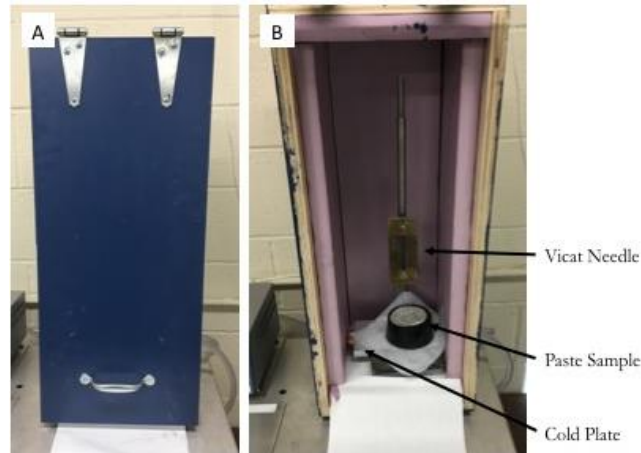


Figure 5-23: Vicat Needle Test, ASTM C191.
Housed in an isothermal box (A) Closed. (B) Open for testing purposes.

5.3.1.2 Testing Matrix and Results

Several different mixture designs were carried out in this project with varying chemical admixtures and dosages. Due to the importance of determining the final set time for the autogenous shrinkage tests, the setting time results shown in Table 5-4 were utilized in all subsequent autogenous shrinkage paste testing chapters. Time of set testing was carried out with two separate samples cast at separate times due to the limitation of only having one sample Vicat setup. Results of time of set were averaged and/or repeated if times differed more than 15 minutes. Table 5-4 shows the mixture proportions alongside averaged initial and final setting times of the two samples. Figure 5-24 presents the values in bar graph form.

Table 5-4: Mixture proportions and averaged time of set through ASTM C191

w/cm	Cement Type	Admixtures		Time of Set (hr)	
		Type	(floz/100 lb cement)	Initial	Final
0.31	PC-III-A	HR-P1	6.5	5.03	5.80
			8.25	4.82	5.67
			12	5.60	7.45
		HR-P2	6.5	5.40	6.88
			8.25	4.58	7.83
			12	5.60	7.65
		HR-P3	6.5	3.18	4.67
			8.25	3.20	5.75
			12	4.02	5.63

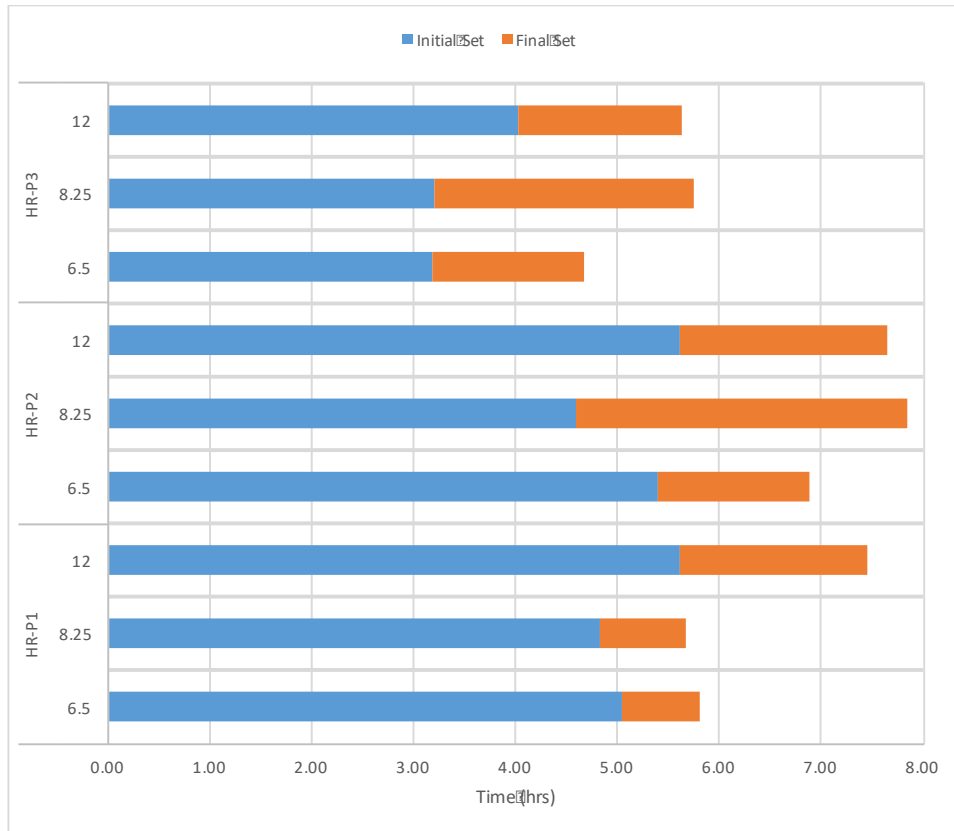


Figure 5-24: Averaged setting times plotted for each paste mixtures

Typically, an increase from HRWR dosage from 6.5 fl oz/100lb cement delays the final set for nearly all HRWR types. HR-P3 retarded the setting times the least, and HR-P2 retarded the setting times the most.

5.3.2 Autogenous Deformation

5.3.2.1 Buoyancy Procedure and Experiment and Experimental Test Setup

In order to measure the autogenous deformation of paste samples via buoyancy method the volumetric deformation of paste was determined using the test setup described in Chapter 2. The setup employed is shown in Figure 5-25.

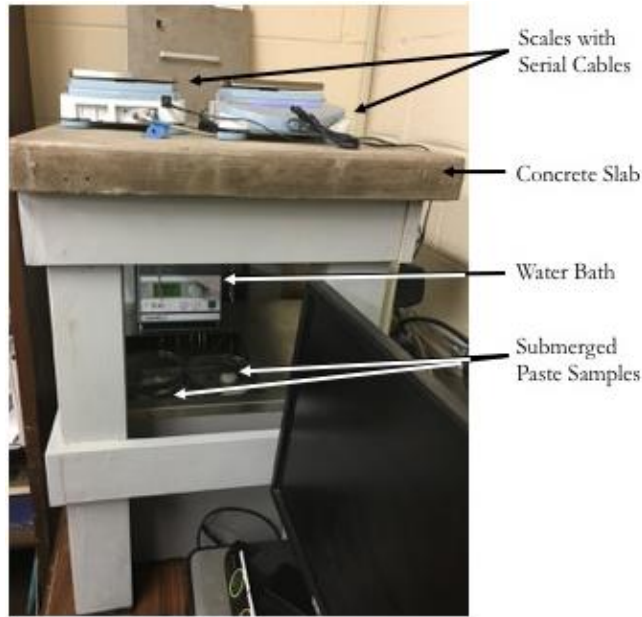


Figure 5-25: Autogenous Shrinkage Test Setup via Volumetric/Buoyancy Method

The setup employed at the University of Texas uses two scales that sit on a concrete slab suspended over a water bath. The setup permits the measurement of two samples at a time. The scales measure to an accuracy of 0.01 grams and are directly connected to computers via serial cables to two separate computers for continuous measurements at 1-minute intervals. The samples suspended from the scales are unlubricated polyurethane condoms (Trojan Supra). The condoms were filled with 100 g to 150 g of paste. The paste was mixed in accordance with ASTM C305. The paste was set into the condoms and sufficient vibration was applied. The condom was twisted and zipped-tied to ensure completely sealed conditions. A pre-tied fishing line and i-hock were attached to the zip-tie in order to allow the paste sample to be quickly immersed into a paraffin oil bath. Measurements commenced immediately upon immersion.

In order to verify initial weight of specimen against the final normal weights of the paste sample the cut off tail end of condom, and zip-tie were collected and recorded. The test was run for a three-day period. At the completion of the test, the paraffin oil was wiped off of the surface of the condom, and the sample was measured. In order to ensure the quality of the test, the final weight and initial weight should not exceed a 2% increase. Otherwise, this can indicate that excessive paraffin oil was absorbed into the membrane.

5.3.2.2 Testing Matrix

Several different mixture designs were carried out in this project with varying chemical admixtures and dosages. Testing was carried out using three separate samples all at 23 °C for a 3-day testing period. Autogenous shrinkage (linear strain, $\mu\epsilon$) was tabulated as a positive value after final set was met (according to time of set results determined in Chapter 4's Section 4.3.2), and 72 hours after the introduction of cement to water. Results of the buoyancy method averaged the three samples cast per mixture design and have been outlined in Table 5-5.

Table 5-5: Autogenous shrinkage according to mixture designs at 72 hours after introduction of cement to water

w/cm	Cement Type	Admixtures		Final Set Time (hr)	Linear Strain ($\mu\epsilon$)
		Type	(floz/100 lb cement)		
0.31	PC-III-A	HR-P1	6.5	5.03	611.20
			8.25	4.82	1614.60
			12	5.60	432.90
		HR-P2	6.5	5.40	422.17
			8.25	4.58	597.97
			12	5.60	651.53
		HR-P3	6.5	3.18	395.47
			8.25	3.20	151.84
			12	4.02	10.10

5.3.2.3 Results

The following sections have composed several comparisons on autogenous shrinkage of the cement pastes samples listed in Table 5-3. Individual mixture design autogenous shrinkage results may be found in Appendix VII of this report.

5.3.2.3.1 Effect of HRWR Dosage

Figure 5-26, Figure 5-27, and Figure 5-28 display the effect of increasing the HRWR dosage for each individual HRWR type. Positive strain was taken after final set as determined through Vicat testing previously explained.

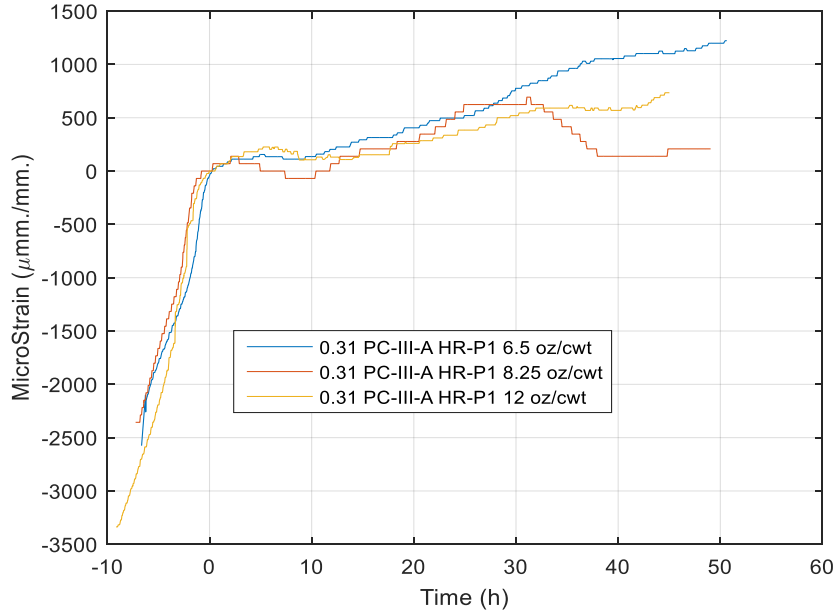


Figure 5-26: Buoyancy shrinkage 0.31 PC-III-A for HR-P1 at 6.5, 8.25, and 12 fl oz/100 lb cement

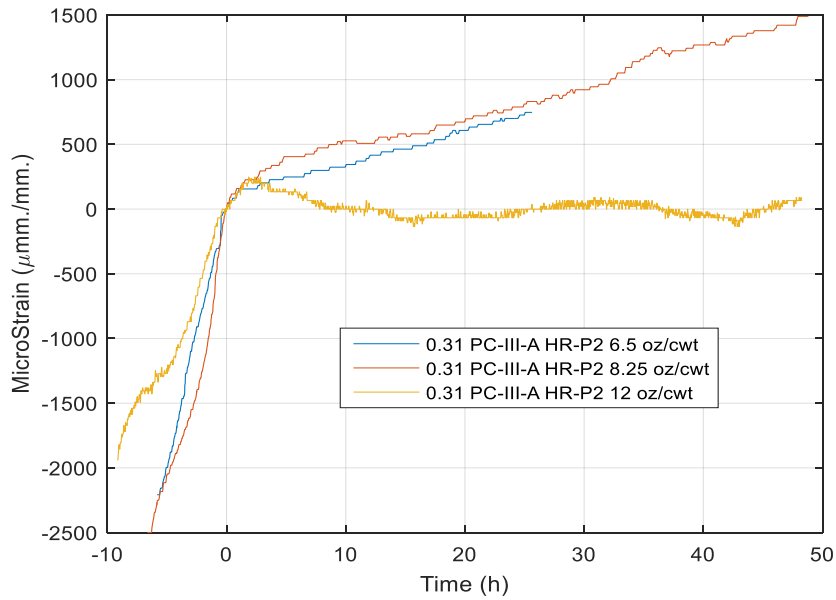


Figure 5-27: Buoyancy shrinkage 0.31 PC-III-A for HR-P2 at 6.5, 8.25, and 12 fl oz/100 lb cement

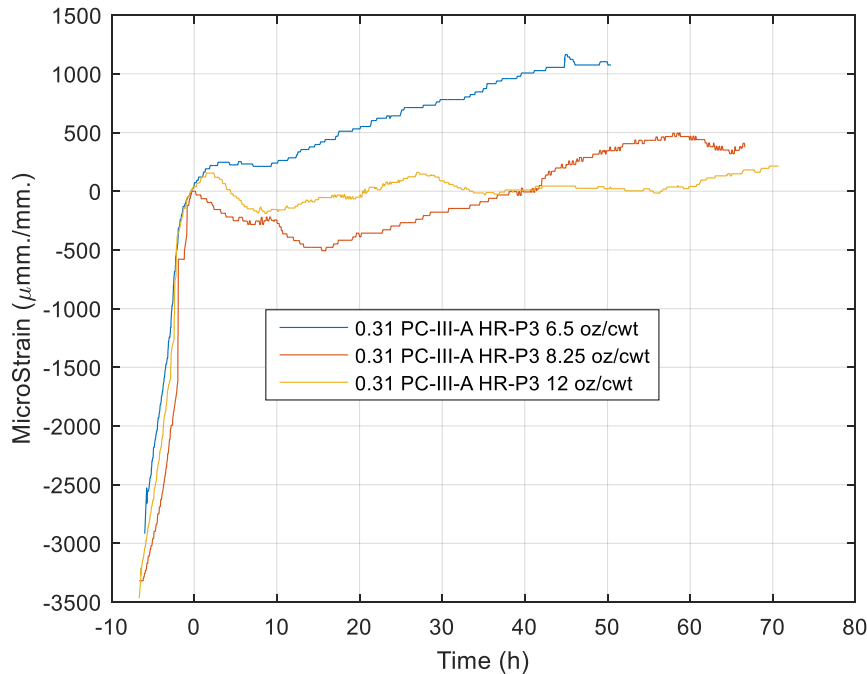


Figure 5-28: Buoyancy shrinkage 0.31 PC-III-A for HR-P3 at 6.5, 8.25, and 12 fl oz/100 lb cement

As shown in all cases, the largest amount of shrinkage strain was observed in the pastes containing the lowest HRWR agent dosage (6.5 oz) except in the case of HRWR HR-P2, where 6.5 and 8.25 oz dosages show similar trends (see Figure 5-27). The higher dosage mixtures again show the increased retardation previously discussed in Section 5.3.1. Retardation may be seen by the slower strain development with respect to time prior to reaching final set. The increase in HRWR dosages showed that, by delaying final set time, the autogenous shrinkage that followed was then delayed.

5.3.2.3.2 Effect of HRWR Type

Figures 5-29 through 5-31 present plots that compare the different HRWR types (HR-P1, HR-P2, and HR-P3) at a series of fixed dosage amount. Again, positive strain was taken after final set as per Vicat measurement.

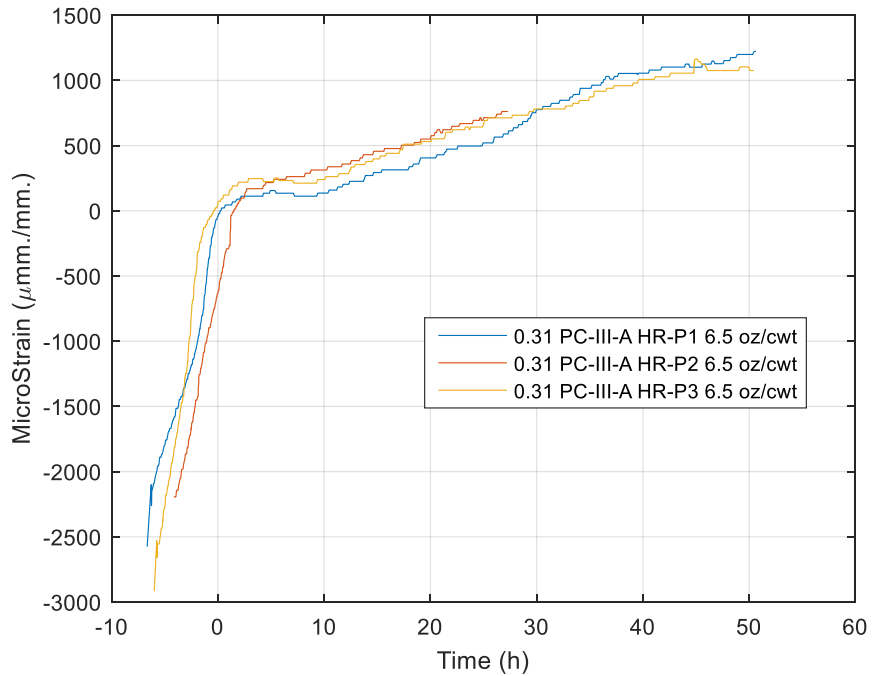


Figure 5-29: Buoyancy shrinkage 0.31 PC-III-A for HR-P1, HR-P2, and HR-P3 at fixed 6.5 fl oz/100 lb cement

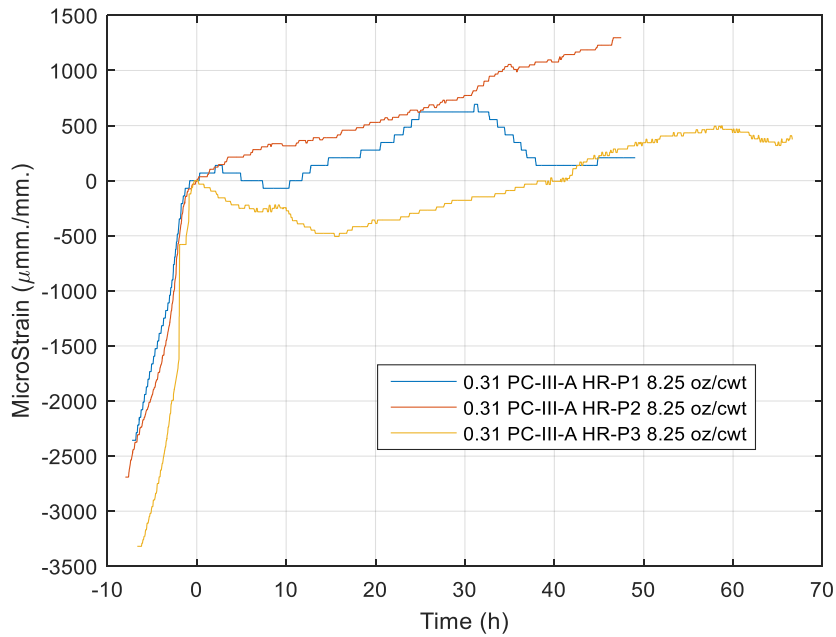


Figure 5-30: Buoyancy shrinkage 0.31 PC-III-A for HR-P1, HR-P2, and HR-P3 at fixed 8.25 fl oz/100 lb cement

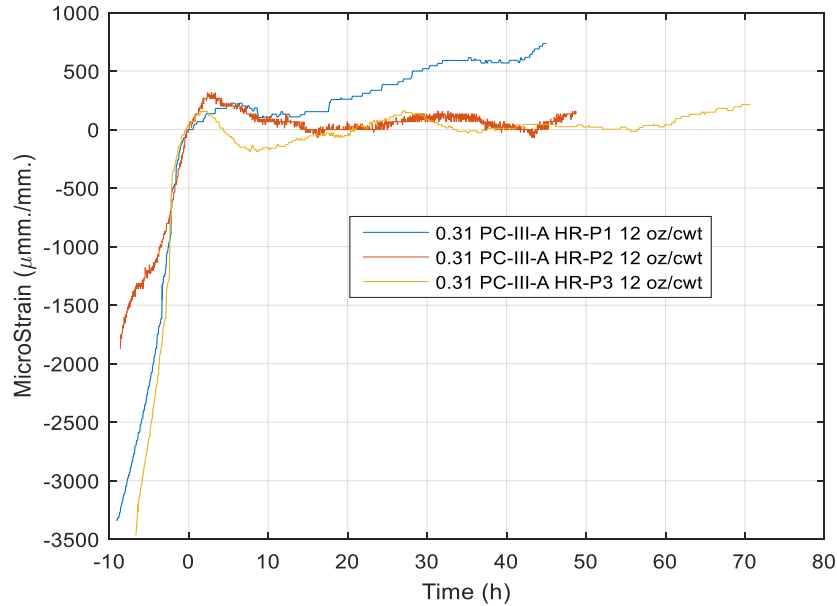


Figure 5-31: Buoyancy shrinkage 0.31 PC-III-A for HR-P1, HR-P2, and HR-P3 at fixed 12 fl oz/100 lb cement

Figure 5-29 illustrates that a fixed dosage of 6.5 oz produces the least amount of variance in shrinkage strain. This erratic variation was concerning to the extent that autogenous deformation was also evaluated using a more accurate corrugated tube method as explained in the following section to evaluate mixture proportioning in more detail.

5.3.2.4 Summary and Conclusions

Based on the results of this section the following conclusions may be drawn:

- Increase in HRWR dosage proved to decrease the autogenous shrinkage after reaching final set. This was aided by the increase time until final set associated with increased HRWR dosage mixtures.
- Due to the high variability in collected strain through the volumetric method, it was difficult to draw further conclusions from the data. Therefore, work towards collecting information on autogenous shrinkage was shifted entirely towards the corrugated tube test methodology.

5.3.3 Corrugated Tube Results

Autogenous shrinkage measurements were conducted on the mortar phase of all the mixture proportions examined as part of this project, as well as some exposure block and restrained shrinkage mixes. The corrugated tube test has been standardized under ASTM C1698, Standard Test Method for Autogenous Strain of Cement Paste and Mortars (2009). The linear method permits the use of mortar or cement paste to be cast in a rigid module with minimal friction, an example of which is shown in Figure 5-32. Two separate versions of the test were employed. One functioned as per the ASTM standard, while the other used noncontact LDVT sensors and monitored the tube's shrinkage while it sat in a temperature controlled bath. The latter approach

was found to be more accurate and details about these modifications to the ASTM standard is presented in the following section.



Figure 5-32: Corrugated polyethylene autogenous test setup (Germann Instruments)

5.3.4 Modifications to ASTM Corrugated Tube Standard Approach

Two modifications were made to the ASTM standard to increase its accuracy:

- the tubes were immersed in a mineral oil bath at 23°C until 72-hour measurement, and
- measurements of shrinkage were automated through the use of noncontact linear variable differential transformers (LVDT).

The purpose of immersing the tubes in a mineral oil bath was to ensure that the paste was maintained at a constant temperature. Noncontact LDVTs were used to ensure friction did not influence the measurement. Normal indicators typically supply a normal force on the end of the tube and therefore cannot take measurements of autogenous shrinkage of the cement at the plastic stage (Tian and Jensen 2005). Indicators widely used on hardened cement pastes such as the Mitutoyo length gage employ as much as 2.5 Newtons in order to make sufficient contact with the sample in question. Likewise, the vertical measurement method may not be used to accurately measure pure autogenous shrinkage because of the error associated with influence of gravity force on the shrinkage of the tube (Bjötengaard and Hammer 2004). Therefore, in order to increase the measurement precision for autogenous shrinkage of cement paste at a very early age, the corrugated tube system was improved through the use of a non-contact LVDT sensor (Gao, Zhang, Luo, Wei and Yu 2013). Continuous measurement of samples paired with non-force protruding measurement indicators confirmed the most accurate and least scatter in the collected data. Measurements are taken at intervals of 1 minute for at least 72 hours after the sample is placed into the testing apparatus. Strain measurements are calculated using the following equation:

$$\varepsilon_{AS} = \left(\frac{S_t}{L_o} \right) * 100\%$$

Where S_t is the displacement of the tube at time t , L_o is the initial length of the paste. In order to measure autogenous shrinkage as accurately as possible, multiple adjustments were made to the corrugated measurement apparatus and method outlined in ASTM 1698. Figure 5-33 shows the

CAD drawings that were developed to have the setup machined and Figure 5-34 shows the annotated photo of the setup employed.

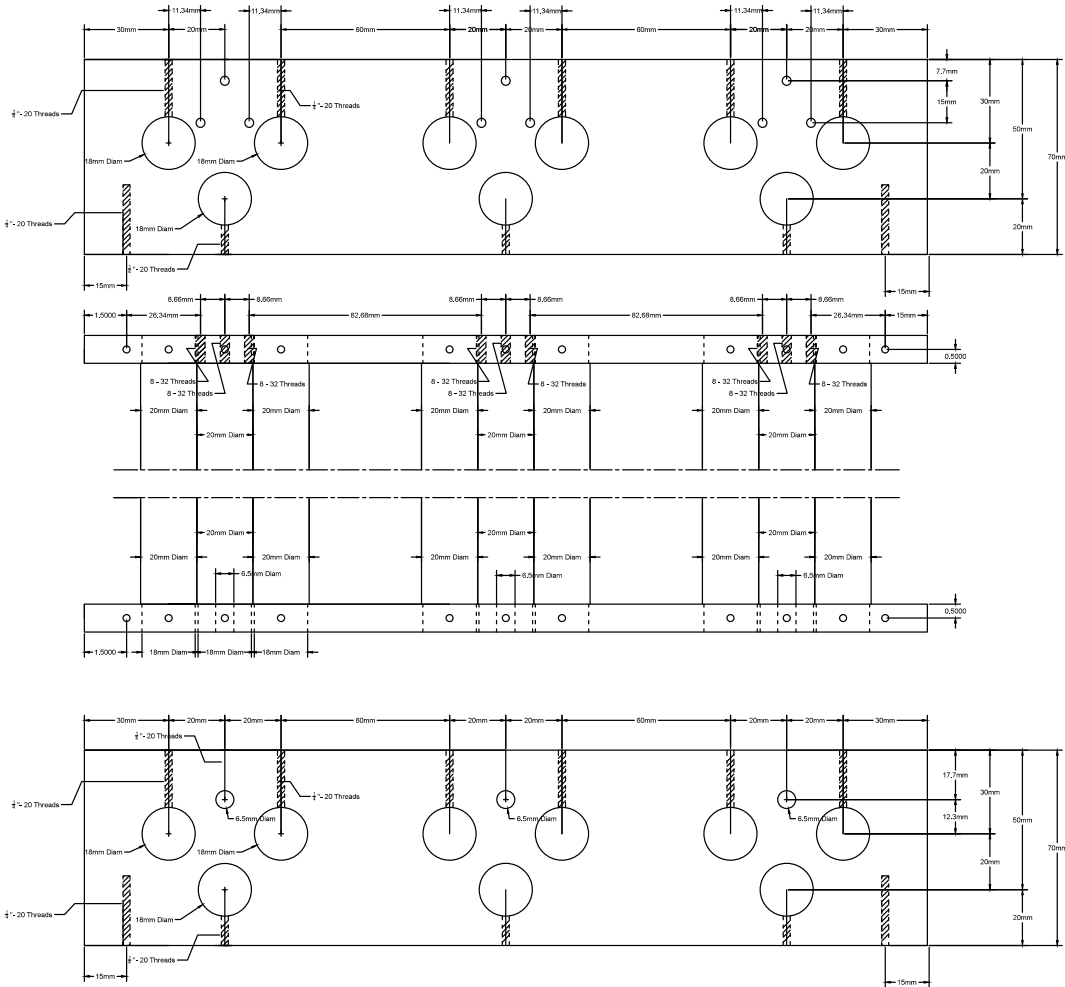


Figure 5-33: CAD drawing of corrugated tube test rig

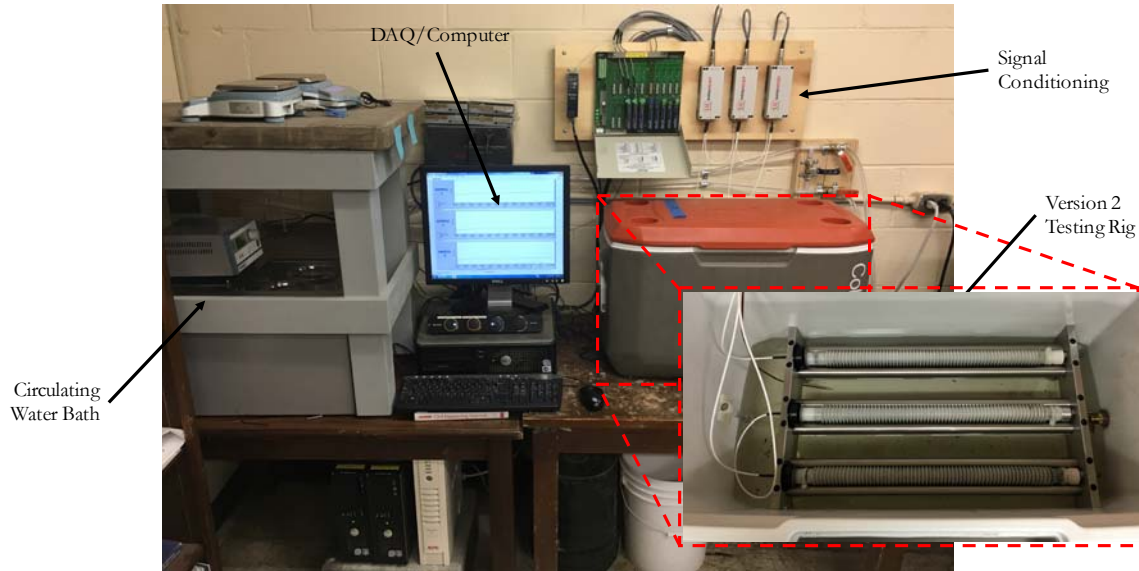


Figure 5-34: Test setup for the corrugated tube test developed at UT Austin.

Note: Testing rig is inside cooler during testing.

Germann Instruments Auto-Shrink corrugated tubes and plastic polyurethane caps were used, as well as specially machined threaded metal caps. A vibrating table was placed under the tube during filling to remove as many entrapped air bubbles in the tube as possible (Figure 5-35). The lower end was capped with the metal cap. Most mixtures had lots of entrapped air so it was impossible to feasibly continuously vibrate until there were no air bubbles visible. Instead, the tubes were filled halfway and vibrated for 15 minutes on each half. Once the tube was completely filled, the upward facing end was capped and sealed with a plastic polyurethane cap. To assure no moisture loss, zip ties are used to further secure the caps at either end of the tube. To assure that the specimens are not lengthened during transport from the mixing room to the testing room, the tubes were carried in PVC pipes that have the approximate desired initial length of the specimens. The corrugated tube was then gently placed into the testing rig. At the conclusion of the initial 72-hour measurement period, the specimens are measured at finite intervals of 1, 3, 7, 14, and 28 days from initial set.

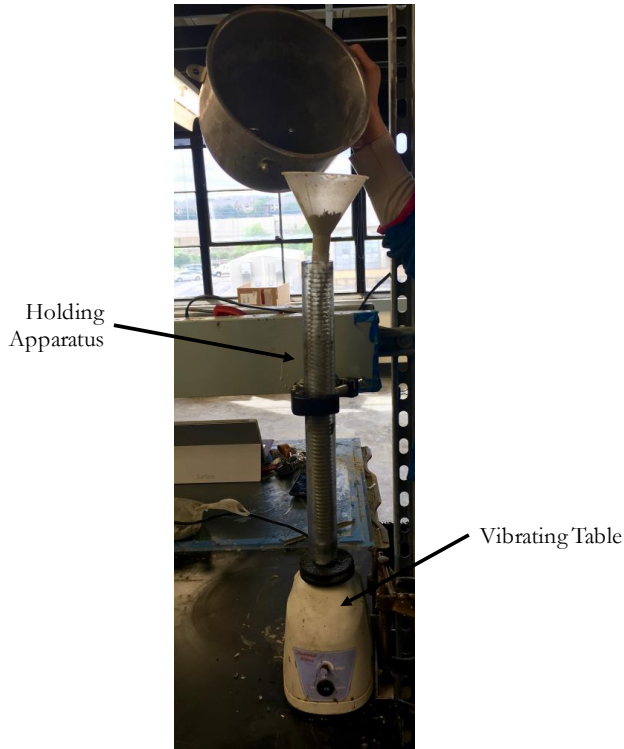


Figure 5-35: Corrugated tube being filled and vibrated

5.3.4.1 Apparatus Construction

The apparatus was designed in a similar fashion to conventional ASTM 1698 standard set-up, except that the apparatus used permits the measurement of three samples simultaneously. Figure 5-36 provides a diagram outlining how the hardware for the Version 2 setup at the University of Texas at Austin was interconnected.

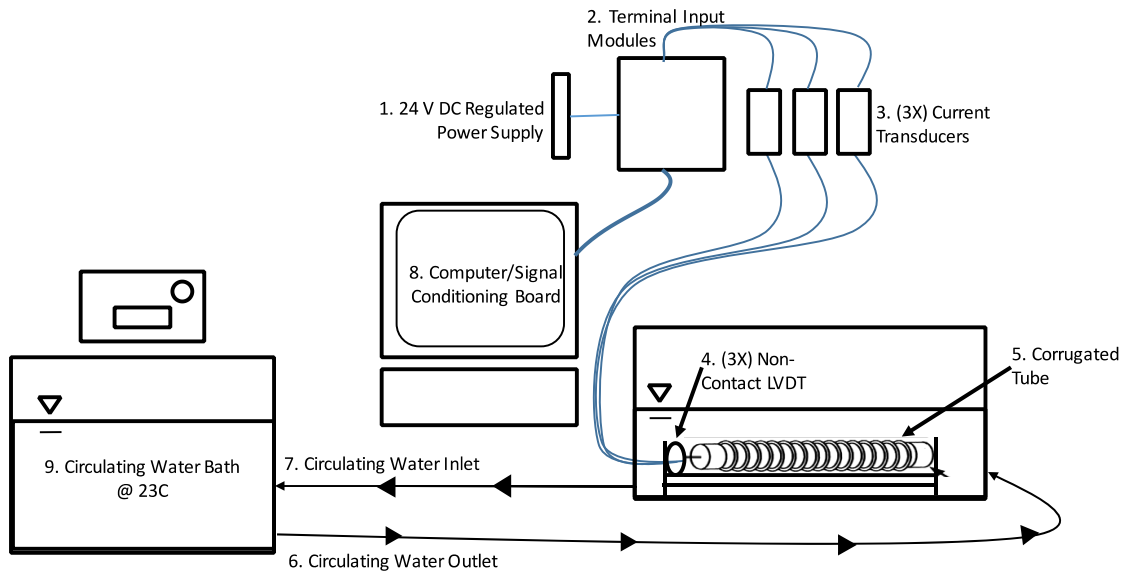


Figure 5-36: Diagram of the non-contact LVDT setup

The corrugated tube testing apparatus is comprised of 3/8 in. stainless steel end plates that are set apart by nine stainless steel rods that have been chamfered and secured into the end plates by set screws. One of the end plates has been tapped to accept all thread that is used to secure one end of the corrugated tube. The caps were made to create a “dead end”; facilitating shrinkage solely from the non-contact LVDT. The end plate with the non-contact LVDTs (Micro Epsilon eddyNCDT 3010 sensor U15) was not fixed and is referred to as the “live-end.” The non-contact LVDTs were selected based on their lower cost relative to a direct contact and waterproof LVDT, as well as for their ability to maintain accuracy, resolution and range consistent with ASTM C1698. The non-contact LVDTs provide a 15-mm range or measurable distance, alongside a 0.75 μm resolution which meets well within the prescribed standard of ASTM C1698. The sensor is adjacently connected to a transducer that is powered by a direct current regulated power supply of 24 volts and 3 amps (National Instruments PS-15). The sensor outputs an eddy current that sends and receives current to and from a ferromagnetic disk (stainless steel 1-in diameter and 0.01-in thick). Each stainless-steel disk was glued to the polyurethane cap using a standard epoxy before it was set into test apparatus. The disk was also placed at an initial 2 mm separation distance from the non-contact LVDT sensor. Figure 5-37 focuses on the non-contact LVDT sensor in line with the stainless-steel disk.

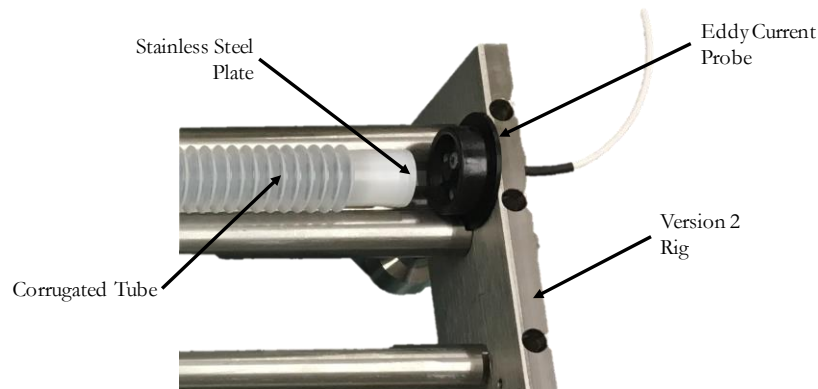


Figure 5-37: Excerpt of Version 2 corrugated tube set-up showing the non-contact LVDT eddy current sensor and adjacent steel plate in situ

The eddyNCDT 3010 transducer was calibrated to accept changes in current received as the targeted ferromagnetic disk moves linearly closer and further away. The calibration curve as shown in Figure 5-38 was used in order to directly correlate a voltage reading (1 mV) as a change in 1 mm distance.

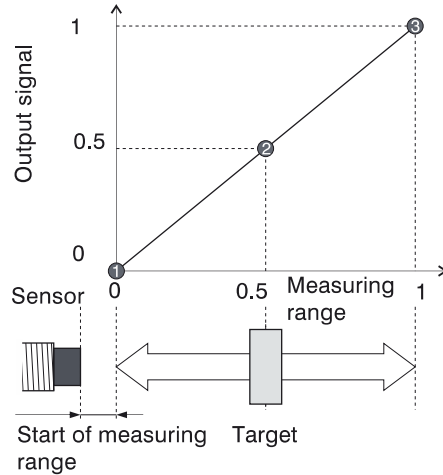


Figure 5-38: Typical LVDT calibration curve

The procurement of the length change in the corrugated tube was performed through the use of a LABview program developed at the University of Texas at Austin. LABview software and National Instruments hardware was used because of the versatility for future testing purposes (e.g., controlling water bath to provide heat ramping effects as seen in the field). The software program was created to compile changes in distance as a function of time for all three samples. The program also monitors temperature of the circulating water bath (VWR 1186D) as well as the separate water bath/cooler that the specimens are housed in. Figure 5-39 provides a screenshot of the LABview program at the conclusion of the three-day testing period.

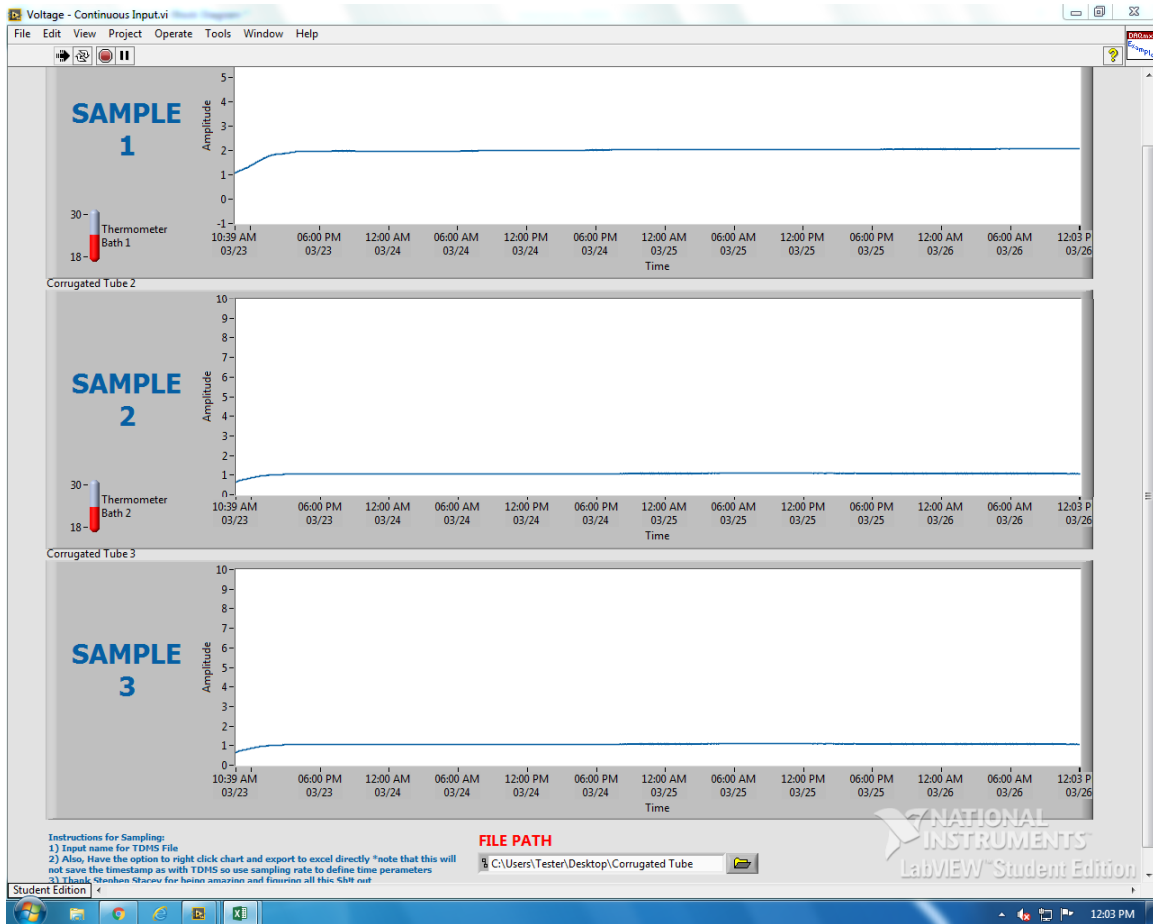


Figure 5-39: LABview program screen of three samples voltage readings with respect to time

The computer not only runs the LABview software but also houses the data acquisition system (DAQ) (National Instruments DAQmx PCI-6220). The DAQ board has a resolution capacity of 16 Bits, well within the tolerance provided by the non-contact sensors and ASTM C 1698. The signal DAQ is connected to a signal conditioning board (National Instruments SC-2345). The signal conditioning board allows the user to have several unique input channels. Figure 5-40 shows the signal conditioning board housing the four separate signal conditioning input modules. Two of the signal conditioning input modules have analog voltage reading (National Instruments SCC-AI03). The analog voltage modules have a voltage range of ± 10 V input and output, which is directly interpreted by the DAQ as function of length change as seen by the LVDT sensor. Each of the analog voltage modules have the capacity to interpret voltage readings from two unique voltage outputs, in this instance, voltage interpreted from the non-contact LVDT sensors. The other two input modules are thermocouple input modules (National Instruments SCC-TI01). The thermocouples are set up to monitor the temperature of the circulating paraffin oil in the corrugated tube cooler. The temperature was spot-checked using a Thermanpen thermometer to ensure accuracy.

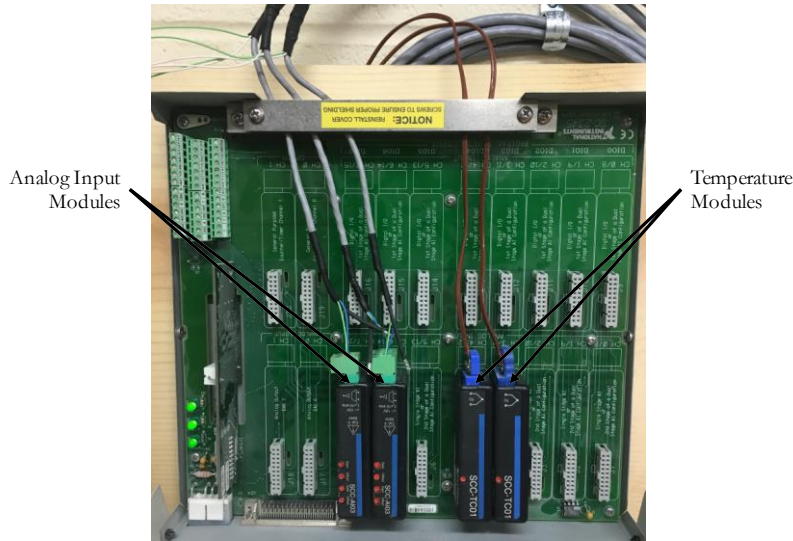


Figure 5-40: Signal conditioning input modules set in the signal conditioning input board

5.3.5 Results from Enhanced Corrugated Tube Test

Autogenous shrinkage results using the enhanced testing set-up discussed in the previous section is presented in the following figures in this section. Figures 5-41 through 5-43 shows the effect of w/c ratio on autogenous shrinkage for a constant dosage of HR-PR1 HRWR. As seen in the figures, when the dosage of HR-P1 is fixed at 6.5 oz/cwt (Figure 5-41), the 0.31 w/cm mixture has highest shrinkage, while 0.33 and 0.28 mixtures have similar and comparatively lower shrinkage. When the dosage is increased to 8.5 oz/cwt (Figure 5-42), a different behavior is seen (0.33 w/cm has the highest shrinkage, while 0.31 and 0.28 w/cm appear to overlap). When the dosage is increased even further to 12 oz/cwt (Figure 5-43), the trend reverses back to the 0.31 w/cm mixture displaying the highest shrinkage, while 0.33 and 0.28 mixtures have similar and comparatively lower shrinkage. Figures 5-44 through 5-46 show the effect of w/c ratio on autogenous shrinkage for a constant dosage of HR-PR2 HRWR. Similar to the results of the HR-PR1 mixture, a positive linear trend between autogenous shrinkage and admixture dosage was not apparent. Figures 5-47 through 5-49 summarize the effect of admixture type and content on reabsorption of bleed water during the autogenous shrinkage test.

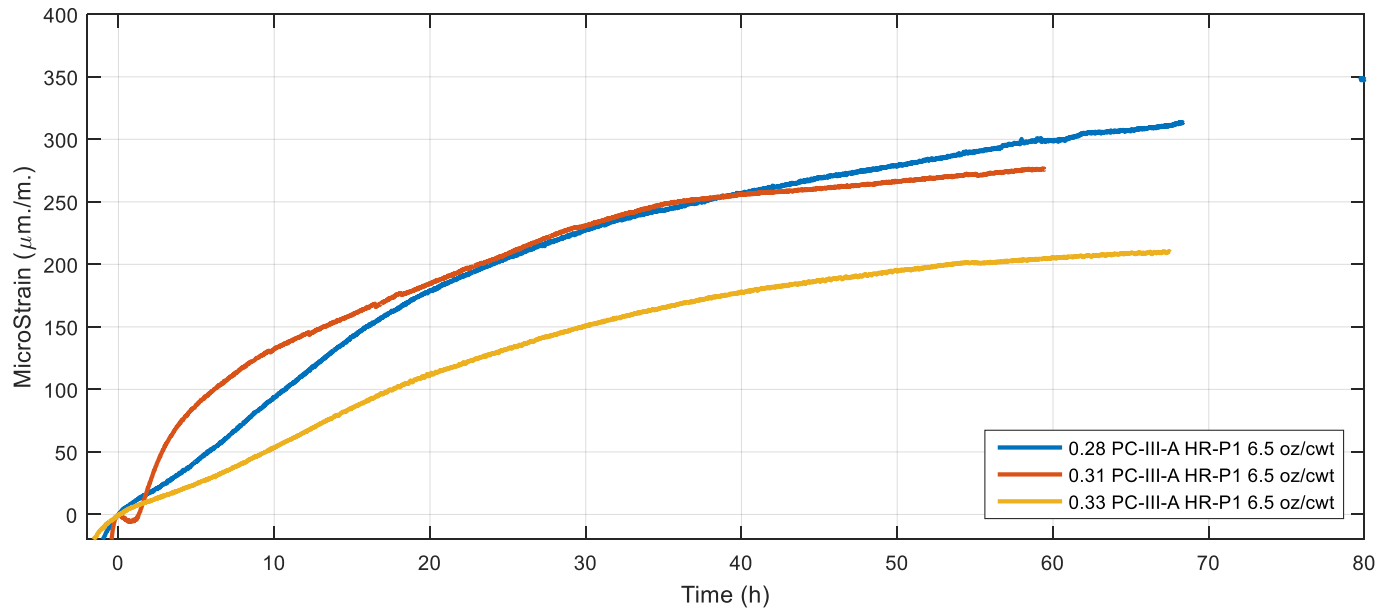


Figure 5-41: Effect of w/cm on autogenous shrinkage of paste containing low dosage of HR-P1 HRWR

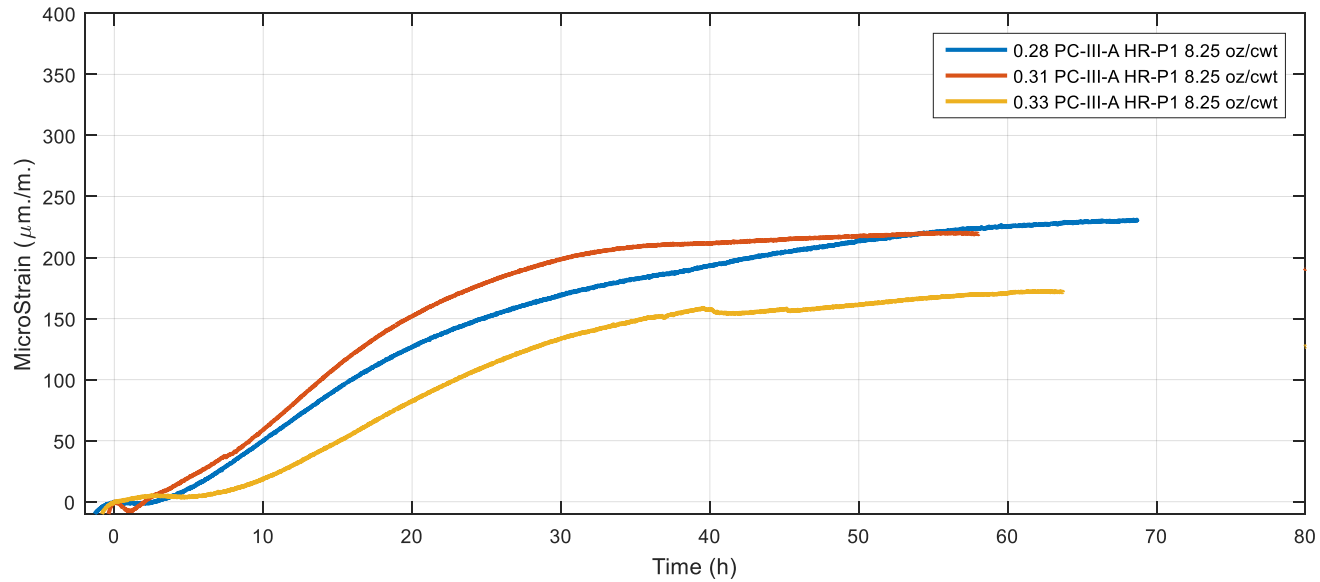


Figure 5-42: Effect of w/cm on autogenous shrinkage of paste containing moderate dosage of HR-P1 HRWR

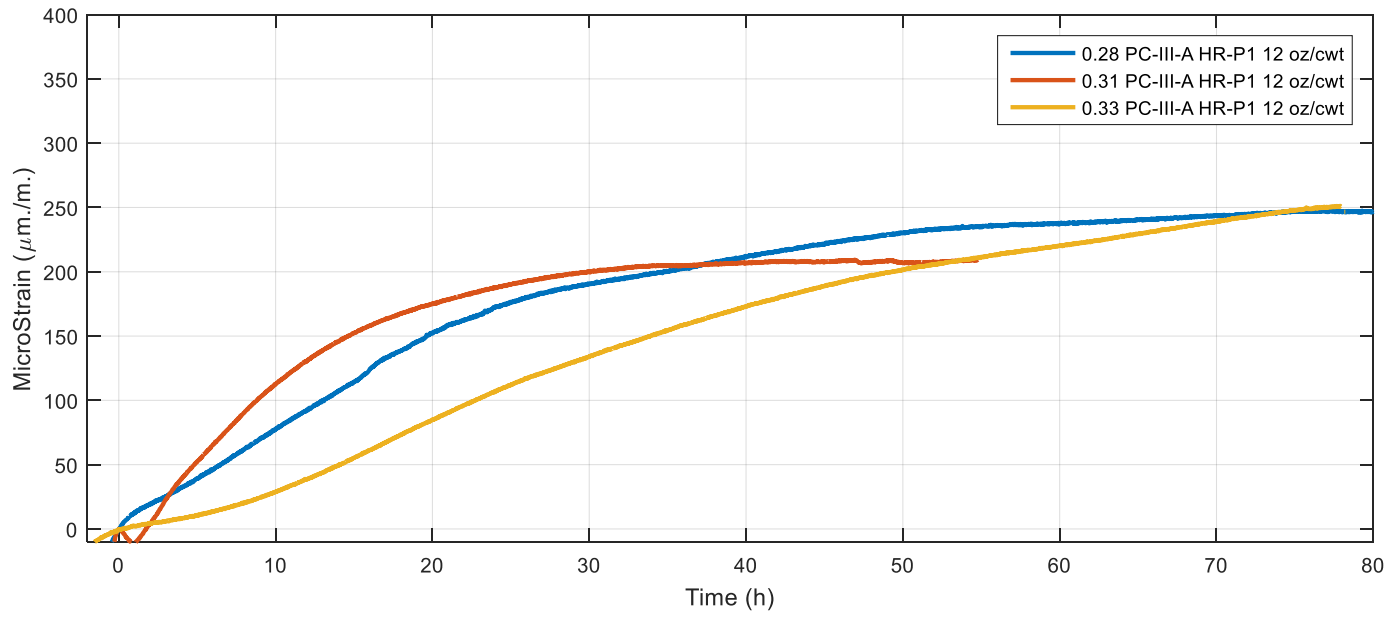


Figure 5-43: Effect of w/cm on autogenous shrinkage of paste containing high dosage of HR-P1 HRWR

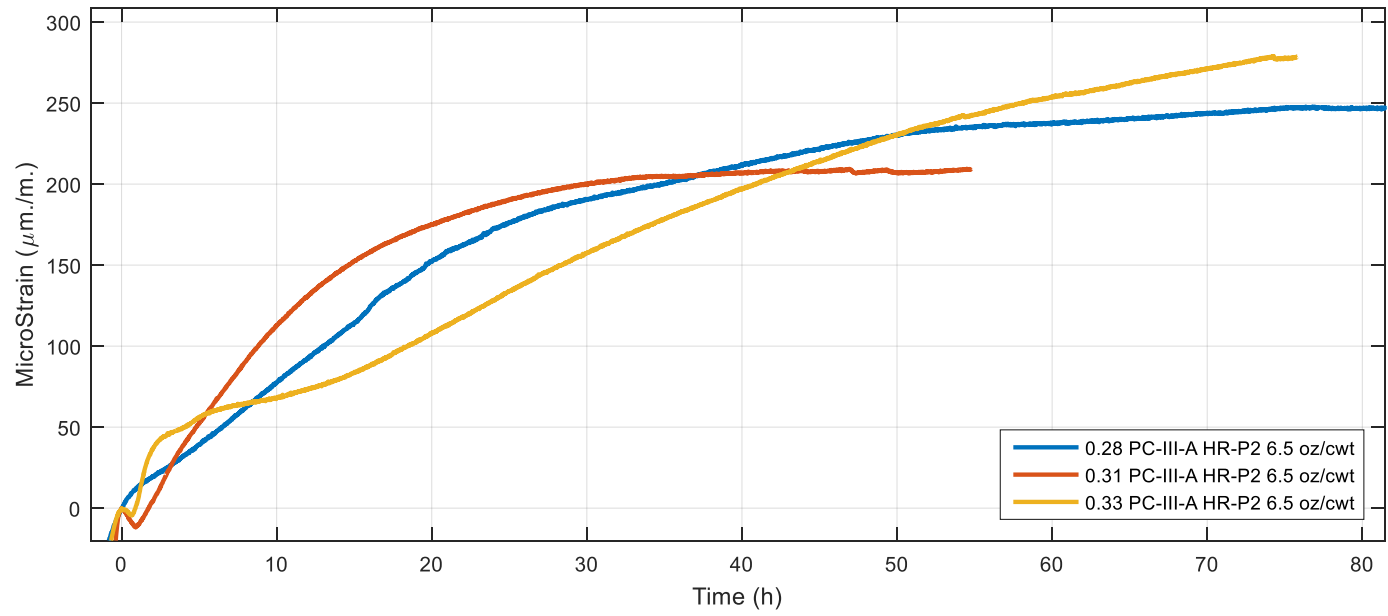


Figure 5-44: Effect of w/cm on autogenous shrinkage of paste containing low dosage of HR-P2 HRWR

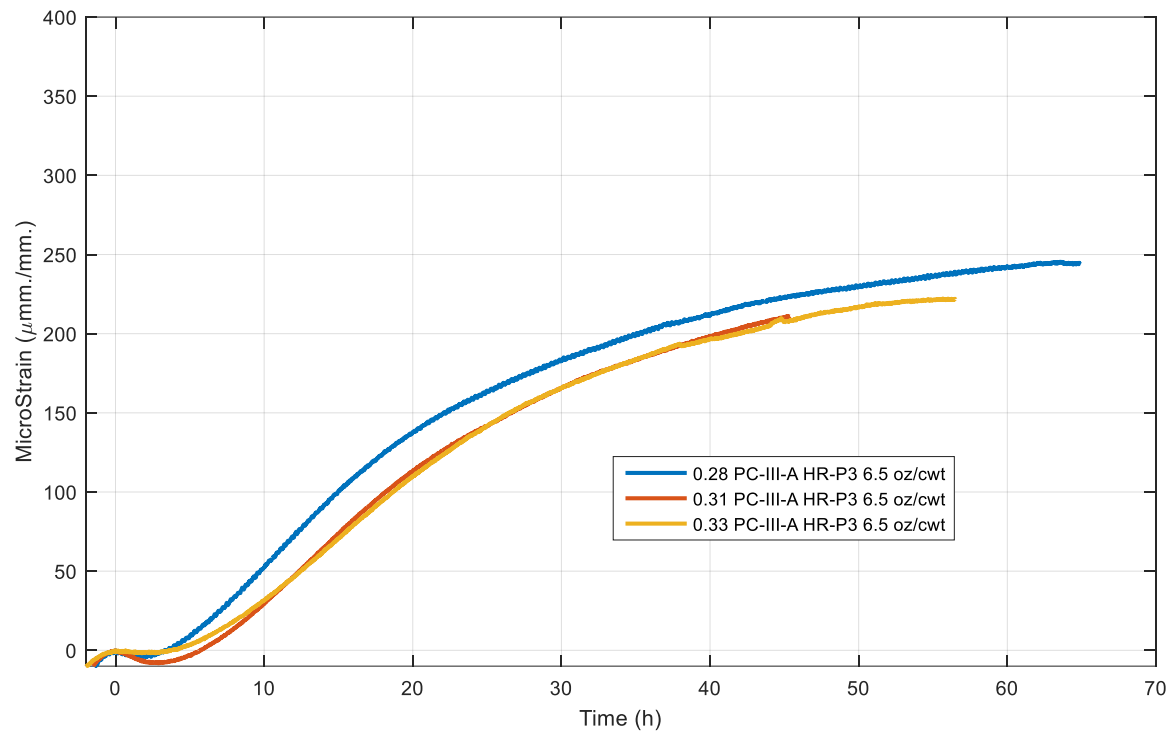


Figure 5-45: Effect of w/cm on autogenous shrinkage of paste containing moderate dosage of HR-P2 HRWR

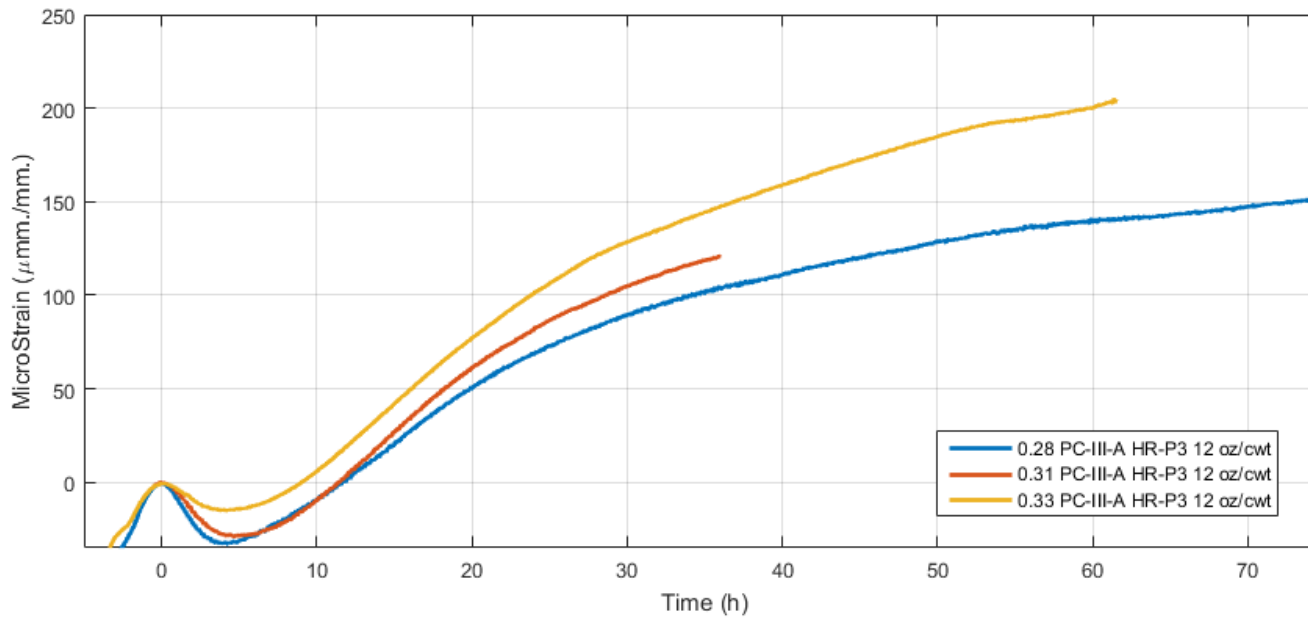


Figure 5-46: Effect of w/cm on autogenous shrinkage of paste containing high dosage of HR-P3 HRWR

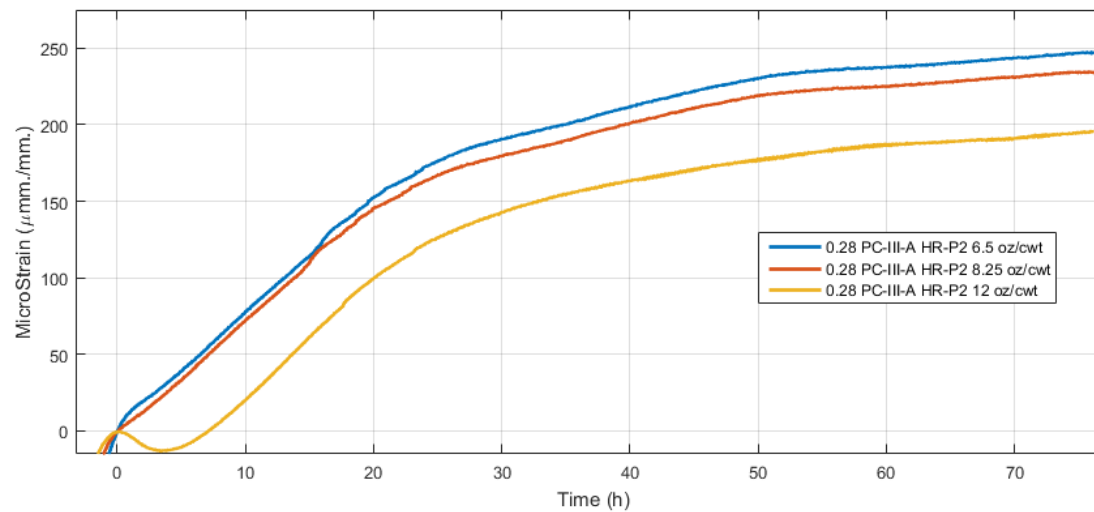


Figure 5-47: 6.5 and 8.25 oz/cwt dosages show no significant bleed bump and overlap at a higher dosage than the 12 oz/cwt dosage

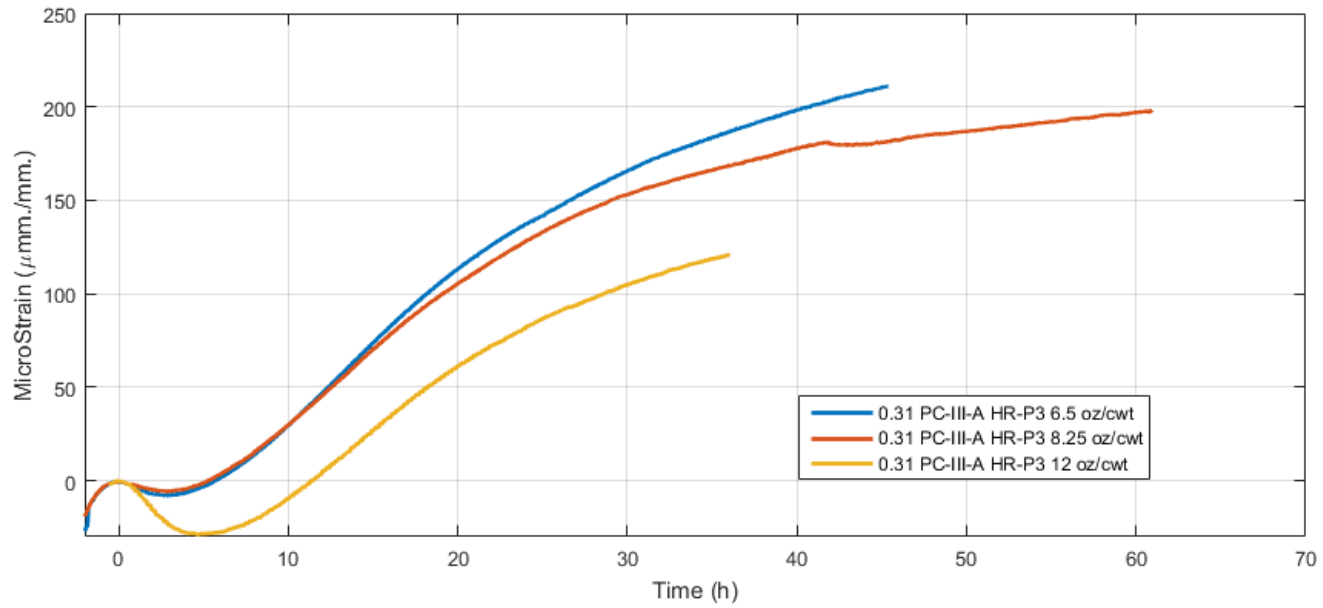


Figure 5-48: 6.5 and 8.25 oz/cwt dosages show a similar, though not as significant bleed bump and both overlap at a higher dosage than the 12 oz/cwt dosage

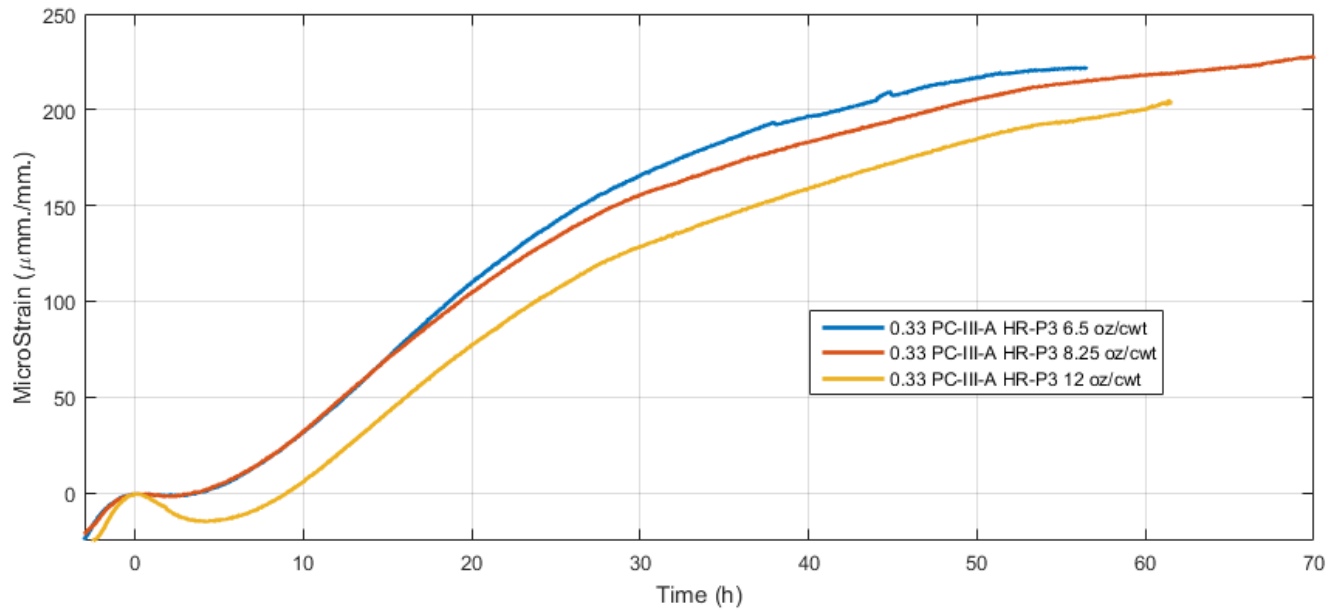


Figure 5-49: 6.5 and 8.25 oz/cwt dosages show a similar, though not as significant bleed bump and both overlap at a higher dosage than the 12 oz/cwt dosage

5.3.6 Conclusions for Parametric Testing

- From the information currently available on which concrete mixtures are good performers and poor performers, there is no evident correlation between autogenous shrinkage and micro-cracking performance (see Figure 5-50).
- There is no apparent correlation between known cracking mixes and autogenous shrinkage expected beyond setting.
- All of the mixes have a similar effective autogenous shrinkage of between 200-400 microstrain, which is very low. This correlates with the extremely long time it takes for the mini-restrained shrinkage test to crack the rings; the autogenous strain is so low that adequate restraint is difficult to reach within a reasonable time frame for testing.

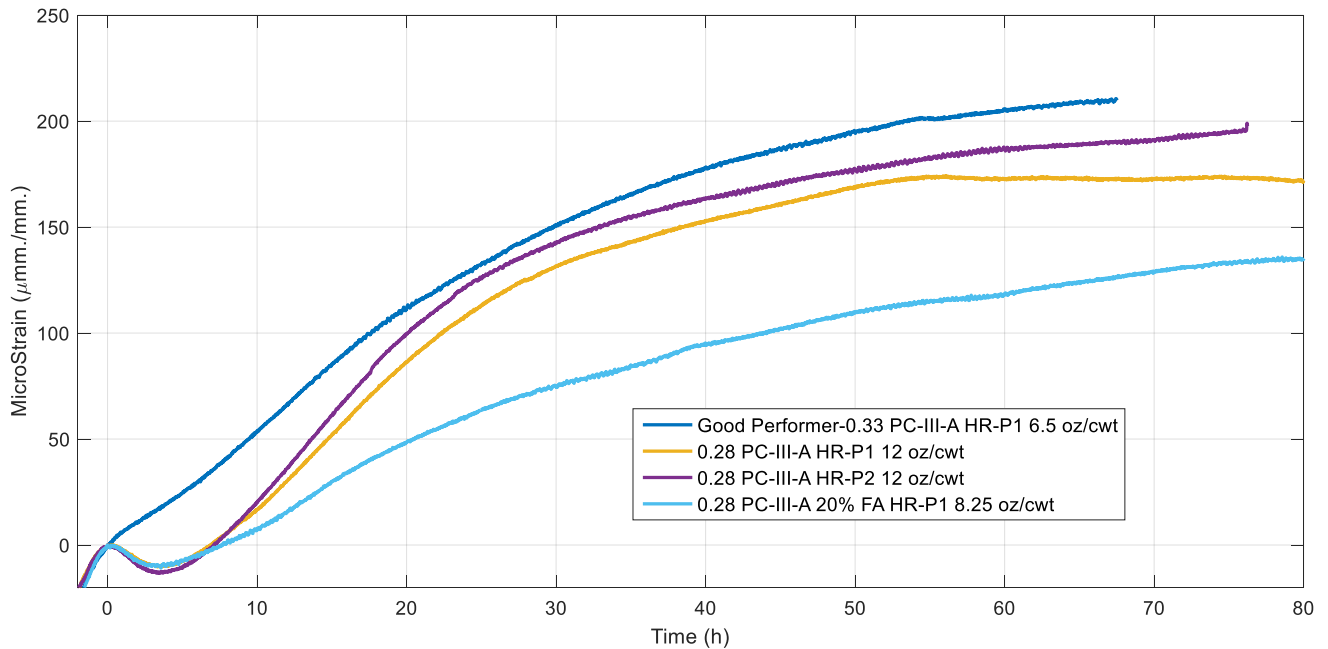


Figure 5-50: Comparison of pastes in concrete mixtures with known performance history, excepting the 0.31 w/cm which did not have a comparable paste mixture.

All are poor performers excepting the 0.33 w/cm paste mixture, which had the highest level of autogenous shrinkage

5.4 Isothermal Calorimetry Testing

5.4.1 Methodology

The hydration process was evaluated via isothermal calorimetry. Figure 5-51 shows the isothermal calorimetry apparatus used. Small plastic cups were filled with a measured amount of cement paste (mixed according to ASTM C305) and placed into the apparatus within 5 minutes. Thermocouples beneath the cups monitored the amount of heat evolved over a 48-hour period as

shown in Figure 5-52. The amount of cement paste placed in the calorimetry cups was limited to 25–30 g so that the bulk of the heat generated would be as close as possible to the thermocouples at the bottom of the cup. The same paste matrix evaluated for autogenous deformation was used to conduct heat of hydration testing. For several initial mixes, three separate tests were performed for each mix. Figure 5-53 shows the results of such a test; the standard deviation among mixes was low enough that it was considered acceptable for only one mix to be performed in future so that the full matrix could be completed efficiently.



Figure 5-51: Isothermal calorimetry apparatus

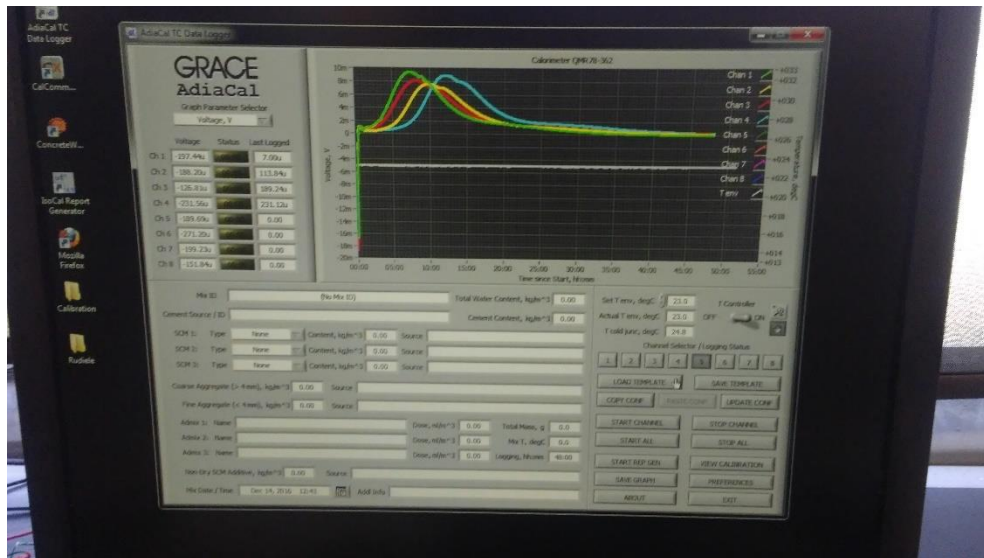


Figure 5-52: A screenshot of the Grace AdiaCal software monitor showing voltage over time from thermocouples underneath cement paste.

Inputs for mass of cement, water, and admixture are available so that the results can be adjusted to be proportional to the mass of cement.

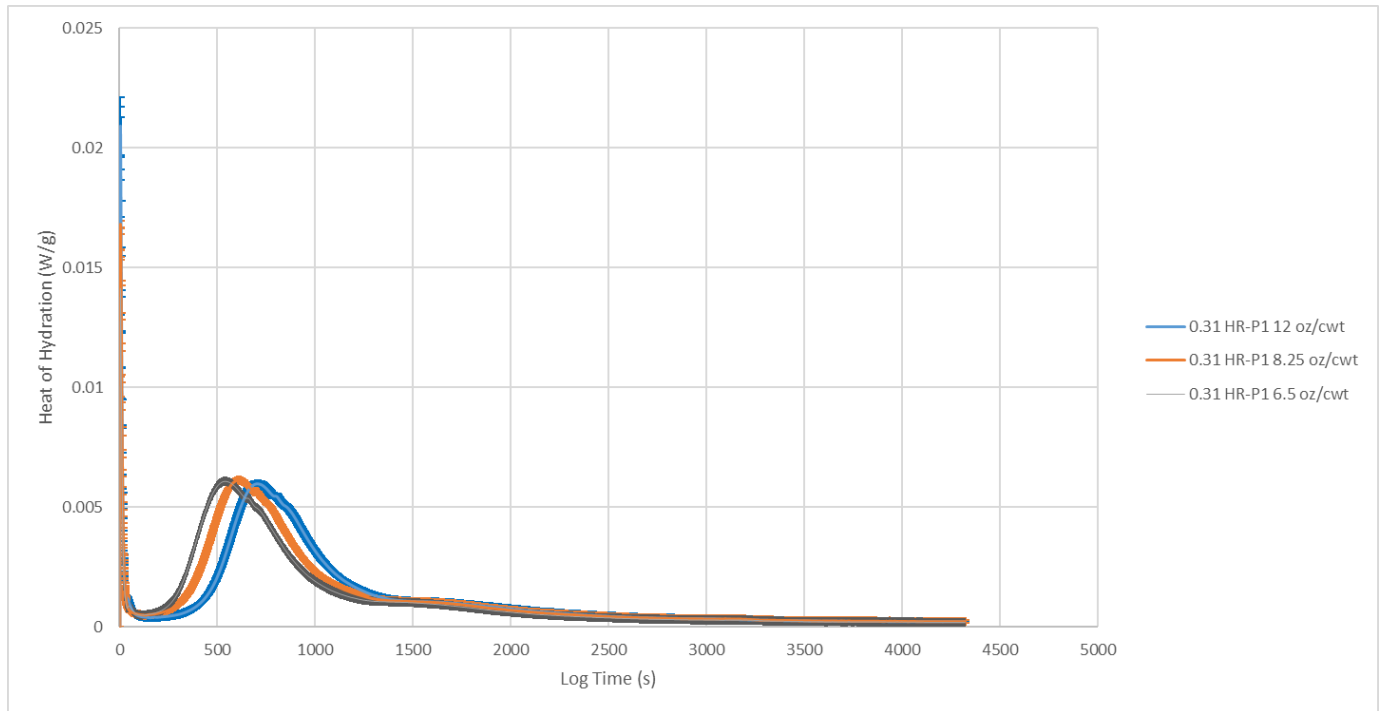


Figure 5-53: Calorimetry results for three mixes.

The colored line illustrates the average of three samples, while the outer colored portion shows the range of +/- the standard deviation among the samples.

5.4.2 Results and Discussion

In order to analyze the hydration kinetics heat flow and total heat evolved curves were created. A typical heat flow curve of cement hydration is shown in Figure 5-54 (Zhang et al. 2015). Variations in lengths and shapes of the various phases give some insight to variations in the hydration process between cement pastes. Additionally, the cumulative heat evolved was monitored. Figures 5-55 through 5-74 present the calorimetry results, and the key findings from analysis of these results are summarized in Section 5.4.3.

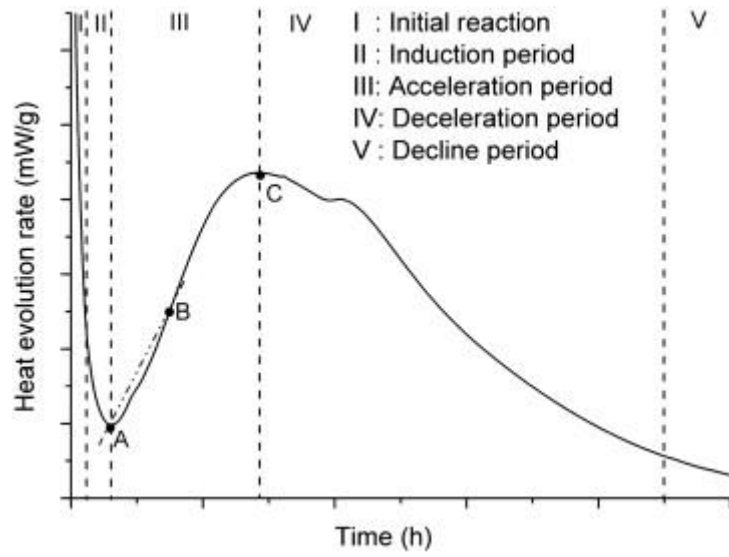


Figure 5-54: Typical heat flow curve with demarcated periods shown (Zhang et al. 2015)

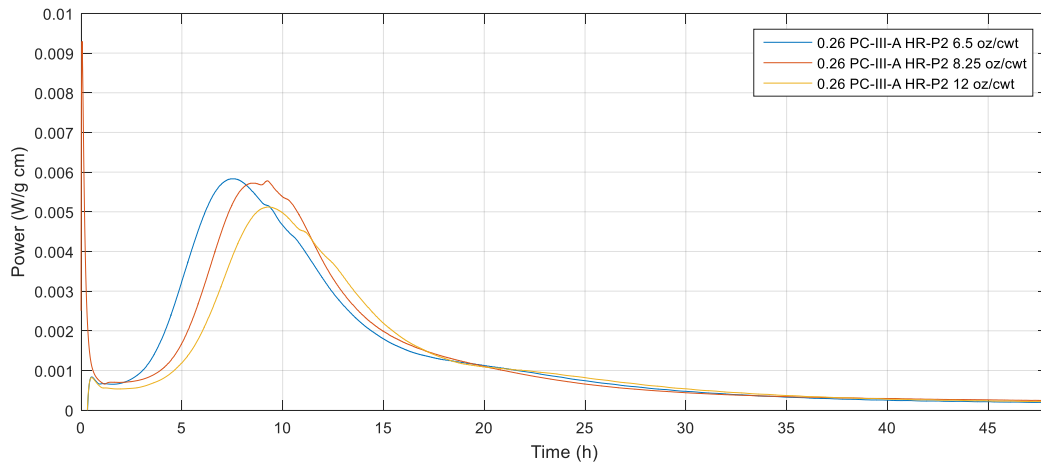


Figure 5-55: Heat flow curve of all 0.26 w/cm mixes using HR-P2 admixture

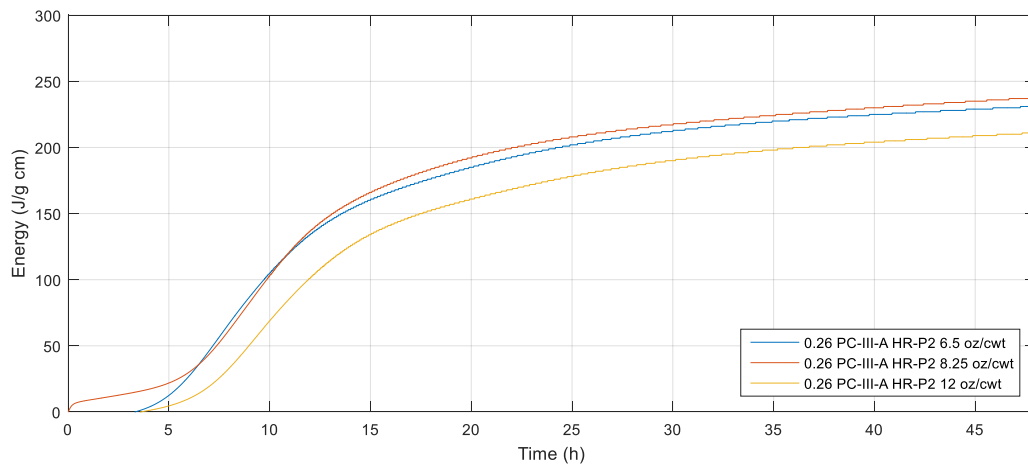


Figure 5-56: Cumulative heat evolved of all 0.26 w/cm mixes using HR-P2 admixture

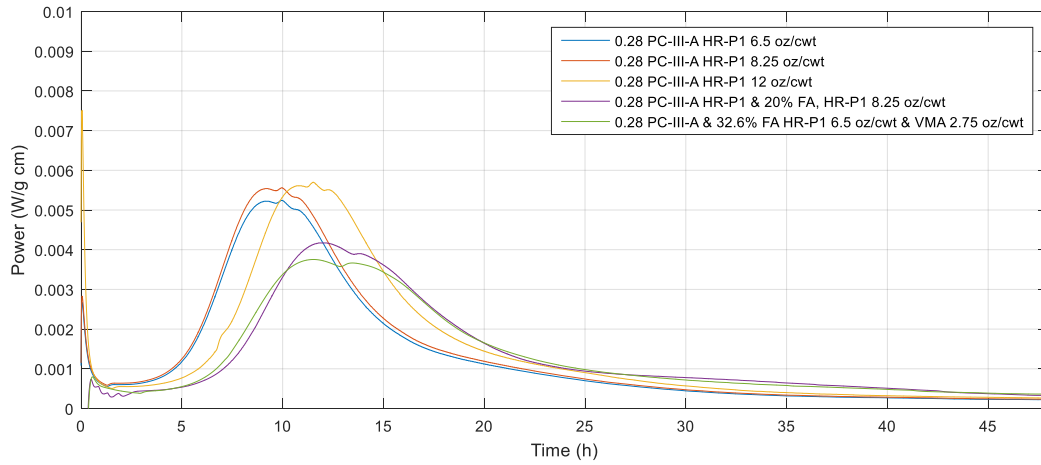


Figure 5-57: Heat flow curve of all 0.28 w/cm mixes using HR-P1 admixture

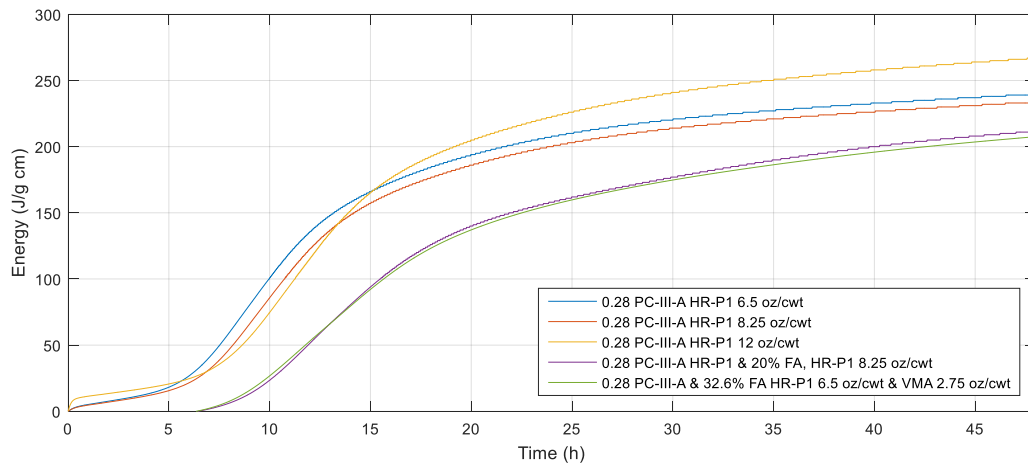


Figure 5-58: Cumulative heat evolved of all 0.28 w/cm mixes using HR-P1 admixture

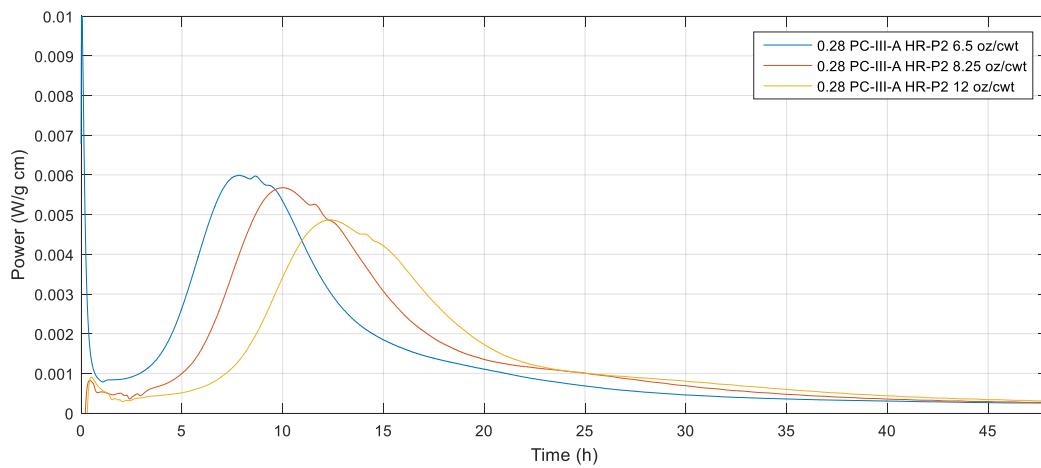


Figure 5-59: Heat flow curve of all 0.28 w/cm mixes using HR-P2 admixture

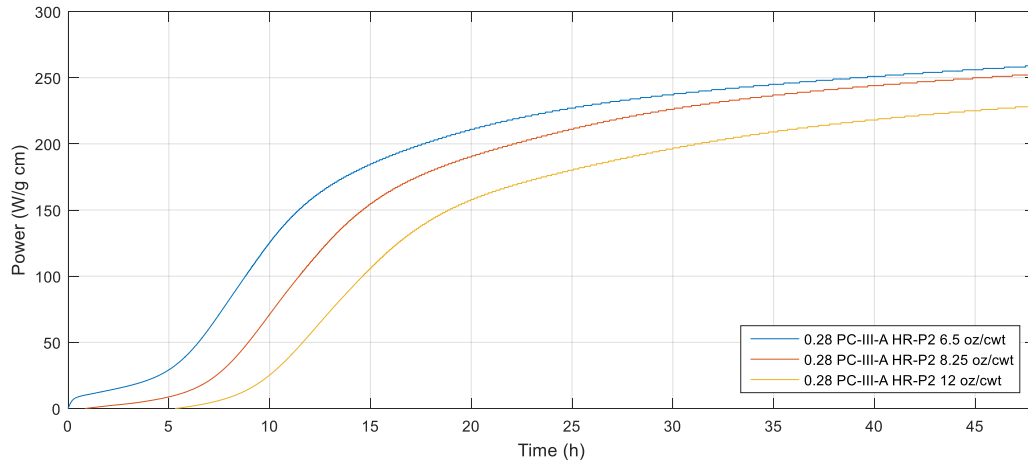


Figure 5-60: Cumulative heat evolved of all 0.28 w/cm mixes using HR-P2 admixture. Total cumulative heat evolved trends higher for a lower dosage of admixture.

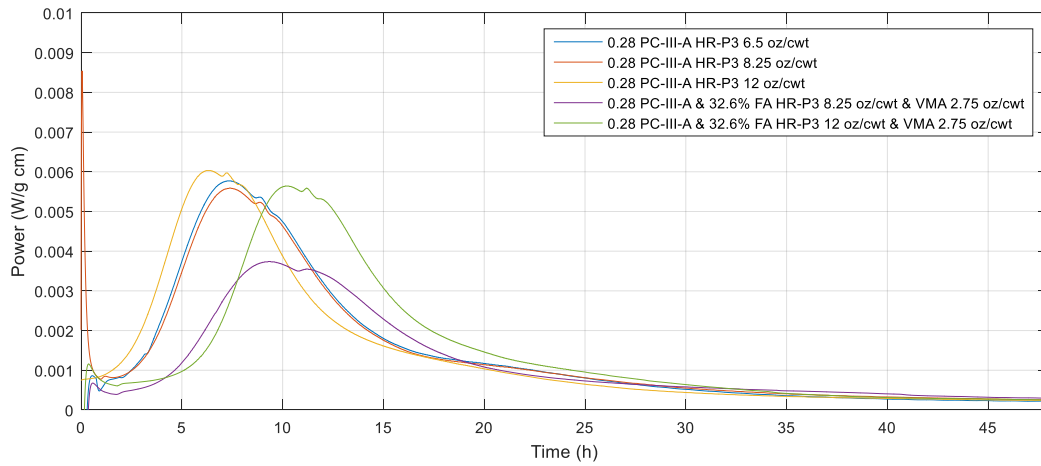


Figure 5-61: Heat flow curve of all 0.28 w/cm mixtures to compare the effect of HRWR dosage and addition of fly ash

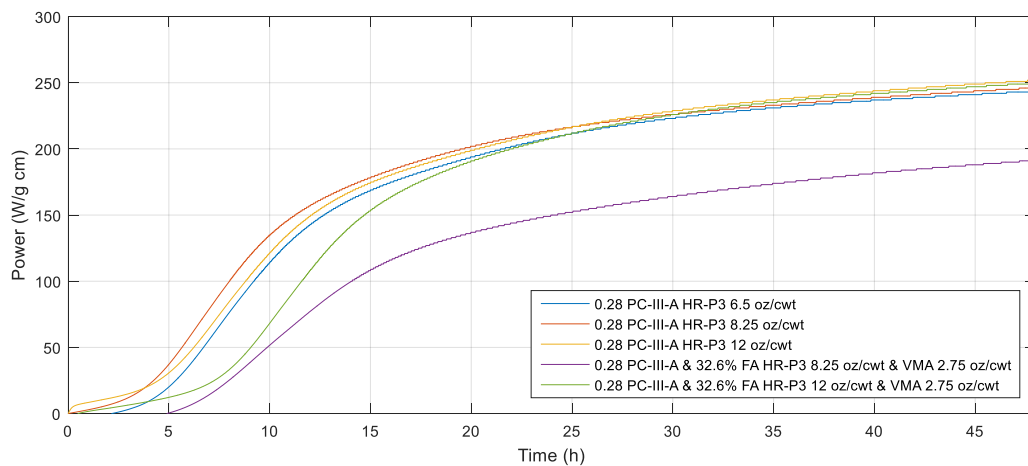


Figure 5-62: Cumulative heat evolved for all 0.28 w/cm mixtures

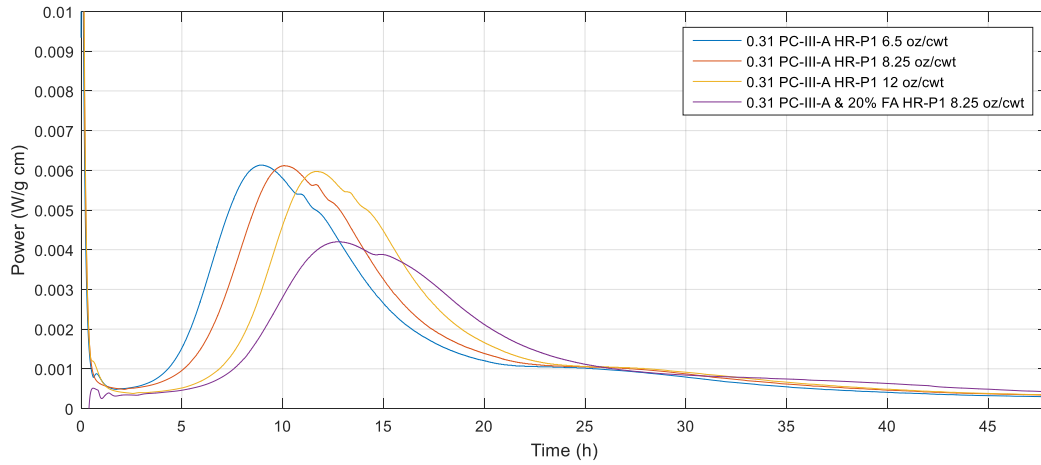


Figure 5-63: Effect of dosage of HR-P1 and fly ash on heat flow over time for 0.31 w/cm

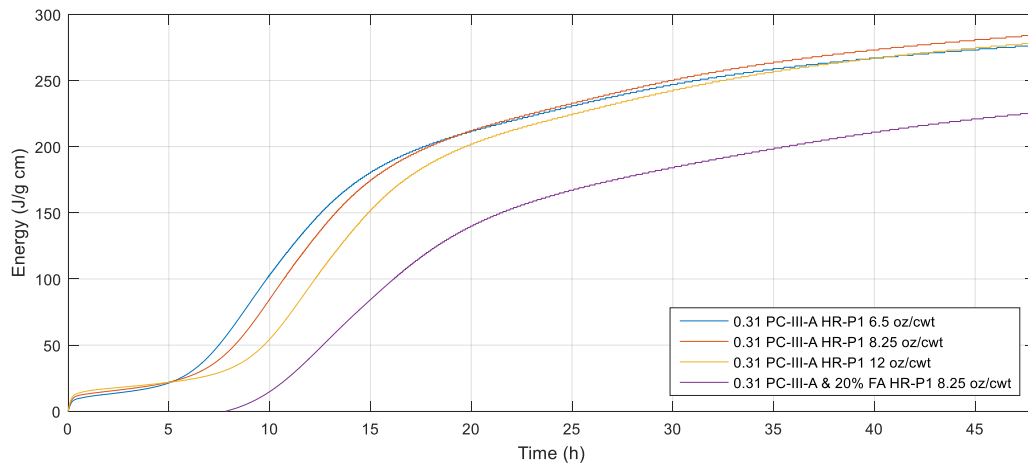


Figure 5-64: Effect of dosage of HR-P1 and fly ash on total heat evolved for 0.31 w/cm

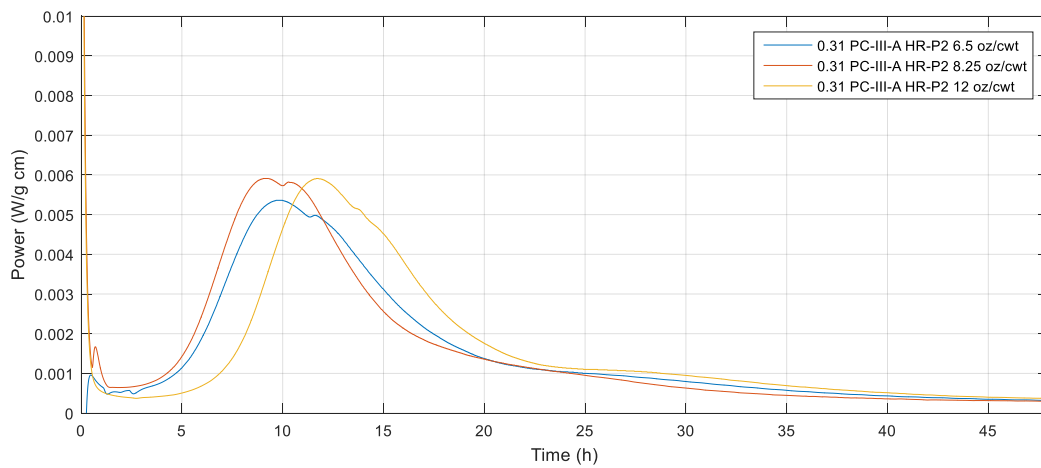


Figure 5-65: Effect of HR-P2 dosage on heat flow curve

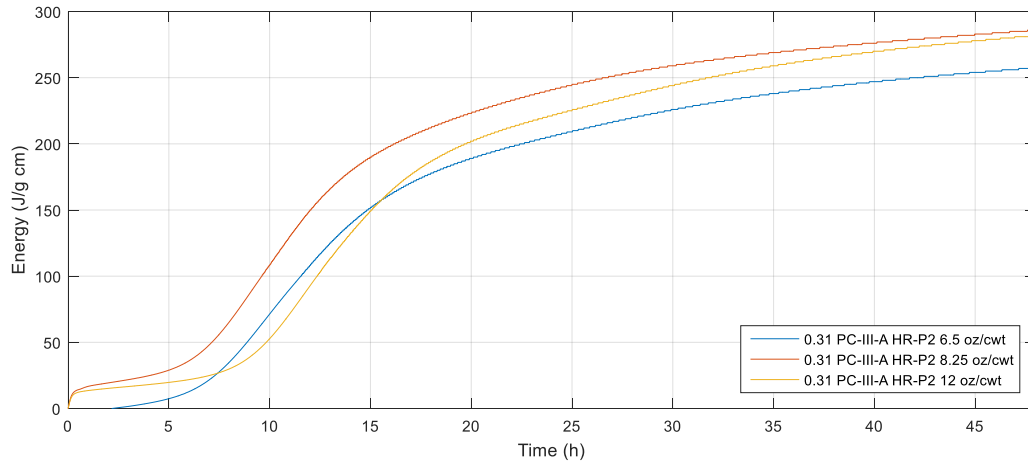


Figure 5-66: Heat flow curve of 0.31 w/cm mixtures evaluated

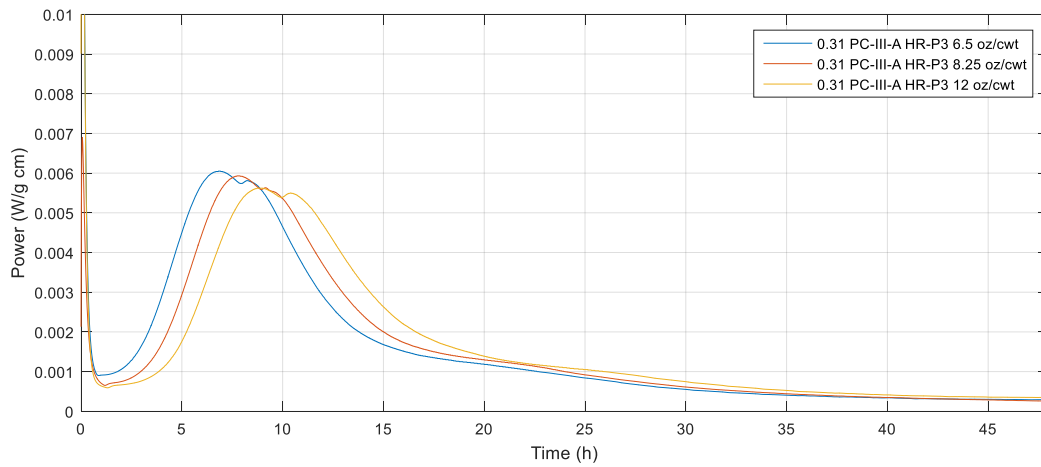


Figure 5-67: Heat flow curve of all 0.31 w/cm mixes using HR-P3 admixture

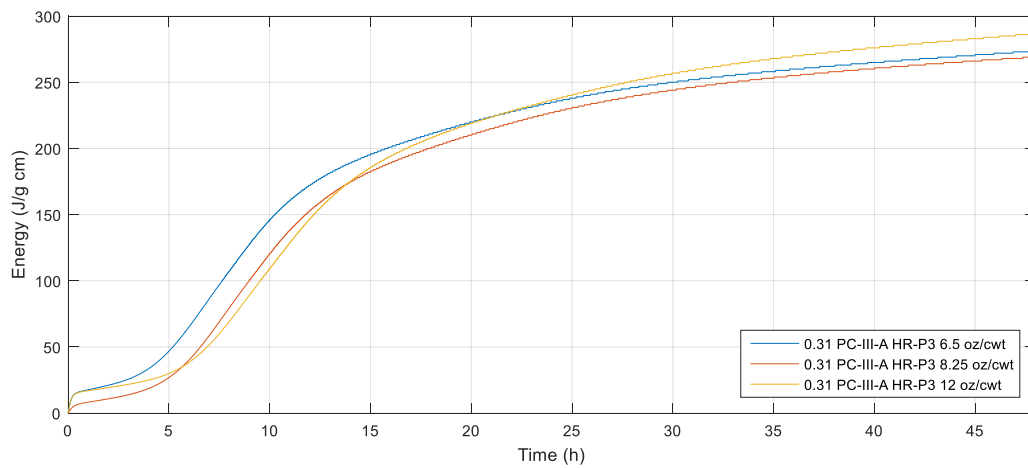


Figure 5-68: Total energy curve of all 0.31 w/cm mixes using HR-P3 admixture

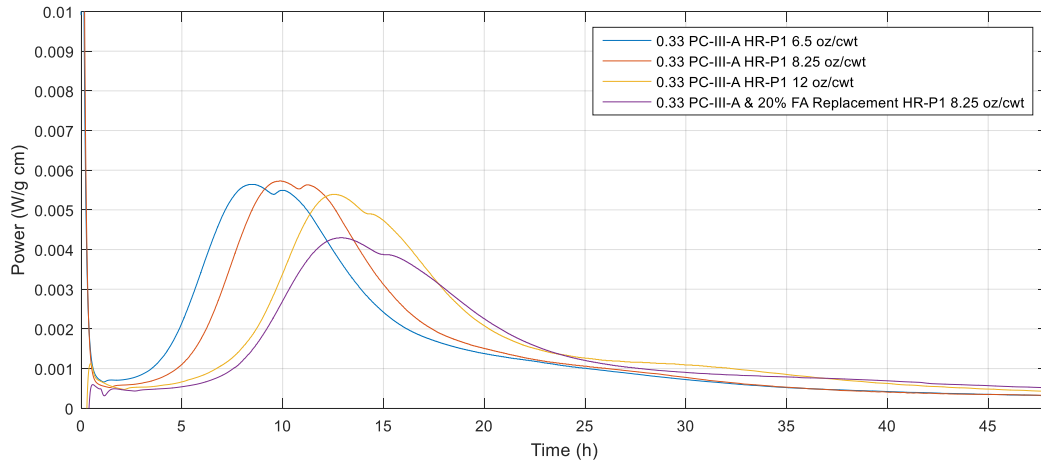


Figure 5-69: Heat flow curve of all 0.33 w/cm mixes evaluated using HR-P1

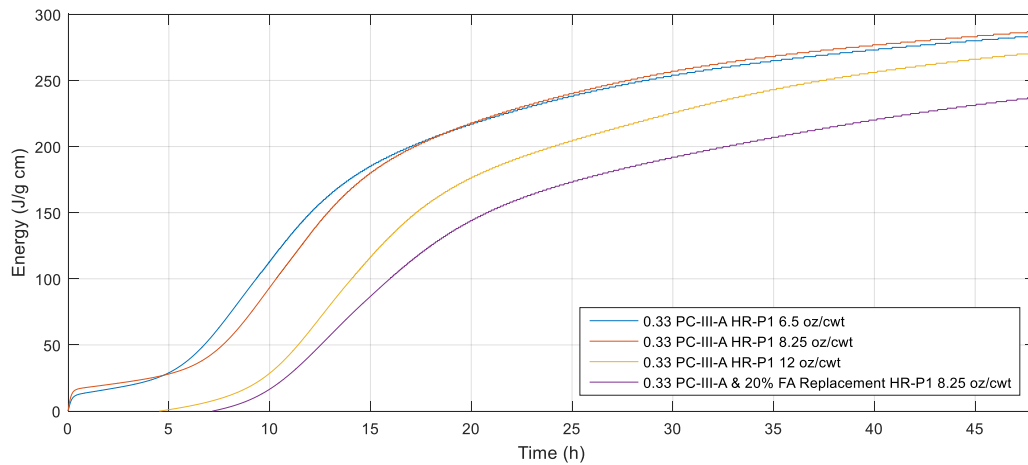


Figure 5-70: Total heat evolved for 0.33 w/cm mixes incorporating HR-P1

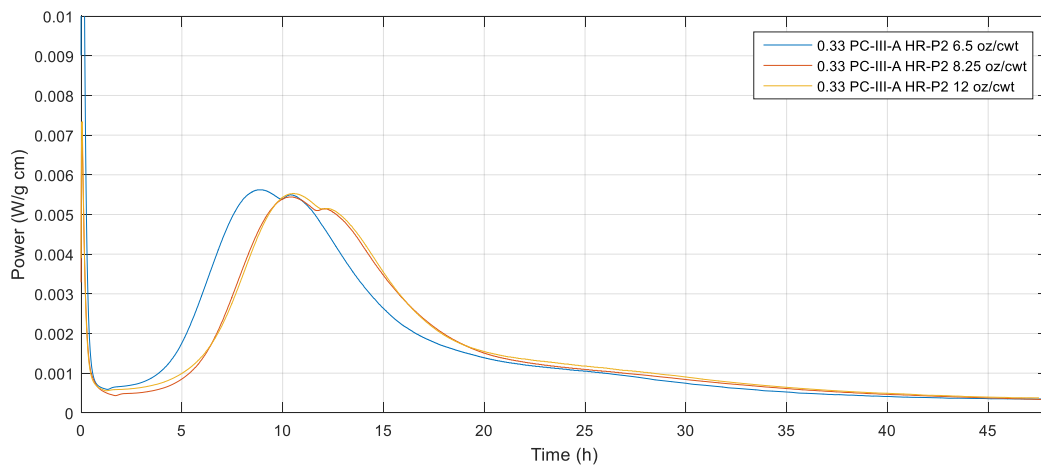


Figure 5-71: Heat flow curve of 0.33 w/cm mixtures incorporating HR-P2

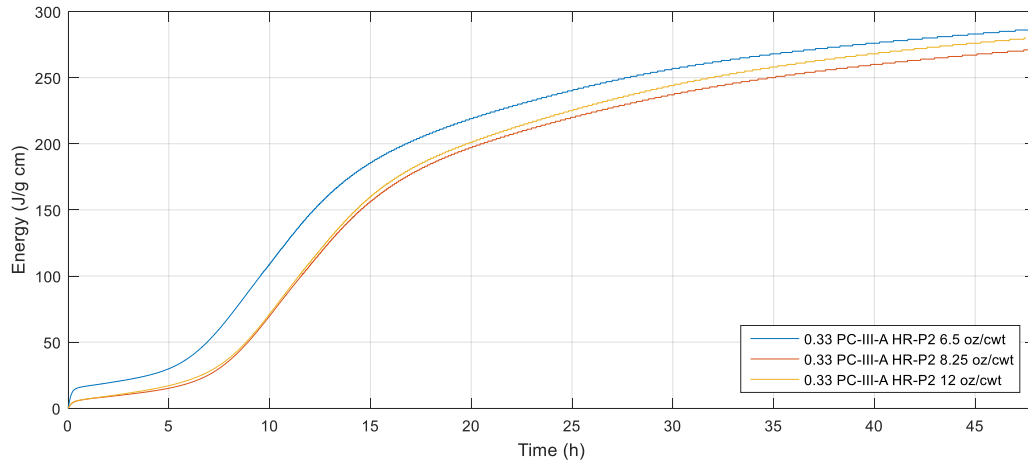


Figure 5-72: Total heat evolved curved of 0.33 w/cm curves incorporating HR-P2

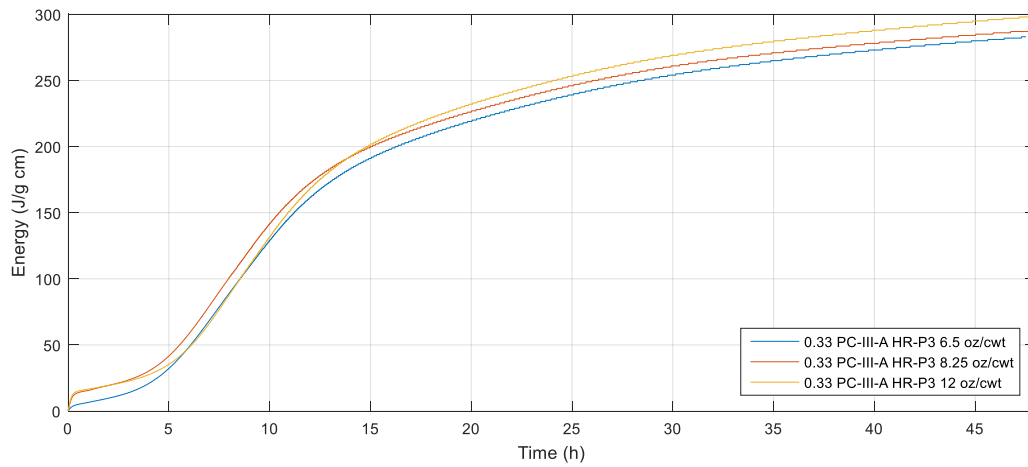


Figure 5-73: Heat flow curve of 0.33 w/cm curves incorporating HR-P3

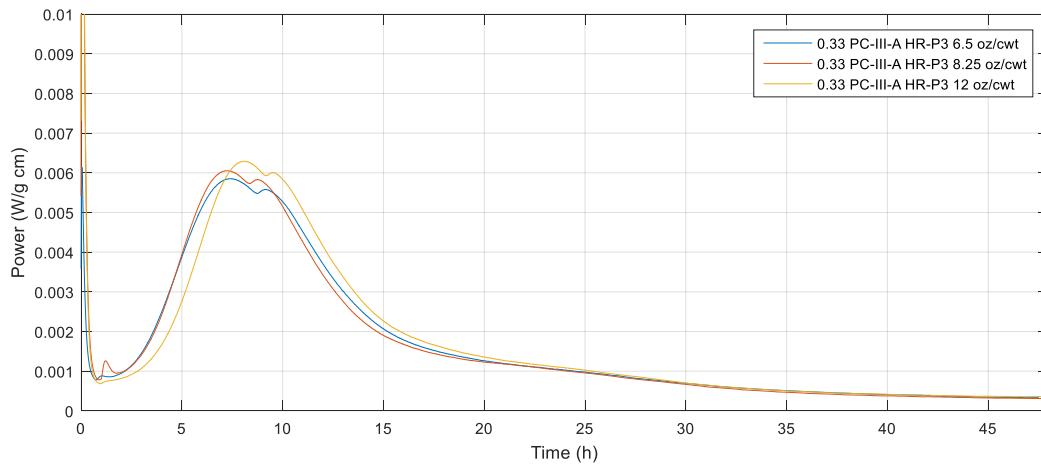


Figure 5-74: Heat flow curves of 0.33 w/cm mixtures incorporating HR-P3

5.4.3 Key Findings and Results

If the admixture was creating some sort of instability at an early age, one would expect the calorimetry plots to reflect that incompatibility issue. Based upon the isothermal calorimetry data collected, hydration is occurring in these mixtures as expected. All brands of HRWR performed similarly. Increased dosage of HRWR results in increased delay of hydration and reduction in peak heat flow, which was expected. The reduction in peak heat flow could explain the correlation between increased dosage of HRWR and reduction in autogenous shrinkage. Incorporation of VMA has little effect on hydration. Incorporation of fly ash reduces heat evolved significantly. This is a significant result as many blocks incorporating fly ash do have cracking. It indicates that there is little reason to that the early age heat evolution of the mixtures has an impact on the cracking.

5.4.4 Mini Ring Test

5.4.4.1 Procedure and Experimental Setup

In order to determine the cracking potential due to autogenous deformation of paste samples, the mini ring test was developed as described in Chapter 2. The setup employed is shown in Figure 5-75.



Figure 5-75: Mini restrained ring test

The samples for were prepared in 1-in. diameter plastic vials that was modified by placing a 5/8-in. diameter stainless steel rod through its center. A 1-in. outer diameter and 5/8-in. inner diameter black rubber tube was inserted into a plastic mold to support and center the rod. Paste was prepared in accordance with ASTM C305. The paste was set into the outer ring of the mold and sufficient vibration was applied until the paste had a smooth radial surface, free of entrapped air. The paste was filled just below the top of the stainless steel rod to create a 1-in. tall specimen

size. After casting, the samples were sealed and placed in a water bath at 23 °C. The samples were left in the water bath and monitored on a daily basis to determine if cracking had occurred. The test is configured under the same principle as the restrained shrinkage ring test, except that the mixtures are only compared under the basis of time to cracking observed. Figure 5-76 provides an example of cracking of a paste sample.

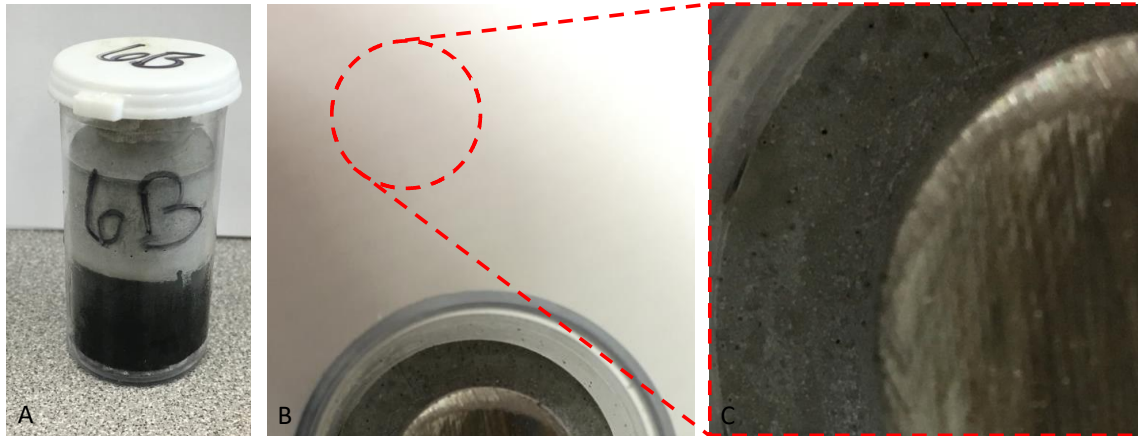


Figure 5-76: Crack development in mini-ring restrained test:

(a) three-month-old paste sample in sample in mini-ring vial; (b) red circle illuminating location of crack; (c) close-up of autogenous formed shrinkage crack

5.4.4.2 Results for Mini Ring Test

The concept of the mini restrained ring test was to create a quick and simple paste test that targets autogenous shrinkage, quantifying it as a function of time to cracking. Unfortunately, the testing period proved longer than expected and no monitored samples developed cracking even over a 2-month period (see Table 5-6).

Table 5-6: Time of cracking for restrained paste mixes that did crack

w/cm	Cement Type	Fly Ash	HRWR	HRWR Dosage (fl. oz./cwt)	Time of Cracking (days)
0.28	Type III	-	Sika 2100	6.5	26
0.31	Type III	-	Sika 4100	8.25	30
0.31	Type III	-	BASF 7700	8.25	28
0.33	Type III	-	Sika 2100	8.25	28
0.33	Type III	-	Sika 4100	8.25	30

5.5 Key Findings

Many test methods were ruled out as effective and simple methods for screening good performers from bad performers. Additionally, the following was indicated by data from test methods contained in this section:

- Increased HRWR dosage correlates with decreased autogenous shrinkage (in 75% of cases)
- All admixture types have a similar effect on hydration, in that they retard it
- Incorporation of fly ash (generally) significantly decreased heat produced

Chapter 6. Field Work

6.1 Introduction

In this section, analysis of the data obtained from field sites (precast plants and exposure sites) is presented. Exposure blocks and mini-girders were cast and placed at the University of Texas at Austin exposure site located at the Pickle Research campus for future testing and analysis. In addition to the exposure blocks located at the University of Texas at Austin, several exposure blocks located at TxDOT Cedar Park were monitored on a bi-annual basis. The blocks at TxDOT's Cedar Park site were cast between August 2010 and October 2012.

6.2 TxDOT Exposure Site Visit

To better quantify the potential cause and effects behind the micro-cracking observed in the field, three visits to the TxDOT exposure site were made. The blocks selected for visual inspection were chosen based on materials used in the concrete, mixture designs, admixtures, and specimen casting date, age of specimen, as well as previous experience and knowledge with respect to the cracking issue.

6.2.1 Block Examination

The TxDOT Concrete Block Exposure Site located in the Cedar Park Campus is composed of more than 1500 exposure blocks that have been cast in order to observe a number of natural concrete deterioration phenomena's. The blocks at the TxDOT Cedar Park site were cast between August 2010 and October 2012. In all, 67 exposure blocks were selected for long-term visual inspection for this project. Table 6-1 summarizes the selection criterion for the exposure blocks that were inspected at the Cedar Park TxDOT Site. With respect to the mixture composition, blocks were selected based on having at least one of the following material from each of the category listed in Table 6-1, i.e., cement type, admixture type, coarse and fine aggregate source and w/c ratio. These materials were selected in consultation with TxDOT and based on previous knowledge with respect to the cracking issue.

Table 6-1: Material Selection Criterion for Crack Investigation of Cedar Park TxDOT Site

Cement	HRWR	Coarse Aggregate	Fine Aggregate	w/c ratio
PC-A-III PC-B-III PC-C-III PC-D-III	HR-PI HR-P2 HR-P3 HR-P4	CA-R CA-L CA-RIII	FA-R FA-L FA-RIII	0.25 through 0.40

Each of the examined exposure blocks were assigned a “crack rating” based upon the worst state of the visible micro-cracking on any of the surfaces exposed to the environment, with a crack rating of 1 corresponding to negligible/no micro-cracking and a crack rating of 5 corresponding to severe micro-cracking (see Figures 6-1 through 6-5 for an example of the cracking rating system

on blocks evaluated at the Cedar Park Exposure site). Appendix VI lists all the evaluated blocks based on their crack rating—ranked no visible cracking (0) to worst case cracking (4.5).



Figure 6-1: Example of Crack Rating = 0



Figure 6-2: Example of Crack Rating = 1



Figure 6-3: Example of Crack Rating = 2



Figure 6-4: Example of Crack Rating = 3



Figure 6-5: Example of Crack Rating = 4.5

In hopes of determining whether there were any trends in the severity of cracks seen amongst the blocks, the blocks were grouped into four categories based on casting date, w/b ratio, cementitious content, and cement source. Figure 6-6 displays the crack rating versus month of casting plot. Figure 6-7, Figure 6-8, Figure 6-9, and Figure 6-10 display the crack rating versus w/b ratio, cement content, and cement source plots, respectively. All crack rating values were collected in March of 2015.

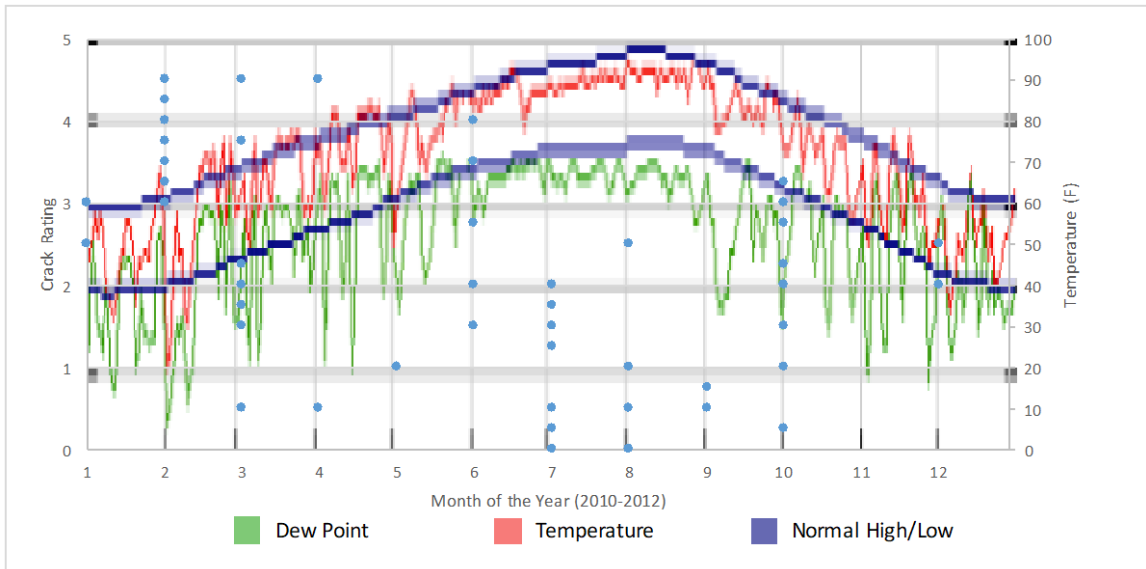


Figure 6-6: Exposure block crack ratings with respect to month of casting.
 Data represents 67 distinct blocks. Dew point is a representation of RH. The “normal high/low” are averages for historical recorded temperatures. Data taken from wunderground.com (2016).

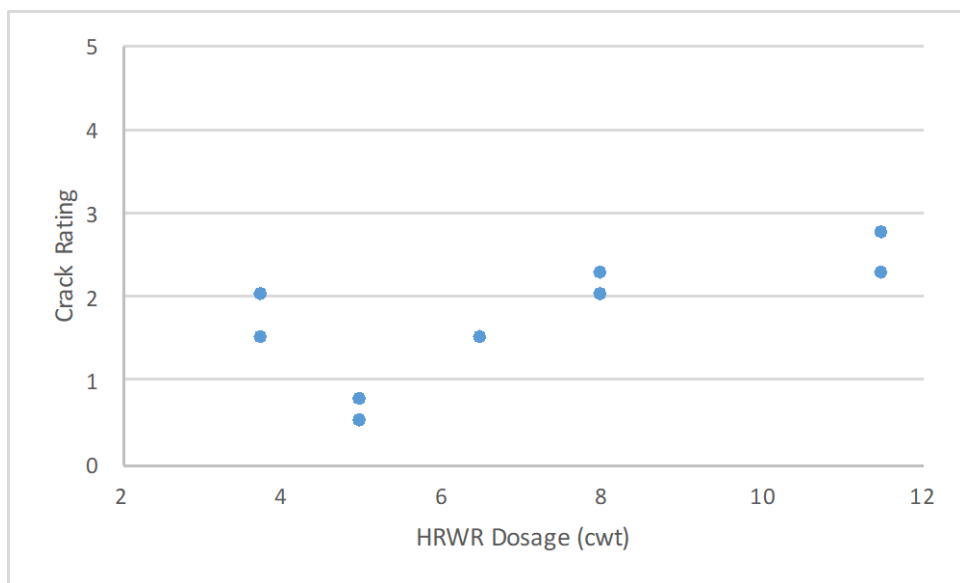


Figure 6-7: Exposure block crack ratings according to variation in HR-P1 dosage with all other properties held constant; data represents nine distinct blocks.

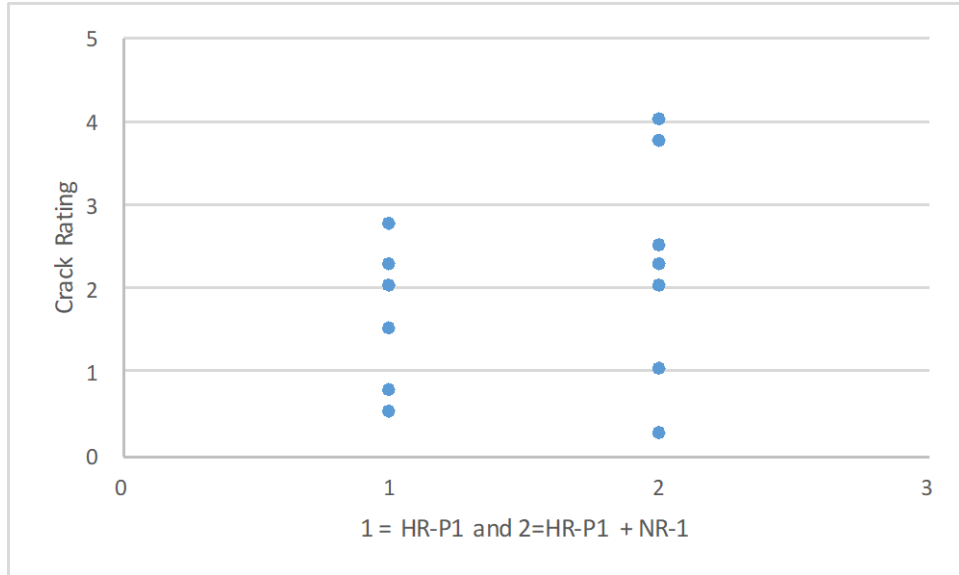


Figure 6-8: Exposure block crack ratings according to variation in HR-P1 and HR-P1+NR-1 with all other properties held constant; data represents 16 distinct blocks.

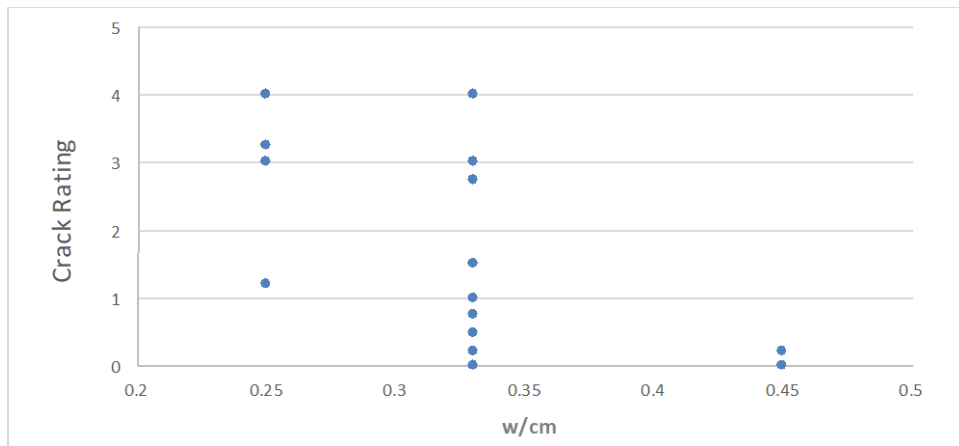


Figure 6-9: Exposure block crack ratings according to a given water-to-cement ratio for a fixed cement content of 658 lb/yd³; data represents 38 distinct blocks.

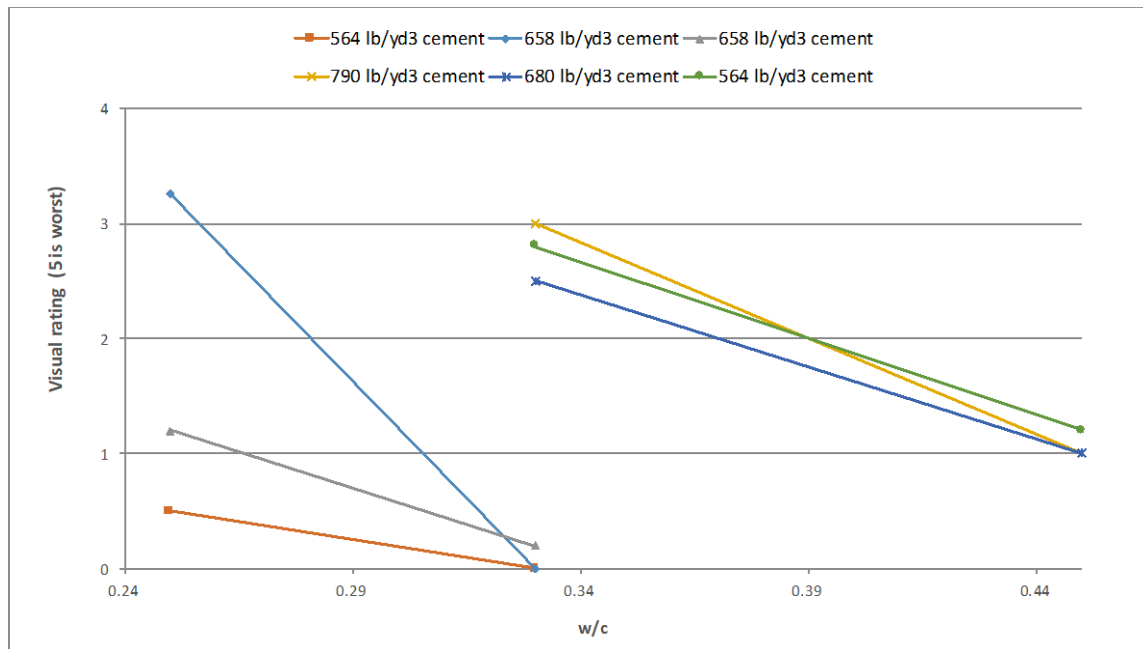


Figure 6-10: Exposure block crack ratings according to a given cementitious content lb/yd³; data represents 12 distinct blocks.

Based on Figures 6-6 through 6-10, alongside the observations made on the TxDOT site regarding the severity of cracking alongside the different faces of the blocks, the following trends are proposed:

- Effect of Casting Date:** It was hypothesized that the exposure conditions in early stages may have played a role in the increased development of the micro-cracking issue. While no definitive relationship can be made from Figure 6-6 between casting date vs. crack rating when only the month of casting is considered, overall it appears as if concrete cast during the colder periods of the year (December, January, and February—months 12, 1, 2, respectively) had higher crack ratings than blocks casts during the warmer months of June (month 6), July (month 7) and August (month 8). Further analysis should be conducted to evaluate the temperature on the date the concrete was cast since temperature can fluctuate greatly from month to month depending on the year, as well as the difference between casting date temperature (or concrete temperature) and maximum and minimum temperatures (concrete or ambient) within the first 24 – 48 hours after casting. Additionally, it should be noted that despite the period between the first block and last block cast for this series being approximately three years, the extent of cracking for short and long term of exposure seems not to be a major governing factor. The first four sets of blocks cast in December of 2010 and January 2011 have a 1.5 through 3.0 crack rating for an average of 2.4 and the last eight blocks cast in October of 2012 have crack ratings of 1.25 through 2.75 for an average of 2.1.
- Effect of HRWR Dosage:** Figure 6-7 confirms that the extent of the micro-cracking issue proves to be independent of solely the HRWR dosage. Note that this comparison using the fixed variables of the following: 658 lb/yd³ of PC-III-A, w/b = 0.33, HR-P1 and CA-A and CA-AII. It is important to rule out the dosage of HRWR as a potential adverse

effect on micro-cracking, however the majority of the exposure blocks cast at the Cedar Park Site did not disclose the dosages used since this was not controlled¹.

- *Effect of HRWR vs. HRWR+NR:* As shown in Figure 6-8 no conclusion can be drawn between the use of solely HRWR HR-P1 and HRWR HR-P1 + NR-1. Since the addition of normal range water reducing retarding admixtures proved non influential with respect to micro-cracking, inclusion of retarders was not considered to be a key factor governing the micro-cracking issue.
- *Effect of HRWR type:* Comparing 4 different HRWRs (HR-P1, HR-P2, HR-P3 and HR-P4) with and without NR-1 with all other mixture variables constant did not provide enough data to determine the effect of admixture type on cracking behavior of field specimens. In order to solely address HRWR type as a source of cracking performance only 16 out of the 67 blocks had the same cement source, aggregate source, w/c ratio and cement content. Since the majority of the blocks (11 out of 16) contained HR-P1, there is not enough data available to evaluate the effect of HRWR composition. Therefore, HRWR type may not be eliminated as a potential variable effecting the extent for the remainder of this analysis.
- *Effect of Aggregate Source:* Aggregate source does not appear to have a strong correlation with worsening of cracking that has been seen in the field. In order to solely address aggregate source as a component of cracking performance only 24 out of the 67 blocks had the same cement source, HRWR type, w/c ratio and cement content. Since the majority of the blocks (19 out of 24) employed the same aggregate, there is not enough data available to evaluate the effect of aggregate source. Therefore, aggregate source may not be eliminated as a potential variable effecting the extent for the remainder of this analysis. It must be noted however, a block with lightweight aggregate, Block 244 from Cedar Park Exposure Site, had the highest crack rating (4.5) of all the blocks observed in this study. Previous research has confirmed that internal curing via soaked lightweight aggregate reduces and in some cases eliminates autogenous shrinkage effect. Block 244 suggests that the extent of micro-cracking is a not solely related to autogenous shrinkage, but that it is due to a culmination of multiple volumetric changing mechanisms.
- *Effect of Cement Source:* Cement source does not appear to have a strong correlation with worsening of cracking that has been seen in the field. In order to solely address cement source as a component of cracking performance only 17 out of the 67 blocks had the same HRWR type, aggregate source, w/c ratio and cement content. Since the majority of the blocks (13 out of 17) employed the same cement source, there is not enough data available to evaluate the effect of cement source. A larger sample size must be taken in order to draw a proper conclusion of this variable. Therefore, cement source may not be eliminated as a potential variable effecting the extent for the remainder of this analysis.
- *Effect of w/c ratio:* In order to address the concern of drying shrinkage cracking on the exposure blocks w/c ratio vs. crack rating (for a fixed cement content) investigated as seen in Figure 6-9. It appears that there is a correlation between lower w/c and crack

¹ From communication with TxDOT employees, we were informed that the HRWR dosage was not recorded since the HRWR was added (sometimes incrementally during mixing) until the desired slump was achieved.

rating. Unfortunately, there is not a large enough sample size to discernibly confirm that higher w/c ratios result in decreased cracking potential.

- *Effect of Cement Content:* Though the data collected and plotted in Figure 6-10 it can be confirmed that lower cementitious contents results in a lower cracking potential.
- *Effect of Drying Orientation:* Visual inspection of the exposure blocks through multiple visits confirmed that the East and West faces of the blocks showed the worst cracking relative to the North and South faces. Therefore, consistent East facing block faces were used for cracking evaluation throughout the field investigations. This suggests that the severity of wetting and drying cycles over the lifetime of the concrete block or temperature effects is impacting the micro-cracking issue, specifically micro-cracking is exacerbated when the wetting and drying occurs quickly and/or blocks faces are subjected to higher temperature variations.

6.3 Precast Plant Site Visit

Since the micro-cracking issue was initially discovered on girders that had been sitting in the precast yard awaiting use in the field, investigating full-scale girders at the precast plants were part of this project. These girders were rejected for use in the field due to micro-cracking. Two separate precast plants were selected to investigate the micro-cracking issue based upon production size, and differences in materials and admixtures employed at each of the plants. The visits to the plants were purely visual inspection. The severity and integrity of the cracking was measured against the following: casting dates, primary location of cracking, and size and spread of cracking. Based upon the two separate precast plant visits the following was documented and proposed:

- *Casting Dates:* Girders that had been exposed to the environment the longest displayed some of the worst cracking. However, the mixture designs were not collected on any of the girders and a majority of the girders with like micro-cracking issues had been demolished by the precast plants. Therefore, although it is well known the delayed micro-cracking issue worsens with time no conclusion can be formally made between the different girders that were investigated at the precast plants due to lack of girders from different casting periods.
- *Location of Cracking:* Several different structural elements were investigated during the precast plant site visits, but in order to provide a more definitive comparison between the two separate precast plants (PP-A and PP-B) the focus was limited to AASHTO Type IV girders. Although the bulk of micro-cracking was widespread across the girders, certain girders displayed a denser allocation of cracking on different faces of the girders. Girders inspected at Precast Plant A displayed micro-cracking focused on the girder's flange, whereas girders located at Precast Plant B was concentrated on the girder's web. Figure 6-11 designates the cracking locations based on general observations at both plants and specific observations at the individual plants.

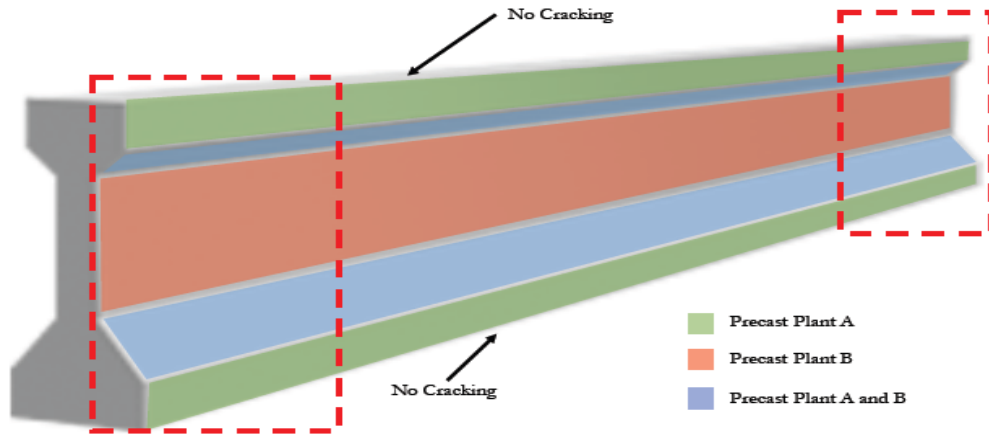


Figure 6-11: Concentration of map cracking pattern.

Note no visible cracking on top or bottom of girders.

Micro-cracking, whether on the flange or the web, propagated onto the angular flange segments of the girders. The cracking was more pronounced on the far ends of the girders and the density of the cracking lessened towards the middle segment of the girder. Cracking was either faint or not visible on either girder end faces and top segment of the girder. Regardless of the cracking intensity or location, the bottom face of the all the girders showed no micro-cracking. The bottom casting face anomaly also proves true in laboratory blocks that have placed on a permeable gravel foundation. Figure 6-12 and Figure 6-13 provide photographs from both PP-A and PP-B showing the differences in micro-cracking allocation on the girder faces.

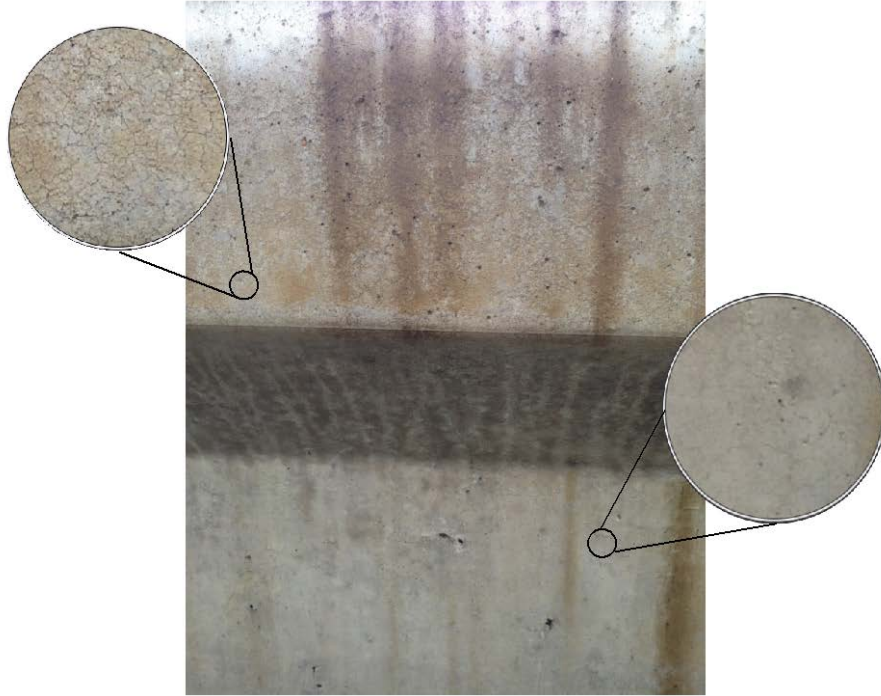


Figure 6-12: Girder located at Precast Plant PP-A (micro-cracking concentrated on upper and lower flange)

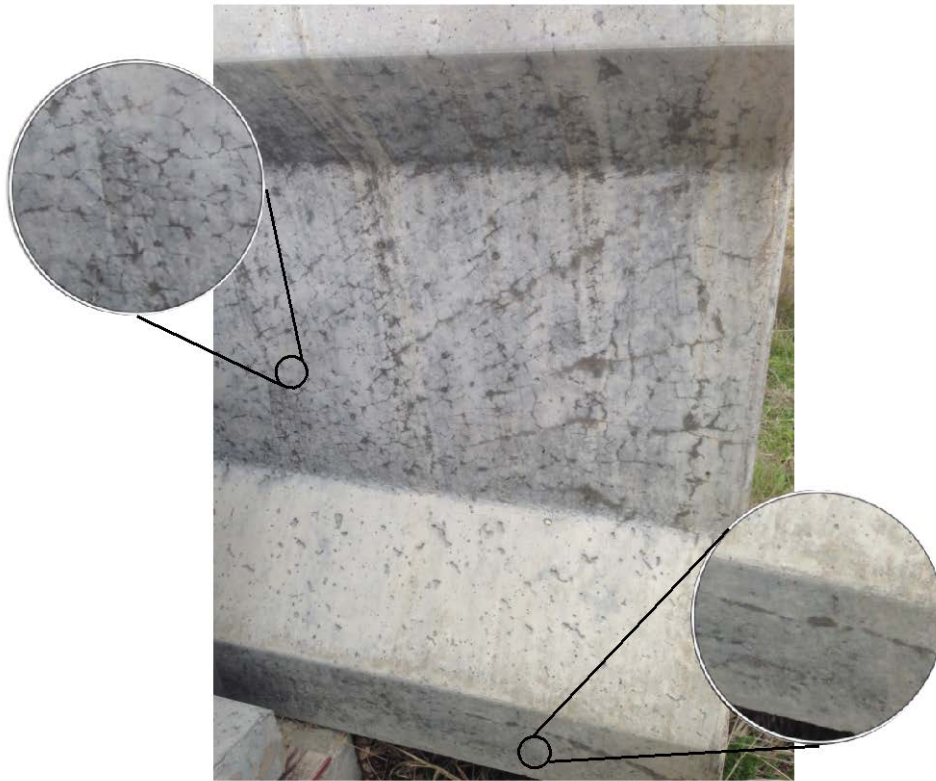


Figure 6-13: Girder located at Precast Plant PP-B (micro-cracking concentrated on web)

- **Size and Spread of Cracking:** Although the scope of this project did not investigate the propagation of crack width with time, visual inspection coupled with correspondence with TxDOT's quality control staff suggests that the cracks increase in density, but not width. The support for limited crack width enlargement with time is attributed to the structural cracks that typically develop on the girders ends. The structural cracks form as a result of the massive force release of the pre-stressed strand. The diagonal cracks as seen in Figure 6-14a have not widened, however the micro-cracking has developed around the structural cracks and the micro-cracks also begin to form away from the structural cracks (see Figure 6-14b).

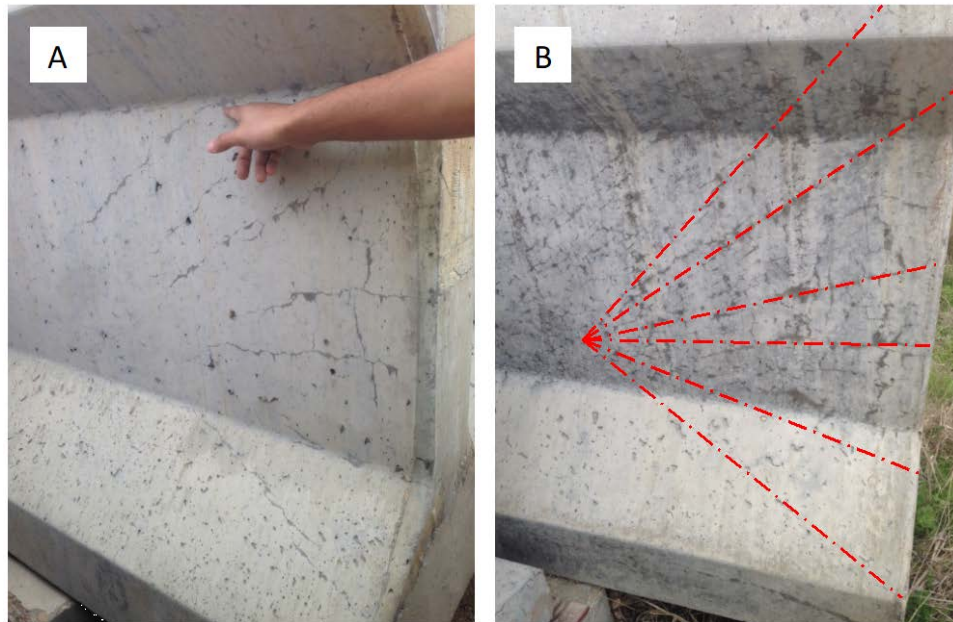


Figure 6-14: (A) Photo of girder located at Precast Plant PP-B with fingers pointing to diagonal release strand cracks. (B) Photo of a separate girder located at Precast Plant PP-B showing that the micro-cracks stem away from the release strand cracks and form in new space between release strand cracks

This reaffirms that this is a material-based issue, otherwise the micro-cracking would just propagate the widening of the structural release strand cracks (least path of resistance) without starting new cracks. Figure 6-15 also shows that the micro cracks develop away and outside of the diagonal release strand cracks, which may possibly be attributed to the moisture that more readily remains in the release strand cracks after a rain. This again, refers back to the wetting and drying cycles that seems to be exacerbating the micro-cracking issue.



Figure 6-15: Close up image of Figure 6-14(b).

This figure emphasizes the micro-cracking development separate from the outlined (dashed red) release strand cracks

6.4 UT Austin Exposure Site

6.4.1 Methodology

26 exposure blocks and 14 “mini-girders” were cast and stored at the exposure site located at the University of Austin to allow for frequent observation of the specimens. The blocks were cast in order to provide a more realistic natural environmental exposure condition as compared to the shrinkage tests (e.g., autogenous free shrinkage, stress development under passive restraint, and free shrinkage) that were being conducted in the laboratory environment. The exposure blocks and girders were assigned qualitative crack ratings (see Figure 6-2, Figure 6-3, Figure 6-4, and

Figure 6-5 for examples of the crack rating system benchmarks). Additionally, carbonation testing was performed was conducted using companion specimens for select mixtures. Figure 6-16 provides a picture of the exposure blocks that have been cast since 2013 as a part of the girder micro-cracking investigation.



Figure 6-16: Investigated blocks located at UT Austin’s exposure site

6.4.2 Exposure Specimen Types

6.4.2.1 Standard 3.4-ft³ Blocks

The exposure blocks were cast in 18x18x18-in. prismatic plywood forms. The plywood surface that makes contact with the concrete was coated with a generous layer of polyurethane form oil to aid in the demolding process and mimic the procedures followed at the precast plants.

6.4.2.2 3.4-ft³ Block with Expansion/Shrinkage Demecs

To better target and quantify the extent of the micro-cracking, select concrete mixtures were cast in exposure blocks that were instrumented with the hex bolts. The bolts were set at 2-in and 1-in depths. In addition, demec points were adhered on the North, South, East and West surfaces of the exposure blocks. The demec points were adhered to the concrete surface with approximately a ¼-in diameter dab of (Devcon 11765) epoxy. Figure 6-17 provides a diagram of the orientation and varying depths for the measurement locations of the measurable exposure blocks.

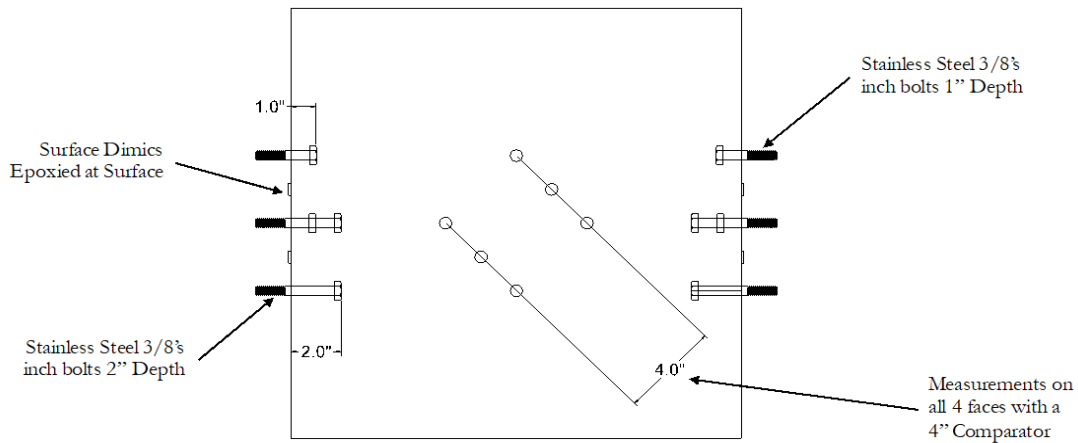


Figure 6-17: (Top) Wood mold used for casting measurable exposure blocks with bolts in place (Bottom) CAD drawing of various depths that bolts and surface demecs were placed for future expansion/shrinkage measurements.

Only the 4 in. diagonally annotated distance figured is measured with the comparator.

“Mini” Girders

In addition to the standard 3.4-ft³ exposure blocks, AASHTO Type IV girders (scaled down to approximately 1/3 from the size cast in the field) were cast for this project (see Figure 6-18) to investigate the effect of volume of concrete to surface area ratio (2.3 in.) that correlates to the true sizing in the field. Each mini girders had a volume of 6.4-ft³ of concrete. The extent of the latent cracking was closely monitored on the girders in order to determine whether cracking location and density occurs more quickly as with the precast plants. The exposure site for the mini girders is shown in Figure 6-19.

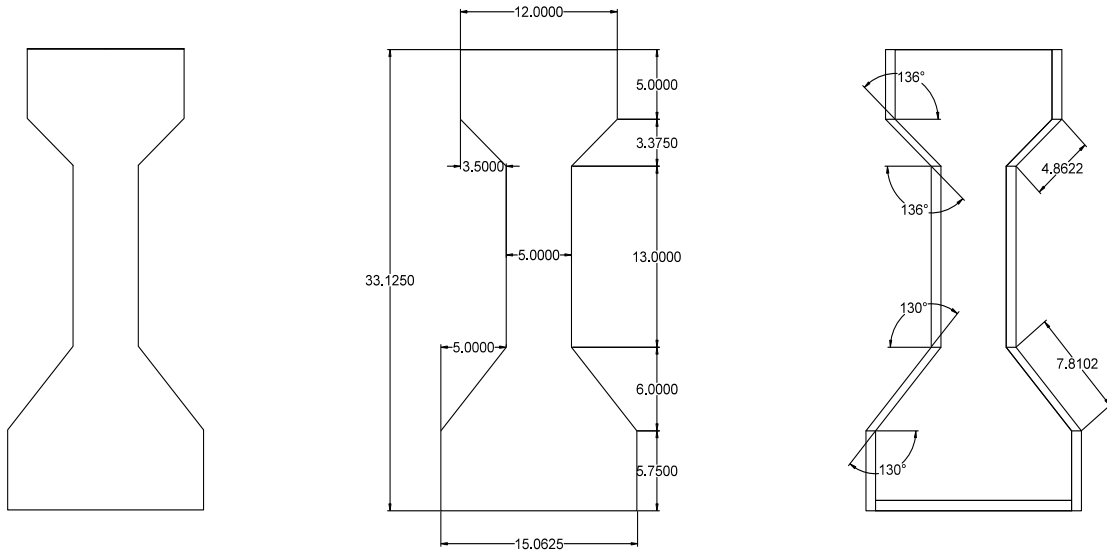


Figure 6-18: CAD drawing of mini-girders (dimensions are inches)



Figure 6-19: Mini girder exposure site (photo taken facing east)

6.4.2.3 Carbonation Specimens

Natural and sheltered carbonation prisms were exposed to the ambient temperatures and ambient CO₂ concentration as provided by the environment at the Construction Materials Research Laboratory located at the University of Texas at Austin's Pickle Research Campus. The 4x4x16 in. specimens were cast from the concrete mixtures used in the blocks and mini-girders. The prisms were cast in order to develop a comparative matrix in the hopes of quantifying crack intensity and

depth of carbonation. Mixed and cast alongside the exposure blocks and mini girders, the prisms were subsequently demolded and stored on a pervious rock bed or sheltered in a Stevenson screen. The prismatic specimens were stored standing up on one end. Figure 6-20 shows the carbonation field site where prisms were either sheltered or exposed to the natural elements.



Figure 6-160: Carbonation exposure site at UT Austin with shelter (Stevenson Screen)

6.4.3 Block and Mini Girder Exposure Results

Table 6-2 and Table 6-3 display the crack ratings (taken December 2016) of the exposure blocks and mini girders stored at the exposure site located at the University of Texas at Austin.

Table 6-2: Blocks cast at UT Austin exposure site for TxDOT 0-6813.

Precast plant mixtures mixed and cast at the precast plants and their laboratory replicates are highlighted. “PP” indicates a precast plant (A for Waco, B for Eagle Lake), “BP” indicates expansion monitored block, and “B” indicates a normal block without expansion monitoring.

w/cm	Cement Type	Cement Content (lb/yd. ³)	SCM Content (lb/yd. ³)	Aggregate Source		HRWR Type	HRWR Dosage (fl.oz./100 cwt)	NR Type	NR Dosage (fl.oz./100 cwt)	Age (months)	Crack Rating	Block ID
				FA	CA							
0.24	PC-III-A	705	-	FA-R	CA-L	HR-P2	12	NR-1	3	24	0	B-3
		705	-	FA-R	CA-L	HR-P4	12	NR-2	3	23	0	B-7
		705	-	FA-R	CA-R	HR-P2	15	NR-1	3	23	1	B-8
0.26	PC-III-A	705	-	FA-R	CA-R	HR-P3	10	NR-2	3	16	0	BP-6
	PC-III-A	700	175	FA-R	CA-R	HR-P2	8.25	NR-1	3	16	1	BP-5
	PC-III-A	705	-	FA-R	CA-R	HR-P2	6.5		3	19	1.75	PP-A Lab NC
	PC-III-B	705	271	FA-R	CA-R	HR-P1	8.25		3	16	0	BP-7
PC-I-A	705	-	FA-R	CA-R	HR-P1	12	NR-1		3	16	0	BP-3
0.28		705	-	FA-R	CA-R	HR-P1		12	3	16	0	B-1
		705	-	FA-R	CA-L	HR-P2		12	3	24	0	B-4
		705	-	FA-R	CA-R	HR-P1	12.5	NR-1	3	23	0 and 0	B2-A, B2-B
	PC-III-A	705	-	FA-R	CA-R	HR-P3	12	NR-2	3	23	0.5	B-5
		705	-	FA-R	CA-L	HR-P3	12		3	22	0.5	BP-1
		705	-	FA-R	CA-L	HR-P3	12		3	22	0.75	B-6
		705	-	FA-R	CA-L	HR-P4	12		3	23	0.1	G-7
		PC-III-B	705	-	FA-R	CA-L	HR-P1		12	NR-1	3	20
0.3	PC-III-A	564	188	FA-RII	CA-RII	HR-P3	8	NR-2	2	22	1.5 and 2	PP-B-A & PP-B-B
		564	188	FA-RII	CA-RII	HR-P3	8		0.5	20	0	PP-B Lab
		564	188	FA-R	CA-R	HR-P3	8		2	16	0	BP-4
		663	271	FA-R	CA-R	HR-P4	5.5		0.5	22	2	PP-A

w/cm	Cement Type	Cement Content (lb/yd. ³)	SCM Content (lb/yd. ³)	Aggregate Source		HRWR Type	HRWR Dosage (fl.oz./100 cwt)	NR Type	NR Dosage (fl.oz./100 cwt)	Age (months)	Crack Rating	Block ID
				FA	CA							
		663	271	FA-R	CA-R	HR-P2	5.5	NR-1	2.5	19	0	PP-A Lab SCC
0.31	PC-III-A	663	271	FA-R	CA-R	HR-P2	7.25		2.5	16	0	BP-8
		663	271	FA-R	CA-R	HR-P3	7.25		2.5	16	0	BP-9
		663	271	FA-R	CA-R	HR-P1	7.25	NR-1	2.5	16	0	BP-10
0.33	PC-III-A	658	-	FA-R	CA-R	HR-P1	12	NR-1	3	16	0	BP-2

Table 6-3: Mini girder matrix at UT Austin Exposure Site.

Precast plant mixtures mixed and cast at the precast plants and their laboratory replicates are highlighted.

w/cm	Cement Type	Cement Content (lb/yd. ³)	SCM Content (lb/yd. ³)	Aggregate Source		HRWR Type	HRWR Dosage (fl.oz./100 cwt)	NR Type	NR Dosage (fl.oz./100 cwt)	Age (months)	Crack Rating	Block ID
				FA	CA							
0.24	PC-III-A	705	-	FA-R	CA-L	HR-P4	12	NR-2	3	23	0.1	G-7
	PC-III-A	705	-	FA-R	CA-R	HR-P2	15	NR-1	3	23	0	G-8
0.26	PC-III-A	705	-	FA-R	CA-R	HR-P2	6.5	NR-1	3	19	0	PP-A LAB NC
0.28	PC-III-A	705	-	FA-R	CA-R	HR-P1	12	NR-1	3	16	0	G-1
		705	-	FA-R	CA-R	HR-P1	12		3	23	0	G-2
		705	-	FA-R	CA-R	HR-P3	12	NR-2	3	23	1	G-5
		705	-	FA-R	CA-L	HR-P2	12.5	NR-1	3	24	0.5	G-3
		705	-	FA-R	CA-L	HR-P2	12	NR-1	3	24	0.25	G-4
	705	-	FA-R	CA-L	HR-P3	12	NR-2	3	22	0	G-6	
	PC-III-B	705	-	FA-R	CA-L	HR-P1	12	NR-1	3	20	0.75	G-11
0.3		564	188	FA-RII	CA-RII	HR-P3	8	NR-2	0.5	20	0.5	PP-B Lab
		564	188	FA-RII	CA-RII	HR-P3	8		2	22	2.5	PP-B
0.31	PC-III-A	663	271	FA-R	CA-R	HR-P4	5.5	NR-2	0.5	22	1	PP-A
		663	271	FA-R	CA-R	HR-P2	5.5	NR-1	2.5	19	0	PP-A Lab SCC

Overall results beyond expected cracking ages of 18 to 24 months show that mixes with a variety of types and dosages of polycarboxylate admixture show distress. Cracked blocks also vary in cement content, aggregate, and water to binder ratio. The matrix adds to the current state of knowledge regarding the micro-cracking issue and allows for several interesting comparisons:

1. **Lab vs. Precast Manufacture (*highlighted in green and orange*):** Precast mixtures (PP-B and PP-A) show very variable results. Both PP-A SCC and PP-B Lab mixtures (girder and block) mixed at the UT CMRG/LIME lab show no micro-cracking. However, the same mixtures made at a precast plant and placed at the exposure site displayed significant micro-cracking: see block PP-A (CR-2) and girder PP-A (CR-1); girder PP-B (CR-2.5) and PP-B (CR-1.5 and 2). The lab mixtures have reached an age of 19 months without showing any micro-cracking and there is only a 3-month age difference between the lab and precast mixtures.

The only difference in mixture proportioning of the lab mixes as opposed to both of the precast plant mixes is the dosage of “NR” or normal range water reducer and retarder. The PP-B uncracked lab-mixed block only used 0.5 fl. oz./cwt, whereas both PP-B cracked blocks mixed by the precast plant have a NR dosage of 2 fl. oz./cwt. Contradicting this result the PP-A uncracked lab-mix was made with a dosage of 2.5 fl. oz./cwt, while the cracked blocks were made with a dosage of 0.5 fl. oz./cwt. Therefore, dosage of NR-1 cannot be a source of the driving mechanism. These results suggest that the mixing and/or casting process has an effect on the micro-cracking. The mixers used at the UT CMRG/LIME are known to be less powerful than those used at a standard precast plant. This is clearly not the only factor, as plenty of lab-mixed blocks did crack, but it is of interest.

2. **Block to Aggregate Comparison (*highlighted in yellow*):** 2 blocks with the same mixture proportions, except for type of aggregate, exhibited the exact same levels of cracking. The blocks were cast within 1 month of each other. Aggregate elasticity or angularity was expected to have an impact on the micro-cracking; in this case the effects seem negligible.
3. **Mini-Girder Comparison:** Multiple mini-girders showed cracking earlier or more severely than those shown by an exposure block made with the same mixture proportions. This may be attributed to the volume to surface area effect and would be expected if drying shrinkage is the driving mechanism of the micro-cracking. 4 examples following the above-mentioned trend are presented below:
 - a. Girder PP-B (CR-2.5) and block PP-B (CR-1.5 and 2).
 - b. Girder PP-B Lab (CR-0.5) and block PP-B Lab (CR-0).
 - c. Girder G-3 (CR-0.5, has a dosage of 12.5 fl.oz./cwt.), Girder G-4 (CR-0.75, dosage of 12.0 fl.oz./cwt.) and Block B-4 (CR-0, dosage of 12.0 fl.oz./cwt.).
 - d. Girder G-5 (CR-1) and block B-5 (CR-0.5).

There are 6 exceptions out of 10 comparisons: block PP-A (CR-2) and girder PP-A (CR-1); block PP-A Lab NC (CR-1.75) and girder PPA Lab NC (CR-0); block B-11 (CR-0.75) and girder G-11 (CR-0.75); block B-6 (CR-0.75) and girder G-6 (CR-0);

block B-8 (CR-1.75) and girder G-8 (CR-0); block B-11 (CR-0.75) and girder G-11 (CR-0.75).

It is likely that girders and blocks that both show no distress are good performers. These likely good performers include: Girder G-7 and Block B-7 (23 months); Girder G-1 and Block B-1 (16 months); Girder G-2 and Block B-2A and B-2B (23 months). Mixtures showing no distress beyond 20 months are considered good performers for reference in testing outside this section.

6.4.4 Exposure Block Expansion/Contraction Results

Visible cracks developed on only three of the exposure blocks (see Table 6-4), though at very low levels and only at the 21-month age for the BP-1 block and 15-month age for BP-2 and BP-5.

Table 6-4: Pinned exposure block matrix at UT Austin exposure site

w/cm	Cement Type	Cement Content (lb/yd. ³)	SCM Content (lb/yd. ³)	Aggregate Source		HRWR Type	HRWR Dosage (fl.oz./100 cwt)	NR Type	NR Dosage (fl.oz./100 cwt)	Age (months)	Crack Rating	Block ID
				FA	CA							
0.26	PC-III-A	705	-	FA-R	CA-R	HR-P3	10	NR-2	3	16	0	BP-6
	PC-III-A	700	175	FA-R	CA-R	HR-P2	8.25	NR-1	3	16	1	BP-5
	PC-III-B	705	271	FA-R	CA-R	HR-P1	8.25		3	16	0	BP-5
0.28	PC-I-A	705	-	FA-R	CA-R	HR-P1	12	NR-1	3	16	0	BP-3
	PC-III-A	705	-	FA-R	CA-L	HR-P3	12		3	22	0.5	BP-1
0.3	PC-III-A	564	188	FA-R	CA-R	HR-P3	8		2	16	0	BP-4
0.31	PC-III-A	663	271	FA-R	CA-R	HR-P2	7.25		2.5	16	0	BP-8
		663	271	FA-R	CA-R	HR-P3	7.25	NR-2	2.5	16	0	BP-9
	PC-III-B	663	271	FA-R	CA-R	HR-P1	7.25	NR-1	2.5	16	0	BP-10
0.33	PC-III-A	658	-	FA-R	CA-R	HR-P1	12	NR-1	3	16	0.1	BP-2

The shrinkage results for overall shrinkage at 1", 2", and surface depths are shown in the Figures 6-21 through 6-30. Consistently among the cracked blocks, there is expansion at 2" depths below the top surface. This could correlate with the observed internal relative humidity differential at 2" depths in in-service cracked girders discussed in Tech Memo 1-B. This moisture gradient depth differential is greater than the maximum moisture gradient depth of 0.6 inches reported in the work of Bisschop (2012). Bisschop work was conducted using mortar specimens (~ 1.5 in x 1.5 in x 6 in) and moisture loss was induced by two different methods (exposure to 50% relative humidity environment or furnace drying at 86 degrees F).

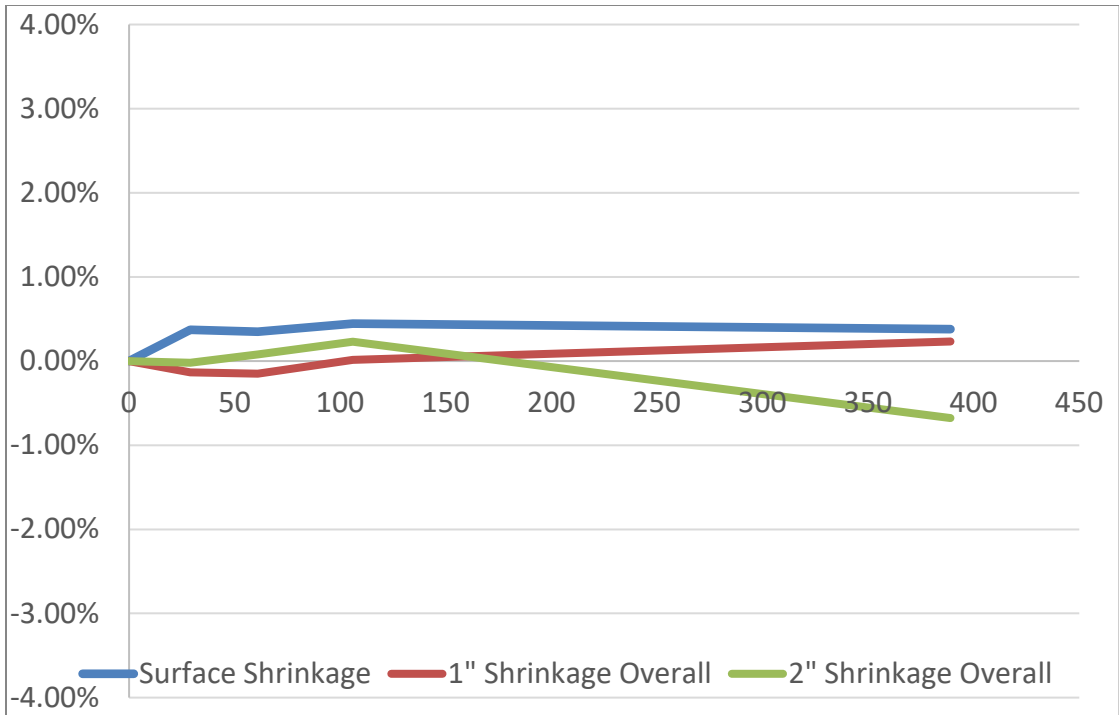


Figure 6-21: Monitored shrinkage results for Block 1 (BP-1); crack rating of 0.5 on western, eastern, and southern side of the blocks

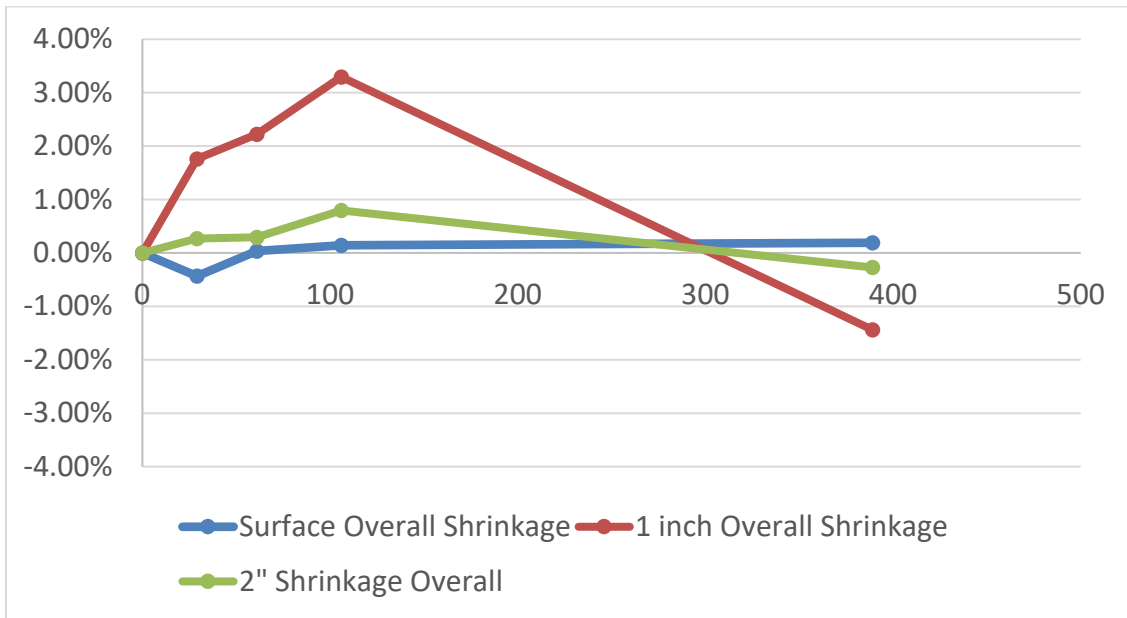


Figure 6-22: Monitored shrinkage results for Block 2 (BP-2); two very small cracks appeared at month 15 on the southern side of the block

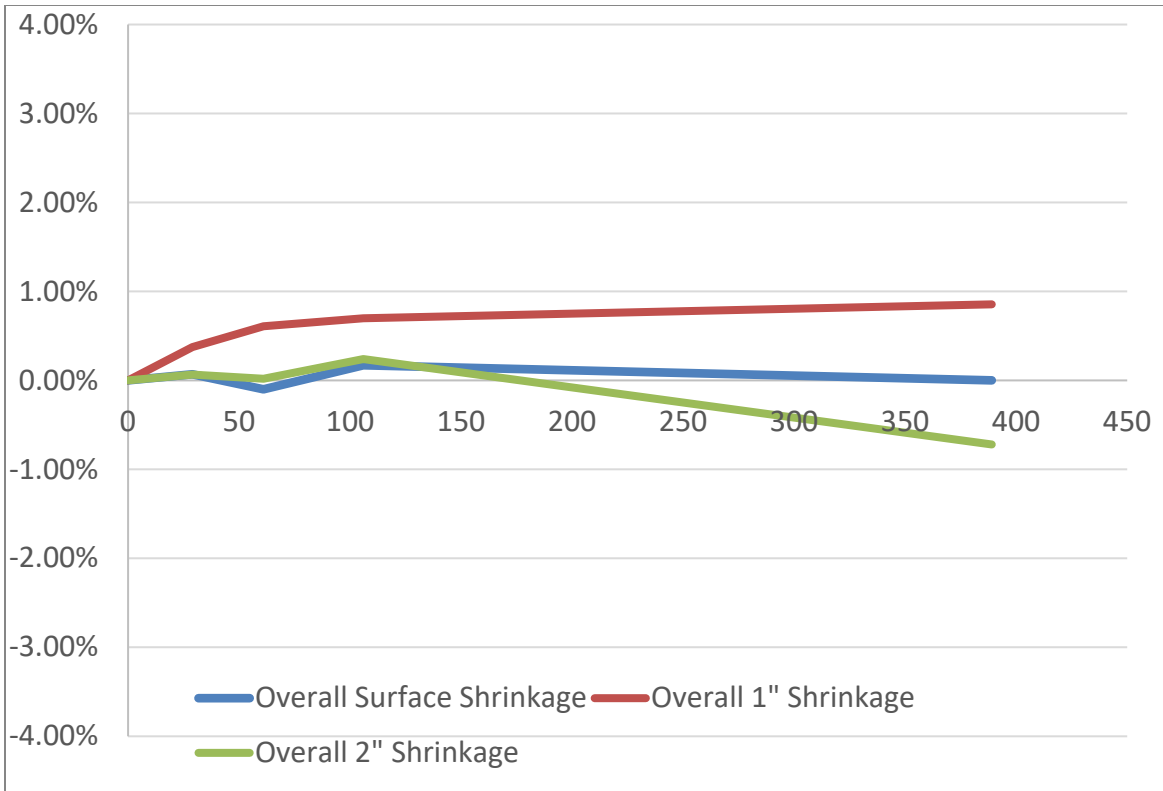


Figure 6-23: Monitored shrinkage results for Block 5 (BP-5); cracking is on the northern, western, and eastern sides

The following figures show blocks that have not cracked within a 16-month period:

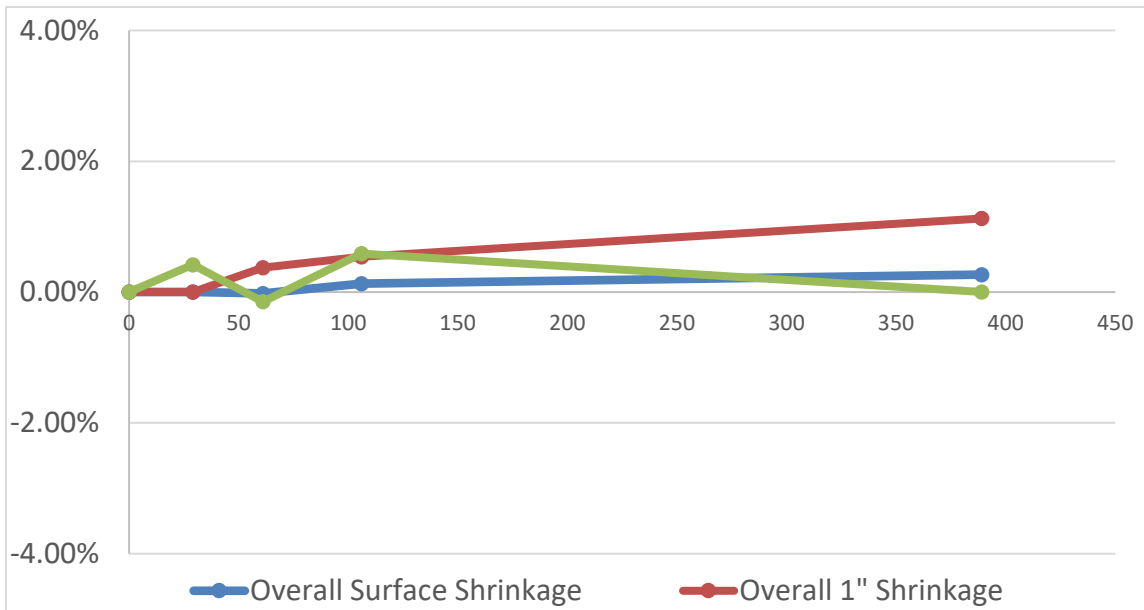


Figure 6-24: Block 3 shrinkage results (BP-3)

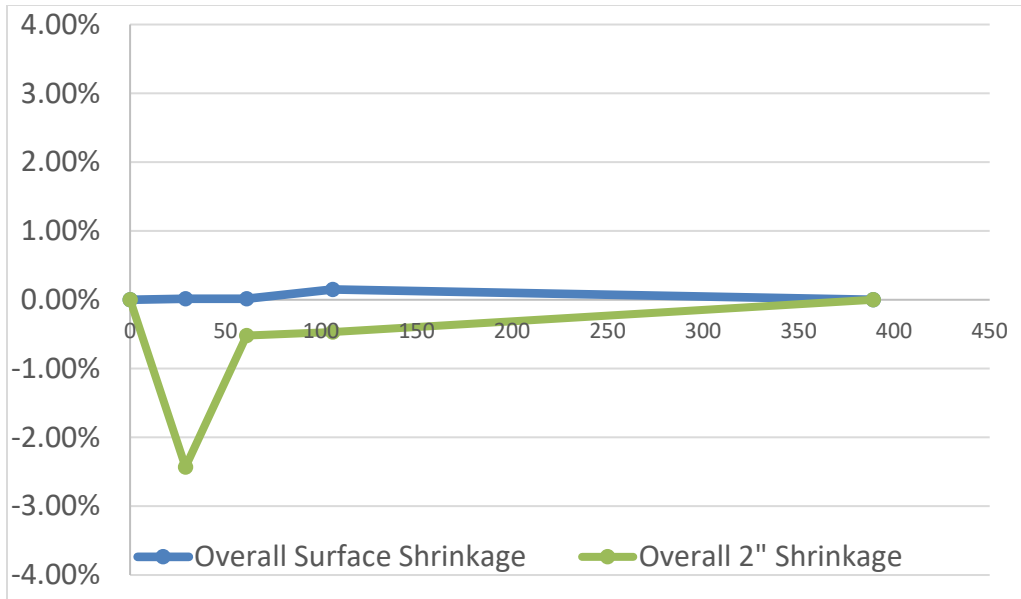


Figure 6-25: Block 4 shrinkage results (BP-4); surface demec fell off of block

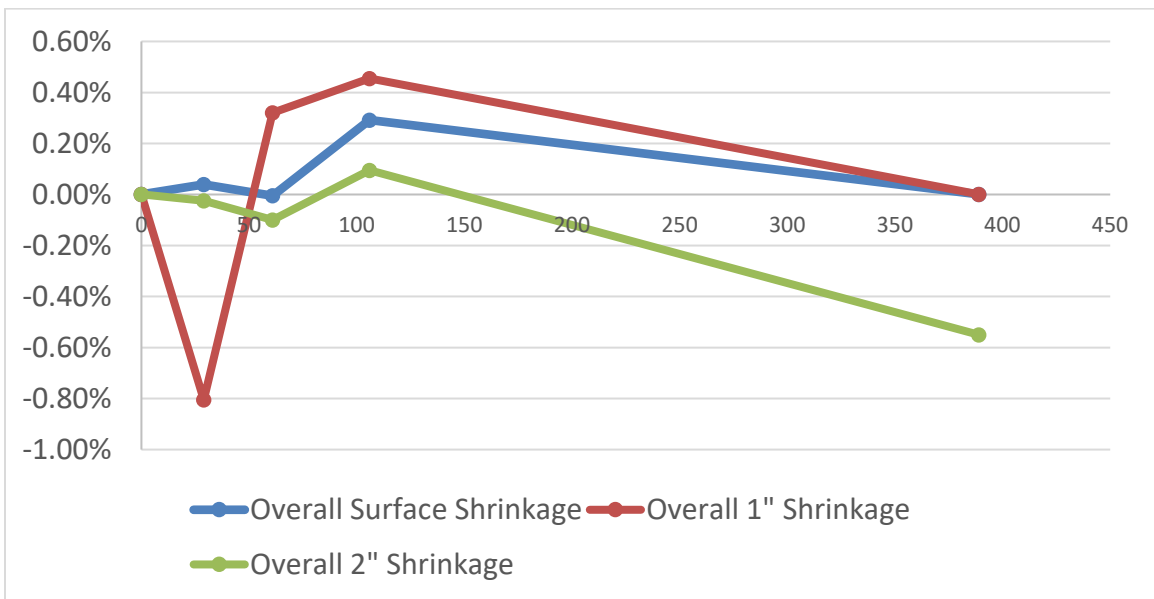


Figure 6-26: Block 6 shrinkage results (BP-6)

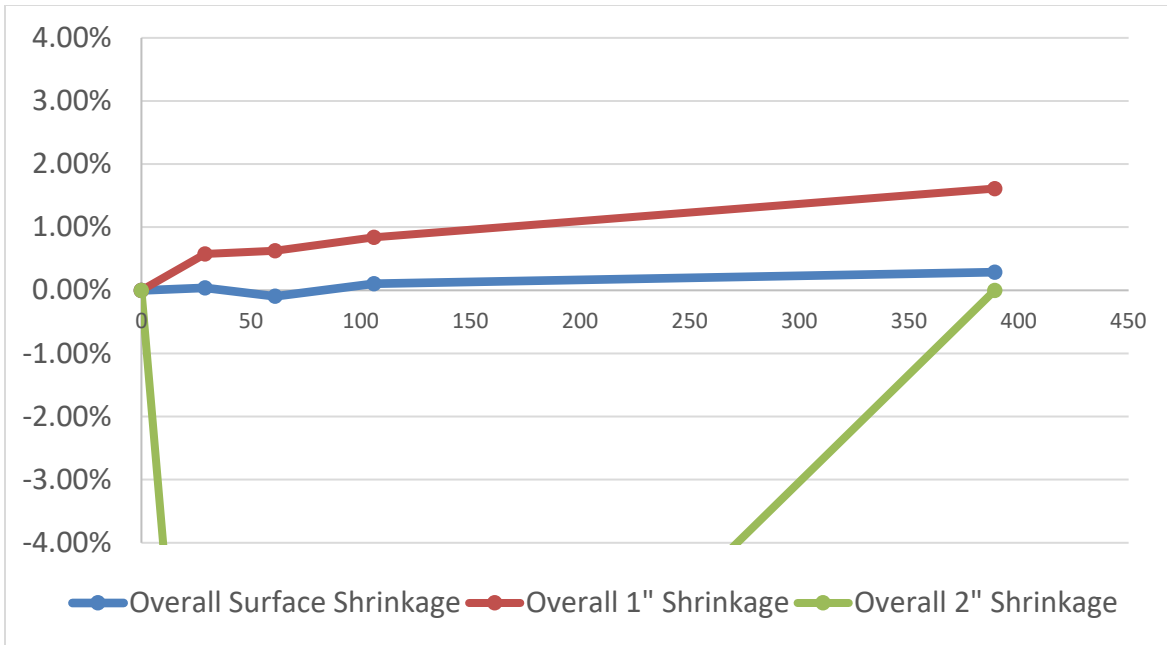


Figure 6-27: Block 7 (BP-7) shrinkage results; demecs fell off of the 2" depth bolts at early age

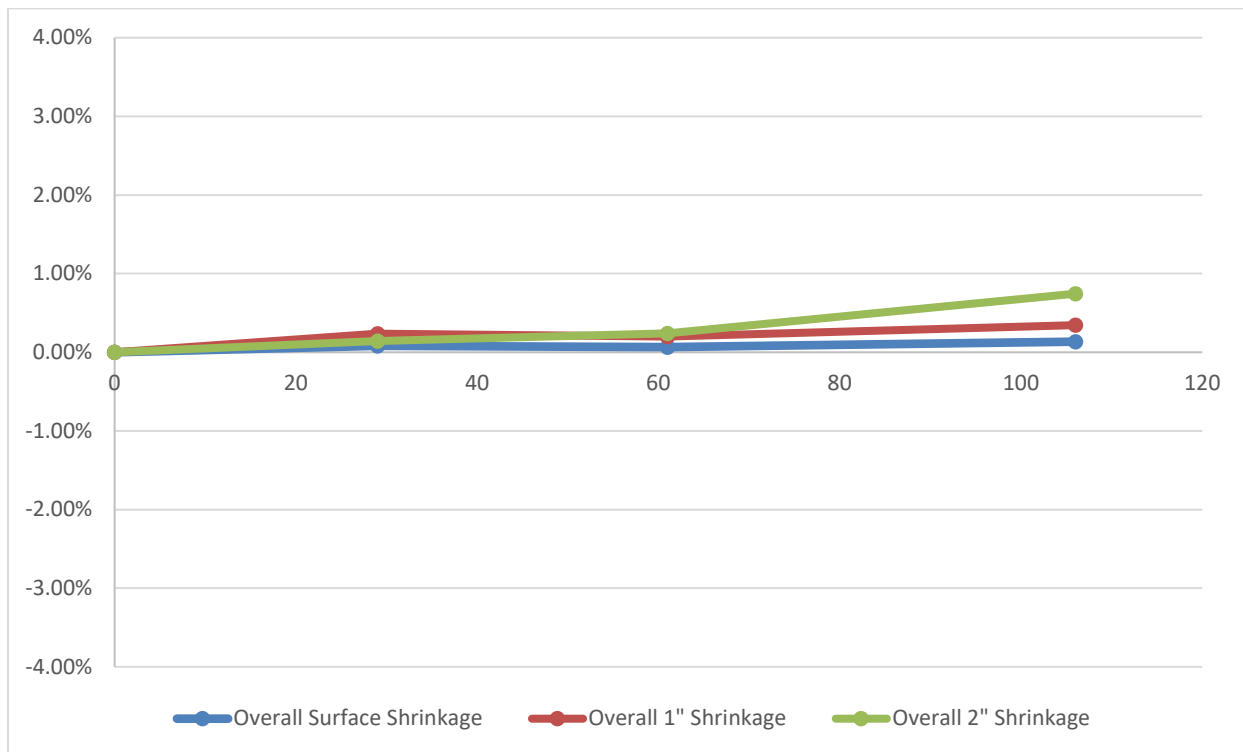


Figure 6-28: Block 8 (BP-8) shrinkage results

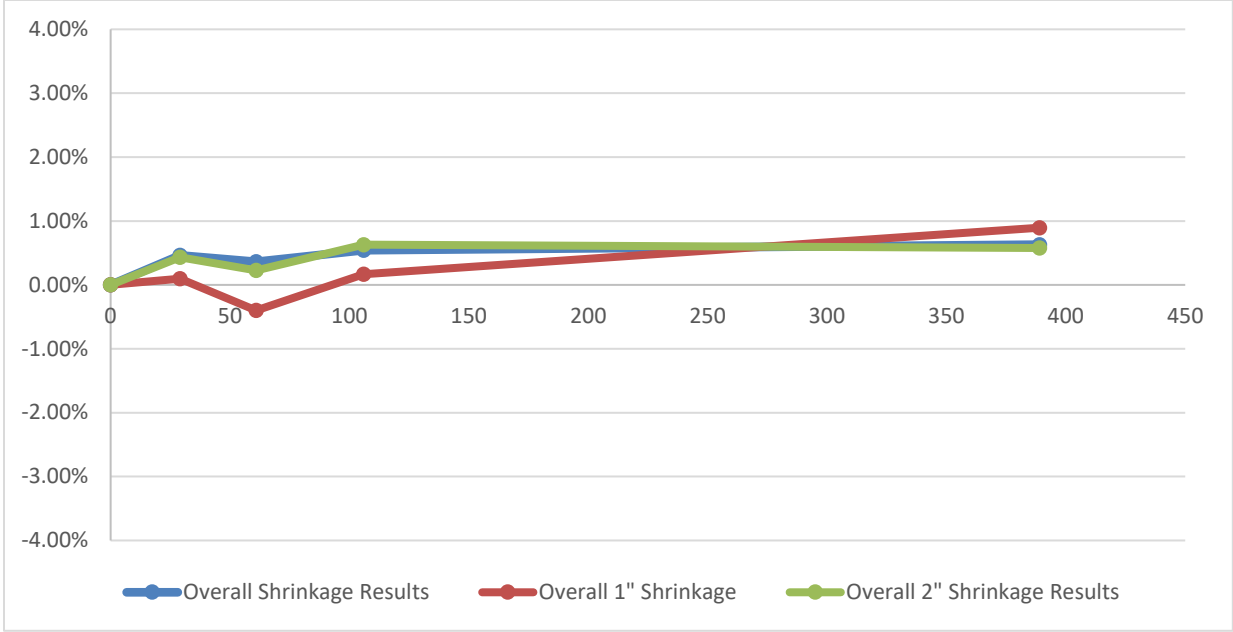


Figure 6-29: Block 9 (BP-9) shrinkage results

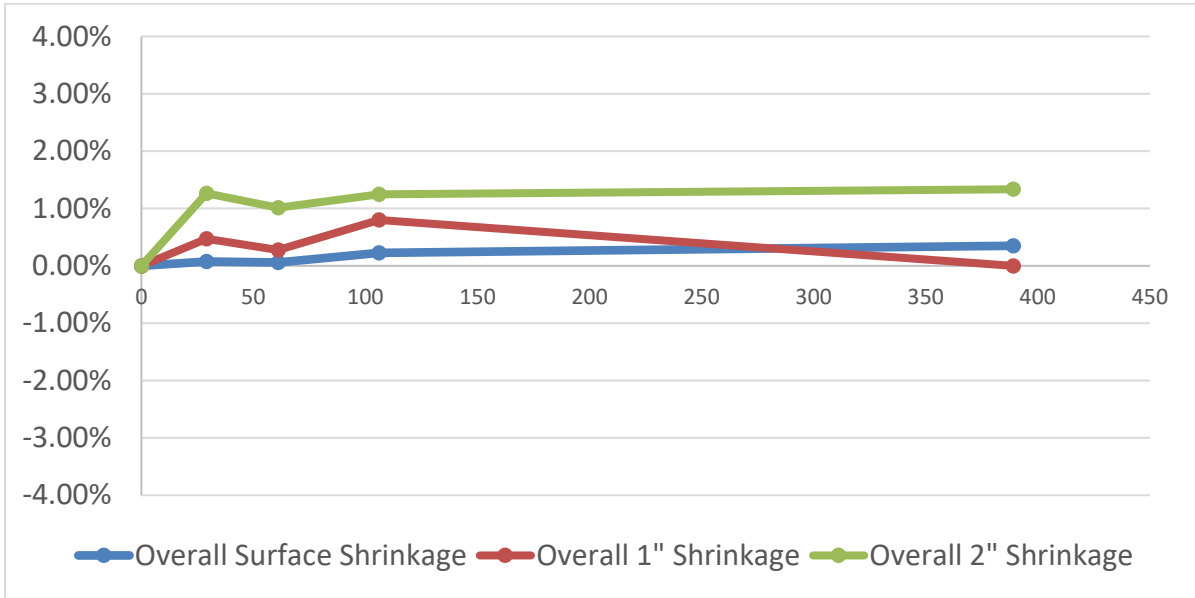


Figure 6-30: Block 10 shrinkage results; demecs fell off of 1" bolts at early age

6.4.5 Carbonation Testing Results

Table 6-5 provides the extent of the carbonation ingress, which was measured perpendicularly to the 4x4-in. prism surfaces for sheltered (IN) and unsheltered (OUT) specimens. As expected, the extremely low w/cm ratio (and therefore low permeability) of the mixtures resulted in shallow carbonation depths for all samples. In order to address the concern that the cracking may be the resultant of carbonation induced shrinkage the concrete displaying the largest

depth of carbonation ingress (G-8) was pulled to determine if the micro-cracking was visible on any of the surfaces.

Table 6-5: Carbonation testing matrix at UT Austin Exposure Site and results comparing sheltered (IN) specimens versus unsheltered (OUT) specimens

w/cm	Mix ID	Cement Type	Cement Content (lb/yd ³)	SCM Content (lb/yd ³)	Aggregate Source		Admixtures				Time Since Cast † (Months)	Carbonation Depth (mm)	
					FA	CA	Type	(floz/100 lb cement)	Type	(floz/ 100 lb cement)		IN	OUT
0.24	G-8	PC-III-A	705	-	FA-R	CA-R	HR-P2	15	NR-1	3	12	0.65	0.35
0.26	PP-A Lab NC	PC-III-A	564	141	FA-R	CA-R	HR-P2	6.5	NR-1	3	8	0	0
0.28	G-2	PC-III-A	705	-	FA-R	CA-R	HR-P2	12	NR-1	3	12	0.10	0.05
	G-5		705	-	FA-R	CA-R	HR-P3	12	NR-2	3	12	0.10	0.075
	G-6		705	-	FA-R	CA-L	HR-P3	12		3	13	0.03	0
	G-7		705	-	FA-R	CA-L	HR-P4	12		3	12	0.10	0.075
	G-13	PC-III-B	705	-	FA-R	CA-L	HR-P1	12	NR-1	3	15	0	0
0.3	PP-B	PC-III-A	564	188	FA-RII	CA-RII	HR-P3	8	NR-2	2	13	0.08	0
	PP-B Lab		564	188	FA-RII	CA-RII	HR-P3	8		0.5	10	0.325	0
0.31	PP-A	PC-III-A	663	271	FA-R	CA-R	HR-P5	5.5	NR-1	0.5	12	0.1	0
	PP-A SCC		663	271	FA-R	CA-R	HR-P2	5.5		2.5	10	0.5	0

Figure 6-31 shows the depth of carbonation for (G-8) prisms exposed to “in” (inside Stevenson screens) and “out” natural outdoor exposure.

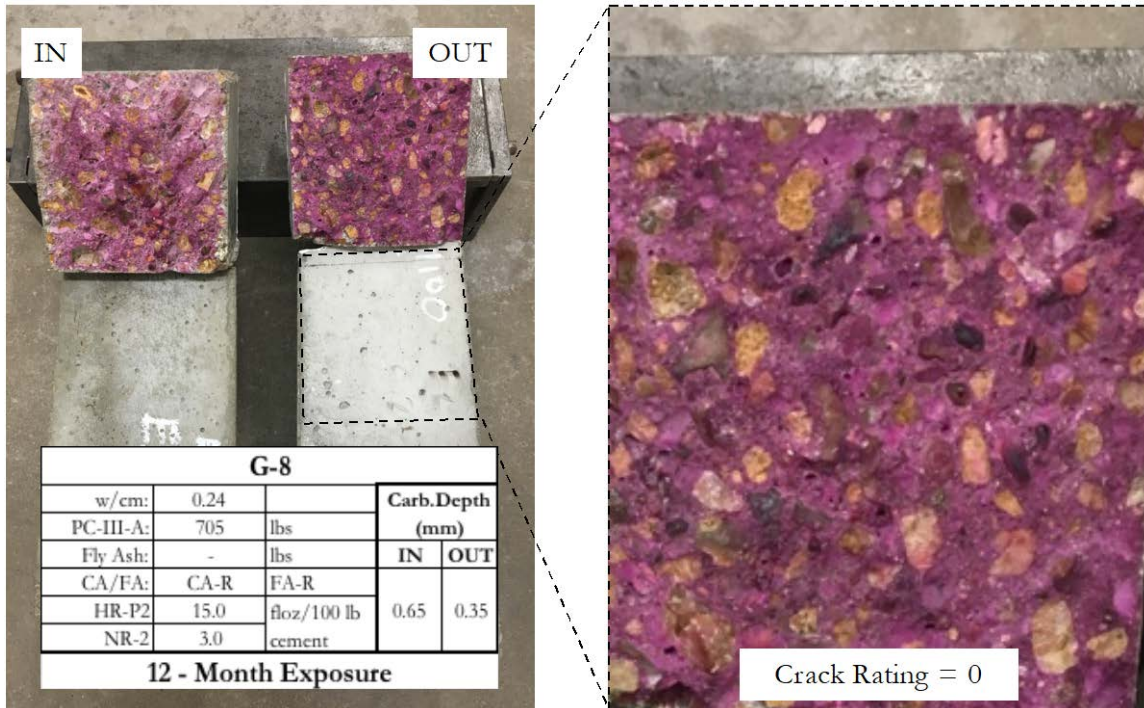


Figure 6-31: Carbonation depth for mixture G-8.

(Left) Comparison of carbonation depth of specimens stored in sheltered conditions and unsheltered. “IN” specimens showed greater carbonation depth with zero visible surface cracking. (Right) Close-up of surface for the unsheltered specimen. No cracks visible on surface (crack rating =0)

The carbonation specimens were used as visual tools in order to learn more about the micro-cracking mechanism. Figure 6-32 suggests that carbonation depth and surface cracking are independent of one another. In all cases, even if a specimen showed development of the surface micro-cracking for the outdoor specimen, no visible cracks proved to develop on the indoor specimens. The following figures were selected based on either visible cracking, the fact that they were cast at precast plants, and/or cast as replicates of precast plant mixtures.

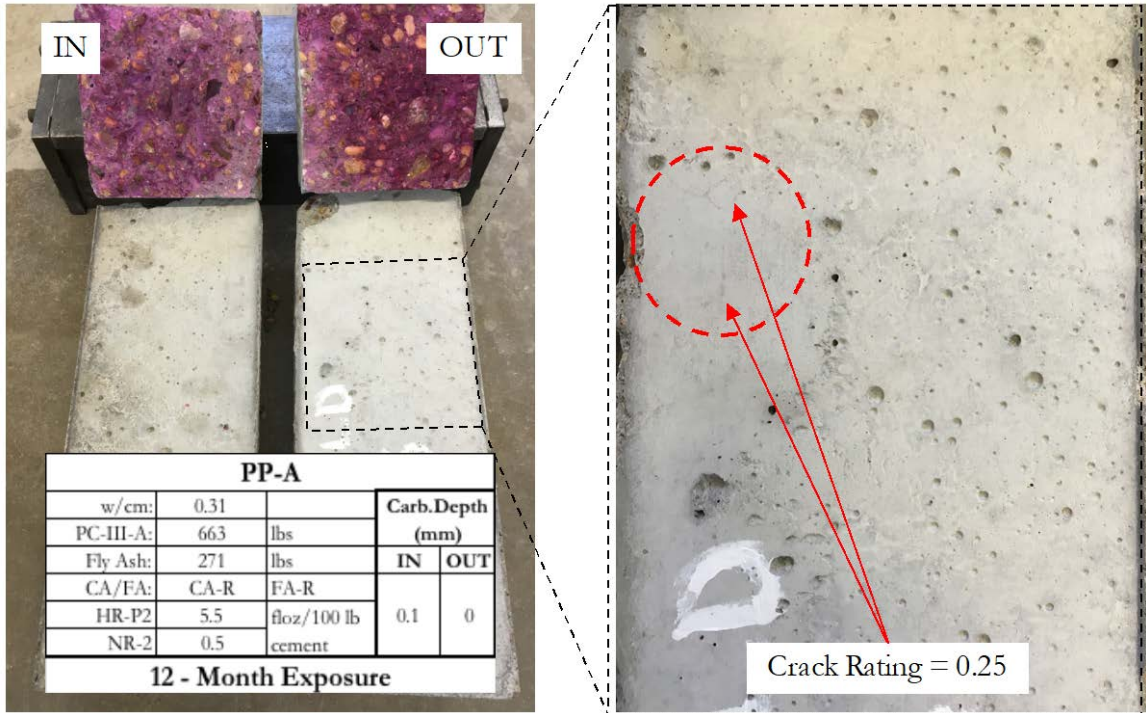


Figure 6-32: Carbonation depth for mixture PP-A; showing very minimal cracking = 0.25

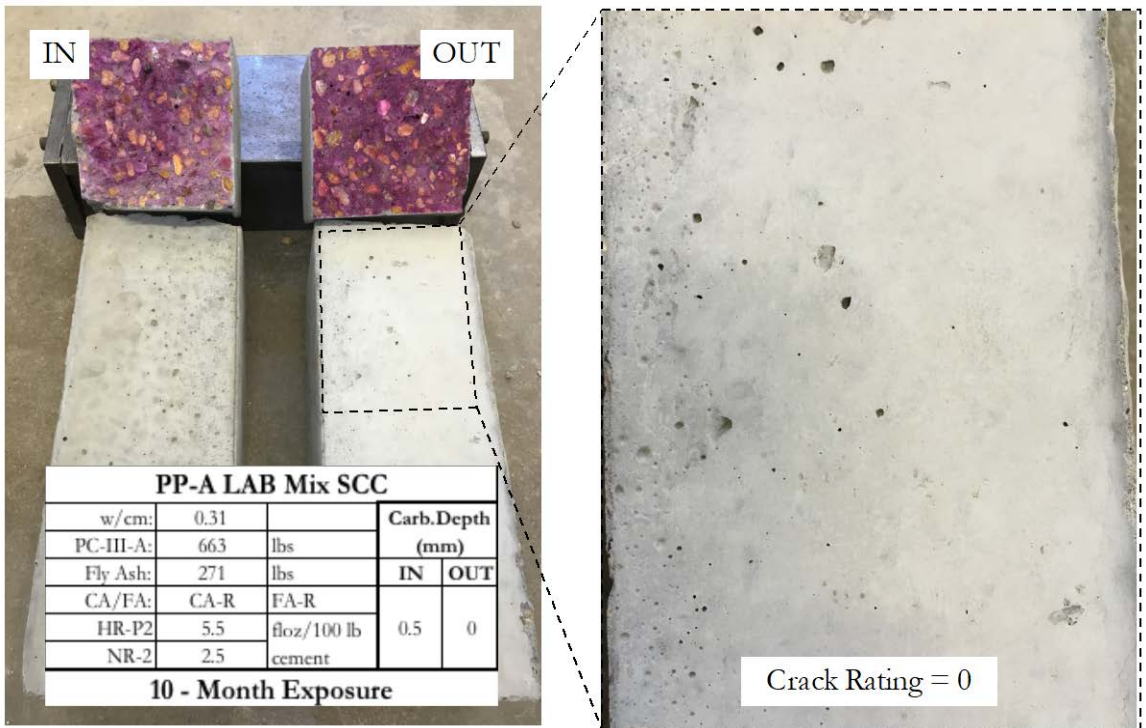


Figure 6-33: Carbonation depth for mixture PP-A Lab Mixture SCC; showing no cracking = 0.0

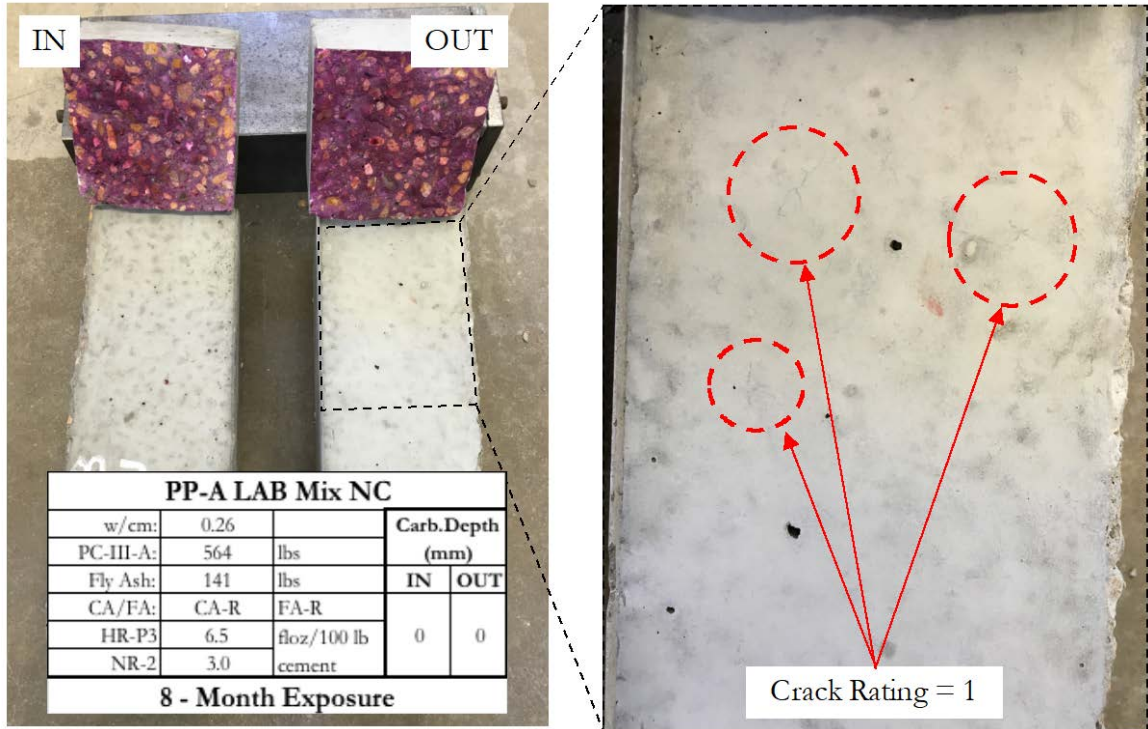


Figure 6-34: Carbonation depth for mixture PP-A Lab Mixture NC; showing very minimal cracking = 1.0

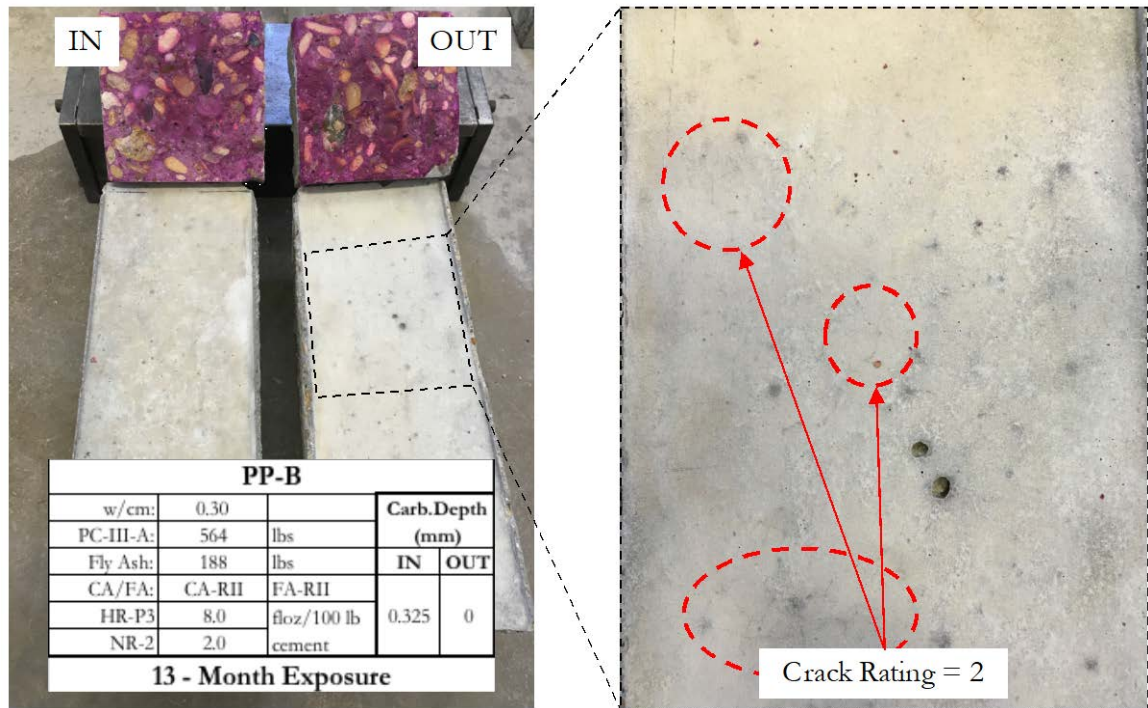


Figure 6-35: Carbonation depth for mixture PP-B; showing very minimal cracking = 2.0

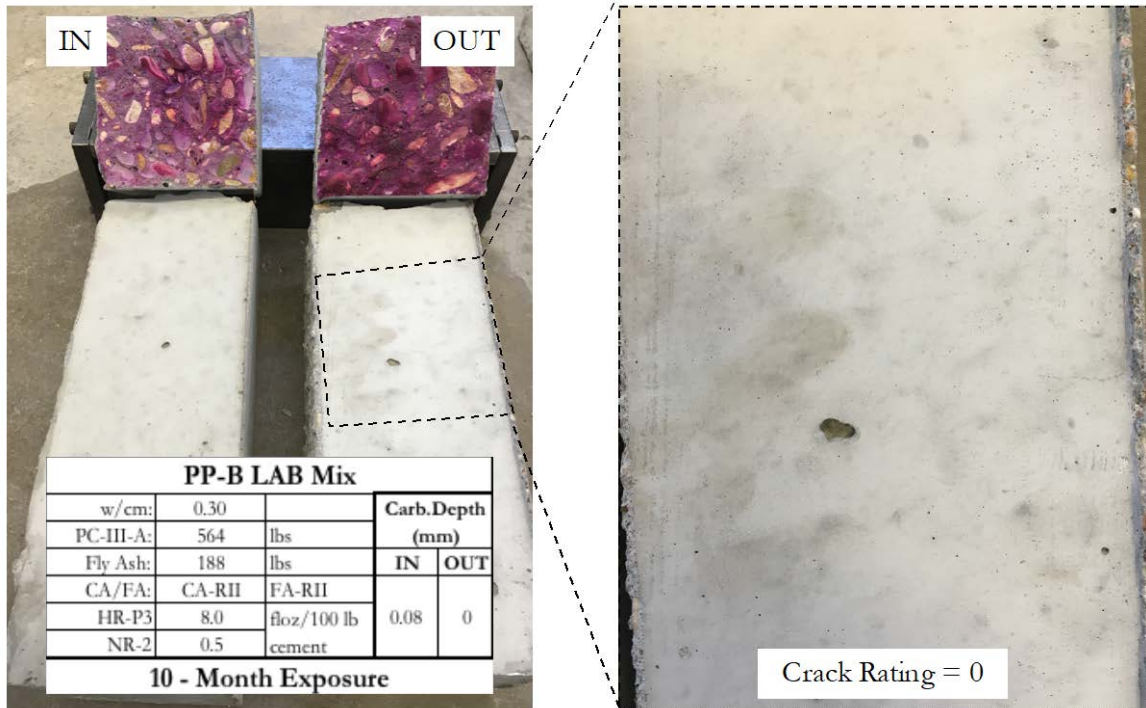


Figure 6-36: Carbonation depth for mixture PP-B Lab Mixture; showing no cracking = 0.0

Based on the results of the carbonation depth ingress and the micro-cracking observed on the carbonation specimens, carbonation does not appear to be a primary mechanism with respect to micro-cracking. The carbonation prisms also reveal that the wetting and drying cycles that the outdoor carbonation specimens experienced clearly exacerbates and provokes the micro-cracking development on the surface of the concrete.

6.4.6 Key Findings

- Surface exposure to the natural elements proves to be the key to exacerbating the surface micro-cracking observed.
- Specimens with measurable pin and demec locations at different depths showed that in cracked blocks expansion occurred at 2 inch depth from the top surface.
- Carbonation shrinkage is not a driving factor inducing the micro-cracks.
- A variety of exposure blocks that were known bad performers, performed well when exposed to the environment at the UT CMRG/LIME Lab, showing no cracking, just as a variety of known good performers performed poorly at the UT CMRG/LIME Lab. This indicates that there is some variability in performance of the concrete mixtures depending on how the mixes are created. The extremely low w/cm of these mixtures likely requires extremely careful quality assurance. Further work should be conducted examining the effect of mixing/concrete processing on the micro-cracking.
- The exposure specimens cast in the shape of girders exhibited cracking more quickly than the exposure specimens cast into the shape of blocks. This suggests that the volume: surface ratio had an impact on mechanism driving the micro-cracking.

Chapter 7. Conclusions

This project has produced a sizable experimental matrix towards the evaluation of the suitability of using ASTM C494 to indicate a mixture propensity to micro-cracks of the nature that is seen in precast concrete girders throughout the state of Texas. In addition, a parametric analysis aimed at determining key factors and mechanisms driving the micro-cracking development seen on precast elements was conducted. ASTM C494 was evaluated by determining the pass and fail rate of select ASTM C494 parameters (water content, time of set, compressive strength and drying shrinkage) of both “good” and “bad” performance mixture designs with respect to micro-cracking observed in the field. Because a true ASTM C494 control mixture is not attainable without the use of HRWR, several pseudo-control mixtures were created for the precast concrete mixtures designs evaluated in this work. The control mixtures were designed to account for the effect of water to binder content, HRWR dosage and type, and lightweight aggregate incorporation on the micro-cracking behavior and the aforementioned ASTM C494 testing parameters.

In addition to the evaluation of ASTM C494 for qualifying HRWR admixtures to eliminate the micro-cracking issue seen in precast applications, an exposure site was developed to monitor the natural development of micro-cracking. Mixtures were selected based on current high performance mixture designs employed at precast plants throughout the state of Texas. The role natural exposure had on micro-cracking behavior was investigated on exposure blocks, mini girders and carbonation specimens.

An additional testing matrix was developed with the goal of evaluating the shrinkage behavior of plant mixtures with the hope of determining whether there was a particular shrinkage mechanism driving micro-crack formation. The testing performed in the parametric study employed autogenous shrinkage measurements on paste mixtures and concrete mixture evaluation through restrained shrinkage ring test to determine both autogenous and drying shrinkage effects. Autogenous paste testing included volumetric (buoyancy) method, corrugated tube and mini-ring test. The autogenous shrinkage evaluation through use of the corrugated tube method is currently being performed to determine the most accurate and repeatable sample preparation procedure for this test.

7.1 Summary of Task Findings

In Tasks 1 and 2, an information survey review of the recent micro-cracking in Texas girders was conducted in collaboration with the (IAC) Project 46-3MTIA034. It was discovered that many girders are affected and all are east of I-35, indicating a relationship between the cracking and environment (potentially related to humidity or moisture). Also, a recent study on the effect of the industry switch from naphthalene to polycarboxylate HRWR’s concluded that concrete mixtures made with polycarboxylate HRWR’s actually had a lower drying shrinkage and overall creep as compared to mixtures made with naphthalene HRWR. As this project is specifically targeting the ASTM standard for limiting the use of HRWR, this information provides good context for results from tasks undergone later in the project indicating that the standard’s limits do not provide a good test to screen for the performance of these concrete mixtures. Additionally, as part of this information survey review, relative humidity measurements and crack ratings were taken at bridges in Dallas and Texarkana. *The relative humidity measurements of girders in the field showed a correlation between a larger relative humidity gradient up to 2” in depth and a larger crack rating. Such a correlation suggests that relative humidity gradients*

within the element is at least somewhat a source of the driving mechanism of the cracks. Through communication with precast plant operators and reviews of a previous thesis on the phenomenon, common mix designs resulting in this cracking (bad performers) and not resulting in cracking (good performers) were determined.

In Task 3, the known good performers and bad performers determined were evaluated through the standards of ASTM C494 in the “specific method.” It was not possible to completely adhere to the ASTM C494 typical “control mix” which consists of the same mix without any HRWR because of the extremely low w/cm ratios currently in use at precast plants. Thus, the “control mix” was designed in several ways as it was desired to have similar workability in the control and non-control mix (Stacey). ***The result of this task showed that no test method within ASTM C494 could effectively evaluate a good performer or a bad performer.***

In Task 4, a matrix of 19 mixes (with performance ultimately unknown) were evaluated to determine the extent of the sensitivity of those tests to a variety of parameters and a more detailed study of drying shrinkage was executed on a matrix of 28 mixes. Key findings gained from this detailed matrix of tests was the reduction of drying shrinkage due to reduction in cementitious content and extending time of curing.

In Task 5, a variety of complementary tests were evaluated in comparison to the results from Task 3 and 4: autogenous shrinkage test, mini-ring tests, ring tests, the casting of an exposure block, calorimetry testing, and carbonation testing. None of these tests yielded promising results that correlated well with results from exposure blocks in the field. Certain phenomena were ruled out as being the cause of the micro-cracking, including carbonation or carbonation shrinkage and no increase in shrinkage with increase in dosage of HRWR was observed. Significant “bleed bumps” in autogenous shrinkage curves were noted, especially for autogenous shrinkage specimens incorporating VMA’s. Nothing significantly irregular was noted through isothermal calorimetry tests. ***The most significant result was determined as a byproduct of carbonation testing: some carbonation specimens were placed within a Stevenson screen. Stevenson screens are used to prevent water from filling up pores in the concrete that may hinder the diffusion of CO₂ through the concrete. The shelters allow air to filter in at the same relative humidity as would be experienced on the exterior of the screen. Although the extent of micro-cracking was not found to be related to the carbonation depth, it was seen that carbonation specimens within a Stevenson screen did not exhibit micro-cracking, while carbonation specimens outside the Stevenson screen did exhibit micro-cracking (Stacey). Therefore, wetting and drying cycles that the outdoor carbonation specimens experienced exacerbated or provoked the micro-cracking development on the surface of the concrete.***

Typical parameters that would affect the overall performance of a mixture were evaluated in Tasks 3-5. However, the results from Task 1 and carbonation testing as part of Task 5 suggest that it is a product of specific environmental exposure. Therefore, plastic shrinkage testing or placement in an environmental chamber would be more likely to yield relevant results. ASTM C494, while it incorporates drying shrinkage, does not accurately evaluate the potential for surface instabilities. This would be consistent with why it shows no potential to screen for micro-cracking potential. ***A clear solution is extending curing time, as Task 4 showed the significant reduction in drying shrinkage when curing goes beyond 1-day. However, in terms of addressing the actual mix design, the solutions are less clear.***

Based on the results of the work performed throughout this project, the following major conclusions are summarized according to their respective subsections:

- **Evaluation of ASTM C494 with HRWR for predicting latent micro cracking effects:**
 - No test required under ASTM C494 Type F guidelines successfully screened out a bad performer, as the guidelines were interpreted in this project. The testing that was performed towards fulfillment of ASTM C494 testing procedures with respect to HRWR agents (Type F) does not provide a proper means of creating a base mixture to compare the admixture agent against. Yet even with the creation of a supplement control mixture a correlation between poor performance in the field and failing in ASTM C494 testing was not apparent.
- **Autogenous shrinkage:**
 - Cement paste analysis with respect to autogenous shrinkage showed that increasing the HRWR dosage retards the final set of the mixture. The delay in set time causes delayed reabsorption of bleed water. The swelling incurred by the paste during reabsorption decrease the ultimate autogenous shrinkage of the paste compared to a paste mixture with a lower HRWR dosage. Correlating this paste study back to field performance, the use of higher admixtures dosages used in the field may be a factor in delaying or minimizing micro-cracking associated with autogenous shrinkage
- **Natural exposure results:**
 - Although the time of year (season) when concrete cast shows to have negligible effect with respect to increasing or decreasing cracking performance, surface exposure to the natural elements (rather than seasonal factors) exacerbates the surface micro-cracking observed.
 - Specimens with measurable pin and demec locations at different depths has the potential to provide better indication of the permissible depth of the micro-cracking as well as create a better quantifiable interpretation of the cracking. Specimens with measurable pin and demec locations at different depths showed that in cracked blocks expansion occurred at 2” depth from the top surface.
 - Carbonation shrinkage is not a driving factor inducing the micro-cracks.
 - Performance variability depends on how the mixes are processed. The processing methods of the concrete was found to effect the time of cracking, suggesting that in order to truly determine the cracking potential of an exposure block, the concrete should be mixed using similar mixing techniques employed at the pre-cast plant or cast at the pre-cast plant; otherwise work, should be conducted to determine the correlation between micro-cracking behavior of concrete mixed using pre-cast plant mixers and concrete mixed using laboratory scale mixtures.
 - The exposure specimens cast in the shape of girders exhibited cracking more quickly than the exposure specimens cast into the shape of blocks. This suggests that the volume:surface ratio had an impact on mechanism driving the micro-cracking.
- **Effect of HRWR dosage/type:**
 - Autogenous shrinkage testing indicates a correlation between a reduction in autogenous shrinkage and an increase in HRWR dosage (this occurred in over 75% of cases). This tendency was also shown by drying shrinkage results.

- **Restrained shrinkage results:**

- The restrained shrinkage testing results correlated poorly with a mixture's field performance. Almost all of the mixtures took a significant number of days to crack (>20 days) due to their high compressive strength, high tensile strength, and high elastic modulus. Based upon their performance in restrained shrinkage, compressive, tensile, and modulus testing, all the mixes would be classified as having a low cracking potential.

7.2 Recommendations and Future Work

Polycarboxylate HRWRs are unlikely to be the source of the cracking. More likely “culprits” include ambient humidity and the extremely low w/cm ratio. One recommendation is that precast plants lower their cementitious content, to the lowest extent possible without compromising strength. This could be accomplished by optimization of aggregate gradation since this enables a paste content reduction and thus mitigates volumetric changes in the concrete. Also recommended is using the highest w/cm ratio that provides adequate durability and strength, as well as re-evaluating concreting procedures to mitigate surface self-desiccation (e.g., better curing) and shrinkage (e.g., chemical shrinkage).

Evaluating the impact of fly ash and other supplementary cementitious mixtures on micro-cracking behavior in low cementitious content precast concrete mixtures should be investigated. Also, since concrete processing (e.g. mixing energy) and specimen geometry (i.e., block vs mini-girder) was found to play a considerable role on micro-cracking developing, it is recommended that future work is concentrated in this area.

Because the mechanism causing the micro-cracking is a function of volume change, additional measurements in the long term of the drying shrinkage specimens is suggested, especially considering that extended time evaluation with respect to control resulted in failing mixtures that would otherwise pass in the 14-day measurement timeline prescribed in ASTM C494 (same limits are used in the extended time evaluation).

Volumetric change of specimens exposed to outdoor weather conditions in Texas appears to be the best current-day approach to capturing the latent micro-cracking as a function of volume change. More work should be performed in the area of measuring outdoor specimen's volume change with respect to time and weather monitoring.

Further investigation of paste to formwork interaction is suggested to examine bleeding effects associated with mixture design that may be influencing the micro-cracking at paste to formwork surface. Variables such as temperature, concrete viscosity and humidity during casting.

Developing an additional exposure site that subjects concrete specimens of like volume to surface area as the girders to daily wetting and drying cycling as a means of potentially expediting the micro-cracking should be examined.

Appendix I: Materials Identification

Table I-1: Cement nomenclature, distributor and oxide analysis

Cement	Distributor	SiO ₂	Al ₂ O ₃	Fe ₂ O	CaO	MgO	SO ₃	Na ₂ O	K ₂ O
		mass %	mass %	mass %	mass %	mass %	mass %	mass %	mass %
PC-III-A	Alamo III	19.8	4.3	3.1	64.2	0.6	4.1	0.1	0.7
PC-III-B	Capitol III	19.8	5.1	1.9	63.5	1.1	5	0.1	0.6
PC-I-A	Alamo I	18.6	5.4	2.6	64.9	1.1	3.3	0.1	1
PC-III-C	Lehigh White								
PC-III-D	Cemex Odessa								

Table I-2: Fly ash nomenclature, distributor and oxide analysis

Fly Ash	Distributor	SiO ₂	Al ₂ O ₃	Fe ₂ O ₃	CaO	MgO	SO ₃	Na ₂ O	K ₂ O
		mass %	mass %	mass %	mass %	mass %	mass %	mass %	mass %
Class F	Rockdale	52.07	23.07	3.95	11.65	2.06	0.48	0.403	0.74

Table I-3: Coarse aggregate nomenclature, source and properties

Coarse Aggregate	Source	Mineralogy Type	Specific Gravity	Absorption Capacity
CA-R	Eagle Lake	Siliceous	2.54	1.31
CA-L	Marble Falls	Limestone	2.47	3.25
CA-RII	Trinity	Siliceous	2.26	1.52

Table I-4: Fine aggregate nomenclature, source and properties

Fine Aggregate	Source	Mineralogy Type	Specific Gravity	Absorption Capacity
FA-R	Eagle Lake	Siliceous	2.47	1.14
FA-RII	Trinity	Siliceous	2.57	1.96
FA-LW	Manufactured	Manufactured	1.86	22.50

Table I-5: Admixture nomenclature, source, classification and properties

Admixture Name	Product Name	C-Polymer Type	ASTM C494 Classification	Specific gravity
HR-P1	Sika 2100	Polycarboxylate	F	1.1
HR-P2	Sika 4100	Polycarboxylate	F	1.1
HR-P3	BASF 7700	Polycarboxylate	F	1.1
HR-P4	BASF Z60	Polycarboxylate	F	1.1
HR-P5	Sika 2110	Polycarboxylate	F	1.1
NR-1	Plastiment	Normal Range Water Reducer and	B & D	1.2
NR-2	Glenium	Normal Range Water Reducer and	B & D	1.2
VMA-1	Sika 4R	Viscosity Modifier	S	1.1

Appendix II: Mixture Identification According to Task

Table II-1: Task 3 Mixture ID's and mixture designs

Mixture ID	w/cm	Cement Type	Cement Content (lb/yd ³)	Admixtures				Other Mixture Parameters
				Type	(floz/100 lb cement)	Type	(floz/ 100 lb cement)	
M1-NC	0.26	PC-III-A	700	HR-P1	6.5	NR-1	1.5	-
M1-CSP					8.25		1.5	-
M2-NC	0.28	PC-III-A		HR-P1	12	NR-1	3	-
M4-SCC	0.31	PC-III-A	663	HR-P1	5.5	NR-1	2.5	-
M5-SCC			640		6		2	-
M3-NC	0.33	PC-III-A	658	HR-P1	6.5	NR-1	3	-
M3-CSP					5.5		2	-
M3-CLWA					5		2.5	### FA-LW
M3-CWB	0.4	PC-III-A		HR-P1	2	NR-1	2	-
M6-CFA					2		2	Fly Ash 25% add.

Table II-2: Task 4 Mixture ID's and mixture designs

Mixture ID		Alteration of Task 3 Mix	w/cm	Cement Type	Admixtures				Other Mixture Parameters		
					Type	(floz/100 lb cement)	Type	(floz/ 100 lb cement)			
1.5	M1-NC	Fly Ash Content	0.26	PC-III-A	HR-P1	6.5	NR-1	3	Fly Ash 33% add.		
1.2		Cement Content				25.75		3	517 lb/yd ³ PC-III-A & Fly Ash 25% add.		
1.1		HRWR Dosage				5.25		NR-1	3	Fly Ash 25% add.	
1.6		HRWR Type				8.25		NR-1	3		
1.7						10		NR-1	3		
1.8		Cement Type				PC-III-B		HR-P1	8.25		NR-1
1.3		w/binder	0.38	PC-III-A	-	-	-	-			
1.4		w/binder	0.45		-	-	-	-			
2.4		M3-NC	Fly Ash Content	0.26	PC-III-A	HR-P1	6.5	NR-1	3	Fly Ash 33% add.	
2.2	Cement Content		0.33	30.5			3		517 lb/yd ³ PC-III-A		
2.1	HRWR Dosage			11.88			3		-		
2.3	w/binder		0.52	-			-		-	-	
2.4	w/binder		0.56	-			-		-	-	
3.1	M4-SCC		w/binder	0.26			PC-III-A		HR-P1	7	NR-1
3.3		Fly Ash Content	0.31	5.5	2.5	Fly Ash 25% add.					
3.4		HRWR Type		5.5	2.5						
3.5				7.25	2.5						
3.6		Cement Type		PC-III-B	HR-P1			6		2.5	
3.2		w/binder	0.33	PC-III-A	HR-P1			5		2.5	

Table II-3: Task 5 Mixture ID's and mixture designs

Mixture ID	w/cm	Cement Type	Admixtures				Other Mixture Parameters	
			Type	(floz/100 lb cement)	Type	(floz/ 100 lb cement)		
G-8	0.24	PC-III-A	HR-P2	15	NR-1	3	-	
G-10	0.26	PC-III-A	HR-P2	6.5	NR-1	3	SCC - Fly Ash 20% add.	
M1-NC-14			HR-P2	8.25	NR-1		2	Fly Ash 25% add.
M1-NC-15			HR-P3	10	NR-2			
M1-NC-16		PC-III-B	HR-P1	8.25	NR-1	3	Fly Ash 38% add.	
G-1	0.28	PC-III-A	HR-P1	12	NR-1	3	-	
G-2			HR-P2					
G-3			HR-P1	12.5				CA-L
G-4			HR-P2					
G-5			HR-P3				-	
G-6			HR-P3					
G-7			HR-P4	12	NR-2		CA-L	
G-13		PC-III-B						
M2-NC-1		PC-III-A	HR-P1		NR-1		-	
T5-3		PC-I-A					-	
T5-4		0.3	PC-III-A	HR-P3	8	NR-2	2	564 lb/yd ³ PC-III-A & Fly Ash 33% add.
G-2-Plant	HR-P3			8	NR-2	2	CA-R-II & Fly ash 25% add.	
G-11-Lab						0.5		
G-1-Plant	0.31	PC-III-A	HR-P4	5.5	NR-1	0.5	Fly Ash 29% add.	
G-9-Lab			HR-P2					
M4-SCC-17			HR-P2	5.5	NR-1	2.5	663 lb/yd ³ PC-III-A & Fly Ash 40%	
M4-SCC-18			HR-P3	7.25	NR-2			
M4-SCC-19		PC-III-B	HR-P1	6	NR-1		663 lb/yd ³ PC-III-B & Fly Ash 40% add.	
M3-NC-6	0.33	PC-III-A	HR-P1	12	NR-1	3	658 lb.yd ³ PC-III-A	

Appendix III: Compressive Strength Data

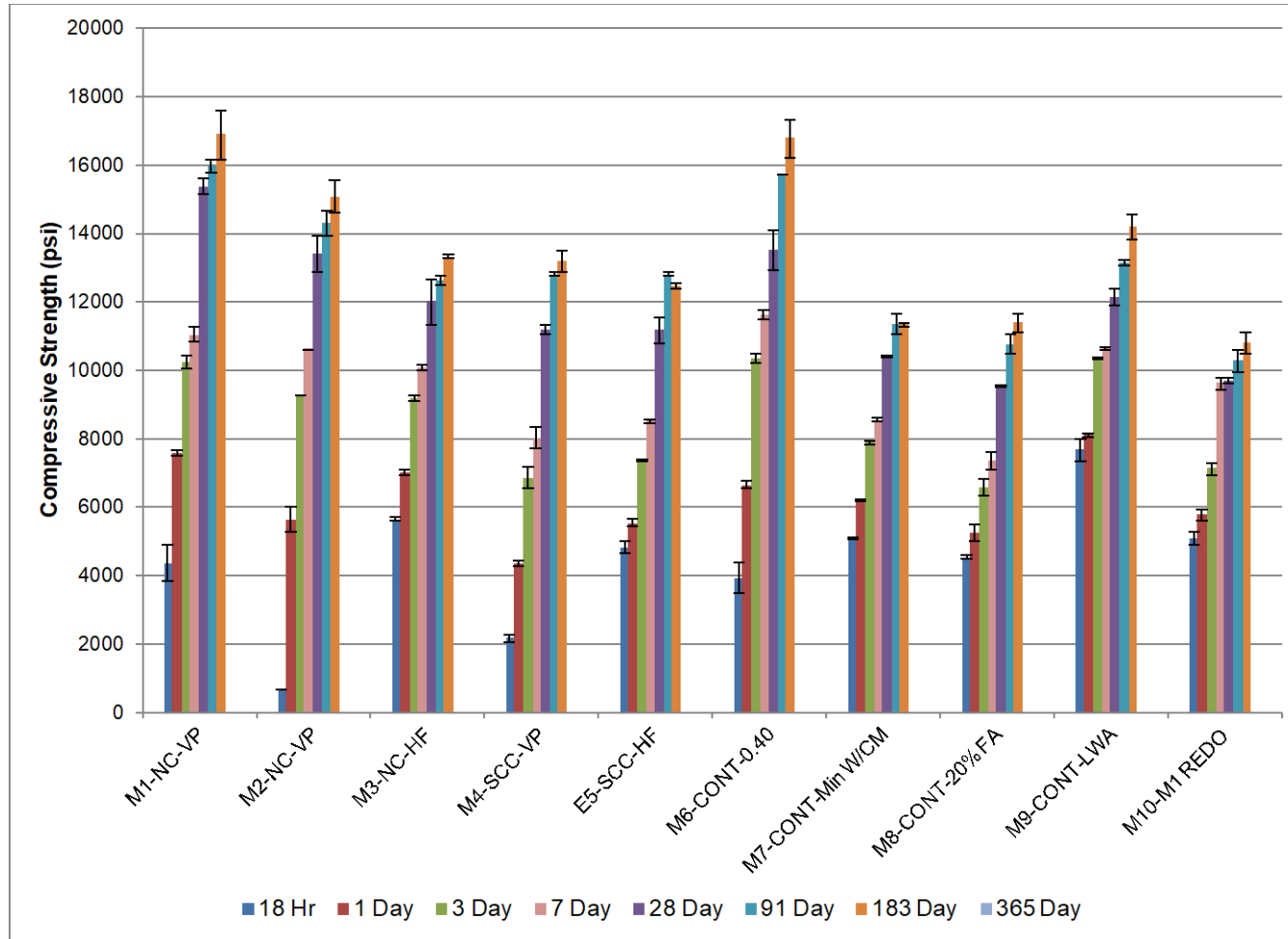


Figure III-1: Compressive Strength Results Task 3

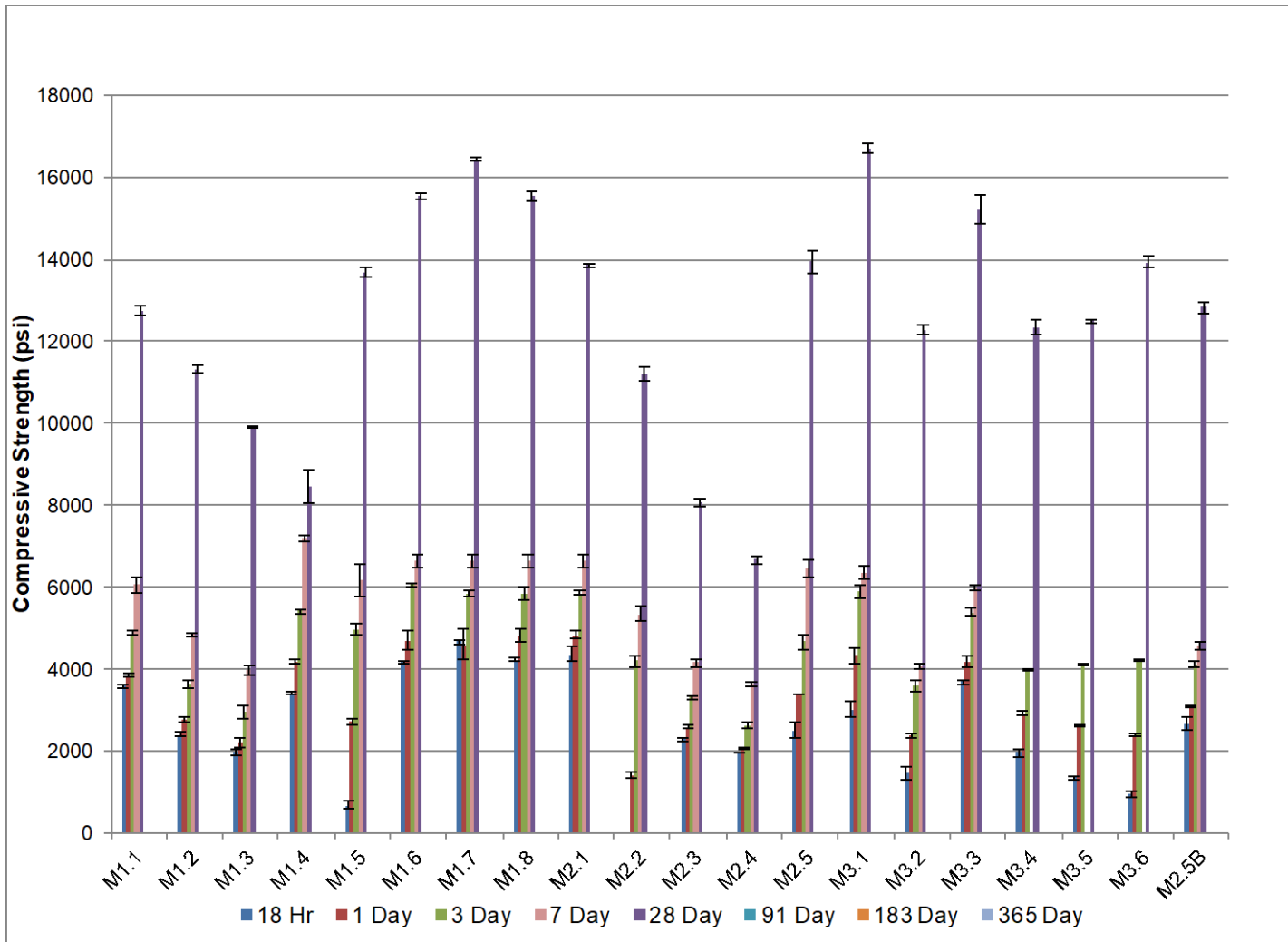


Figure III-2: Compressive Strength Results Task 4

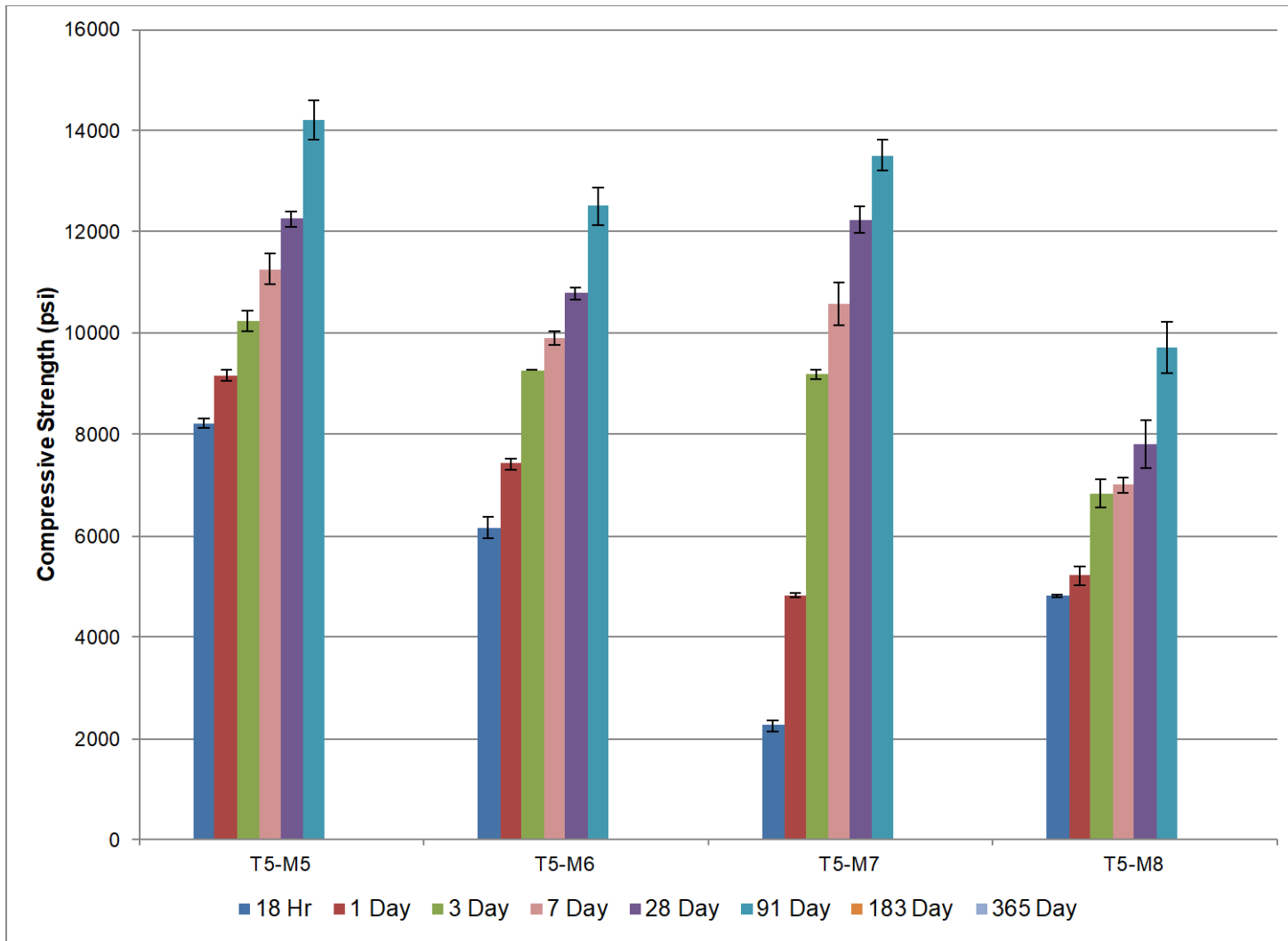


Figure III-3: Compressive Strength Results Task 5

Appendix IV: Additional Cited Sources

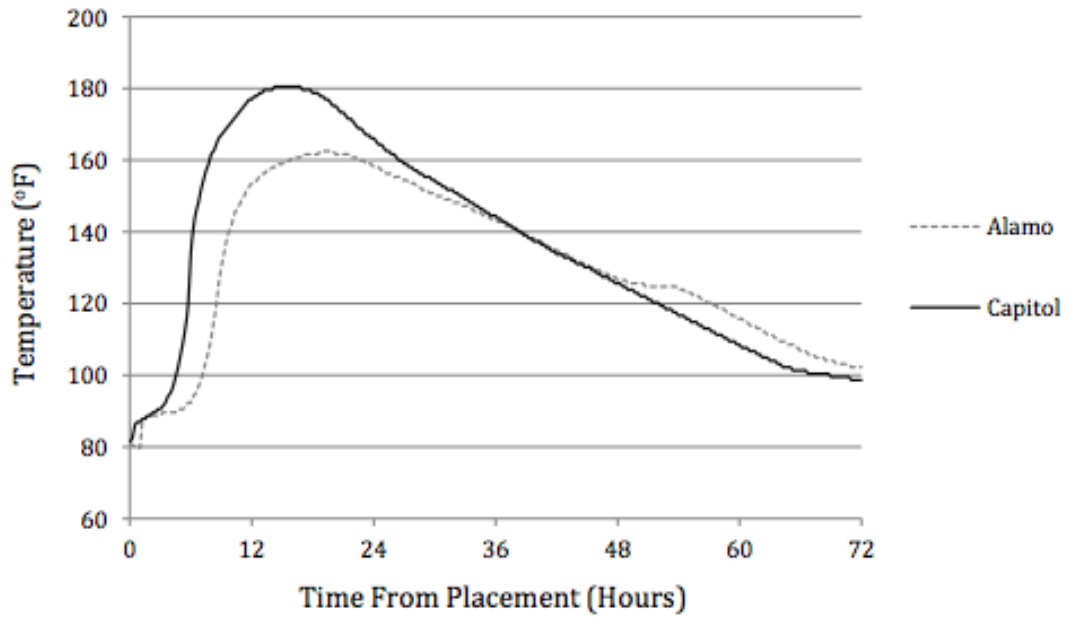


Figure IV-1: Time vs Temperature curve for precast concrete elements containing Alamo III and Capitol III cement taken from Implementation of Concrete Works Software in Texas Highway Construction (Meeks 2012).

Appendix V: Drying Shrinkage Curves

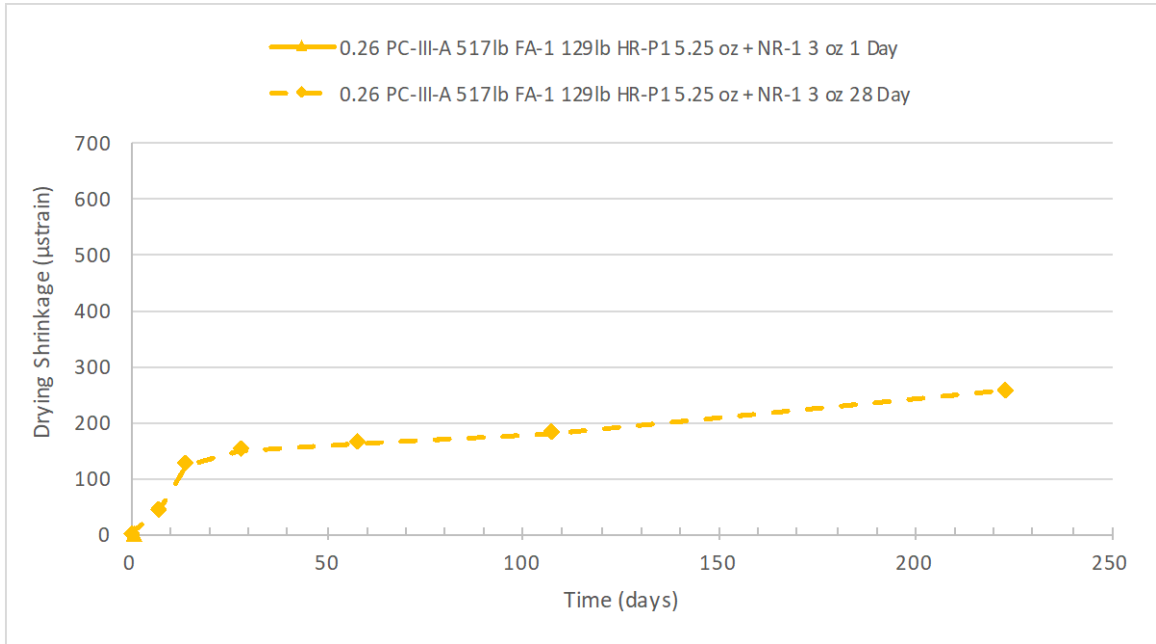


Figure VI-1: Drying Shrinkage 0.26 PC-III-A 517lb + FA-1 129lb HR-P1 5.25 oz + NR-1 3 oz

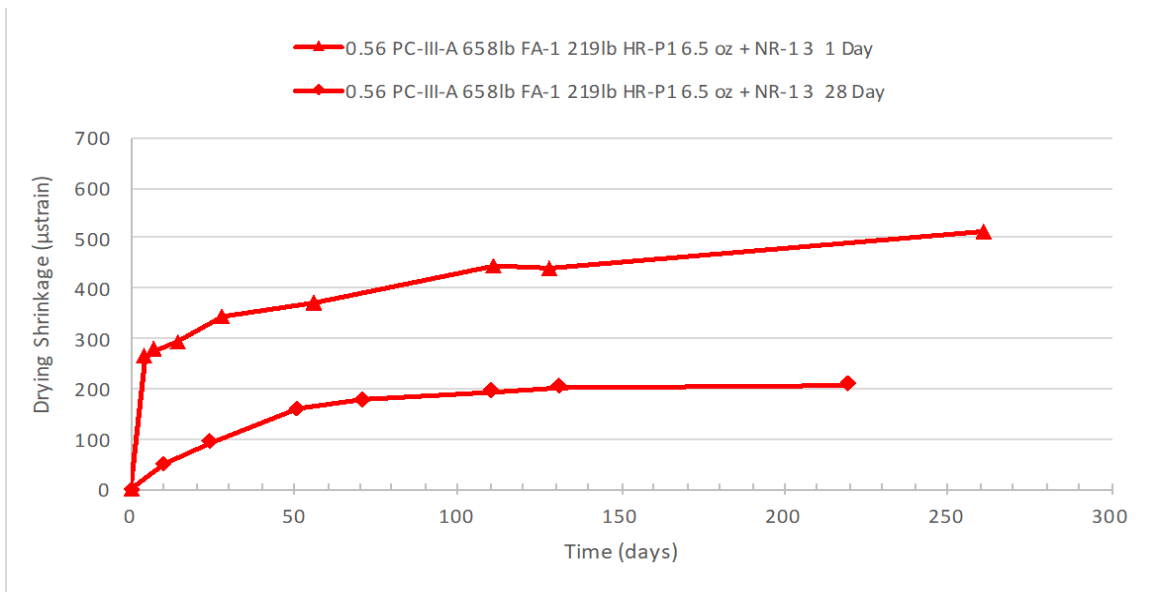


Figure VI-2: Drying Shrinkage 0.56 PC-III-A 658lb FA-1 219lb HR-P1 6.5 oz + NR-1 3 oz
TRIAL A

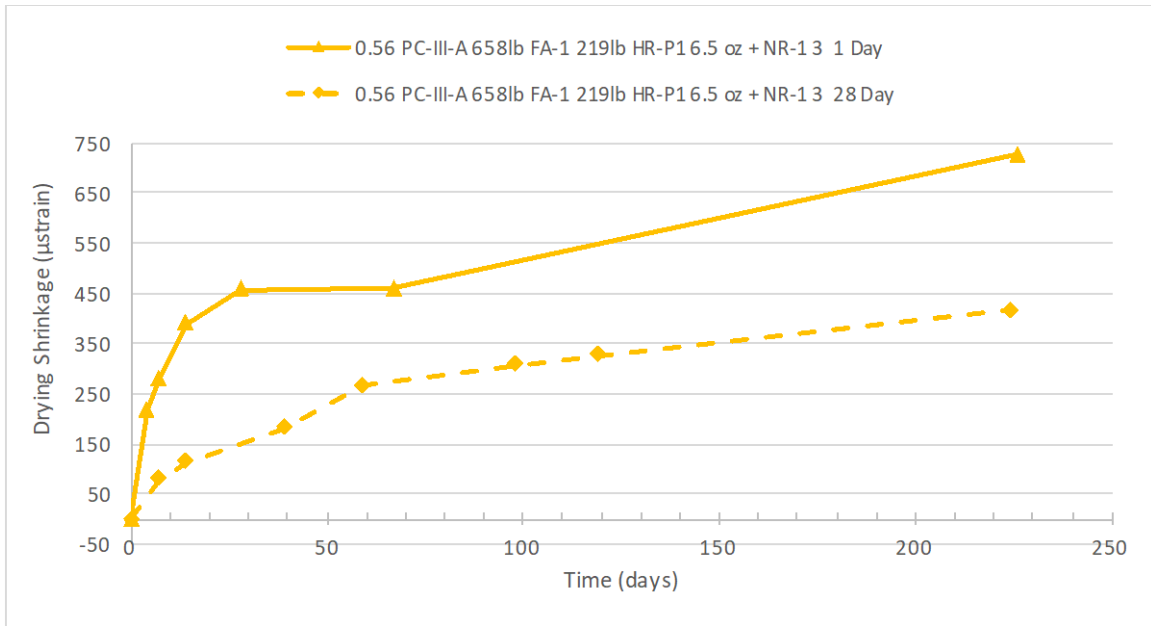


Figure VI-3: Drying Shrinkage 0.56 PC-III-A 658lb FA-1 219lb HR-P1 6.5 oz + NR-1 3 oz TRIAL B

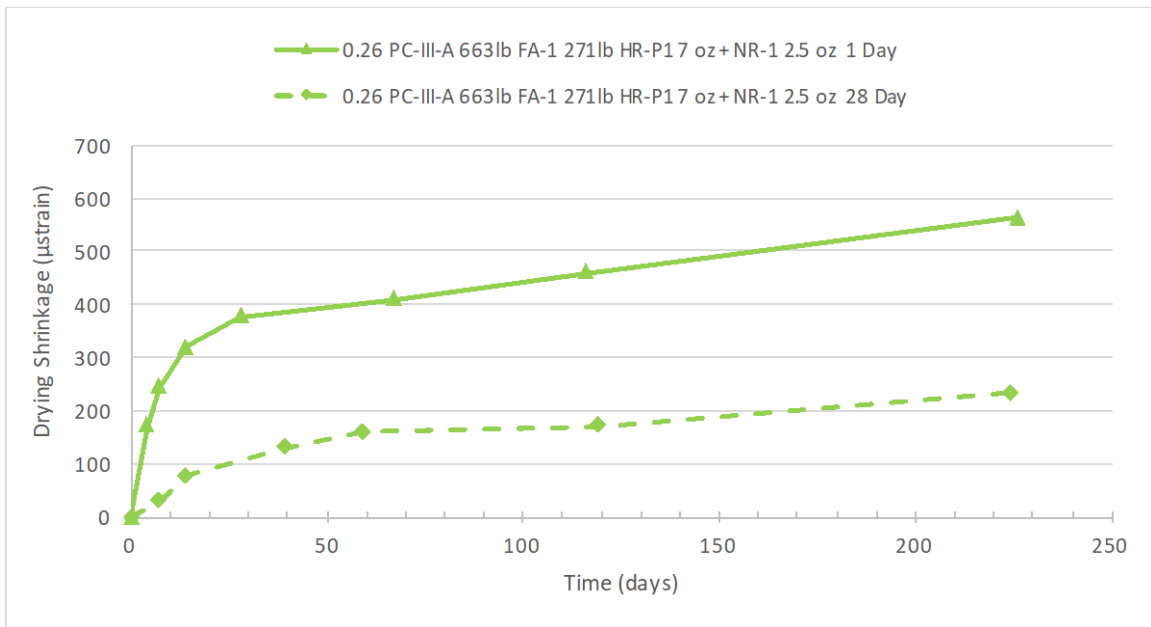


Figure VI-4: Drying Shrinkage 0.26 PC-III-A 663lb FA-1 271lb HR-P1 7 oz + NR-1 2.5 oz

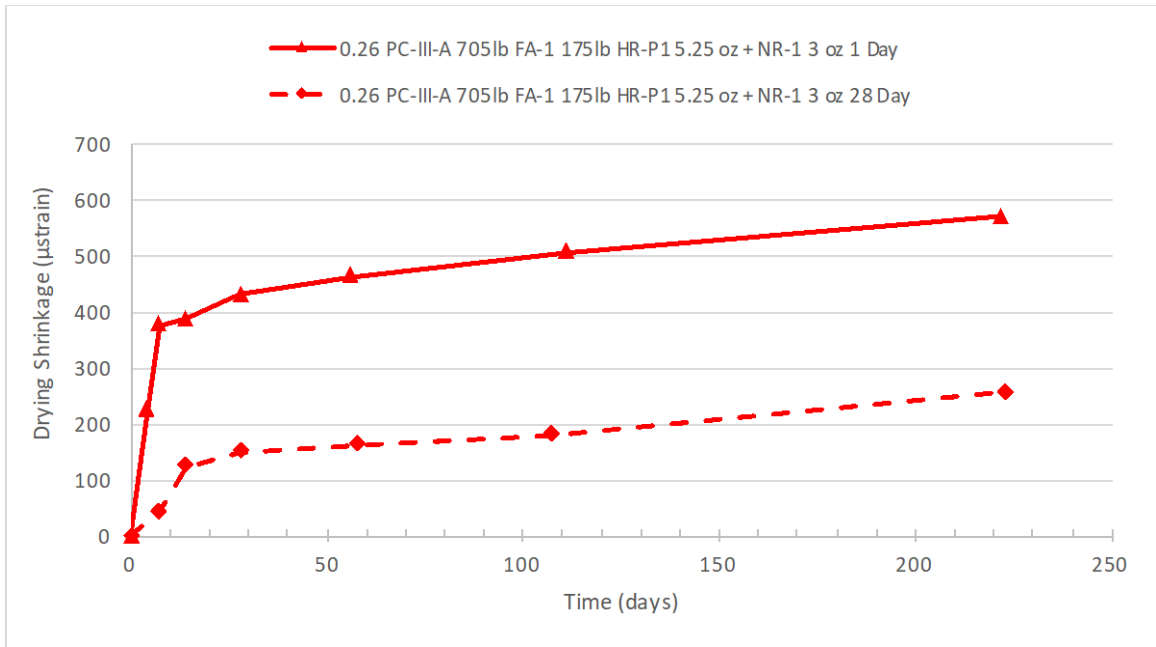


Figure VI-5: Drying Shrinkage 0.26 PC-III-A 705lb FA-1 175lb HR-P1 5.25 oz + NR-1 3 oz

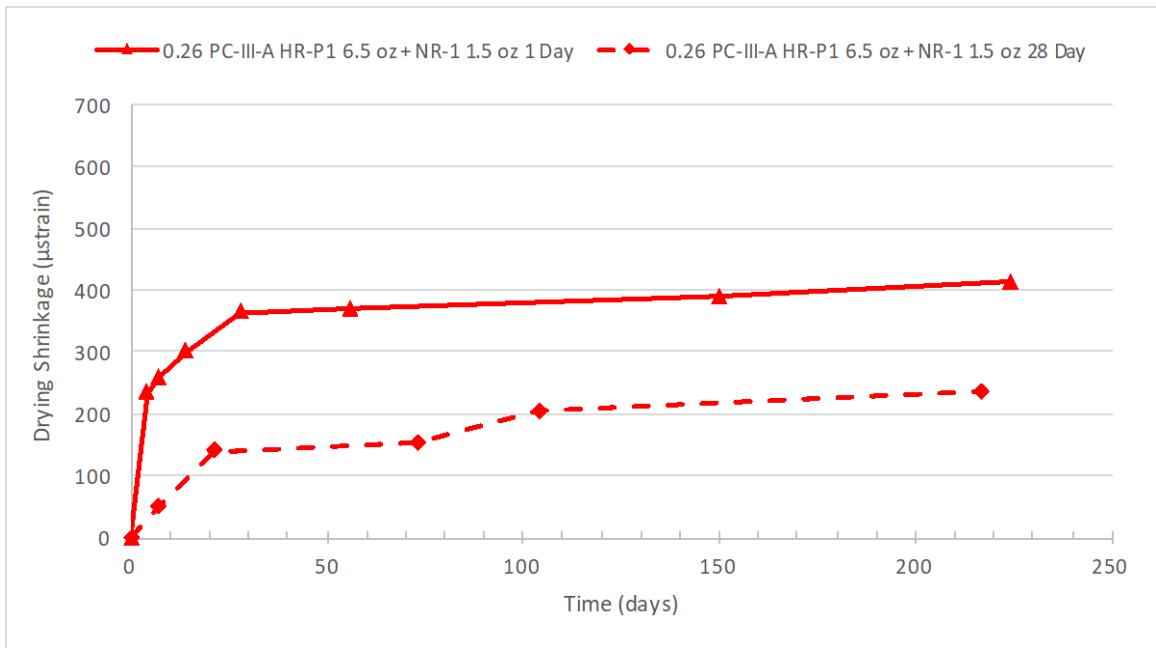


Figure VI-6: Drying Shrinkage 0.26 PC-III-A 705lb FA-1 175lb HR-P1 6.5 oz + NR-1 1.5 oz

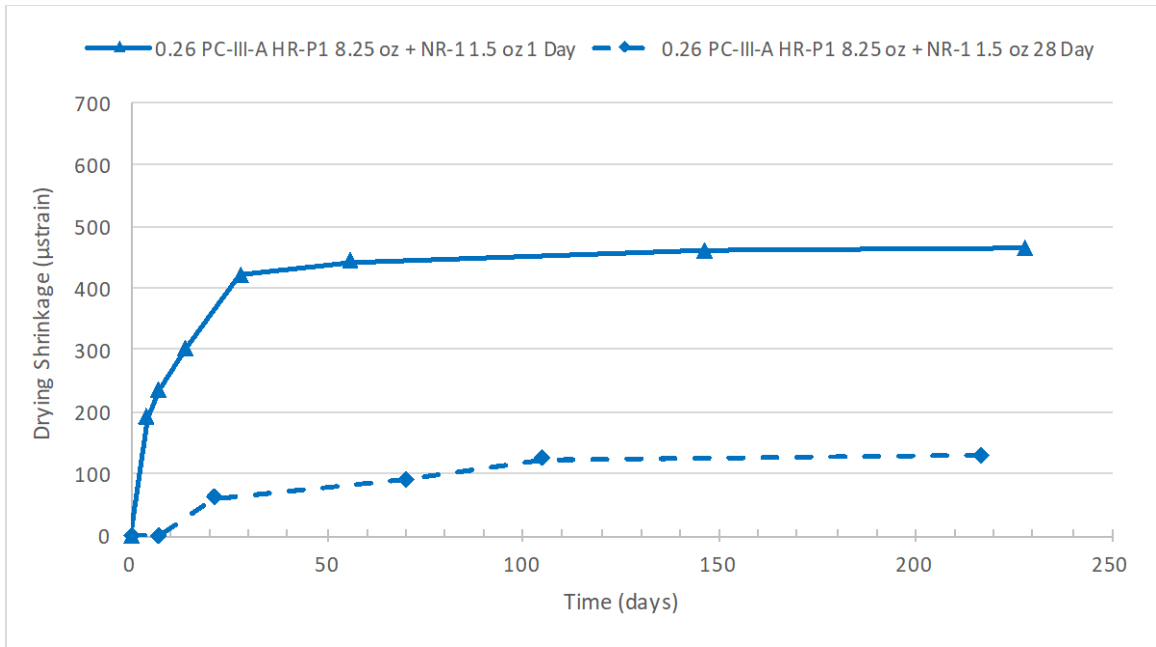


Figure VI-7: Drying Shrinkage 0.26 PC-III-A 705lb FA-1 175lb HR-P1 8.25 oz + NR-1 1.5 oz

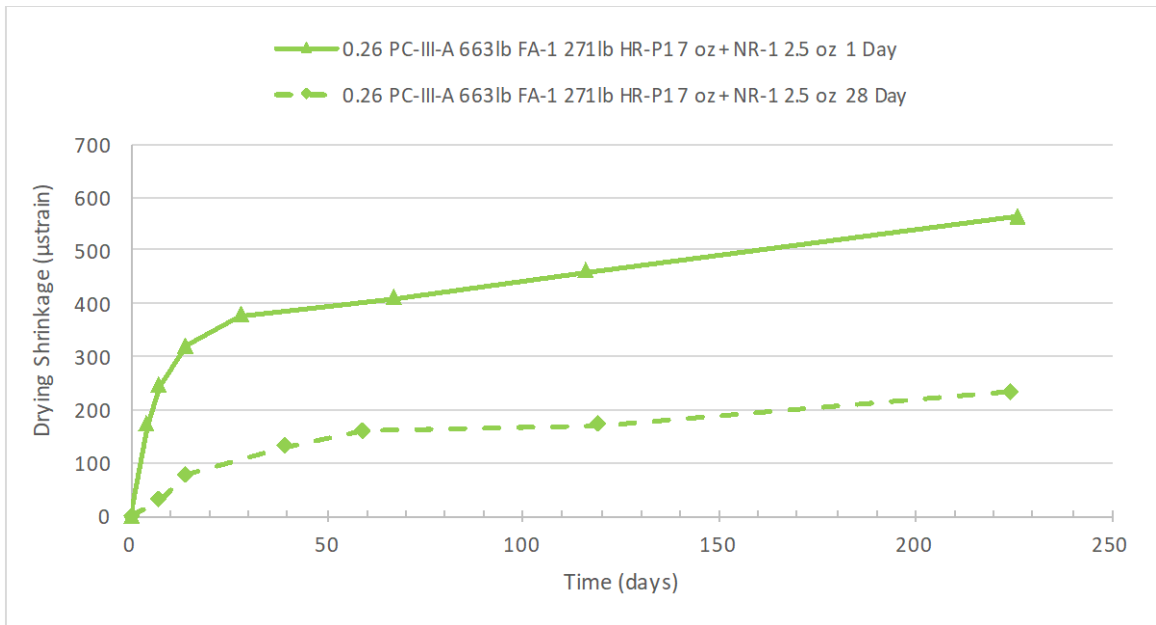


Figure VI-8: Drying Shrinkage 0.26 PC-III-A 663lb FA-1 271lb HR-P1 7 oz + NR-1 2.5 oz

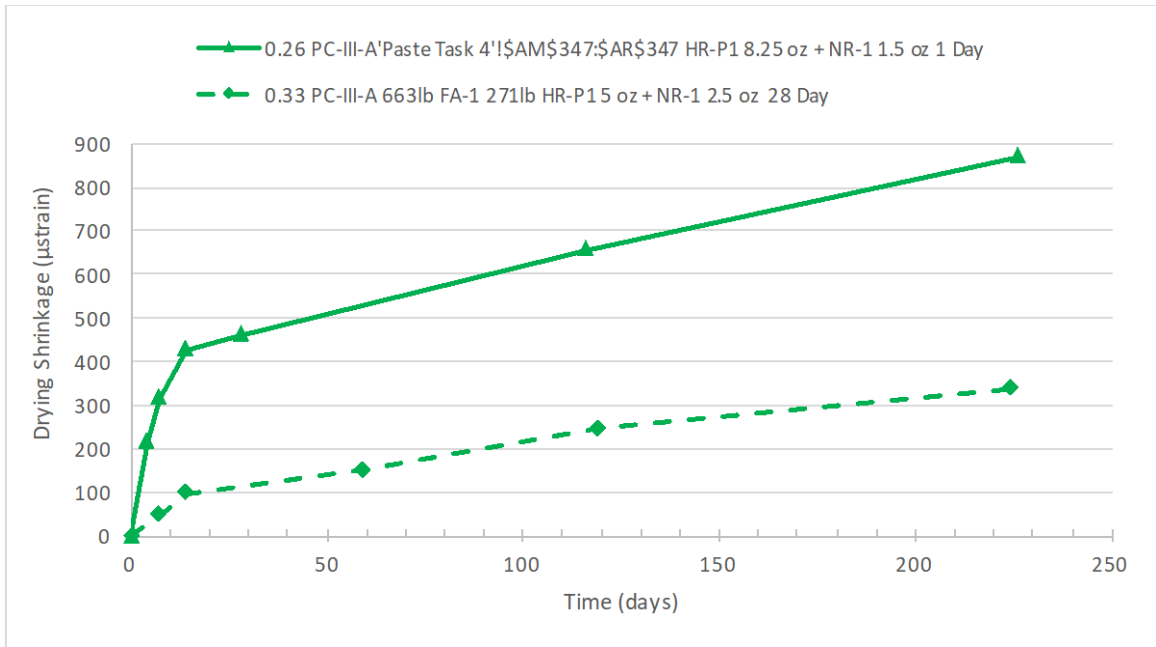


Figure VI-9: Drying Shrinkage 0.33 PC-III-A 663lb FA-1 271lb HR-P1 5 oz + NR-1 2.5 oz

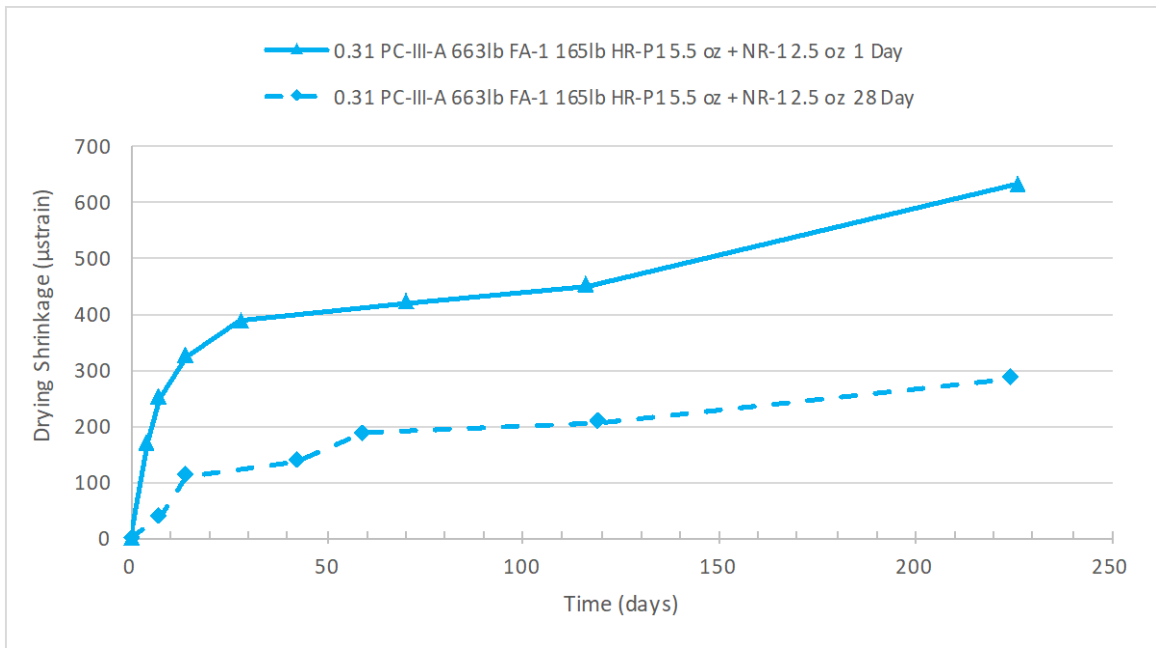


Figure VI-10: Drying Shrinkage 0.31 PC-III-A 663lb FA-1 165lb HR-P1 5.5 oz + NR-1 2.5 oz

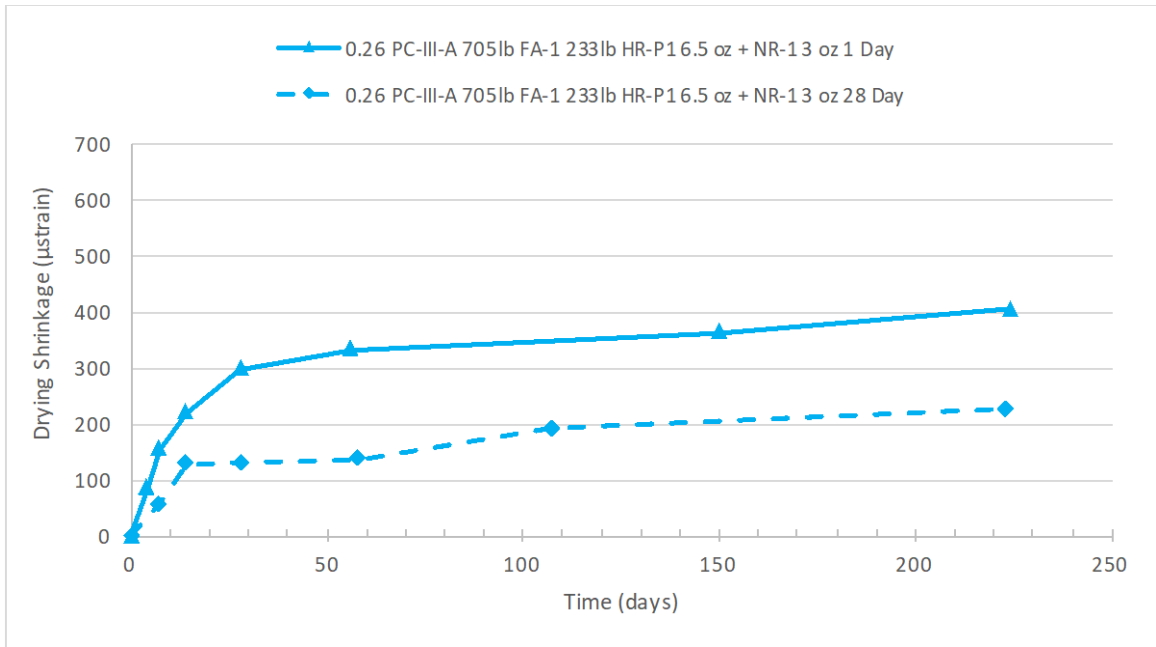


Figure VI-11: Drying Shrinkage 0.26 PC-III-A 705lb FA-1 233lb HR-P1 6.5 oz + NR-1 3 oz

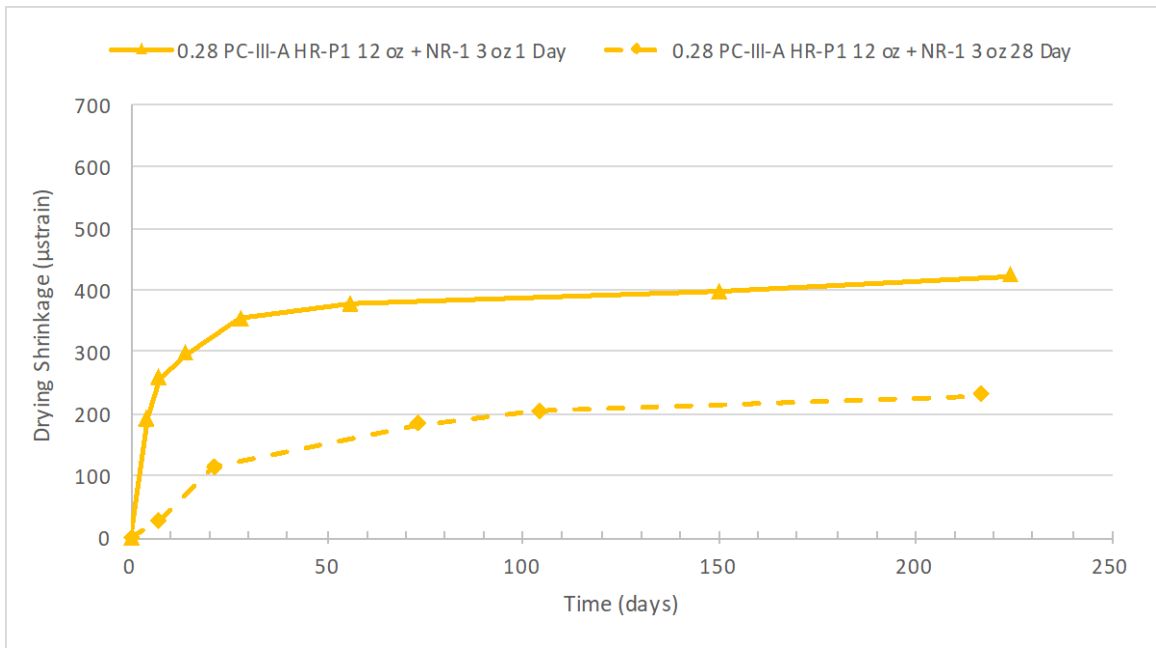


Figure VI-12: Drying Shrinkage 0.28 PC-III-A 705lb FA-1 175lb HR-P1 12 oz + NR-1 3 oz

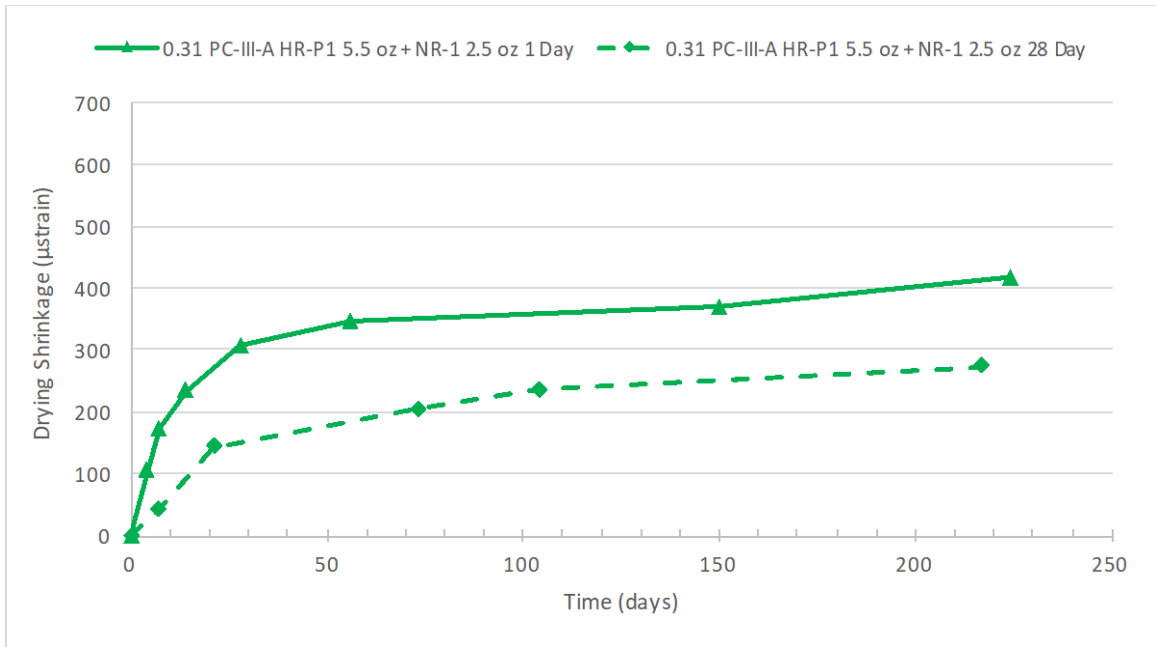


Figure VI-13: Drying Shrinkage 0.31 PC-III-A 663lb FA-1 271lb HR-P1 5.5 oz + NR-1 2.5 oz

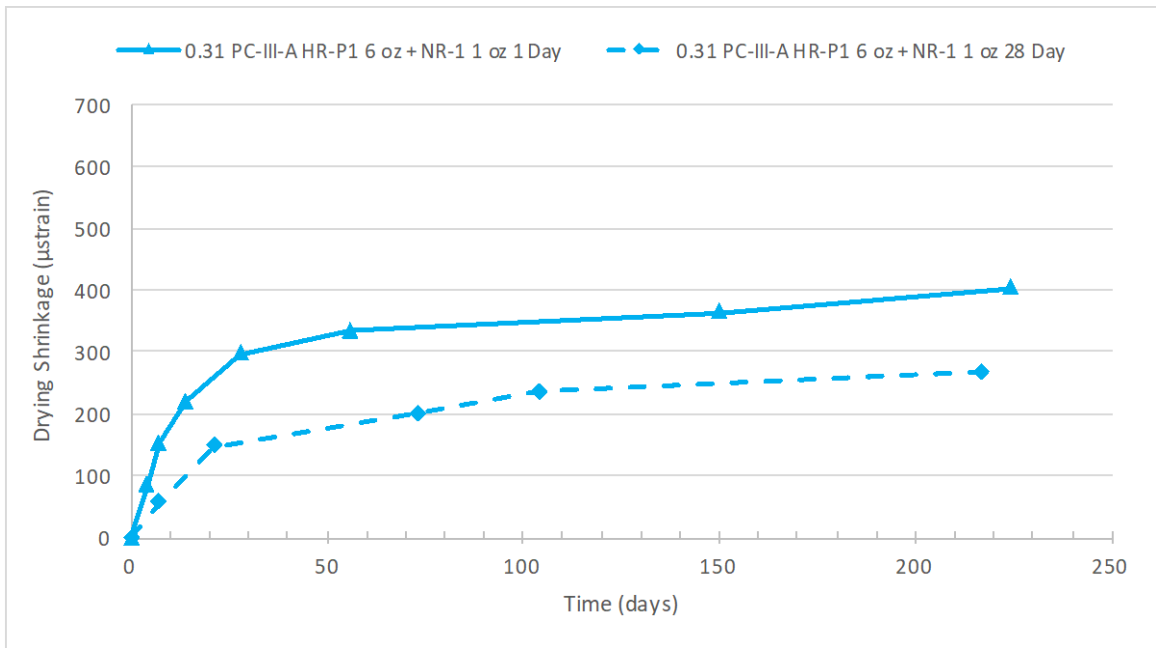


Figure VI-14: Drying Shrinkage 0.31 PC-III-A 640lb FA-1 213lb HR-P1 6 oz + NR-1 2 oz

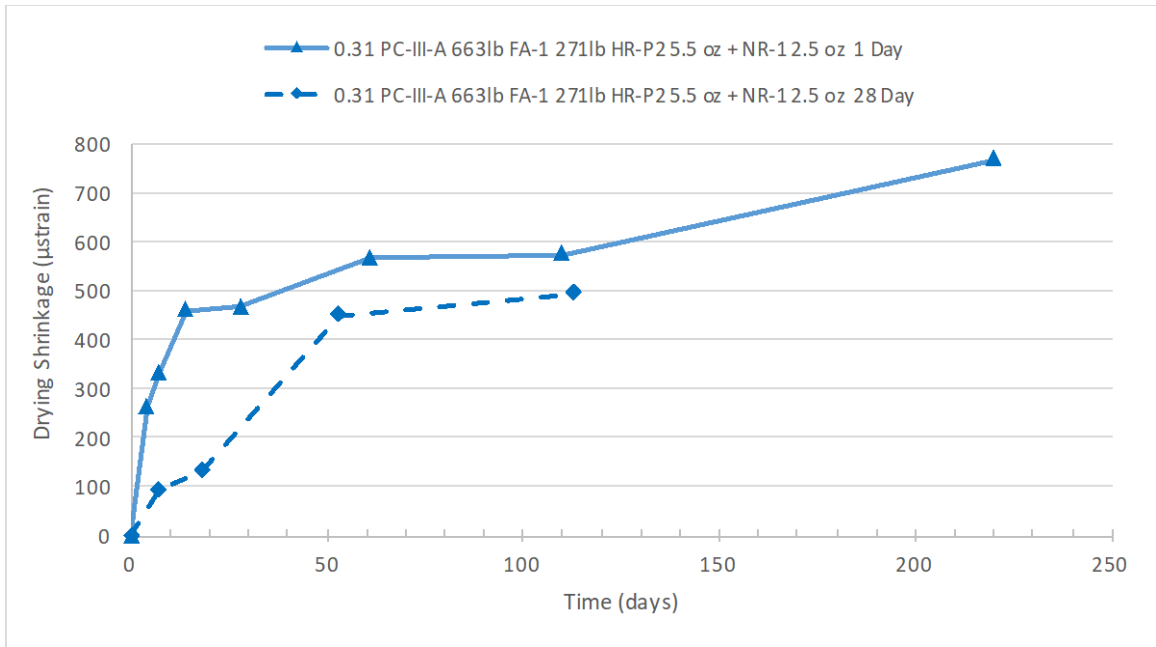


Figure VI-15: Drying Shrinkage 0.31 PC-III-A 663lb FA-1 271lb HR-P2 5.5 oz + NR-1 2.5 oz

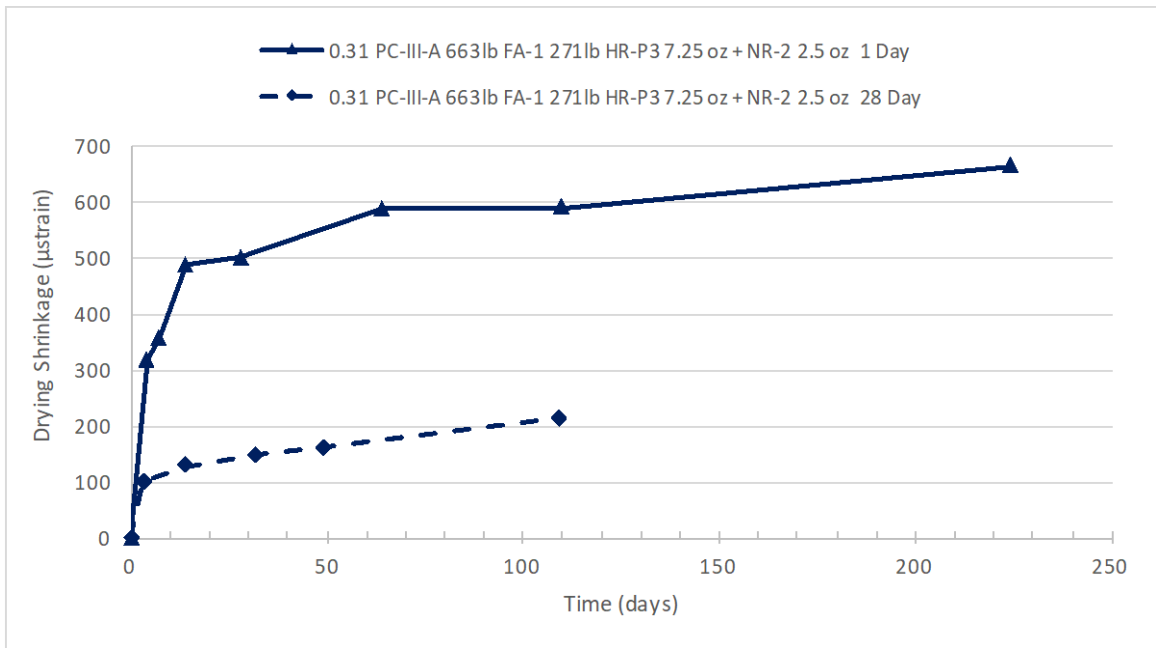


Figure VI-16: Drying Shrinkage 0.31 PC-III-A 663lb FA-1 271lb HR-P3 7.25 oz + NR-2 2.5 oz

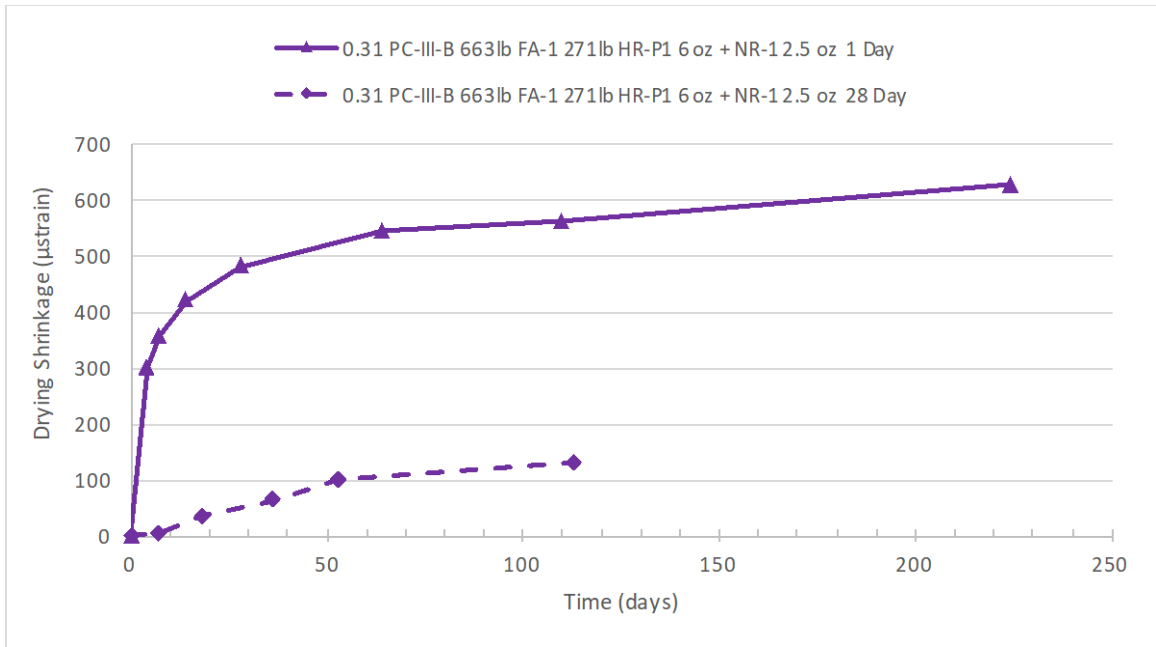


Figure VI-17: Drying Shrinkage 0.31 PC-III-B 663lb FA-1 271lb HR-P1 6 oz + NR-1 2.5 oz

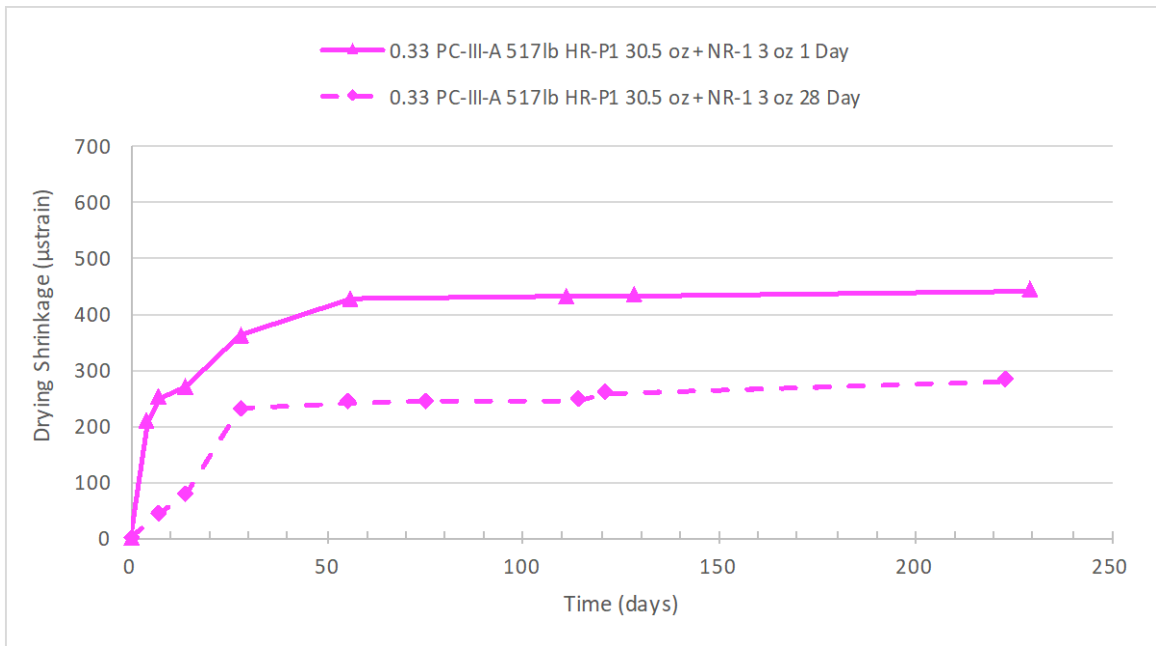


Figure VI-18: Drying Shrinkage 0.33 PC-III-A 517lb HR-P1 30.5 oz + NR-1 3 oz

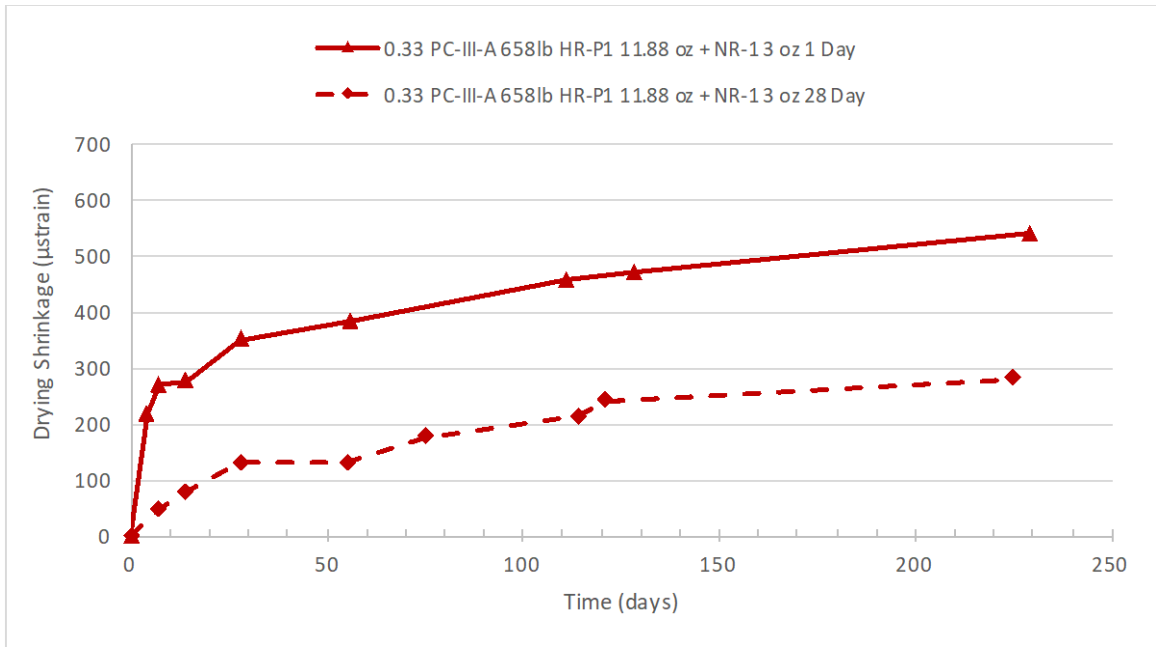


Figure VI-19: Drying Shrinkage 0.33 PC-III-A 658lb HR-P1 11.88 oz + NR-1 3 oz

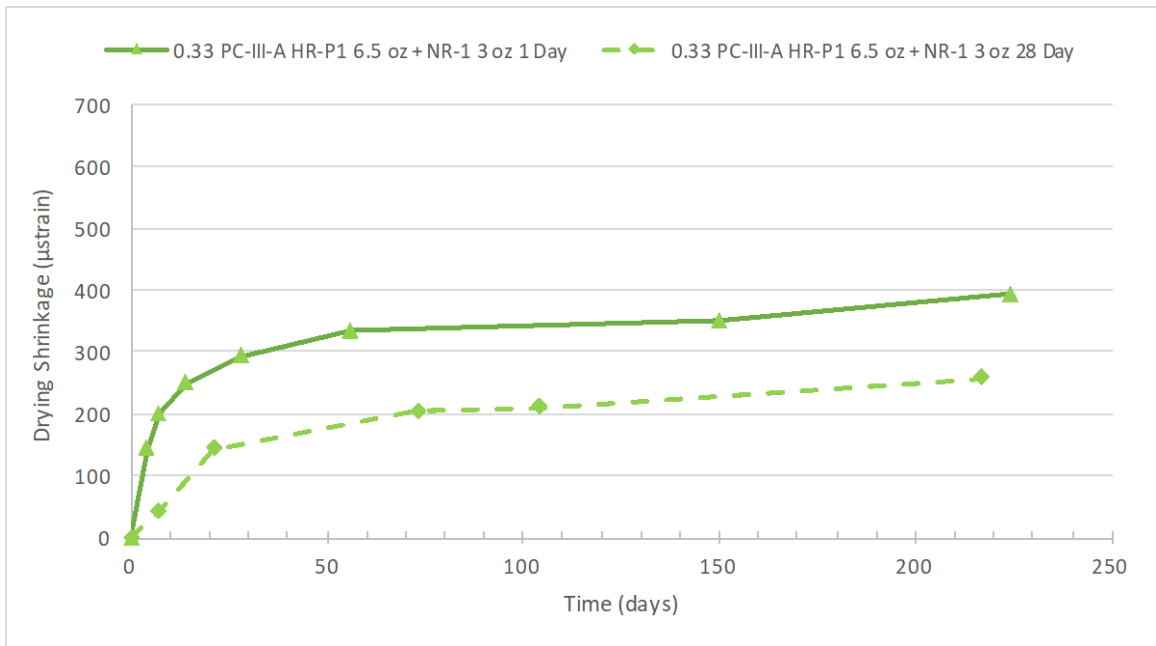


Figure VI-20: Drying Shrinkage 0.33 PC-III-A 658lb HR-P1 6.5 oz + NR-1 3 oz

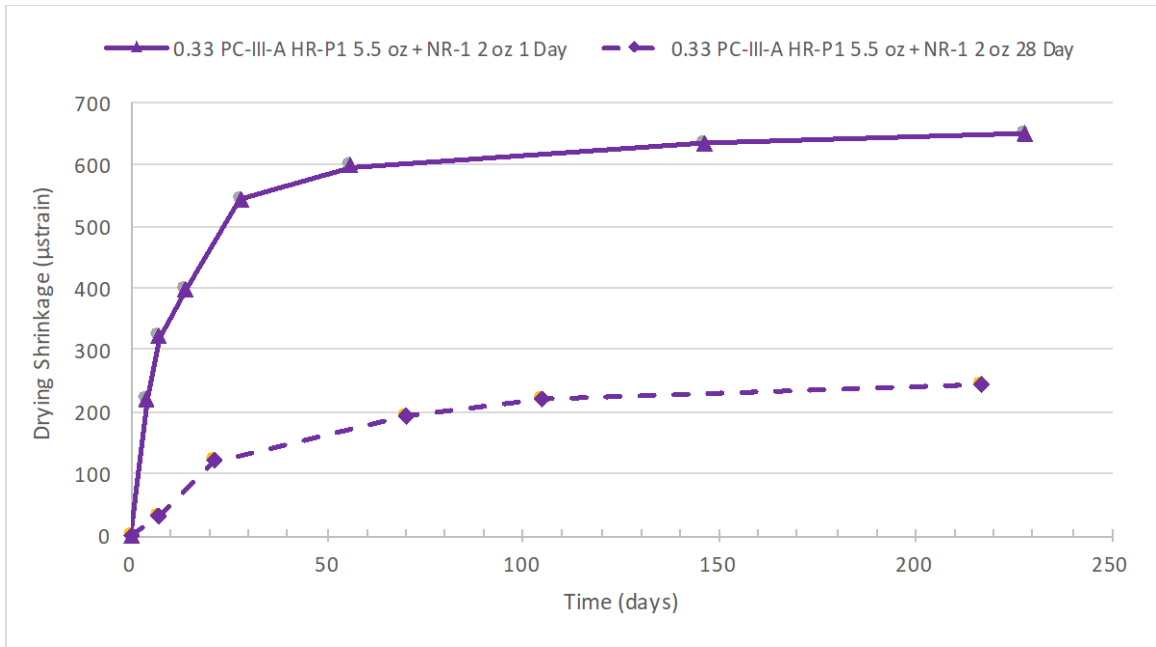


Figure VI-21: Drying Shrinkage 0.33 PC-III-A 658lb HR-P1 5.5 + NR-1 2 oz

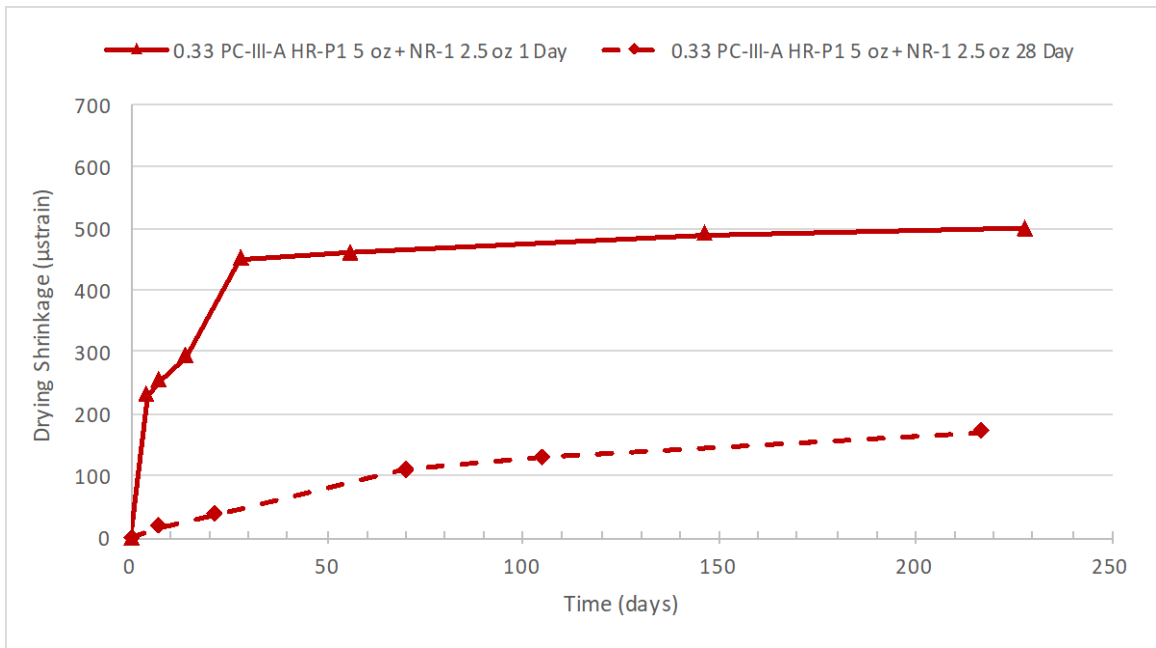


Figure VI-22: Drying Shrinkage 0.33 PC-III-A 658lb HR-P1 5 + NR-1 2.5 oz w/ FA-LW

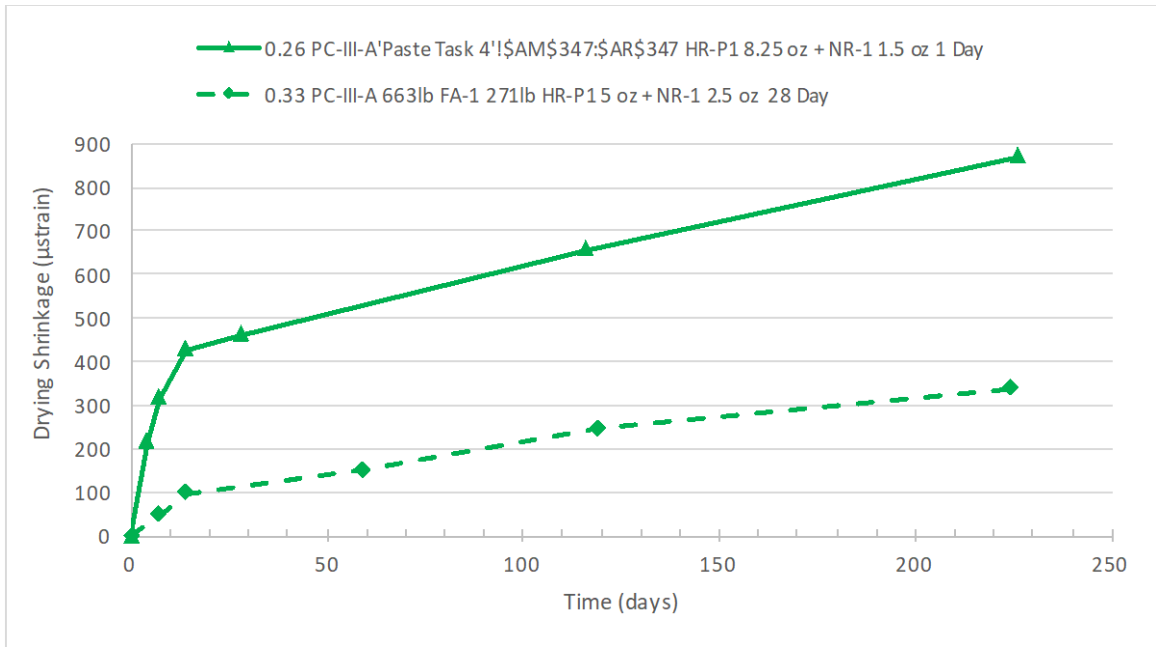


Figure VI-23: Drying Shrinkage 0.33 PC-III-A 663lb FA-1 271lb HR-P1 5 oz + NR-1 2.5 oz

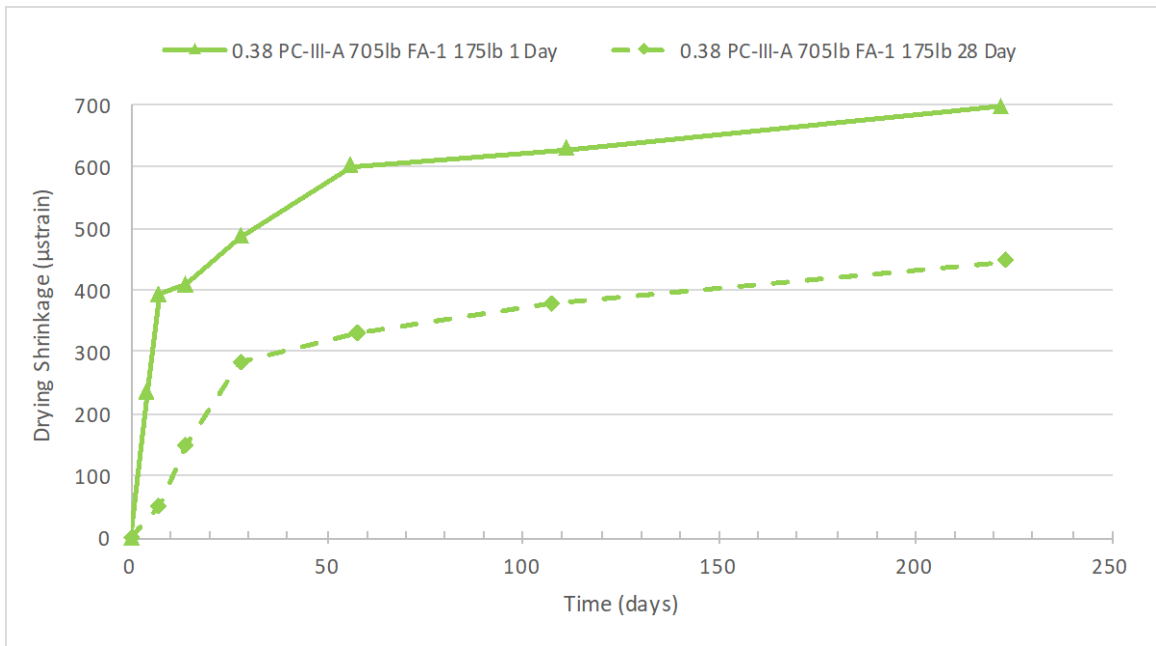


Figure VI-24: Drying Shrinkage 0.38 PC-III-A 705lb FA-1 175lb

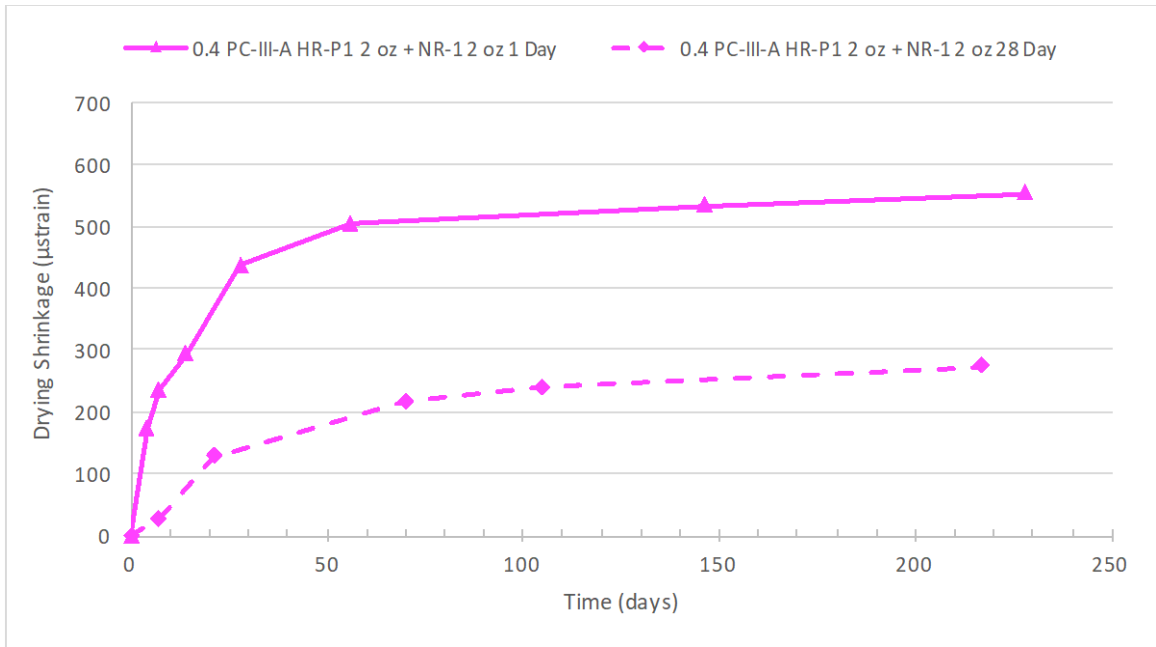


Figure VI-25: Drying Shrinkage 0.4 PC-III-A 658lb FA-1 165lb HR-P1 2 oz + NR-1 2 oz

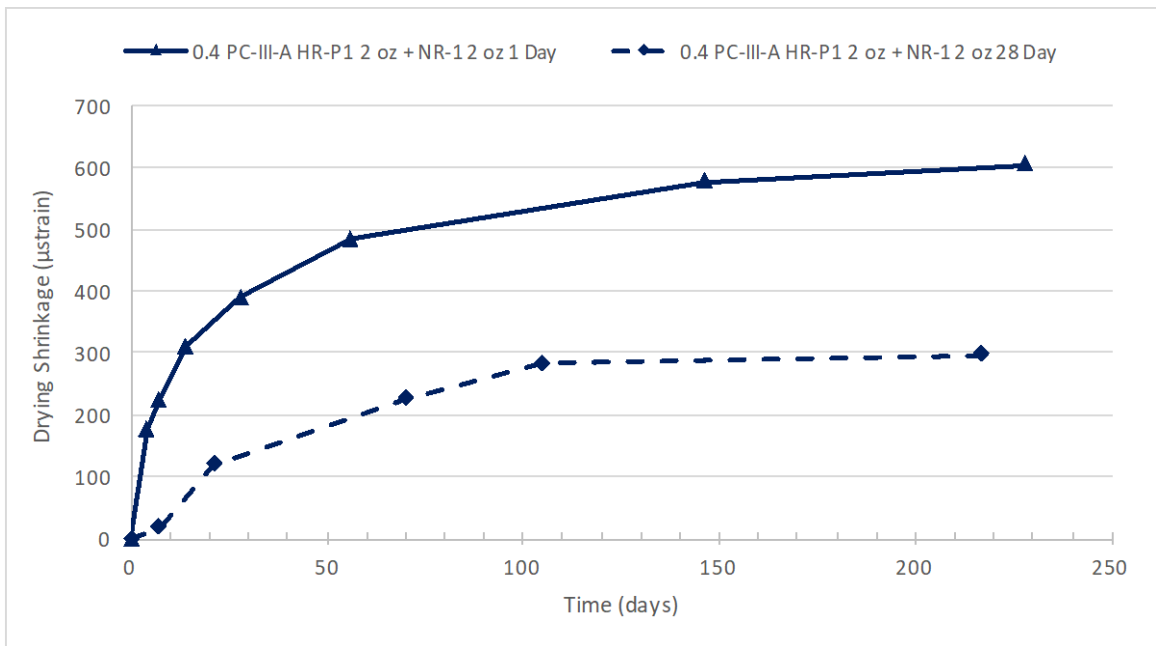


Figure VI-26: Drying Shrinkage 0.4 PC-III-A 658lb HR-P1 2 oz + NR-1 2 oz

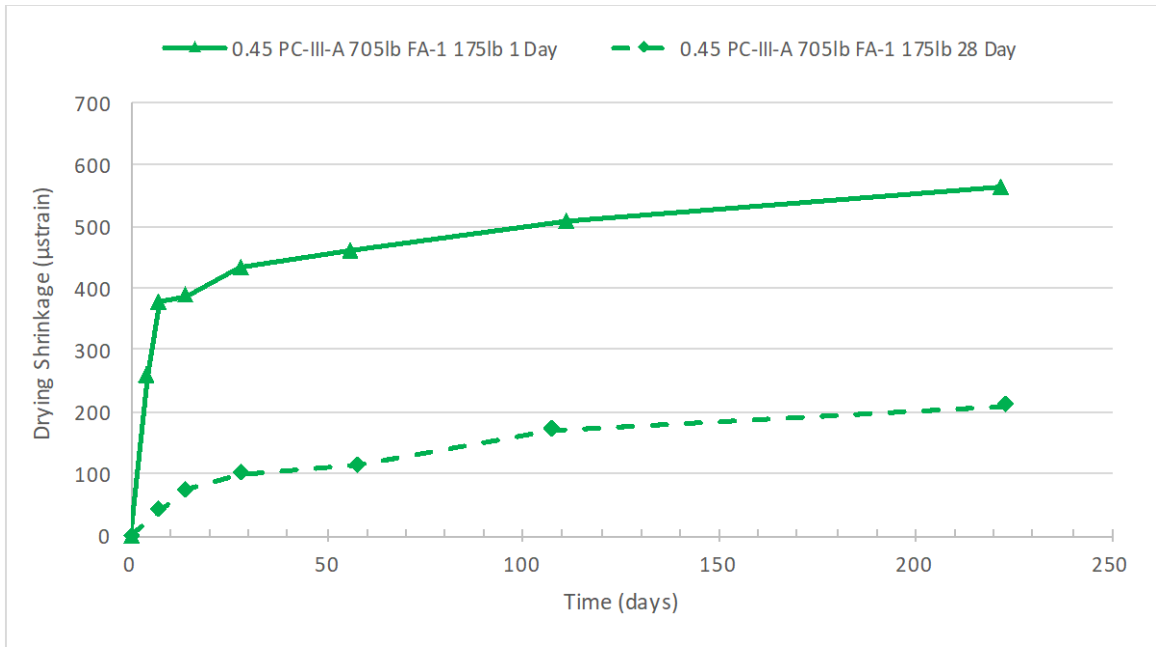


Figure VI-27: Drying Shrinkage 0.45 PC-III-A 705lb FA-1 175lb

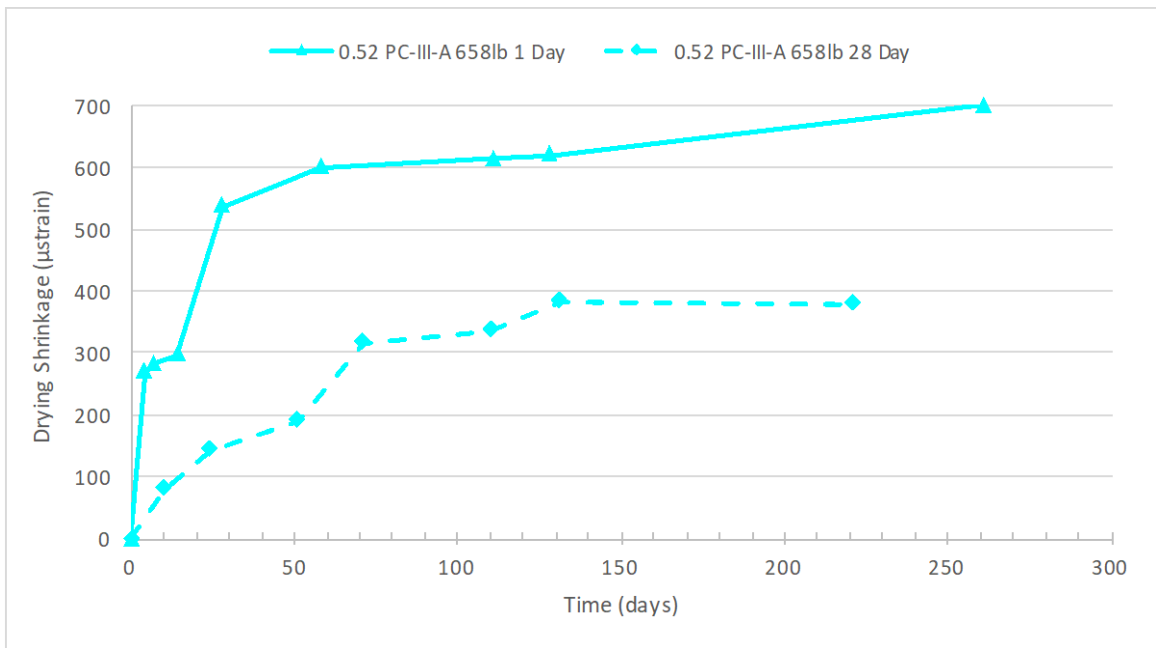


Figure VI-28: Drying Shrinkage 0.52 PC-III-A 658lb

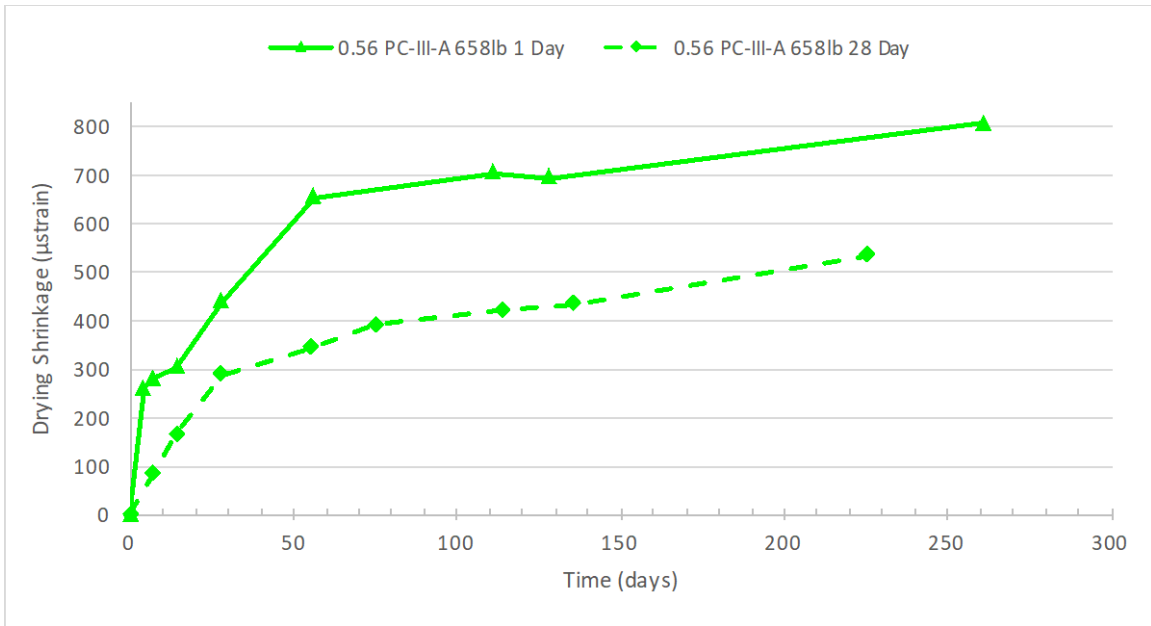


Figure VI-29: Drying Shrinkage 0.56 PC-III-A 658lb

Appendix VI: Restrained Shrinkage Ring Program

```
'CR5000
'Created by Stephen Stacey 2015

'Declare Variables and Units
Public BattV
Public FCLoaded
Public PTemp_C
Public CReps
Public ZMode
Public QBSSMode
Public CIndex
Public CAvg
Public LCount
Public Strain(16)
Public Vr1000(16)
Public GFAdj(16)
Public BrZero(16)
Public CKnown(16)
Public CReps_2
Public ZMode_2
Public QBSSMode_2
Public CIndex_2
Public CAvg_2
Public LCount_2
Public Strain_2(16)
Public Vr1000_2(16)
Public GFAdj_2(16)
Public BrZero_2(16)
Public CKnown_2(16)
Public CReps_3
Public ZMode_3
Public QBSSMode_3
Public CIndex_3
Public CAvg_3
Public LCount_3
Public Strain_3(16)
Public Vr1000_3(16)
Public GFAdj_3(16)
Public BrZero_3(16)
Public CKnown_3(16)
Public CReps_4
Public ZMode_4
Public QBSSMode_4
Public CIndex_4
Public CAvg_4
Public LCount_4
Public Strain_4(16)
Public Vr1000_4(16)
Public GFAdj_4(16)
Public BrZero_4(16)
```



```

Public CKnown_4(16)
Public CReps_5
Public ZMode_5
Public QBSSMode_5
Public CIndex_5
Public CAvg_5
Public LCount_5
Public Strain_5(16)
Public Vr1000_5(16)
Public GFAdj_5(16)
Public BrZero_5(16)
Public CKnown_5(16)
Public
GFsRaw(16)={2.13,2.13,2.13,2.13,2.12,2.12,2.12,2.12,2.12,2.12,2.12,2.1
2,2.12,2.12,2.12,2.12}
Public
GFsRaw_2(16)={2.13,2.13,2.13,2.13,2.12,2.12,2.12,2.12,2.13,2.12,2.13,2
.12,2.12,2.12,2.12,2.12}
Public
GFsRaw_3(16)={2.12,2.12,2.12,2.12,2.12,2.12,2.12,2.12,2.12,2.12,2.12,2
.12,2.12,2.12,2.12,2.12}
Public
GFsRaw_4(16)={2.13,2.13,2.13,2.13,2.13,2.12,2.13,2.12,2.12,2.12,2.12,2
.12,2.12,2.12,2.12,2.12}

Units BattV=Volts
Units PTemp_C=Deg C
Units Strain=mic
Units Vr1000=mV/V
Units GFAdj=unitless
Units BrZero=mV/V
Units Strain_2=mic
Units Vr1000_2=mV/V
Units GFAdj_2=unitless
Units BrZero_2=mV/V
Units Strain_3=mic
Units Vr1000_3=mV/V
Units GFAdj_3=unitless
Units BrZero_3=mV/V
Units Strain_4=mic
Units Vr1000_4=mV/V
Units GFAdj_4=unitless
Units BrZero_4=mV/V

'Define Data Tables Simply Change the Mix_XX to a new number each
time.
'Check How data is stored after in collection.

```

```

DataTable(Mix_7,True,-1)
  DataInterval(0,5,Min,10)

  Sample(1,Strain_3(5),IEEE4)
  Sample(1,Strain_3(6),IEEE4)
  Sample(1,Strain_3(7),IEEE4)
  Sample(1,Strain_3(8),IEEE4)
  Sample(1,Strain_3(9),IEEE4)
  Sample(1,Strain_3(10),IEEE4)
  Sample(1,Strain_3(11),IEEE4)
  Sample(1,Strain_3(12),IEEE4)
  Sample(1,Strain_3(13),IEEE4)
  Sample(1,Strain_3(14),IEEE4)
  Sample(1,Strain_3(15),IEEE4)
  Sample(1,Strain_3(16),IEEE4)
EndTable

DataTable(Mix_6,True,-1)
  DataInterval(0,5,Min,10)

  Sample(1,Strain_4(1),IEEE4)
  Sample(1,Strain_4(2),IEEE4)
  Sample(1,Strain_4(3),IEEE4)
  Sample(1,Strain_4(4),IEEE4)
  Sample(1,Strain_4(5),IEEE4)
  Sample(1,Strain_4(6),IEEE4)
  Sample(1,Strain_4(7),IEEE4)
  Sample(1,Strain_4(8),IEEE4)
  Sample(1,Strain_4(9),IEEE4)
  Sample(1,Strain_4(10),IEEE4)
  Sample(1,Strain_4(15),IEEE4)
  Sample(1,Strain_4(16),IEEE4)
EndTable

DataTable(Extra_Ring,True,-1)
  DataInterval(0,5,min,10)

  Sample(1,Strain_4(11),IEEE4)
  Sample(1,Strain_4(12),IEEE4)
  Sample(1,Strain_4(13),IEEE4)
  Sample(1,Strain_4(14),IEEE4)
EndTable

'Main Program
BeginProg
  'Initialize calibration variables for
  'Full Bridge Strain, 120 ohm measurement 'Vr1000()'
  CIndex=1 : CAvg=1 : CReps=16
  For LCount = 1 To 16

```

```
DataTable(Mix_5,True,-1)
  DataInterval(0,5,Min,10)

  Sample(1,Strain(1),IEEE4)
  Sample(1,Strain(2),IEEE4)
  Sample(1,Strain(3),IEEE4)
  Sample(1,Strain(4),IEEE4)
  Sample(1,Strain(5),IEEE4)
  Sample(1,Strain(6),IEEE4)
  Sample(1,Strain(7),IEEE4)
  Sample(1,Strain(8),IEEE4)
  Sample(1,Strain(9),IEEE4)
  Sample(1,Strain(10),IEEE4)
  Sample(1,Strain(15),IEEE4)
  Sample(1,Strain(16),IEEE4)
EndTable
```

```
DataTable(Mix_8,True,-1)
  DataInterval(0,5,Min,10)

  Sample(1,Strain(11),IEEE4)
  Sample(1,Strain(12),IEEE4)
  Sample(1,Strain(13),IEEE4)
  Sample(1,Strain(14),IEEE4)
  Sample(1,Strain_2(1),IEEE4)
  Sample(1,Strain_2(2),IEEE4)
  Sample(1,Strain_2(3),IEEE4)
  Sample(1,Strain_2(4),IEEE4)
  Sample(1,Strain_2(5),IEEE4)
  Sample(1,Strain_2(6),IEEE4)
  Sample(1,Strain_2(7),IEEE4)
  Sample(1,Strain_2(8),IEEE4)
EndTable
```

```
DataTable(Mix_3,True,-1)
  DataInterval(0,5,Min,10)

  Sample(1,Strain_2(9),IEEE4)
  Sample(1,Strain_2(10),IEEE4)
  Sample(1,Strain_2(11),IEEE4)
  Sample(1,Strain_2(12),IEEE4)
  Sample(1,Strain_2(13),IEEE4)
  Sample(1,Strain_2(14),IEEE4)
  Sample(1,Strain_2(15),IEEE4)
  Sample(1,Strain_2(16),IEEE4)
  Sample(1,Strain_3(1),IEEE4)
  Sample(1,Strain_3(2),IEEE4)
  Sample(1,Strain_3(3),IEEE4)
  Sample(1,Strain_3(4),IEEE4)
EndTable
```

```

        GFAdj(LCount)=GFsRaw(LCount)
    Next
    'Initialize calibration variables for
    'Full Bridge Strain, 120 ohm measurement 'Vr1000_2()'
    CIndex_2=1 : CAvg_2=1 : CReps_2=16
    For LCount_2 = 1 To 16
        GFAdj_2(LCount_2)=GFsRaw_2(LCount_2)
    Next
    'Initialize calibration variables for
    'Full Bridge Strain, 120 ohm measurement 'Vr1000_3()'
    CIndex_3=1 : CAvg_3=1 : CReps_3=16
    For LCount_3 = 1 To 16
        GFAdj_3(LCount_3)=GFsRaw_3(LCount_3)
    Next
    'Initialize calibration variables for
    'Full Bridge Strain, 120 ohm measurement 'Vr1000_4()'
    CIndex_4=1 : CAvg_4=1 : CReps_4=16
    For LCount_4 = 1 To 16
        GFAdj_4(LCount_4)=GFsRaw_4(LCount_4)
    Next

    'Load the most recent calibration values from the CalHist
table
    FCLoaded=LoadFieldCal(True)
    'Main Scan
    Scan(1,Min,1,0)
    'Default Datalogger Battery Voltage measurement
'BattV'
    Battery(BattV)
    'Default Wiring Panel Temperature measurement
'PTemp_C'
    PanelTemp(PTemp_C,_60Hz)
    'Turn AM16/32 Multiplexer On
    PortSet(2,1)
    Delay(0,1,mSec)
    LCount=1
    SubScan(0,uSec,16)
        'Switch to next AM16/32 Multiplexer channel
        PortSet(1,1)
        Delay(0,1,mSec)
        PortSet(1,0)
        Delay(0,1,mSec)
        'Full Bridge Strain, 120 ohm measurement
'Vr1000()'
        BrFull(Vr1000(LCount),
1,mV20,1,Vx1,1,5000,True,True,50000,_60Hz,1,0)
        LCount=LCount+1
    NextSubScan
    'Calculated strain result 'Strain()' for

```

```

'Full Bridge Strain, 120 ohm measurement 'Vr1000()'
StrainCalc(Strain(),16,Vr1000(),BrZero(),-1,GFAdj(),0)
'Bending full bridge strain shunt calibration for
'Full Bridge Strain, 120 ohm measurement 'Vr1000()'
FieldCalStrain(13,Strain(),1,GFAdj(),
0,QBSSMode,CKnown(),CIndex,CAvg,GFsRaw(),0)
'Zeroing calibration for
'Full Bridge Strain, 120 ohm measurement 'Vr1000()'
FieldCalStrain(10,Vr1000(),CReps,0,BrZero(),ZMode,
0,CIndex,CAvg,0,Strain())
'Turn AM16/32 Multiplexer Off
PortSet(2,0)
Delay(0,1,mSec)
'Turn AM16/32 Multiplexer On
PortSet(4,1)
Delay(0,1,mSec)
LCount_2=1
SubScan(0,uSec,16)
'Switch to next AM16/32 Multiplexer channel
PortSet(3,1)
Delay(0,1,mSec)
PortSet(3,0)
Delay(0,1,mSec)
'Full Bridge Strain, 120 ohm measurement
'Vr1000_2()'
BrFull(Vr1000_2(LCount_2),
1,mV20,2,Vx2,1,5000,True,True,50000,_60Hz,1,0)
LCount_2=LCount_2+1
NextSubScan
'Calculated strain result 'Strain_2()' for
'Full Bridge Strain, 120 ohm measurement 'Vr1000_2()'
StrainCalc(Strain_2(),
16,Vr1000_2(),BrZero_2(),-1,GFAdj_2(),0)
'Bending full bridge strain shunt calibration for
'Full Bridge Strain, 120 ohm measurement 'Vr1000_2()'
FieldCalStrain(43,Strain_2(),1,GFAdj_2(),
0,QBSSMode_2,CKnown_2(),CIndex_2,CAvg_2,GFsRaw_2(),0)
'Zeroing calibration for
'Full Bridge Strain, 120 ohm measurement 'Vr1000_2()'
FieldCalStrain(10,Vr1000_2(),CReps_2,0,BrZero_2(),ZMode_2,0,CIndex_2,C
Avg_2,0,Strain_2())
'Turn AM16/32 Multiplexer Off
PortSet(4,0)
Delay(0,1,mSec)
'Turn AM16/32 Multiplexer On
PortSet(6,1)
Delay(0,1,mSec)
LCount_3=1
SubScan(0,uSec,16)

```

```

        'Switch to next AM16/32 Multiplexer channel
        PortSet(5,1)
        Delay(0,1,mSec)
        PortSet(5,0)
        Delay(0,1,mSec)
        'Full Bridge Strain, 120 ohm measurement
'Vr1000_3()'
        BrFull(Vr1000_3(LCount_3),
1,mV20,3,Vx3,1,5000,True,True,50000,_60Hz,1,0)
        LCount_3=LCount_3+1
        NextSubScan
        'Calculated strain result 'Strain_3()' for
        'Full Bridge Strain, 120 ohm measurement 'Vr1000_3()'
        StrainCalc(Strain_3(),
16,Vr1000_3(),BrZero_3(),-1,GFAdj_3(),0)
        'Bending full bridge strain shunt calibration for
        'Full Bridge Strain, 120 ohm measurement 'Vr1000_3()'
        FieldCalStrain(43,Strain_3(),1,GFAdj_3(),
0,QBSSMode_3,CKnown_3(),CIndex_3,CAvg_3,GFsRaw_3(),0)
        'Zeroing calibration for
        'Full Bridge Strain, 120 ohm measurement 'Vr1000_3()'
FieldCalStrain(10,Vr1000_3(),CReps_3,0,BrZero_3(),ZMode_3,0,CIndex_3,C
Avg_3,0,Strain_3())
        'Turn AM16/32 Multiplexer Off
        PortSet(6,0)
        Delay(0,1,mSec)
        'Turn AM16/32 Multiplexer On
        PortSet(8,1)
        Delay(0,1,mSec)
        LCount_4=1
        SubScan(0,uSec,16)
        'Switch to next AM16/32 Multiplexer channel
        PortSet(7,1)
        Delay(0,1,mSec)
        PortSet(7,0)
        Delay(0,1,mSec)
        'Full Bridge Strain, 120 ohm measurement
'Vr1000_4()'
        BrFull(Vr1000_4(LCount_4),
1,mV20,4,Vx4,1,5000,True,True,50000,_60Hz,1,0)
        LCount_4=LCount_4+1
        NextSubScan
        'Calculated strain result 'Strain_4()' for
        'Full Bridge Strain, 120 ohm measurement 'Vr1000_4()'
        StrainCalc(Strain_4(),
16,Vr1000_4(),BrZero_4(),-1,GFAdj_4(),0)
        'Bending full bridge strain shunt calibration for
        'Full Bridge Strain, 120 ohm measurement 'Vr1000_4()'
        FieldCalStrain(43,Strain_4(),1,GFAdj_4(),

```

```
0,QBSSMode_4,CKnown_4(),CIndex_4,CAvg_4,GFsRaw_4(),0)
  'Zeroing calibration for
  'Full Bridge Strain, 120 ohm measurement 'Vr1000_4()'

FieldCalStrain(10,Vr1000_4(),CReps_4,0,BrZero_4()),ZMode_4,0,CIndex_4,C
Avg_4,0,Strain_4())
  'Turn AM16/32 Multiplexer Off
  PortSet(8,0)
  Delay(0,1,mSec)

  'Call Data Tables and Store Data
  CallTable Mix_5
  CallTable Mix_8
  CallTable Mix_3
  CallTable Mix_7
  CallTable Mix_6
  CallTable Extra_Ring

      NextScan
EndProg
```

Appendix VII: Cedar Park Blocks Included in Parametric Study

Block Number	Cement	Admixture	Coarse Aggregate	Fine Aggregate	W-C Ratio	Fly Ash (Replacement %)	Cement (lbs/cu.yd ¹)	Na2Oeq (lbs/cu.yd ¹)	Crack Rating (1-5) 11/4/15
366	Alamo III	Sika 2100 and Sika Plastiment	Hanson Eagle Lake	Hanson Eagle Lake	0.25		658	3.1	0
438	Alamo III	Sika 2100 and Sika Plastiment	Capitol Marble Falls	Capitol Marble Falls	0.40		658	3.1	0
438	Alamo III	Sika 2100 and Sika Plastiment	Capitol Marble Falls	Capitol Marble Falls	0.40		658	3.1	0
7	Alamo III	Sika 2110 and Sika Plastiment	Trinity Lockett	Trinity Lockett	0.33		564	2.7	0
29	Alamo III	Sika 2100 and Sika Plastiment	Trinity Lockett	Trinity Lockett	0.33		658	3.1	0
367	Alamo III	Sika 2100 and Sika Plastiment	Hanson Eagle Lake	Hanson Eagle Lake	0.33		658	3.1	0.25
368	Alamo III	Sika 2100 and Sika Plastiment	Hanson Eagle Lake	Hanson Eagle Lake	0.40		658	3.1	0.25
528	Capitol IP	Sika 2100 and Sika Plastiment	Hanson Servtex	TXI Webberville	0.33		658		0.25
196	Alamo III	Sika 2100 and Sika Plastiment	Hanson Servtex	TXI Webberville	0.33		519	2.5	0.5
277	Capitol III	Sika 2100 and Sika Plastiment	Hanson Servtex	TXI Webberville	0.33		700		0.5
278	Alamo III	Sika 2100 and Sika Plastiment	Hanson Servtex	TXI Webberville	0.33	25	700		0.5
362	Alamo III	Sika 2100 and Sika Plastiment	Hanson Arena	Hanson Arena	0.33		658	3.1	0.5
363	Alamo III	Sika 2100 and Sika Plastiment	Hanson Arena	Hanson Arena	0.40		658	3.1	0.5
437	Alamo III	Sika 2100 and Sika Plastiment	Capitol Marble Falls	Capitol Marble Falls	0.33		658	3.1	0.5
474	Alamo III	Sika - ViscoCrete 2100 (5 cwt)	Hanson Servtex	TXI Webberville	0.33		658		0.5
106	Alamo III	Sika 2100 and Sika Plastiment	Trinity Lockett	Trinity Lockett	0.25		564	2.7	0.5
617	Alamo III	Sika 2100 and Sika Plastiment	Hanson Servtex	TXI Webberville	0.33		658		0.5
794	Alamo III	Sika 2100 and Sika Plastiment	Trinity Lockett	Trinity Lockett	0.33		564		0.5
797	Alamo III	Sika 2100 and Sika Plastiment	Trinity Lockett	Trinity Lockett	0.33		564		0.5
474	Alamo III	Sika - ViscoCrete 2100 (5 cwt)	Hanson Servtex	TXI Webberville	0.33		658		0.75
522	Capitol IP	Sika 2100 and Sika Plastiment	Hanson Servtex	Trinity Lockett	0.33		658		0.75
279	Texas Lehigh III	Sika 2100 and Sika Plastiment	Hanson Servtex	TXI Webberville	0.33	25	700		1
437	Alamo III	Sika 2100 and Sika Plastiment	Capitol Marble Falls	Capitol Marble Falls	0.33		658	3.1	1
531	Capitol IIP	Sika 2100 and Sika Plastiment	Hanson Servtex	TXI Webberville	0.33		658		1
791	Alamo III	Sika 2100 and Sika Plastiment	Trinity Lockett	Trinity Lockett	0.33		564		1.25
217	Capitol III	Sika 2100 and Sika Plastiment	Hanson Servtex	TXI Webberville	0.33	2	575	2.5	1.5
564	Alamo III	Sika - ViscoCrete 2100 (3.75 cwt)	Hanson Servtex	TXI Webberville	0.33		658		1.5

586	Alamo III	Sika - ViscoCrete 2100 (6.5 cwt)	Hanson Servtex	TXI Webberville	0.33		658		1.5
616	Alamo III	Sika 2100 and Sika Plastiment	Hanson Servtex	TXI Webberville	0.33		658		1.5
617	Alamo III	Sika 2100 and Sika Plastiment	Hanson Servtex	TXI Webberville	0.33		658		1.5
792	Alamo III	Sika 2100 and Sika Plastiment	Trinity Lockett	Trinity Lockett	0.33		564		1.5
793	Alamo III	Sika 2100 and Sika Plastiment	Trinity Lockett	Trinity Lockett	0.33		564		1.5
618	Alamo III	Sika 2100 and Sika Plastiment	Hanson Servtex	TXI Webberville	0.33		658		1.75
619	Alamo III	Sika 2100 and Sika Plastiment	Hanson Servtex	TXI Webberville	0.33		658		1.75
361	Alamo III	Sika 2100 and Sika Plastiment	Hanson Arena	Hanson Arena	0.25		658	3.1	1.75
192	Lehigh White	Sika 2100 and Sika Plastiment	Hanson Servtex	TXI Webberville	0.33		658	1.5	2
219	Capitol III	Sika 2100 and Sika Plastiment	Hanson Servtex	TXI Webberville	0.33	2	806	3.5	2
221	Capitol III	Sika 2100 and Sika Plastiment	Hanson Servtex	TXI Webberville	0.33	25	703	3.0	2
285	Capitol III	Sika 2100 and Sika Plastiment	Hanson Servtex	TXI Webberville	0.33	25	700		2
361	Alamo III	Sika 2100 and Sika Plastiment	Hanson Arena	Hanson Arena	0.25		658	3.1	2
617	Alamo III	Sika 2100 and Sika Plastiment	Hanson Servtex	TXI Webberville	0.33		658		2
220	Capitol III	Sika 2100 and Sika Plastiment	Hanson Servtex	TXI Webberville	0.33	25	586	2.5	2
616	Alamo III	Sika 2100 and Sika Plastiment	Hanson Servtex	TXI Webberville	0.33		658		2
618	Alamo III	Sika 2100 and Sika Plastiment	Hanson Servtex	TXI Webberville	0.33		658		2
564	Alamo III	Sika - ViscoCrete 2100 (3.75 cwt)	Hanson Servtex	TXI Webberville	0.33		658		2

Block Number	Cement	Admixture	Coarse Aggregate	Fine Aggregate	W-C Ratio	Fly Ash (Replacement %)	Cement (lbs/cu.yd ¹)	Na ₂ O _{eq} (lbs/cu.yd ¹)	Crack Rating (1-5) 11/4/15
628	Alamo III	Sika - ViscoCrete 2100 (8 cwt)	Hanson Servtex	TXI Webberville	0.33		658		2
619	Alamo III	Sika 2100 and Sika Plastiment	Hanson Servtex	TXI Webberville	0.33		658		2.25
628	Alamo III	Sika - ViscoCrete 2100 (8 cwt)	Hanson Servtex	TXI Webberville	0.33		658		2.25
629	Alamo III	Sika - ViscoCrete 2100 (11.5 cwt)	Hanson Servtex	TXI Webberville	0.33		658		2.25
798	Alamo III	Sika 2100 and Sika Plastiment	Hanson Servtex	TXI Webberville	0.33		658		2.25
191	Cemex Odessa V	Sika 2100 and Sika Plastiment	Hanson Servtex	TXI Webberville	0.33		658	3.0	2.5
198	Alamo III	Sika 2100 and Sika Plastiment	Hanson Servtex	TXI Webberville	0.33		764	3.5	2.5
436	Alamo III	Sika 2100 and Sika Plastiment	Capitol Marble Falls	Capitol Marble Falls	0.25		658	3.1	2.5
218	Capitol III	Sika 2100 and Sika Plastiment	Hanson Servtex	TXI Webberville	0.33	2	691	3.0	2.75
220	Capitol III	Sika 2100 and Sika Plastiment	Hanson Servtex	TXI Webberville	0.33	25	586	2.5	2.75
222	Capitol III	Sika 2100 and Sika Plastiment	Hanson Servtex	TXI Webberville	0.33	25	820	3.5	2.75
648	Alamo III	BASF - PS1466	Hanson Servtex	TXI Webberville	0.33		658		2.75
710	Alamo III	BASF - Glenium 3400 NV	Hanson Servtex	TXI Webberville	0.33		658		2.75
629	Alamo III	Sika - ViscoCrete 2100 (11.5 cwt)	Hanson Servtex	TXI Webberville	0.33		658		2.75
197	Alamo III	Sika 2100 and Sika Plastiment	Hanson Servtex	TXI Webberville	0.33		643	3.0	3
270	Texas Lehigh III	Sika 2100 and Sika Plastiment	Hanson Servtex	TXI Webberville	0.33		700		3
646	Alamo III	BASF - Rheobuild 1000	Hanson Servtex	TXI Webberville	0.33		658		3
647	Alamo III	BASF - Glenium 7700	Hanson Servtex	TXI Webberville	0.33		658		3.25
268	Capitol III	Sika 2110 and Sika Plastiment	Hanson Servtex	TXI Webberville	0.33		658	3.0	3.25
267	Alamo III	Sika 2110 and Sika Plastiment	Hanson Servtex	TXI Webberville	0.33		658	3.1	3.5
268	Capitol III	Sika 2110 and Sika Plastiment	Hanson Servtex	TXI Webberville	0.33		658	3.0	3.5
222	Capitol III	Sika 2100 and Sika Plastiment	Hanson Servtex	TXI Webberville	0.33	25	820	3.5	3.5
381	Alamo III	Sika 2100 and Sika Plastiment	Trinity Lockett	Trinity Lockett	0.25		658	3.1	3.5
248	Alamo III	Sika 2100 and Sika Plastiment	Hanson Servtex	TXI Webberville	0.33		658	3.0	3.75
249	Alamo III	Sika 2100 and Sika Plastiment	Hanson Servtex	TXI Webberville	0.33		658	3.0	3.75
259	Alamo III	Sika 2100 and Sika Plastiment	Hanson Servtex	TXI Webberville	0.33		658	3.1	3.75
260	Capitol III	Sika 2100 and Sika Plastiment	Hanson Servtex	TXI Webberville	0.33		658	3.0	4
306	Capitol III	Sika 2100 and Sika Plastiment	Hanson Servtex	TXI Webberville	0.33		658	2.8	4
250	Capitol III	Sika 2100 and Sika Plastiment	Hanson Servtex	TXI Webberville	0.33		658	2.8	4.25
229	Capitol III	Sika 2100 and Sika Plastiment	Hanson Servtex	TXI Webberville	0.33		719	3.0	4.5
244	Alamo III	Sika 2100 and Sika Plastiment	Hanson Servtex	TXI Web/TXI Light	0.33		658	3.0	4.5
257	Alamo III	Sika 2110 and Sika Plastiment	Hanson Servtex	TXI Webberville	0.33		658	2.9	4.5
258	Capitol III	Sika 2110 and Sika Plastiment	Hanson Servtex	TXI Webberville	0.33		658	3.0	4.5

References

- Acker, P. "Swelling, Shrinkage and Creep: A Mechanical Approach to Cement Hydration." *Mat. Struct. Materials and Structures* 37.4 (2004): 237-43. Web.
- Ai, Hua, J. Francis Young, and George W. Scherer. "Thermal expansion kinetics: method to measure permeability of cementitious materials: II, application to hardened cement pastes." *Journal of the American Ceramic Society* 84.2 (2001): 385-91.
- Al-Fadhala, Manal, and Kenneth C. Hover. "Rapid evaporation from freshly cast concrete and the Gulf environment." *Construction and Building Materials* 15.1 (2001): 1-7.
- Almusallam, A. A., et al. "Effect of mixture proportions on plastic shrinkage cracking of concrete in hot environments." *Construction and Building Materials* 12.6 (1998): 353-358.
- Altoubat, Salah A., and David A. Lange. "Creep, shrinkage, and cracking of restrained concrete at early age." *ACI Materials Journal* 98.4 (2001): 323-331.
- Assaf, G and Ghezal, A. (2015). Time-Dependent Behavior of Self-Consolidating Concrete Loaded at Early Age: Influence of Chemical Admixtures. ASCE, *Journal of Materials in Civil Engineering*.
- ASTM C 192, Standard Practice for Making and Curing Concrete Test Specimens in the Laboratory, American Society of Testing and Materials, (2015)
- ASTM C150, Standard Specification for Portland Cement, American Society of Testing and Materials, (2012).
- ASTM C157, Standard Test Method for Length Change of Hardened Hydraulic-Cement Mortar and Concrete, American Society of Testing and Materials, (2008).
- ASTM C1579, Standard Test Method for Evaluating Plastic Shrinkage Cracking of Restrained Fiber Reinforced Concrete (Using a Steel Form Insert), American Society of Testing and Materials, (2013).
- ASTM C1581, Standard Test Method for Determining Age at Cracking and Induced Tensile Stress Characteristics of Mortar and Concrete under Restrained Shrinkage, (2009).
- ASTM C1608, Standard Test Method for Chemical Shrinkage of Hydraulic Cement Paste, American Society of Testing and Materials, (2012).
- ASTM C1679, Standard Practice for Measuring Hydration Kinetics of Hydraulic Cementitious Mixtures Using Isothermal Calorimetry, American Society of Testing and Materials, (2014).
- ASTM C305, Standard Practice for Mechanical Mixing of Hydraulic Cement Pastes and Mortars of Plastic Consistency, American Society of Testing and Materials, (2014).

- ASTM C33, Standard Specification for Concrete Aggregates, American Society of Testing and Materials, (2013).
- ASTM C39, Standard Test Method for Compressive Strength of Cylindrical Concrete Specimens, American Society of Testing and Materials, (2014).
- ASTM C403, Test Method for Time of Setting of Concrete Mixtures by Penetration Resistance, ASTM International, (2008).
- ASTM C469, Standard Test Method for Static Modulus of Elasticity and Poisson's Ratio of Concrete in Compression, American Society of Testing and Materials, (2010).
- ASTM C494, Standard Specification for Chemical Admixtures for Concrete, American Society of Testing and Materials, (2013).
- ASTM C496, Standard Test Method for Splitting Tensile Strength of Cylindrical Concrete Specimens, American Society of Testing and Materials, (2011).
- ASTM C511, Standard Specification for Mixing Rooms, Moist Cabinets, Moist Rooms, and Water Storage Tanks Used in the Testing of Hydraulic Cements and Concretes, American Society of Testing and Materials, (2013).
- ASTM C618, Standard Specification for Coal Fly Ash and Raw or Calcined Natural Pozzolan for Use in Concrete, American Society of Testing and Materials, (2012).
- Barcelo, Laurent, Micheline Moranville, and Bernard Clavaud. "Autogenous shrinkage of concrete: a balance between autogenous swelling and self-desiccation." *Cement and Concrete Research* 35.1 (2005): 177-183.
- Bažant, Z. P. "Delayed thermal dilatations of cement paste and concrete due to mass transport." *Nuclear Engineering and Design* 14.2 (1970): 308-318.
- Bazant, Zdenek P., and Yunping Xi. "Continuous retardation spectrum for solidification theory of concrete creep." *Journal of Engineering Mechanics* 121.2 (1995): 281-288.
- Bentur, A., and K. Kovler. "Evaluation of early age cracking characteristics in cementitious systems." *Materials and Structures* 36.3 (2003): 183-190.
- Bentz, D. P., and W. J. Weiss. "REACT: reducing early-age cracking today." *Concrete Plant International* 3 (2008): 56-61.
- Bentz, Dale P., and Ole Mejlhede Jensen. "Mitigation strategies for autogenous shrinkage cracking." *Cement and Concrete Composites* 26.6 (2004): 677-685.
- Bisschop and van Mier 2002 Bisschop, J & Mier, JGM van (2002). *Drying shrinkage microcracking in concrete*. Heron, 47(3), 163-184.

- Bouasker, Marwen, et al. "Chemical shrinkage of cement pastes and mortars at very early age: effect of limestone filler and granular inclusions." *Cement and Concrete Composites* 30.1 (2008): 13-22.
- Cohen, Menashi D., Jan Olek, and William L. Dolch. "Mechanism of plastic shrinkage cracking in portland cement and portland cement-silica fume paste and mortar." *Cement and Concrete Research* 20.1 (1990): 103-119.
- "Concrete Rated Source Quality Catalog." (2016): n. pag. [Ftp://ftp.dot.state.tx.us/pub/txdot-info/cmd/mpl/crsqc.pdf](ftp://ftp.dot.state.tx.us/pub/txdot-info/cmd/mpl/crsqc.pdf). TxDOT Construction Division – Materials & Pavements (CST-M&P). Web.
- Czernin, Wolfgang. *Zementchemie für Bauingenieure*. Bau-Verlag, 1977.
- Dao, V. T. N., et al. "Plastic shrinkage cracking of concrete." *Australian Journal of Structural Engineering* 10.3 (2010): 207-214.
- Davis H.E. (1940) *Autogenous Volume Change of Concrete*, Proceedings of the 43rd Annual American Society for Testing Materials, Atlantic City, N.J., June, pp. 1103-1113
- Dela, Birgitte Friis, and Henrik Stang. "Two-dimensional analysis of crack formation around aggregates in high-shrinkage cement paste." *Engineering Fracture Mechanics* 65.2 (2000): 149-164.
- Douglas KS, Hover KC (2002) *Measuring non-drying bulk shrinkage of cement paste and mortar using Archimedes' principle: Part I*. In: Jensen OM, Bentz DP, Lura P (eds) *Autogenous deformation of concrete*, ACI SP 220, American Concrete Institute, Farmington Hills, Michigan, pp 39–51
- Gao, Peng, et al. "Improvement of autogenous shrinkage measurement for cement paste at very early age: Corrugated tube method using non-contact sensors." *Construction and Building Materials* 55 (2014): 57-62.
- Grube, H. *Causes of shrinkage of concrete and its effect on concrete structures* (In German). Dusseldorf 1991.
- Hammer, Tor Ame, O. Bjontegaard, and E. Sellevold. "Measurement methods for testing of early age autogenous strain." *RILEM Proceedings of Conference on Early Age Cracking in Cementitious Systems EAC*. Vol. 1. 2002.
- Hewlett, P. C. *Lea's Chemistry of Cement and Concrete*. 4th Edition. St. Edmundsbury Pres Ltd., 1998.
- Holt, E., and M. Leivo. "Cracking risks associated with early age shrinkage." *Cement and Concrete Composites* 26.5 (2004): 521-530.
- Holt, Erika E. *Early age autogenous shrinkage of concrete*. Vol. 446. Technical Research Centre of Finland, 2001.

- Hossain, Akhter, Brad Pease, and Jason Weiss. "Quantifying early-age stress development and cracking in low water-to-cement concrete: restrained-ring test with acoustic emission." *Transportation Research Record: Journal of the Transportation Research Board* 1834 (2003): 24-32.
- Houst, Y. F., and F. H. Wittmann. "Depth profiles of carbonate formed during natural carbonation." *Cement and Concrete Research* (Pergamon Press) 32 (2002): 1923-1930.
- Interagency Contract (IAC) No. 463MTIA034: "Evaluation of Long-Term Durability of Concrete."
- Jensen, O. Mejlhede, and P. Freiesleben Hansen. "A dilatometer for measuring autogenous deformation in hardening Portland cement paste." *Materials and structures* 28.7 (1995): 406-409.
- Jensen, O.M., Hansen, P.F.: Autogenous deformation and RH-change in perspective. In: *Cement and Concrete Research* 31 (2001), pp. 1859-1865
- Jensen, Ole Mejlhede, and Per Freiesleben Hansen. "Autogenous deformation and RH-change in perspective." *Cement and Concrete Research* 31.12 (2001): 1859-1865.
- Khunthongkeaw, Jittbodee, Somnuk Tangtermsirikul, and Thatchavee Leelawat. "A study on carbonation depth prediction for fly ash concrete." *Construction and Building Materials* 20.9 (2006): 744-753.
- Kosmatka, S. K. (2008). *Design and Control of Concrete Mixtures*. Skokie, IL: Portland Cement Association.
- Kovler, K. "Testing system for determining the mechanical behaviour of early age concrete under restrained and free uniaxial shrinkage." *Materials and Structures* 27.6 (1994): 324-330.
- Kovler, Konstantin. "Interdependence of creep and shrinkage for concrete under tension." *Journal of materials in civil engineering* 7.2 (1995): 96-101.
- Kronlof, A., Leivo, M., and Sipari, P., (1995), "Experiment study on the basic phenomena of shrinkage and cracking of fresh Mortar", *Cement and Concrete Research*, Vol. 25, No.9. pp. 1747-1754.
- Kropp et al. 1995 – Kropp, j. And Hilsdorf, H.K. (eds.). 1995: *Performance Criteria for Concrete Durability – State of the art Report Prepared by RILEM Report 12*, E & F N Spon, Longdon, U.K., (pp Rilem, Paris), 341 pp.
- Kwak, H-G., and S-J. Ha. "Plastic shrinkage cracking in concrete slabs. Part I: a numerical model." *Magazine of Concrete Research* 58.8 (2006): 505-516.
- Lam, L., and J. G. Teng. "Ultimate condition of fiber reinforced polymer-confined concrete." *Journal of Composites for Construction* 8.6 (2004): 539-548.

- Le Chatelier, H. "Sur les changements de volume qui accompagnent le durcissement des ciments." Bulletin Societe de l'encouragement pour l'industrie nationale 5 (1900).
- Locher, F.W.: Zement - Grundlagen der Herstellung und Verwendung. Düsseldorf, Germany, Verlag Bau und Technik 2000. English: Cement – Principles of production and use. Düsseldorf, Germany, 2006
- Lura, Pietro, and Ole Mejlhede Jensen. Volumetric Measurement in Water Bath-An Inappropriate Method to Measure Autogenous Strain of Cement Paste. No. PCA R&D Serial No. 2925. 2005.
- Lura, Pietro, Ole Mejlhede Jensen, and Jason Weiss. "Cracking in cement paste induced by autogenous shrinkage." Materials and structures 42.8 (2009): 1089-1099.
- Lura, Pietro, Ole Mejlhede Jensen, and Klaas van Breugel. "Autogenous shrinkage in high-performance cement paste: an evaluation of basic mechanisms." Cement and Concrete Research 33.2 (2003): 223-232.
- Lynam, C. G. "Growth and Movement in Portland Cement Paste Concrete, London." (1934): 139.
- M. Won, Improvements of Testing Procedures for Concrete Coefficient of Thermal Expansion, Transportation Research Record: Journal of the Transportation Research Board No. 1919, (2005).
- Meeks, Corey Franklin. "Implementation of ConcreteWorks software in Texas highway construction." (2011).
- Mora-Ruacho, José, Ravindra Gettu, and Antonio Aguado. "Influence of shrinkage-reducing admixtures on the reduction of plastic shrinkage cracking in concrete." Cement and Concrete Research 39.3 (2009): 141-146.
- P.K Mehta, P.J.M Monteiro, Concrete: Structure, Properties and Materials, Third Edition, McGraw-Hill, (2006).
- Pease, B., Adam Neuwald, and W. J. Weiss. "The influence of aggregates on early age cracking in cementitious systems." Celebrating concrete: role of concrete in sustainable development, International symposium dedicated to Prof. S. Shah, Northwestern University. 2003.
- Pease, B., Neuwald, A., and Weiss, W. J., The Influence of Aggregates on Early Age Cracking in Cementitious Systems, Celebrating Concrete: Role of Concrete in Sustainable Development, An International Symposium dedicated to Professor Surendra Shah, Northwestern University, pp. 329~338, (September 2003)
- Persson, Bertil. "Experimental studies on shrinkage of high-performance concrete." Cement and Concrete Research 28.7 (1998): 1023-1036.

- Plastic Cracking in Concrete," Technical Information Letter No. 171-NRMCA, Modern Concrete, Oct. 1960, pp. 63-64.
- Plastic Cracking in Concrete," Technical Information Letter No. 171-NRMCA, Modern Concrete, Oct. 1960, pp. 63-64.
- Powers, T. C. "The thermodynamics of volume change and creep." *Matériaux et Construction* 1.6 (1968): 487-507.
- Powers, T. C. "TL Brownyard Proc. Am. Concrete Institute, 43 (1946–1947)." *Proc. Am. Concrete Institute* 43 (1946): 149.
- Powers, T. C., and T. L. Brownyard. "Studies of the physical properties of hardened Portland cement paste." *Bulletin* 22 (1946).
- Qi, Chengqing, Jason Weiss, and Jan Olek. "Characterization of plastic shrinkage cracking in fiber reinforced concrete using image analysis and a modified Weibull function." *Materials and Structures* 36.6 (2003): 386-395.
- Radjy, Fariborz, Erik J. Sellevold, and Kurt Kielsgaard Hansen. *Isoteric vapor pressure: temperature data for water sorption in hardened cement paste: enthalpy, entropy and sorption isotherms at different temperatures*. 2003.
- Radocea, A. "A model of plastic shrinkage." *Magazine of Concrete Research* 46.167 (1994): 125-132.
- Radocea, Adrian. "A new method for studying bleeding of cement paste." *Cement and concrete research* 22.5 (1992): 855-868.
- Roziere, E., A. Loukili, and F. Cussigh. "A performance based approach for durability of concrete exposed to carbonation." *Construction and Building Materials (Elsevier Ltd.)* 23 (2009): 190-199.
- Sant, G. L. (2006). *A Discussion of Analysis Approaches for Determining 'Time-zero' from Chemical Shrinkage and Autogenous Strain Measurements in Cement Paste*. International RILEM Conference on Volume Changes of Hardening Concrete: Testing and Mitigation (p. 9). Lyngby, Denmark: RILEM.
- Sant, G. L. (2006). *Measurement of Volume Change in Cementitious Materials at Early Ages*. *Transportation Research Record*, 21-29.
- Sant, L. a. (2006). *Measurement of Volume Change in Cementitious Materials at Early Ages; Review of Testing Protocols and Interpretation of Results*. *Transportation Research Record: Journal of the Transportation Research Board*, 21-29.
- Scherer, George W. "Thermal expansion kinetics: method to measure permeability of cementitious materials: I, theory." *Journal of the American Ceramic Society* 83.11 (2000): 2753-2761.

- See HT, Attiogbe EK, Miltenberger MA. Potential for restrained shrinkage cracking of concrete and mortar. In: Proceedings of the ASTM symposium on early-age cracking of concrete, December 2003.
- Sellevoid, E. J., and Ø. Bjøntegaard. "Coefficient of thermal expansion of cement paste and concrete: Mechanisms of moisture interaction." *Materials and Structures* 39.9 (2006): 809-815.
- Sellevoid, E., et al. "High performance concrete: early volume change and cracking tendency." *RILEM PROCEEDINGS. CHAPMAN & HALL*, 1995.
- Shaeles, Christos A., and Kenneth C. Hover. "Influence of mixture proportions and construction operations on plastic shrinkage cracking in thin slabs." *ACI Materials Journal* 85.6 (1988): 495-504.
- Simpkins, P.G., Johnson, D.W., and Fleming, D.A., "Drying Behavior of Colloidal Silica 2 Gels," *Journal of the American Ceramic Society*, V. 72, No. 10, 1986, pp. 1816-1821.
- Slowik, Volker, Markus Schmidt, and Roberto Fritsch. "Capillary pressure in fresh cement-based materials and identification of the air entry value." *Cement and Concrete composites* 30.7 (2008): 557-565.
- Stacey, Stephen. "Evaluation of ASTM C494 Procedures for Polycarboxylate Admixtures Used in Precast Concrete Elements." Thesis. 2016.
- Tazawa, E. "Autoshrink'98." *Proc. of the Int. Workshop on Autogenous Shrinkage of Concrete*. 1998.
- Tazawa, E. And Miyazawa, S. (1992) Autogenous shrinkage of cement paste with condensed silica fume, *Proceedings of the 4th CANMET/ACI International Conference on Fly Ash, Silica Fume, Slag and Natural Pozzolans in Concrete*, ACI, pp.875-894.
- Tazawa, Eiichi. *Autogenous Shrinkage of Concrete: Proceedings of the International Workshop, Organized by JCI (Japan Concrete Institute), Hiroshima, June 13-14, 1998*. New York: Routledge, 1999. Print.
- Thomas, M. D. A., and J. D. Matthews. "Carbonation of fly ash concrete." *Magazine of Concrete Research* 44.160 (1992): 217-228.
- Tian, Qian, and Ole Mejlhede Jensen. "Measuring autogenous strain of concrete with corrugated moulds." *Microstructure related durability of cementitious composites* (2008): 1501-1511.
- Tiburzi, Nicolás Bruno. *Evaluation of Volume Changes and Cracking Potential of Low Water-to-cementitious Material Ratio Concrete Mixtures*. Thesis. University of Texas at Austin, 2015. N.p.: n.p., n.d. UT Electronic Theses and Dissertations. Web.
- Weiss, William Jason. *Prediction of early-age shrinkage cracking in concrete elements*. 1999.

Weyers, R. E., J. C. Conway, and P. D. Cady. "Photoelastic analysis of rigid inclusions in fresh concrete." *Cement and Concrete Research* 12.4 (1982): 475-484.

Wittmann, F. H. "On the action of capillary pressure in fresh concrete." *Cement and Concrete Research* 6.1 (1976): 49-56.

Young, J. Francis, Sidney Mindess, and David Darwin. *Concrete*. Prentice Hall, 2002.

Zou, Dinghua, and Jason Weiss. "Early age cracking behavior of internally cured mortar restrained by dual rings with different thickness." *Construction and Building Materials* 66 (2014): 146-153.

12390, CEN/TS. *Determination of the Relative Carbonation Resistance of Concrete*. 2008.